



**HAL**  
open science

# Dendrimers as a powerful tool in theranostic applications

Flonja Liko

► **To cite this version:**

Flonja Liko. Dendrimers as a powerful tool in theranostic applications. Human health and pathology. Université d'Angers, 2016. English. NNT : 2016ANGE0039 . tel-01618646

**HAL Id: tel-01618646**

**<https://theses.hal.science/tel-01618646>**

Submitted on 18 Oct 2017

**HAL** is a multi-disciplinary open access archive for the deposit and dissemination of scientific research documents, whether they are published or not. The documents may come from teaching and research institutions in France or abroad, or from public or private research centers.

L'archive ouverte pluridisciplinaire **HAL**, est destinée au dépôt et à la diffusion de documents scientifiques de niveau recherche, publiés ou non, émanant des établissements d'enseignement et de recherche français ou étrangers, des laboratoires publics ou privés.

# Thèse de Doctorat

**Flonja LIKO**

Mémoire présenté en vue de l'obtention du :

**Grade de Docteur de l'Université d'Angers**

sous le sceau de l'Université Bretagne Loire

École doctorale : *Biologie Santé*

Discipline : *Sciences de la vie et de la santé*

Spécialité : *Pharmacologie expérimentale et clinique*

Unité de recherche : *UMR\_S 1066 INSERM MINT, l'Université d'Angers*

**Grade de Docteur de l'Université Santiago de Compostela**

sous le sceau de l'Université Santiago de Compostela

École doctorale : *Erasmus Mundus Doctoral Program on Nanomedicine and Pharmaceutical Innovation*

Discipline : *Nanomedicine*

Unité de recherche : *Center for Research in Biological Chemistry and Molecular Materials (CIQUS) at the USC*

Soutenue le 16.12.2016

Thèse N° : 107857

## Dendrimers as a powerful tool in theranostic applications

### JURY

- Rapporteurs : **Claire BILLOTEY**, Professeur des universités, Université Jean Monnet, Saint-Étienne.  
**Diego PENA**, Professeur étranger, Université Santiago de Compostela.
- Examineurs : **Emmanuel GARCION**, Directeur de recherche, MINT, UMR-S 1066 Inserm.  
**Nicolas NOIRET**, Professeur des universités, École nationale supérieure de chimie de Rennes.
- Directeur de Thèse : **François HINDRE**, Maître de conférences, Université d'Angers.
- Co-directeur de Thèse : **Eduardo FERNANDEZ-MEGIA**, Professeur étranger, Université Santiago de Compostela.

## Thèse de Doctorat

Flonja LIKO

### Potentiel des dendrimères comme outil d'applications théranostiques

#### Dendrimers as a powerful tool in theranostic applications

##### Résumé

Une nouvelle stratégie oncologique, basée sur l'intégration de la radiothérapie nanovectorisée et l'administration loco-régionale, a été évaluée pour le traitement et l'imagerie du glioblastome, le type le plus commun des tumeurs cérébrales primaires. Les dendrimères Gallic Acid-Triéthylène Glycol (GATG) sont des nanovecteurs de choix pour délivrer simultanément l'agent thérapeutique (le radioisotope  $^{188}\text{Re}$  par son rayonnement bêta a été retenu) et l'agent diagnostique (le gadolinium est un agent paramagnétique utilisé en Imagerie par Résonance Magnétique (IRM)). Leur évaluation a été réalisée par administration loco-régionale par stéréotaxie sur un modèle de rat F98. Les données pharmaco-cinétiques ont été également obtenues après injection intraveineuse permettant d'apprécier les propriétés des différents dendrimères synthétisés. Leur apport en terme de confinement au site d'injection représente un avantage majeur de ce nouveau type de radiopharmaceutiques.

##### Mots clés

GATG, dendrimères, radiothérapie interne, MRI, glioblastoma,  $^{188}\text{Re}$ ,  $\text{Gd}^{3+}$ ,  $^{99\text{m}}\text{Tc}$ .

##### Abstract

A new oncologic strategy, based on the integration of nanovectorized radiotherapy and locoregional delivery, was evaluated for the treatment and imaging of glioblastomas, the most common and lethal type of primary brain tumors. Gallic acid-triethylene glycol (GATG) dendrimers were the nanovectors of choice to deliver the radiotherapeutic  $^{188}\text{Re}$  and paramagnetic nuclei  $\text{Gd}^{3+}$ , with a minimally invasive stereotactic injection, directly depositing the radiotherapeutic dose to the tumor site in a F98 rat glioma model. Intravenous injection was used to further investigate the pharmacokinetics, throughout body distribution and clearance profiles of these dendrimers. Molecular weight and architecture had an important role on the *in vivo* behavior of the dendrimers. Their use as nanovectors prevented the fast brain clearance of the radionuclide alone, and prolonged the confinement of the internal radiation at the tumor site.

##### Key words

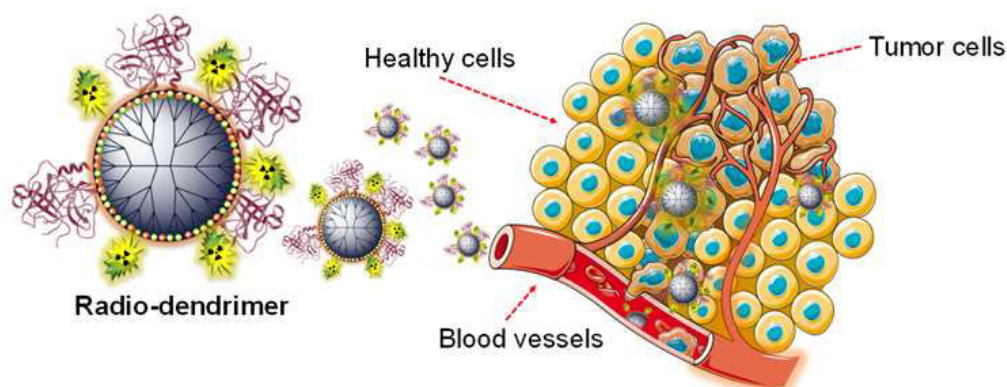
GATG, dendrimer, internal radiotherapy, MRI, glioblastoma,  $^{188}\text{Re}$ ,  $\text{Gd}^{3+}$ ,  $^{99\text{m}}\text{Tc}$ .

2016-2017

Doctorat de l'Université d'Angers  
Biomolécules, pharmacologie, thérapeutique

2016-2017

Doctorat de l'Université Santiago de Compostela  
Nanomedicine, chimie organique, synthèse organique



# Dendrimers as a powerful tool in theranostic applications

**Liko Flonja**

Sous la direction de

Dr. Hindré François

Dr. Fernandez-Megia Eduardo

Membres du jury

Billotey Claire, PU-PH | Rapporteur

Peña Diego, PU | Rapporteur

Garcion Emmanuel, DR | Examineur

Noiret Nicolas, PU | Examineur

Hindr e Fran ois, MCU | Directeur de th ese

Fernandez-Megia Eduardo, MCU | Directeur de th ese



**L'auteur du présent document vous autorise à le partager, reproduire, distribuer et communiquer selon les conditions suivantes :**



- Vous devez le citer en l'attribuant de la manière indiquée par l'auteur (mais pas d'une manière qui suggérerait qu'il approuve votre utilisation de l'œuvre).
- Vous n'avez pas le droit d'utiliser ce document à des fins commerciales.
- Vous n'avez pas le droit de le modifier, de le transformer ou de l'adapter.

**Consulter la licence creative commons complète en français :**

**<http://creativecommons.org/licences/by-nc-nd/2.0/fr/>**



Ces conditions d'utilisation (attribution, pas d'utilisation commerciale, pas de modification) sont symbolisées par les icônes positionnées en pied de page.







---

*In loving memory of my father  
and to my wonderful mother.*

---





## Acknowledgements

Firstly, I would like to express my sincere gratitude to my directors, François Hindre (Associate Professor, University of Angers, France) and Eduardo Fernandez-Megia (Associate Professor, University of Santiago de Compostela, Spain) for the continuous support of my PhD study and related research, their motivation and immense knowledge. Their guidance helped me in all the time of research and writing of this thesis.

Besides my advisors I would like to thank Prof. Frank Boury, as the coordinator of the European Doctorate in Nanomedicine and Pharmaceutical Innovation (NanoFar) that made possible the realization of this PhD research.

I would like to thank the rest of my thesis committee: Claire Billotey (Professor at the University of Jean Monnet, Saint-Étienne, France) and Diego Peña (Associate Professor at the University of Santiago de Compostela, Spain) for giving me the honor of being reviewers for this PhD; my sincere gratitude to Nicolas Noiret (Professor at ENSCR, Rennes, France) and Emmanuel Garcion (Director of Research at Inserm U646, Angers, France) for the time dedicated to evaluate and examine this work.

My heartfelt thanks also goes to Juan Francisco Correa Chinea, not only for the great and unlimited help during my work at the Center for Research in Biological Chemistry and Molecular Materials in Spain, but also for his friendship.

Thank you to Florence Franconi for her extremely valuable MRI technical support and to Benedicte Lelievre for the ICP-MS measurements and very professional attitude.

I am grateful to Jérôme Roux and Pierre Legras from the Service Commun d'Animalerie Hospitalo-Universitaire (SCAHU, Angers, France) for the sympathy and help for during the animal experimentation. I would also like to thank Clement Tetaud with Natacha Galopin for their very important technical support, during the *in vivo* work.

Many thanks to Marion Toucheteau (responsible for Erasmus Mundus and communication at the University of Angers), Edith Greleau (UMR 1066 Micro et Nanomédecines Biomimétiques (MINT), University of Angers), and Purificación Domínguez (CIMUS, University of Santiago de Compostela) for their valuable help with the administrative procedures, during this joint PhD program, both in France and Spain.

I would like to thank all of my colleagues, who in one way or another, helped me during this PhD. One page of acknowledgements is not enough to thank all of them. Thank you for making these last three years such a memorable time.



## Table of Contents

List of Figures .....	4
List of Tables .....	9
List of Abbreviations .....	10
PART 1. Glioblastoma management .....	20
1.1. Diagnosis modalities of glioblastoma (PET, SPECT, CT, MRI) .....	24
MRI, in diagnostic imaging of glioblastoma.....	28
$T_1/ T_2$ relaxation times and $T_1/ T_2$ mapping .....	30
Spin/gradient echo ( $T_1/T_2$ weighting) and inversion recovery sequences .....	33
Tissue characterization with and without injection of Gd CA .....	35
Relaxivity of Gd CA .....	38
Dendrimer-based Gd CA and their effect on proton/water exchange.....	39
1.2. Glioblastoma treatment .....	44
Radionuclides for the therapy of malignant gliomas .....	48
Vectors for internal radiotherapy of glioblastoma .....	50
Dendrimers as the vectors of choice .....	53
The role of dendrimers in biomedical applications.....	58
1.3. Review Article: Dendrimers as innovative radiopharmaceuticals in cancer radionanotherapy.....	63
Conclusions.....	78
PART 2. Strategies and Objectives.....	82
2.1. Modern strategies for the accelerated synthesis of dendrimers .....	86
Results and Discussion.....	91
Synthesis and characterization of novel building blocks for carbamate dendrimers .....	91

Experimental Information .....	109
Materials and Instrumentation.....	109
Synthesis and characterization of new compounds.....	112
Conclusions .....	121
2.2. GATG dendrimers for integrated radiotherapy and MRI of glioblastoma .....	124
Preamble .....	124
2.2.1. Materials and methods .....	128
Characterization of starting dendrimers .....	130
Synthesis and characterization of new compounds.....	131
NMR spectra .....	134
IR spectra.....	137
Technetium radiolabeling.....	138
<i>In vivo</i> study of <sup>99m</sup> Tc-2[Gn]-DTPA dendrimers following <i>iv</i> injection.....	139
Gadolinium labeling .....	141
Molar relaxivity measurements of Gd-2[Gn]-DTPA dendrimers .....	141
Ethic statement .....	143
Preparation of the glioma animal model .....	143
CED procedure of Gd-2[G3]-DTPA dendrimers .....	145
MRI with Gd-2[G3]-DTPA dendrimers in F98 glioma rats, following CED.....	145
Dual labeling with radioactive 188-rhenium and gadolinium.....	147
Experimental conditions for the tissue distribution study following the CED of dual labeled dendrimers.....	147
2.2.2. Results and Discussion .....	152
2.3. Complementary results .....	167
2.3.1. Materials and methods .....	167

Synthesis and characterization of 2[Gn]-DOTA dendrimers .....	169
2.3.2. Results and discussion.....	180
Comparison of relaxivity properties between Gd-2[Gn]-DTPA and Gd-2[Gn]-DOTA dendrimers.....	180
2.4. Conclusions.....	183
PART 3. General Conclusions.....	187
Bibliography.....	195
PART 4. Bibliography .....	197

## List of Figures

<b>Figure 1.1</b> Brain, nervous system tumors: ASR (World) per 100 000 (all ages).....	21
<b>Figure 1.2</b> A simplified algorithm for classification of the diffuse gliomas based on histological and genetic features. ....	22
<b>Figure 1.3</b> Histologic characteristics of glioblastoma tumors. (a) Three zones can be recognized: central necrosis, proliferation, and infiltration zone. H&E, 25x; (b) Area of disrapture with high cell density, vessels of different size and edema dissociation of the tissue; (c) Circumscribed necrosis with pseudo-palisading in an area with high cell density (H&E, 100x) and area with a high Ki-67/MIB.1 proliferation index (DAB, 100x). ....	23
<b>Figure 1.4</b> MRI scans of a patient with a right temporal glioblastoma illustrating the spread of the disease. (A) Pre-surgical scan, GBM (arrow) is surrounded with edema. (B) Scan after surgery and radiation therapy showing “gross total resection” and clear resection cavity, and (C) six months later, showing recurrence not only at the resection margin (arrow) but a second focus of GBM across the Sylvian fissure in the frontal lobe (arrow). (D) Postresection scans of both recurrent tumors. (E) Scan 3 months later, showing the tumor recurring at the resection margin and crossing the corpus callosum to the other hemisphere (arrow) .....	29
<b>Figure 1.5</b> Behavior of $T_1$ and $T_2$ as a function of correlation time. ....	31
<b>Figure 1.6</b> (a) Return to equilibrium of the magnetization, (b) return to equilibrium on the z axis:.....	32
( $M_z = M_0 \times [1 - e(-tT_1)]$ ), (c) return to equilibrium in the xy plane ( $M_y = M_0 \times e(-tT_2)$ ).....	32
<b>Figure 1.7</b> Gd contrast agent was selectively taken up in the tumor region due to pathological changes in the BBB, whereas an intact BBB prevented contrast agent accumulation in unaffected brain tissue.....	37
<b>Figure 1.8</b> Activation of a Microglia cell during a pathological state in the brain. ....	53
<b>Figure 1.9</b> Schematic of three main architectural components of dendrimers.....	54
<b>Figure 1.10</b> Schematic depicting the building blocks of the dendrimer and generation growth. ....	55
<b>Figure 1.11</b> Schematic resuming the divergent and convergent growth of dendrimers. ....	56

<b>Figure 1.12</b> Schematic of the iterative sequence of reactions, needed for the generation growth of the dendrimers.....	56
<b>Figure 1.13</b> Applications of dendrimers with high potential.....	59
<b>Figure 2.1</b> Convergent approach toward triazole dendrimers. a) CuSO <sub>4</sub> (5 mol%), sodium ascorbate (10 mol%), H <sub>2</sub> O/tBuOH (1:1); b) 1.5 eq. NaN <sub>3</sub> , CH <sub>3</sub> COCH <sub>3</sub> /H <sub>2</sub> O (4:1), 60 °C, 1–3 h.....	87
<b>Figure 2.2</b> Synthetic scheme for carbamate dendrimers .....	90
<b>Figure 2.3.</b> Synthetic scheme for RU-1 .....	91
<b>Figure 2.4</b> Fragment of the core: 2 .....	92
<b>Figure 2.5</b> The synthetic scheme of the G1cb-1 .....	94
<b>Figure 2.6</b> The synthetic scheme of the G1cb-2.....	97
<b>Figure 2.7</b> Elongation of the carbamate repeating unit from RU-1 to RU-2 .....	98
<b>Figure 2.8</b> Scheme depicting the steps for the synthesis of RU-2; 1. first step for the synthesis of product A; 2. second step for the synthesis of product B; 3. third step for the combination of A and B to give RU-2-OH; 4. fourth step resulting in RU-2. ....	99
<b>Figure 2.9</b> Disappearance of the azide band during the coupling reaction .....	101
<b>Figure 2.10</b> The synthetic scheme of the G1cb-4.....	102
<b>Figure 2.11.</b> Scheme for the azide substitution reaction .....	103
Time (min) .....	103
<b>Figure 2.12</b> Structure of G2cb-4.....	104
<b>Figure 2.13</b> The synthetic scheme of <b>1</b> .....	105
<b>Figure 2.14</b> The chemical structure of G1cb-5.....	106
<b>Figure 2.15</b> The synthetic scheme of the azide substitution of the G1cb-5 .....	106

<b>Figure 2.16</b> Structure of G2cb-5 .....	108
<b>Figure 2.17</b> Structure of G1cb-6 .....	108
<b>S1.</b> $^1\text{H}$ and $^{13}\text{C}$ NMR spectra of RU-1 .....	112
<b>S2.</b> $^1\text{H}$ and $^{13}\text{C}$ NMR spectra of RU-2 .....	114
<b>S3.</b> $^1\text{H}$ and $^{13}\text{C}$ NMR spectra of G1cb-4 .....	115
<b>S4.</b> $^{13}\text{C}$ - $^{13}\text{C}$ HMQC of G1cb-4 .....	116
<b>S5.</b> $^1\text{H}$ - $^1\text{H}$ COSY of G1cb-4 .....	116
<b>S6.</b> $^1\text{H}$ NMR spectrum of the chlorinated core 1 .....	117
<b>S7.</b> $^1\text{H}$ NMR spectrum of the core 1 .....	118
<b>S8.</b> $^1\text{H}$ and $^{13}\text{C}$ NMR spectra of G1cb-5 .....	119
<b>S9.</b> $^{13}\text{C}$ - $^{13}\text{C}$ HMQC and $^1\text{H}$ - $^1\text{H}$ COSY of G1cb-5 .....	120
<b>S10.</b> $^1\text{H}$ NMR spectrum of 2[G2]-N <sub>3</sub> .....	130
<b>S11.</b> $^1\text{H}$ NMR spectrum of 2[G3]-N <sub>3</sub> .....	131
<b>S12.</b> $^1\text{H}$ NMR spectrum of 2[G4]-N <sub>3</sub> .....	131
<b>S13.</b> $^1\text{H}$ NMR spectrum of 2[G2]-DTPA (Dfilter 50 ms) .....	134
<b>S14.</b> $^{13}\text{C}$ NMR spectrum of 2[G2]-DTPA .....	134
<b>S15.</b> $^1\text{H}$ NMR spectrum of 2[G3]-DTPA (Dfilter 200 ms) .....	135
<b>S16.</b> $^{13}\text{C}$ NMR spectrum of 2[G3]-DTPA .....	135
<b>S17.</b> $^1\text{H}$ NMR spectrum of 2[G4]-DTPA .....	136
<b>S18.</b> $^{13}\text{C}$ NMR spectrum of 2[G4]-DTPA .....	136

<b>S19.</b> IR spectrum of 2[G2]-DTPA.....	137
<b>S20.</b> IR spectrum of 2[G3]-DTPA.....	137
<b>S21.</b> IR spectrum of 2[G4]-DTPA.....	138
<b>S22.</b> Elution profile detected by the gamma counter following the radiolabeling reaction of 2[Gn]-DTPA dendrimers with pertechnetate in rt. ....	139
<b>S23.</b> Rat in a metabolic cage.....	140
<b>S24.</b> CED procedure .....	145
<b>S25.</b> F98 glioma rat ready to be put in the MRI system.....	146
<b>Figure 2.18.</b> Functionalization of GATG dendrimers with DTPA ligands. (a) Chemical structure of 2[Gn]-N <sub>3</sub> dendrimers. (b) One-pot DTPA functionalization reaction. (c, d) <sup>1</sup> H NMR and IR confirming complete reduction of azide groups. (e, f) GPC and DLS of 2[Gn]-DTPA dendrimers with concentration of 1 mg/mL in 10 mM PB pH 7.4/ 150 mM LiCl.....	153
<b>Figure 2.19</b> Degree of Conjugation of DTPA ligands to 2[Gn] dendrimers.....	155
<b>Figure 2.20</b> (a) Biodistribution analyses (n=3/group). (b) <i>In vivo</i> blood clearance in adult female Wistar rats, injected via the tail vein with 3.7 Mbq of <sup>99m</sup> Tc-2[Gn]-DTPA in 0,2 mL saline.....	158
<b>Figure 2.21.</b> Evaluation of 2[Gn]-DTPA dendrimers by MRI following Gd labeling. (a) Schematic including CED of Gd-2[G3]-DTPA dendrimers in F98 glioma tumor bearing rats. An extensive invasion of normal brain with islands of F98 tumor cells at varying distances from the tumor mass is observed. (b) <i>R<sub>1</sub></i> and <i>R<sub>2</sub></i> plots for Gd-2[G2]-DTPA (pink), Gd-2[G3]-DTPA (orange), Gd-2[G4]-DTPA (black), and Gd-DTPA (blue); (c) <i>T<sub>1</sub>W</i> and <i>T<sub>1</sub></i> maps of the F98 glioma rats 0.5h post-CED (7T MRI). Orange circles indicate the presence of 2[Gn]-DTPA-Gd. ....	162
<b>Figure 2.22.</b> Brain retention and clearance of 2[Gn]-DTPA dendrimers following dual labeling with Gd and <sup>188</sup> Re. Tissue distribution comparison between <sup>188</sup> Re-perrhenate (3.7 MBq) and of [ <sup>188</sup> Re, Gd]-2[G3]-DTPA dendrimers (3.7 MBq) (a) 24 hours (b) and 96 hours following their CED in F98-glioma rats (n=3). ....	164
<b>S26.</b> <sup>1</sup> H NMR spectrum of 2[G2]-DOTA.....	171

<b>S27.</b> $^{13}\text{C}$ NMR spectrum of 2[G2]-DOTA.....	171
<b>S28.</b> IR spectrum of 2[G2]-DOTA. ....	172
<b>S29.</b> $^1\text{H}$ NMR spectrum of 2[G3]-DOTA.....	172
<b>S30.</b> $^{13}\text{C}$ NMR spectrum of 2[G3]-DOTA.....	173
<b>S31.</b> IR spectrum of 2[G3]-DOTA. ....	173
<b>S32.</b> $^1\text{H}$ NMR spectrum of 2[G4]-DOTA.....	174
<b>S33.</b> $^{13}\text{C}$ NMR spectrum of 2[G4]-DOTA.....	174
<b>S34.</b> IR spectrum of 2[G4]-DOTA. ....	175
<b>S35.</b> Purity check of [Gn]-DOTA dendrimers by SEC.....	175
<b>S36.</b> DLS measurements of 2[Gn]-DOTA dendrimers (2[G2]-DOTA-2[G4]-DOTA from left to right) .....	175
<b>Figure 2.23.</b> Chemical structure of 2[G2]-DOTA/DTPA .....	176
<b>Figure 2.24.</b> NMR interpretation of 2[G2]-DTPA structures.....	177
<b>Figure 2.25</b> NMR interpretation of 2[G2]-DOTA structures. ....	178
<b>Figure 2.26.</b> a) $R_1$ plots for Gd-2[G2]-DOTA (violet), Gd-2[G3]-DOTA (red), Gd-2[G4]-DOTA (green), Gd-2[G2]-DTPA (pink), Gd-2[G3]-DTPA (orange), Gd-2[G4]-DTPA (black), and Gd-DTPA (blue); b) $R_2$ plots for Gd-2[G2]-DOTA (violet), Gd-2[G3]-DOTA (red), Gd-2[G4]-DOTA (green), Gd-2[G2]-DTPA (pink), Gd-2[G3]-DTPA (orange), Gd-2[G4]-DTPA (black), and Gd-DTPA (blue). ....	182

## List of Tables

Table 1.1. Features of modalities used for glioma imaging .....	27
Table 1.2 General characteristic of therapeutic radionuclides used for malignant gliomas treatment.....	49
Table 2.1 Stability tests of the RU-1 in various microwave assisted AAC conditions .....	91
Table 2.2 Results of the tests following the reactions of the RU-1 with core fragment 2, in various microwave assisted AAC conditions .....	93
Table 2.3 Results of various microwave assisted AAC conditions tested for the synthesis of G1cb-1 .....	95
Table 2.4 Results of various microwave assisted AAC conditions tested for the synthesis of G1cb-2 .....	96
Table 2.5 Stability tests of the RU-2 in various microwave assisted AAC conditions .....	100
Table 2.6 Microwave assisted AAC conditions tested for the synthesis of G1cb-4.....	101
Table 2.7 Microwave assisted AAC conditions tested for the azide substitution reaction.....	103
Table 2.8 Microwave assisted AAC condition tested for the synthesis of G2cb-4 .....	104
Table 2.9 Microwave assisted reaction conditions tested for the azide substitution reaction .....	105
Table 2.10 Microwave assisted AAC conditions tested for the synthesis of G1cb-5 (AAC 16), the azide substitution reaction of G1cb-5, the synthesis of G2cb-5 (AAC 17) and the synthesis of G1cb-6 (AAC 18).107	
Table 2.11. Relaxivities of macromolecular CAs compared with Gd-DTPA in 7T.....	160
Table 2.12 Relative NMR integration data to measure the % DC of chelates to 2[Gn]-DTPA/DOTA dendrimers .....	179
Table 2.13 Characterization of 2[Gn]-DTPA and 2[Gn]-DOTA dendrimers.....	179
Table 2.14 Relaxivities of macromolecular CAs compared with Gd-DTPA in 7T.....	183

## List of Abbreviations

% IA:	percentage of injected activity.
$1/T_{i,d}$ :	diamagnetic relaxation rate.
$1/T_{i,obs}$ :	observed solvent relaxation rate.
$1/T_{i,p}$ :	paramagnetic relaxation rate.
$^{11}\text{C-MET}$ :	$^{11}\text{C}$ -methionine.
$^{123}\text{I}$ :	iodine-123.
$^{125}\text{I}$ :	iodine-125.
$^{131}\text{I}$ :	iodine-131.
$^{188}\text{Re}$ :	rhenium-188
$^{18}\text{FET}$ :	$^{18}\text{F}$ -fluor-ethyl-tyrosine.
$^1\text{H}$ :	proton.
$^{201}\text{Tl}$ :	thallium-201.
$^{90}\text{Y}$ :	yttrium-90.
$^{99m}\text{Tc}$ :	technetium-99m.
AAC:	azide-alkyne cycloaddition.
Ar:	argon.
ATCC:	American Type Culture Collection.
BBB:	blood brain barrier.
BCNU:	biodegradable polymer releasing carmustine.
BTEAC:	benzyltriethylammonium chloride.
CA:	contrast agents.
CED:	convection-enhanced delivery.
$\text{CHCl}_3$ :	chloroform.
CNS:	central nervous system.
COSY:	homonuclear correlation spectroscopy.
CSF:	cerebrospinal fluid.
CT:	computed tomography.
CuAAC:	copper-catalyzed azide-alkyne cycloaddition reaction.
DEPT:	distortionless enhancement by polarization transfer.
DLS:	dynamic light scattering.
DMEM:	Dulbecco's modified Eagle's medium.

DMSO:	dimethyl sulfoxide.
DSC:	disuccinimidyl chloride.
DTPA:	diethylenetriaminepentaacetic acid.
DOTA:	1,4,7,10-tetraazacyclododecane-1,4,7,10-tetraacetic acid
EBRT:	external beam radiotherapy.
EPR:	enhanced permeability and retention.
EI:	experimental information.
EtOAc:	ethyl acetate.
FCS:	fetal calf serum.
FDA:	U.S. Food and Drug Administration.
FDG:	[ <sup>18</sup> F]fluoro-2-deoxy-2-glucose.
FOV:	Field of View.
G:	generation of dendrimer.
G1cb:	first generation carbamate dendrimer.
GATG:	gallic acid triethylene glycol.
GBM:	glioblastoma.
Gd:	gadolinium.
Gd CA:	gadolinium contrast agents.
GE:	gradient echo.
GPC:	gel permeation chromatography.
HMQC:	heteronuclear multiple quantum correlation spectroscopy
HN <sub>3</sub> :	hydrazoic acid.
ICP-MS:	inductively coupled plasma-mass spectrometry.
IMT:	3-[ <sup>123</sup> I]iodo- $\alpha$ -methyl-l-tyrosine.
IR:	Inversion recovery.
<i>iv</i> :	intravenous.
LET:	linear energy transfer.
LiCl:	lithium chloride.
LNCs:	lipid nanocapsules.
MeCN:	acetonitrile.
MeOH:	methanol.
MGMT:	O6-methylguanine-DNA-methyltransferase.
moAbs:	monoclonal antibodies.

MPLC:	medium pressure liquid chromatography.
MRI:	magnetic resonance imaging.
NIR:	near-infrared.
NMR:	nuclear magnetic resonance.
PB:	phosphate buffer.
Pd/C:	palladium on activated charcoal.
PEG:	poly(ethylene glycol).
PET:	positron emission tomography.
Ph <sub>3</sub> P:	triphenylphosphine.
Py:	pyridine.
RES:	reticuloendothelial system.
RF:	radiofrequency.
RIT:	radioimmunotherapy.
rt:	room temperature.
RU:	repeating unit of dendrimers.
SE:	spin echo.
SLNs:	sentinel lymph nodes.
SOCl <sub>2</sub> :	thionyl chloride.
SPECT:	single photon emission computed tomography.
SRS:	stereotactic radiosurgery.
$T_1$ :	longitudinal relaxation time.
$t_{1/2}$ :	half-life.
$T_1W$ :	$T_1$ -weighted.
$T_2$ :	transverse relaxation time.
$T_2W$ :	$T_2$ weighted.
<i>t</i> BuOAc:	tert-butyl acetate.
TE:	echo time.
$TI$ :	inversion time.
TMZ:	temozolomide.
TR:	repetition time.
$V_d$ :	volume of distribution.
$V_i$ :	volume of infusion.
WHO:	World Health Organization.

$\alpha$ : alpha.  
 $\beta$ : beta.  
 $\rho$ : proton density.

## RÉSUMÉ

Une nouvelle stratégie oncologique, basée sur l'intégration de la radiothérapie nanovectorisée et l'administration loco-régionale, a été évaluée pour le traitement et l'imagerie du glioblastome, le type le plus commun des tumeurs cérébrales primaires. Les dendrimères Gallic Acid-Triéthylène Glycol (GATG) sont des nanovecteurs de choix pour délivrer simultanément l'agent thérapeutique (le radioisotope  $^{188}\text{Re}$  par son rayonnement bêta a été retenu) et l'agent diagnostique (le gadolinium est un agent paramagnétique utilisé en Imagerie par Résonance Magnétique (IRM)). Leur évaluation a été réalisée par administration loco-régionale par stéréotaxie sur un modèle de rat F 98. Les données pharmaco-cinétiques ont été également obtenues après injection intraveineuse permettant d'apprécier les propriétés des différents dendrimères synthétisés. Leur apport en terme de confinement au site d'injection représente un avantage majeur de ce nouveau type de radiopharmaceutiques.

**mots-clés :** GATG, DTPA, dendrimères théranostic, radiothérapie interne MRI, glioblastoma,  $^{188}\text{Re}$ ,  $\text{Gd}^{3+}$ ,  $^{99\text{m}}\text{Tc}$ .

## ABSTRACT

A new oncologic strategy, based on the integration of nanovectorized radiotherapy and locoregional delivery, was evaluated for the treatment and imaging of glioblastomas, the most common and lethal type of primary brain tumors. Gallic acid-triethylene glycol (GATG) dendrimers were the nanovectors of choice to deliver the radiotherapeutic  $^{188}\text{Re}$  and paramagnetic nuclei  $\text{Gd}^{3+}$ , with a minimally invasive stereotactic injection, directly depositing the radiotherapeutic dose to the tumor site in a F98 rat glioma model.

Intravenous injection was used to further investigate the pharmacokinetics, throughout body distribution and clearance profiles of these dendrimers. Molecular weight and architecture had an important role on the *in vivo* behavior of the dendrimers. Their use as nanovectors prevented the fast brain clearance of the radionuclide alone, and prolonged the confinement of the internal radiation at the tumor site.

**keywords:** GATG, DTPA, *theranostic dendrimers*, *localized radiotherapy*, MRI, F98 glioma rats, glioblastoma,  $^{188}\text{Re}$ ,  $\text{Gd}^{3+}$ ,  $^{99\text{m}}\text{Tc}$ .

Présidence de l'université  
40 rue de rennes – BP 73532  
49035 Angers cedex

– Tél. 02 41 96 23 23 | Fax 02 41 96 23 00



# ENGAGEMENT DE NON PLAGIAT

Je, soussigné(e) Flonja LIKO

déclare être pleinement conscient(e) que le plagiat de documents ou d'une partie d'un document publiée sur toutes formes de support, y compris l'internet, constitue une violation des droits d'auteur ainsi qu'une fraude caractérisée.

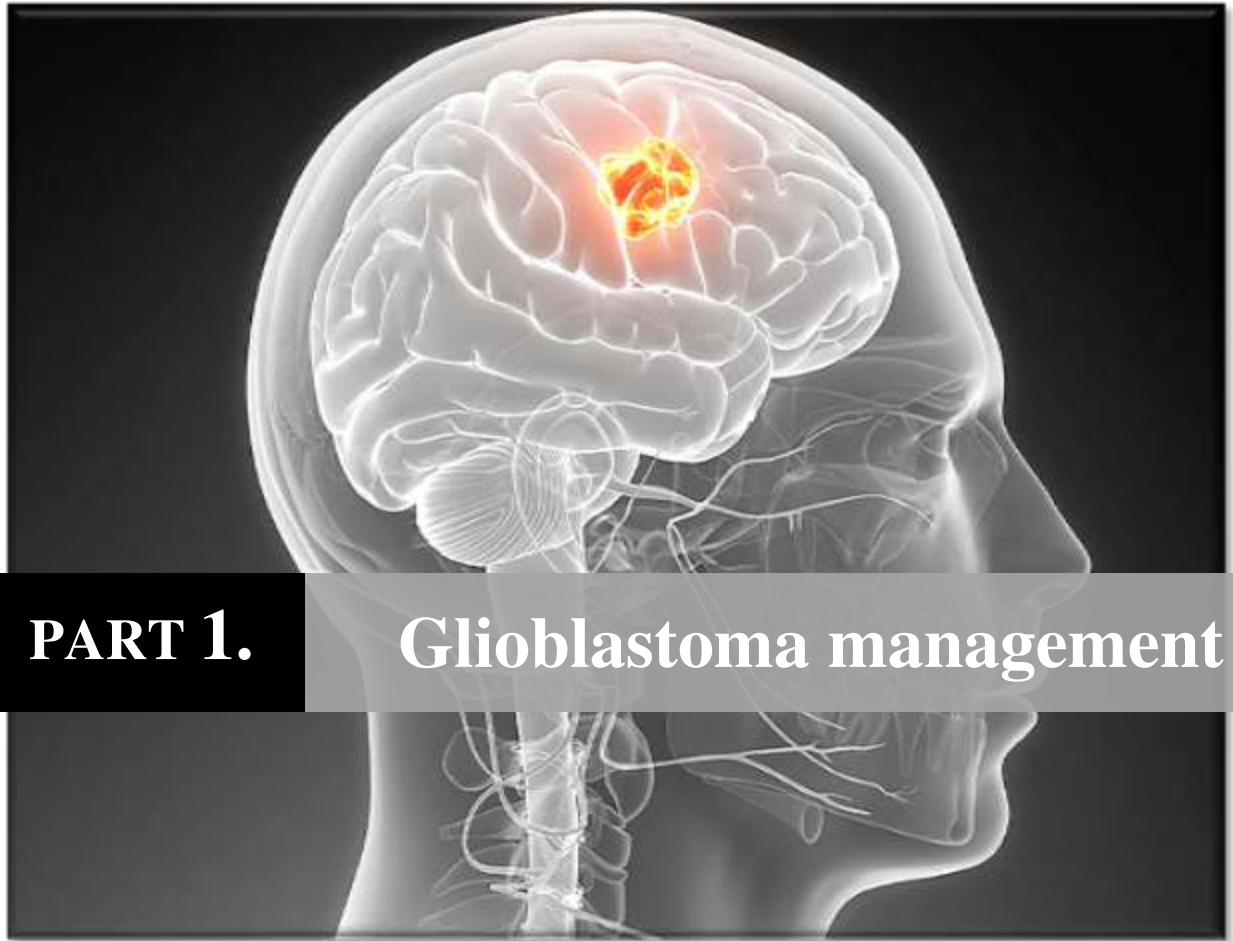
En conséquence, je m'engage à citer toutes les sources que j'ai utilisées pour écrire ce rapport ou mémoire.

signé par l'étudiant(e) le **10 / 10 / 2016**

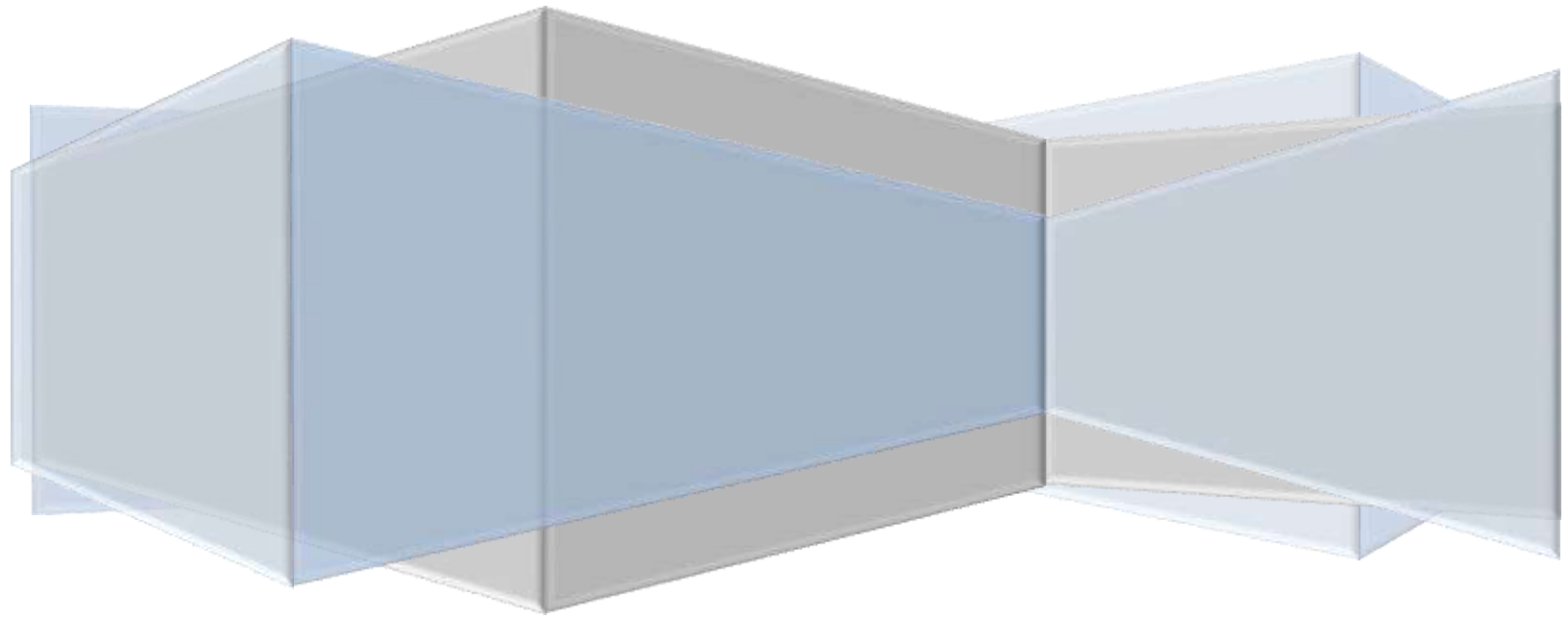
**Cet engagement de non plagiat doit être signé et joint  
à tous les rapports, dossiers, mémoires.**

Présidence de l'université  
40 rue de rennes – BP 73532  
49035 Angers cedex  
Tél. 02 41 96 23 23 | Fax 02 41 96 23 00





**PART 1.**      **Glioblastoma management**





## General Introduction

---

The main objective of this thesis was to develop a new oncologic strategy, based on the integration of nanovectorized radiotherapy, with radiolabeled dendrimers, and intratumoral injection, via convection enhanced delivery, for the theranostics of glioblastomas. In the first part of this manuscript the general characteristics of glioblastoma will be introduced, while exposing the urgent need to find new diagnosis and treatment regimens for the improvement of this brain cancer prognosis. It will be continued with the currently used diagnosis modalities in clinical settings, focusing on the magnetic resonance imaging (MRI), which is considered at this time as the gold standard for the diagnosis and follow up of the glioblastoma. MRI parameters, important for the second part of this thesis, are going to be explained shortly, continuing with the preparation of contrast agents used for MRI, such as diethylenetriaminepentaacetic acid (DTPA) and 1,4,7,10-tetraazacyclododecane-1,4,7,10-tetraacetic acid (DOTA) derivatives for MRI enhancement.

It is known that in order to increase the relaxation rate of bulk solvent the paramagnetic ion should (1) efficiently relax the water that comes into contact with it, and (2) the relaxed water should exchange rapidly with the bulk water, to be able to transmit the relaxation effect to it. For fast tumbling complexes, such as Gd-DTPA, it is relaxation of the bound water that is the rate limiting process. On the other hand, slower tumbling will result in a more efficient relaxation mechanism of the bound water. For most biological targets of interest for imaging, multiple gadolinium ions are required to provide the necessary relaxation rate change. However, linking complexes in a linear fashion gives an oligomer, where rotation about the short axis of the molecule is fast and limits relaxivity. Since relaxivity is so dependent on molecular motion, the rotational dynamics of the final molecule are critical. The architectural characteristics of the dendrimers

## General Introduction

---

comprised of gadolinium complexes impose a more isotropic rotational dynamic, resulting in a better translation of the effect of the high molecular weight in the increase of the relaxivity.

Following the presentation of the most important methods used nowadays in clinics for the diagnosis and follow up of glioblastoma, new modalities in locoregional therapy, for a localized irradiation to glioblastoma tumor cells will be introduced. The introduction part of this thesis will be concluded after paying special attention to the localized internal radiotherapy for glioblastoma treatment, including the used radionuclides, innovative vectors and their characteristics. The reason why dendrimers were our nanovector of choice as a multifunctional platform, to be dual labeled with Gd for MRI and  $^{188}\text{Re}$  for glioblastoma treatment, is discussed when assessing the role of dendrimers in biomedical applications and in our review on the use of dendrimers in cancer radionanotherapy.

## **PART 1. Glioblastoma management**

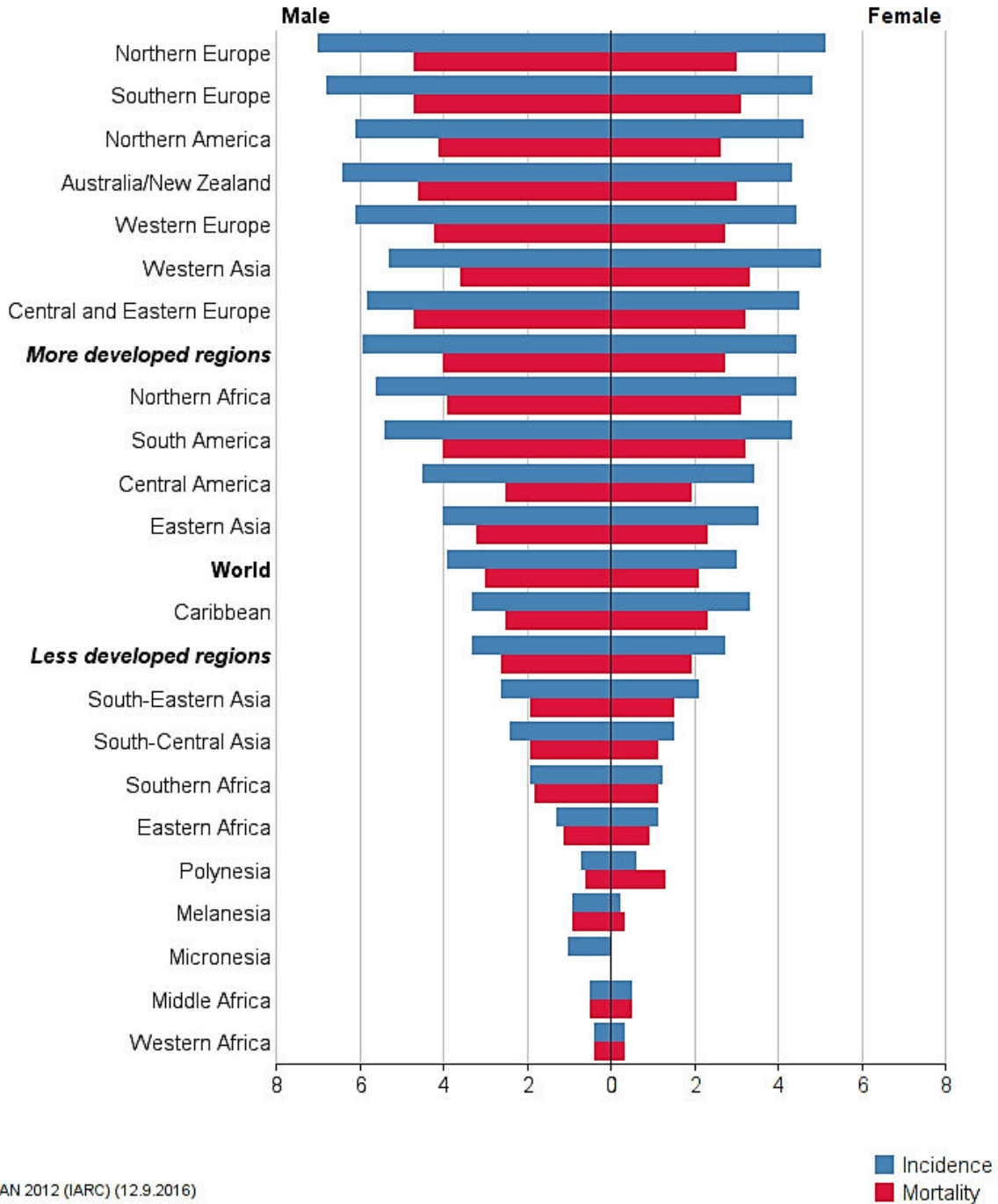
Gliomas are the most common primary intracranial tumor, representing 81% of malignant brain tumors. Glioblastoma, the most occurring glioma histology (45% of all gliomas), has a 5-year relative survival of less than 5%. It develops from star-shaped glial cells (astrocytes and oligodendrocytes) that support the health of the nerve cells within the brain. These are the most invasive type of glial tumors, rapidly growing and commonly spreading into nearby brain tissue. Incidence rates for brain and other central nervous system (CNS) cancer are highest in Northern Europe and lowest in Western Africa (Figure 1.1), with the highest world age-standardized incidence rates in Albania for men and Sweden for women (2012).<sup>1</sup>

For the first time in 2016, the World Health Organization (WHO) Classification of Tumors of the CNS introduced molecular parameters in addition to histology to diagnose many tumor entities.<sup>2</sup> This new classification from a pathogenetic point of view is based on both phenotype and genotype; from a prognostic point of view, it groups tumors with similar prognostic markers; and from the patient management point of view, it guides the use of therapies (conventional or targeted) for biologically and genetically similar entities (Figure 1.2).

Most notably, while in the past all astrocytic tumors had been grouped together, now all diffusely infiltrating gliomas (whether astrocytic or oligodendroglial) are grouped together: based not only on their growth pattern and behaviors, but also more pointedly on the shared genetic driver

# General Introduction

mutations in the *IDH1* and *IDH2* genes. This is aimed to facilitate clinical, experimental and epidemiological studies that will lead to improvements in the lives of patients with brain tumors.



GLOBOCAN 2012 (IARC) (12.9.2016)

**Figure 1.1** Brain, nervous system tumors: ASR (World) per 100 000 (all ages). Reprinted with permission from reference 1. Copyright: International Agency for Research on Cancer (IARC), 2016.

# General Introduction

In this new classification, glioblastomas are divided into (1) glioblastoma, IDH-wildtype (about 90% of cases), which corresponds most frequently with the clinically defined primary or *de novo* glioblastoma and predominates in patients over 55 years of age<sup>3</sup>; (2) glioblastoma, IDH-mutant (about 10% of cases), which corresponds closely to so-called secondary glioblastoma with a history of prior lower grade diffuse glioma and preferentially arises in younger patients<sup>3</sup> and (3) glioblastoma, a diagnosis that is reserved for those tumors for which full IDH evaluation cannot be performed.

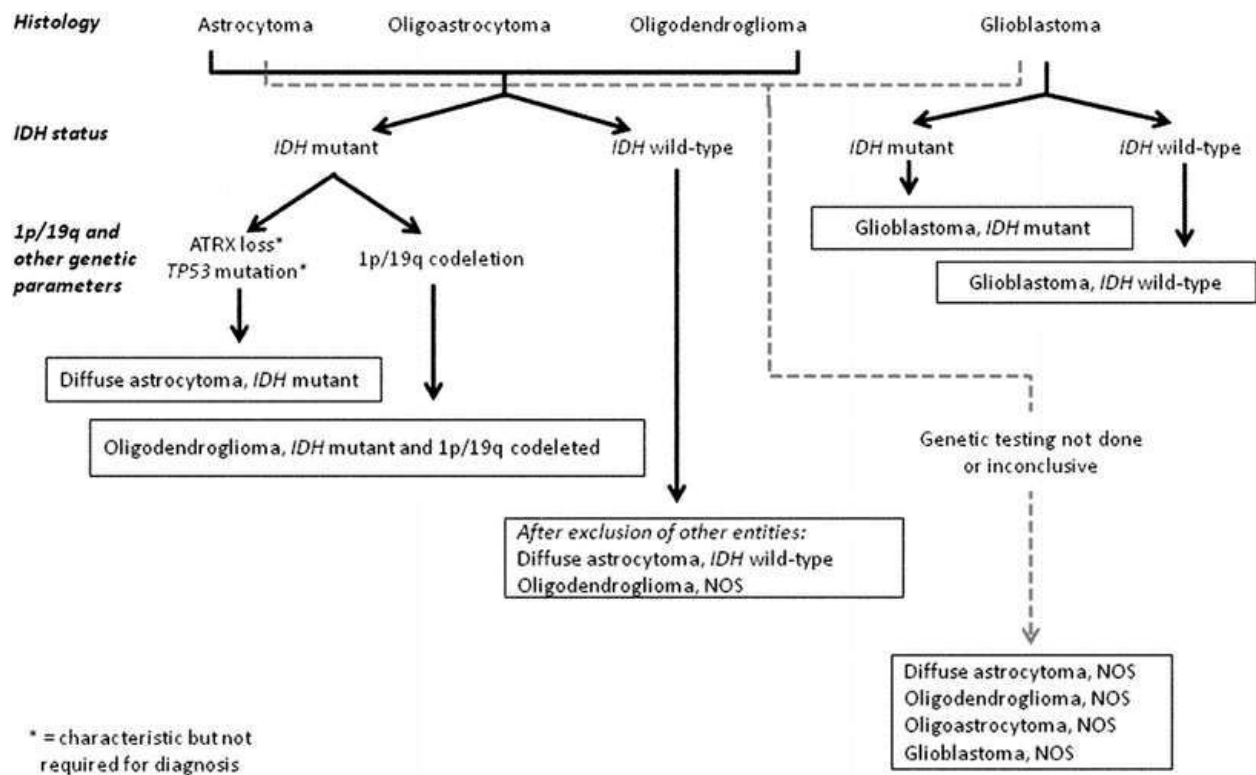


**Figure 1.2** A simplified algorithm for classification of the diffuse gliomas based on histological and genetic features. Reprinted with permission from reference 2.

## General Introduction

The tumor corresponds to WHO Grade IV, and it is composed of three zones: central necrosis, proliferation and infiltration zones (Figure 1.3a). Proliferation region is characterized by hypercellularity, nuclear polymorphism, brisk mitotic activity, prominent microvascular proliferation, and/or necrosis (Figure 1.3b and c).<sup>4-5</sup> Circumscribed necrosis and angiogenesis are the absolute features of glioblastoma and their occurrence is needed for its recognition, because they are direct signs of malignancy. Infiltration zone represents the invasion into the brain of tumor cells that acquire a particular phenotypic and molecular signature. It is not uniform along the tumor borders and often it is so mild that it is hardly detectable, also histologically.<sup>6</sup>

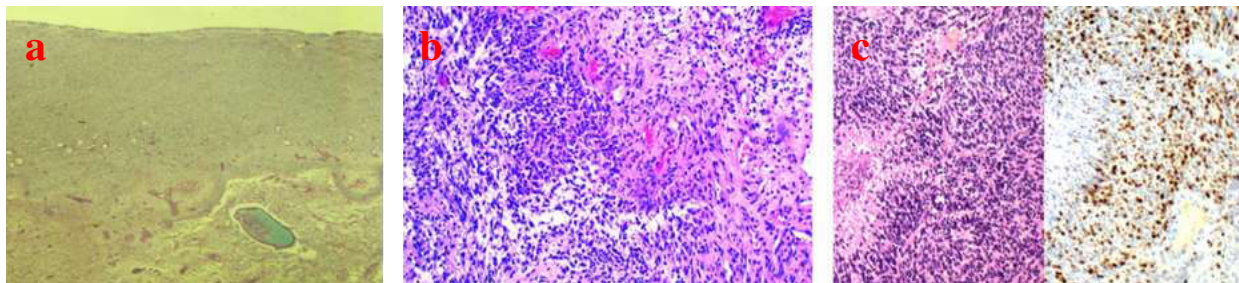


**Figure 1.3** Histologic characteristics of glioblastoma tumors. (a) Three zones can be recognized: central necrosis, proliferation, and infiltration zone. H&E, 25x; (b) Area of disruption with high cell density, vessels of different size and edema dissociation of the tissue; (c) Circumscribed necrosis with pseudo-palisading in an area with high cell density (H&E, 100x) and area with a high Ki-67/MIB.1 proliferation index (DAB, 100x). Reprinted with permission from reference 6.

The most conclusive prognostic factors for glioblastoma are extent of tumor resection, age at diagnosis, and Karnofsky performance status, which allows patients to be classified as to their functional impairment.<sup>7</sup> Age is significantly associated with survival after diagnosis for all glioma, but the effect is most pronounced for glioblastoma.<sup>8</sup> In general, gliomas with an oligodendroglial component have increased survival, as opposed to those with an astrocytic component.<sup>7-9</sup> The complex character of this tumor is one of the main reasons of the resistance of glioblastoma to

therapeutic intervention. Glioblastoma treatment challenges can be summarized as due to the following characteristics:

- Localization of tumors in the brain;
- Inherent resistance to conventional therapy;
- Limited capacity of the brain to repair itself;
- Migration of malignant cells into adjacent brain tissue;
- The variably disrupted tumor blood supply which inhibits effective drug delivery;
- Tumor capillary leakage, resulting in an accumulation of fluid around the tumor; (peritumoral edema) and intracranial hypertension;
- A limited response to therapy;
- The resultant neurotoxicity of treatments directed at gliomas.

Despite new diagnostic and treatment opportunities such as magnetic resonance imaging (MRI), microneurosurgery, neuronavigation, and the development and testing of various cytotoxic agents this cancer remains incurable.

## **1.1. Diagnosis modalities of glioblastoma (PET, SPECT, CT, MRI)**

Neuroimaging has become invaluable in the management of glioblastoma. Routine diagnosis of glioblastoma critically relies on MRI, owing to the variety of soft tissue contrasts available and its ability to provide morphological, physiological and metabolic information about the tumor. MRI is used at all stages of glioma management, from the detection and localization of the tumor to the planning of neurosurgery and radiotherapy, followed by the assessment of treatment efficacy.

## General Introduction

---

Positron emission tomography (PET) and Single Photon Emission Tomography (SPECT) can complement MRI by providing access to molecular targets with high sensitivity. Both SPECT and PET give information based on the spatial concentration of injected radiopharmaceuticals. PET uses short-lived positron-emitting radiotracers, which can be replace an atom or a molecule of a biological subtrat, enzyme or other biological active compounds (e.g. with  $^{11}\text{C}$ ,  $^{18}\text{F}$ ), or linked with them via a radioligand (e.g. with  $^{68}\text{Ga}$ ). These radiopharmaceuticals allow to evaluate with PET imaging of proliferation and metabolic activity, to assess differential diagnosis,<sup>10-11</sup> biological tumor volume, intratumoral heterogeneity<sup>12</sup> and to monitor therapy.<sup>12-13</sup> SPECT uses gamma emitting radionuclides.<sup>14</sup>

PET can utilize biochemically active molecules<sup>15</sup> radiolog of [ $^{18}\text{F}$ ]fluoro-2-deoxy-2-glucose (FDG), and amino acids as radiotracers. It is well known that the transport of amino acids and subsequent protein synthesis is upregulated in many tumor types. Thus, labelled amino acids, such as  $^{11}\text{C}$ -methionine ( $^{11}\text{C}$ -MET),  $^{18}\text{F}$ -fluor-ethyl-tyrosine ( $^{18}\text{F}$ FET) are the most commonly applied for the imaging of gliomas.  $^{11}\text{C}$ -MET and  $^{18}\text{F}$ FET are superior for the detection of gliomas even in the regions of infiltrative tumor cells, not detectable by MRI.<sup>16</sup> They are more useful than  $^{18}\text{F}$ -FDG, which produces a high background signal in the brain (because of high glucose consumption) and has limited sensitivity in detecting brain tumors.<sup>17</sup> PET also allows the monitoring of tumor hypoxia, an important feature of high grade gliomas.

Similar to PET tracers, most SPECT tracers are metabolism substrates that are labeled with radionuclides. The simple preparation make SPECT more attractive than PET, the most used radionuclides in SPECT ( $^{99\text{m}}\text{Tc}$ ), which restricts the compounds, which can be labeled with these nuclides. Four nuclides are used currently in SPECT imaging: thallium-201 ( $^{201}\text{Tl}$ ), technetium-

## General Introduction

---

$^{99m}\text{Tc}$ ), iodine-123 ( $^{123}\text{I}$ ), and indium-111 ( $^{111}\text{In}$ ).<sup>15, 18</sup> Several radioisotope-labeled compounds including  $^{201}\text{Tl}$ , technetium-99m-hexakis-2-methoxyisobutyl isonitrile ( $^{99m}\text{Tc}$ -MIBI), and 3- $^{123}\text{I}$ iodo- $\alpha$ -methyl-L-tyrosine (IMT) have been developed and utilized for glioma imaging.<sup>13, 19</sup> The poor targeting and specificity of these chelates prohibit their widespread use. Mainly due to its limited availability and associated costs, metabolic imaging has not yet been routinely implemented into a current standard of care algorithm for glioblastoma patients.

Computed tomography (CT) often provides the anatomical context in PET and SPECT studies, but can also be used to detect tumors (after injection of contrast) and in perfusion studies. However, CT may cause small tumors to be missed and may not depict all multifocal lesions.

Given the poor prognosis of patients with glioblastoma the overall clinical utility of SPECT and PET is mostly suited to the evaluation of treatment response in experimental protocols designed to improve the patients' outcome.<sup>13</sup> Functional images can provide additional information, useful to determine the degree of malignancy and as a guide for biopsy, by locating tumor hot spots. Ultimately, tissue samples are needed for definite histological diagnosis.

Table 1.1. provides an overview of some of the most important features of the different modalities used for the imaging of gliomas.<sup>20</sup>

## General Introduction

**Table 1.1. Features of modalities used for glioma imaging.**

Modality	Key features
MRI	<p>Based on the magnetic properties of hydrogen nuclei placed in a high magnetic field (non-ionizing radiations)</p> <p>Versatile modality with wide variety of soft tissue contrasts available</p> <p>High spatial resolution (0.2–1 mm) and fair sensitivity (<math>10^{-3}</math>–<math>10^{-5}</math> mol/L)</p> <p>Provide anatomical, functional and metabolic information</p>
PET	<p>Nuclear imaging technique that uses positron emitting radionuclides with fluorine-18 (110 min)</p> <p>High sensitivity (<math>10^{-11}</math>–<math>10^{-12}</math> mol/L) and limited spatial resolution (5–10 mm)</p> <p>Production of radiolabeled isotopes is expensive and requires the proximity of a cyclotron</p> <p>Molecular imaging of targets such as receptors, enzymes or protein sites</p> <p>Biodistribution of tracers may depend on blood–brain barrier, trapping of enzyme substrates, cell surface internalization, protein binding and metabolism</p>
SPECT	<p>Nuclear imaging technique that uses the direct gamma radiations emitted by radioisotopes such as technetium-99 m (6 h) or iodine-123 (13 h)</p> <p>Well established, widely available and cheaper than PET</p> <p>Good sensitivity (<math>10^{-10}</math>–<math>10^{-11}</math> mol/l) and limited spatial resolution (7–15 mm)</p> <p>Simultaneously image several radionuclides (differentiated by their energy)</p>
CT	<p>Fast, effective and high resolution technique based on X-ray attenuation in tissues</p> <p>Often used to provide the anatomical context in PET or SPECT studies</p>

### **MRI, in diagnostic imaging of glioblastoma**

MRI is used at all stages of glioblastoma management, from the detection and localization of the tumor, to the planning of neurosurgery and radiotherapy and the assessment of treatment efficacy.<sup>21</sup> Even though MRI scans for glioblastoma diagnosis frequently visualize mass lesions that enhance with contrast in  $T_1$ -weighted sequences, accompanied by perifocal edema as being depicted on  $T_2$ -/fluid-attenuated inversion recovery-weighted images, the neoplastic cells extend far beyond the area of enhancement. A typical result of “gross total resection” of a temporal lobe of glioblastoma, followed 6 months later by recurrence at the surgical margin and elsewhere, is shown in Figure 1.4.<sup>22</sup>

MRI technique is based on the principles of nuclear magnetic resonance (NMR), and takes advantage of the tissue contrast generated from the NMR signals received from hydrogen nuclei of water molecules located in different physiological environments throughout an organism.<sup>21</sup> MRI has excellent soft-tissue specificity, and can be used to identify many types of lesions in the brain and spinal cord.

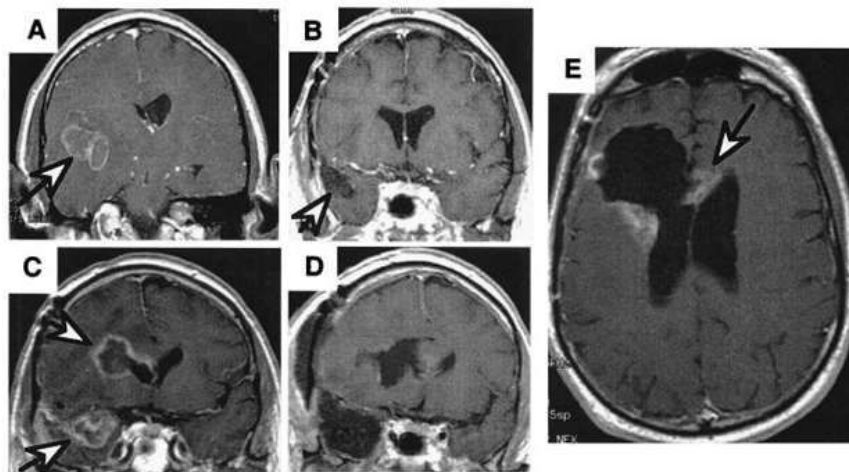


**Figure 1.4** MRI scans of a patient with a right temporal glioblastoma illustrating the spread of the disease. (A) Pre-surgical scan, GBM (arrow) is surrounded with edema. (B) Scan after surgery and radiation therapy showing “gross total resection” and clear resection cavity, and (C) six months later, showing recurrence not only at the resection margin (arrow) but a second focus of GBM across the Sylvian fissure in the frontal lobe (arrow). (D) Postresection scans of both recurrent tumors. (E) Scan 3 months later, showing the tumor recurring at the resection margin and crossing the corpus callosum to the other hemisphere (arrow). Copyright© 2000, the National Academy of Sciences.

The predominant factors that influence the amount of signal and contrast are the longitudinal relaxation time ( $T_1$ ), transverse relaxation time ( $T_2$ ) and spin density ( $\rho$ ) of the different area.. The patients are often injected with a contrast agent such as gadolinium (Gd) chelates, which alter the  $T_1$  and/or  $T_2$  of the water protons in the vicinity of the agent and, thus, help to improve image contrast (bright/dark) for diagnosis.<sup>21</sup>

MRI is a non-invasive diagnostic technique based on computer-assisted imaging of the relaxation signals of nuclei spins following their excitation by radiofrequency (RF) waves in a strong magnetic field.<sup>23</sup> The proton ( $^1\text{H}$ ) has been the most studied nuclei due to its high gyromagnetic ratio and abundance in biological tissue, particularly in the human body. Placed inside a magnetic field, all nuclei spins are aligned, more in the same direction of the magnetic field, with a precession movement depending on the gyromagnetic moment of the spin. This

## General Introduction

---

precessional frequency, known as the Larmor frequency, depending to the magnetic field level ( $B_0$ ) and the gyromagnetic ratio of the proton spin, is calculated from the equation:  $\nu_0 = (\gamma/2\pi)B_0$ , where:  $\nu_0$  is the Larmor frequency in MHz,  $\gamma$  is the gyromagnetic ratio in MHz/Tesla and  $B_0$  is the strength of the static magnetic field in Tesla.<sup>24</sup> The majority of contrast agents available at present belong to the class of  $T_1$  materials, and are essentially based on metal ions such as  $Gd^{3+}$  and  $Mn^{2+}$  or  $Mn^{3+}$  bound to chelating ligands with a labile site for coordination of water molecules.

### **$T_1/T_2$ relaxation times and $T_1/T_2$ mapping**

Spin-lattice (longitudinal) or  $T_1$  relaxation is the process by which the longitudinal magnetization recovers after the RF pulse, which has been traditionally associated to the enthalpic interaction of the excited nucleus with its environment (the lattice), and in particular with the magnetic active agents of this environment ( $^1H$  protons, unpaired electrons  $e^-$ ). The longitudinal relaxation time  $T_1$  is characteristic of the return to equilibrium of the magnetization along the z direction. It corresponds to the time required for the system to return to 63% of its equilibrium value, after it has been exposed to a  $90^\circ$  RF pulse. In most situations  $T_1$  relaxation is optimal if the average rate of molecular reorientation in space is at the Larmor precession frequency. In mobile liquids near room temperature the average rates of molecular rotation are several orders of magnitude higher than  $\nu_0$ , leading to very inefficient relaxation (long  $T_1$ ). For larger molecules and more viscous solutions molecular motions become slower and  $T_1$  shortens. However, at some point the average molecular motions become slower than  $\nu_0$ , and  $T_1$  becomes longer again (Figure 1.5).<sup>25</sup>

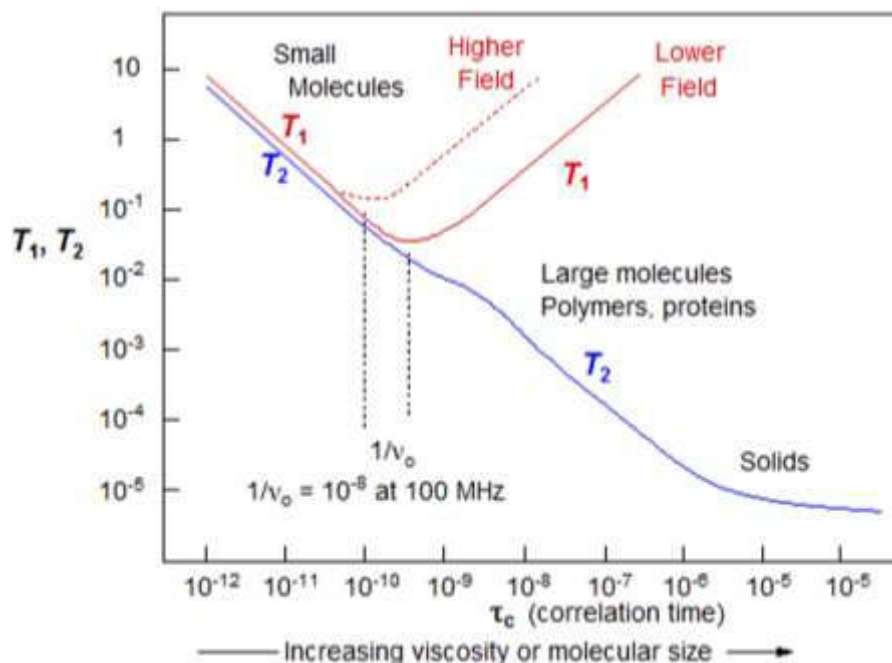


**Figure 1.5** Behavior of  $T_1$  and  $T_2$  as a function of correlation time.<sup>25</sup>

Spin-spin (transverse) or  $T_2$  relaxation is the process by which the transverse magnetization decays due to dephasing of proton spins. The contribution of all the spins precessing around the external magnetic field  $B_0$  produces a net magnetization  $M_0$ . After a  $90^\circ$  RF pulse is applied, the magnetization flips at the same angle from the longitudinal axis to the xy-plane (Figure 1.6). Dephasing of the spins is an entropy phenomenon that results in a quick exponential decrease of the net magnetization in the xy plane.  $T_2$  is caused by transient magnetic fields at any frequency. Thus  $T_2$  keeps getting shorter as molecular reorientation rates slowdown, as shown in Figure 1.5. Different scan sequences show up differences in these relaxation times generating what are referred to as  $T_1$ ,  $T_2$  or proton density (the concentration of protons) weighted images.

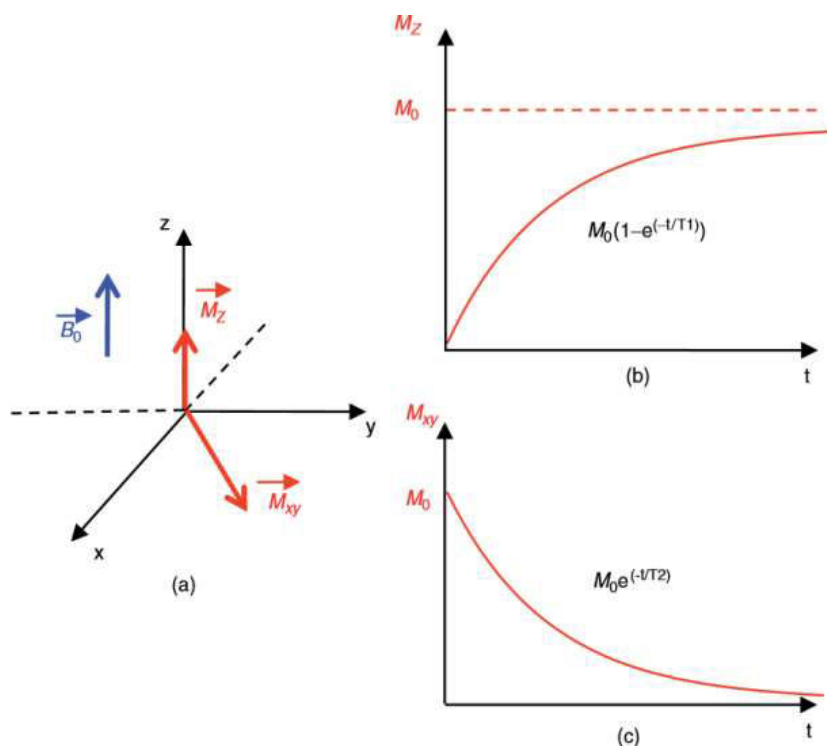


**Figure 1.6** (a) Return to equilibrium of the magnetization, (b) return to equilibrium on the z axis: ( $M_z = M_0 \times [1 - e^{-t/T_1}]$ ), (c) return to equilibrium in the xy plane ( $M_y = M_0 \times e^{-t/T_2}$ ).<sup>25</sup>

The high-resolution rapid computation and the intensity consistency provided by modern  $T_1$  mapping renders it a new and straightforward candidate data type in MRI.<sup>26</sup>  $T_1$  maps are quantitative images of  $T_1$  relaxation times. The image intensity of a parametric image is known to be proportional to the  $T_1$  relaxation times and it can give a quick view of how these values differ across an image. Since  $T_1$  maps are parametric images of pure  $T_1$ , they are expected to contain reduced bias and other distortions, compared with conventional  $T_1$ -weighted ( $T_1W$ ) images, and are believed to improve the performance of segmentation.<sup>27</sup>

For commonly used  $T_1W$  imaging, the accumulation of paramagnetic contrast agent is associated with local changes in signal intensity. However, signal intensity is an indirect and qualitative measure of concentration, because it is influenced by several other factors, such as coil

sensitivities, gain calibration, sequence timing parameters and fluctuations in electrocardiogram or respiratory triggering intervals.

While  $T_1$  maps are not immune to artifacts, they are measurements of a physical property, and so are comparable across subjects and scanners. This stability of the intensity profile reduces the complexity of registration and segmentation and may provide information about complex changes in tissue composition.<sup>28-29</sup> New segmentation frameworks either directly take  $T_1$  maps as input<sup>28</sup> or combine them with  $T_1$ -weighted images in multi-channel image segmentation.<sup>29</sup>

An important question is whether the *in vivo* MRI contrast change can be quantitatively related to local contrast agent concentration in the tissue. In case of paramagnetic nanoparticles, robust  $T_1$  mapping techniques are needed to address this issue.<sup>30</sup> The group of Gustav<sup>31</sup> found that regional elevations in longitudinal relaxation rates  $R_1$  ( $R_1=1/T_1$ ) following injection of paramagnetic liposomes in a mouse model of myocardial infarction, correlated well with local Gd-concentrations as determined by Inductively Coupled Plasma-Mass Spectrometry (ICP-MS).

$T_2$  parametric maps are generated on the basis of a similar principle of  $T_1$  mapping, where a series of images are obtained to calculate a  $T_2$  decay curve.  $T_2$  mapping techniques have not yet received the same focus as  $T_1$  mapping.<sup>32</sup> A comparison of diagnostic efficacy between the two techniques will be better served in future investigations.

### **Spin/gradient echo ( $T_1/T_2$ weighting) and inversion recovery sequences**

There are two principle types of pulse sequence, called spin echo (SE) and gradient echo (GE). SE sequences use two RF pulses to create the echo, which measures the signal intensity and produce  $T_1$ -,  $T_2$ -, or proton density ( $\rho$ ) weighted images depending on the choice of TR and TE.

## General Introduction

---

SE sequences generally produce the best quality images but they take a relatively long time, several minutes rather than seconds. GE sequences use a single RF pulse followed by a gradient pulse to create the echo, which also measures the signal intensity and produce images with  $T_1$ -,  $T_2$ - or  $\rho$  weighting. Generally, these sequences have much shorter TRs than SE, resulting in shorter scan times. However, they are influenced to an extent by the inhomogeneity of the main magnetic field and timing parameters.<sup>33</sup>

$T_1W$  imaging is one of the basic pulse sequences in MRI and demonstrates differences in the  $T_1$  relaxation times of tissues. The  $T_1$  of a tissue reflects the amount of time needed for its protons' spins to realign with the main magnetic field ( $B_0$ ), and to get back to equilibrium.  $T_1$  weighting tends to have short TE and TR times, to minimize  $T_2$  relaxations effect. If  $T_1W$  images did not have short TR's, then all the protons would recover their alignment with the main magnetic field and the image would be uniformly intense. Selecting a TR shorter than the tissues' recovery time allows one to differentiate them. Tissues with high fat content quickly realign their longitudinal magnetization with  $B_0$ , and therefore appear to be bright on a  $T_1$  weighted image. Conversely, compartments filled with water have much slower longitudinal magnetization realignment after an RF pulse, and therefore less transverse magnetization. Thus, water has low signal and appears as dark. This is useful to demonstrate anatomy.  $T_1W$  sequences provide the best contrast for paramagnetic contrast agents.

$T_2W$  imaging is useful to differentiate anatomical structures mainly on the basis of  $T_2$  values. The scanning parameters are set as long TR/long TE to minimize  $T_1$  relaxation effects. If the TE is extended out over a very long time, only tissues with a very long  $T_2$  relaxation time will retain signal. Compartments filled with water appear bright and tissues with high fat content appear dark.

## General Introduction

---

This is useful for demonstrating pathology since most lesions/tumors are associated with an increase in water content. Paramagnetic contrast agents (e.g. gadolinium (Gd) containing compounds) do not cause the same bright tissue contrast as they do on  $T_1W$  imaging. Gd shortens  $T_2$  relaxation time and actually results in hypointense signal.

The traditional inversion recovery (IR) pulse sequence is a variation of the spin echo sequence. It is a spin echo sequence with an additional  $180^\circ$  pulse, usually slice-selective, which is applied prior to the initial excitation pulse. IR pulse sequences are used to give heavy  $T_1$ -weighting. The inversion time (TI) is a user-selectable delay time between the  $180^\circ$  pulse and the excitation pulse and determines the amount of  $T_1$  relaxation that occurs between the two pulses. The inversion pulse also allows for the suppression of signals through the proper choice of TI. If the TI time is chosen so that the tissue of interest has no longitudinal component at the time of the excitation pulse, then that tissue contributes no signal to the final image. The two most common applications of IR sequences are for the suppression of cerebrospinal fluid (CSF) and fat.

### **Tissue characterization with and without injection of Gd CA**

MRI signal intensity is expressed in gray levels: a high intensity signal appears in white and a weak intensity signal in black or dark gray. An MRI is obtained by contrasts between different biological tissues. The contrast-to-noise ratio is chosen by the MRI user who can modify the sequence parameters (TR: Repetition Time, TE: Echo Time, flip angle, FOV: Field Of View, etc.) in order to obtain the desired contrast between tissues. The choice of the MRI parameters allows the image contrast to be varied according to the values of their intrinsic physical parameters. If  $T_1$  or  $T_2$  are selected as parameters, then the MR image is defined as  $T_1$ , or  $T_2$  weighted. The contrasts

## General Introduction

---

are defined by the choice of TR and TE, taking into account the repetition of the basic sequence. The transverse magnetization is the maximum at a short TE. The rate at which each tissue recovers its longitudinal magnetization depends on its  $T_1$  value.

The efficacy of contrast agents with regard to their application in MRI is defined by their relaxivity. This property describes the ability of a 1 mM solution of CA to enhance the relaxation rate of solvent nuclei in close vicinity of the paramagnetic entity, which increases signal intensity in a magnetic resonance image. The effect of the contrast agent on the signal intensity can either be positive (increase in signal or  $T_1$ -enhancement) or negative (signal reduction or  $T_2$ -enhancement). Almost all MR contrast agents will affect both  $T_1$ - and  $T_2$ - relaxation times and the distinction between them will depend on many MR-specific parameters as well as contrast agent dose. The most widely used class of MRI contrast agents is based on the mechanism of longitudinal relaxation ( $T_1$ ).<sup>34-36</sup> It is usually the motion of the neighboring  $^1\text{H}$  protons which creates an oscillating magnetic field that stimulates a return to equilibrium of the  $\text{H}_2\text{O}$  protons. If molecules containing unpaired electrons ( $e^-$ ) are introduced into the  $\text{H}_2\text{O}$  molecule environment, they will trigger the return to equilibrium of the  $\text{H}_2\text{O}$  protons much more effectively, because the magnetic moment of the electron is 658 times stronger than that of the proton.

Lanthanides contain unpaired electrons, including Gd that contains seven unpaired electrons. Although Gd is very effective, it is always used as a very stable chelate, to prevent toxicity issues. Gd complexes reduce the value of neighboring water hydrogens  $T_1$  (and  $T_2$ ), generating a reduction in signal intensity (line broadening) in an acquisition. Taking into consideration that the production of an image requires the accumulation of many acquisitions for a sufficient signal to noise ratio (SNR), the Gd contrast agent shorten the time of return to equilibrium of the magnetization (z

## General Introduction

---

axis). This results in a shorter TR, offering the opportunity for more accumulations per unit time (several TRs), and therefore recording more signal per unit time for spins with reduced  $T_1$ .

The presence of the contrast agent Gd in a particular location of a living tissue will result in a stronger signal (positive enhancement) in this region of the image. For example, in normal tissue, the “large” Gd chelate cannot cross the blood–brain barrier; by contrast, in certain tumors the vascularization is higher than the surrounding tissues and the blood brain barrier is locally porous, so Gd chelate can penetrate the tumor that appears hyperintense on the corresponding MRI, as shown in the Figure 1.7.

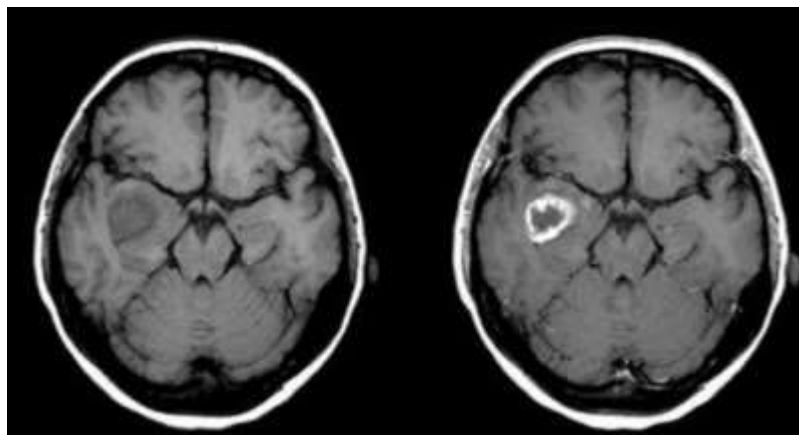


**Figure 1.7** Gd contrast agent was selectively taken up in the tumor region due to pathological changes in the BBB, whereas an intact BBB prevented contrast agent accumulation in unaffected brain tissue. Adapted from ref. <sup>37</sup>.

Preparation of lanthanide complexes is mostly simple. The formation kinetic of the complexes differs for two main ligand families, the open-chain ligands (DTPA derivatives) and macrocycles (DOTA derivatives). The open-chain ligands form complexes at room temperature immediately once pH is in the appropriate range. Generally, a careful control of solution pH is very important and the base should be added very slowly to avoid precipitation of uncomplexed

## General Introduction

---

ions as hydroxides during the reaction course. The most common reaction pH range is 5–7 and should be kept unchanged during the complexation reaction. The labeling reaction is commonly done in water, using lanthanide (III) salts of non-complexing anions. Ligands are mostly polyvalent acids, which must be at least partially, deprotonated to form the complexes. The metal ions and ligands can be reacted in the equimolar amounts or in an excess of the metal ion or ligand. A slight ligand excess is used to ensure a complete binding of the metal ion.<sup>38</sup> If excess of metal ion is present, it must be removed. The simplest way is raising the pH above 8 leading to precipitation of the excessive metal ion as metal hydroxide, which is removed by filtration (e.g., through syringe filters) or by centrifugation.<sup>39</sup>

### Relaxivity of Gd CA

The aim of using a contrast agent in MRI is to accelerate the relaxation of water protons in the surrounding tissue. Nowadays, Gd complexes are far the most widely used MRI contrast agents in the clinical practice. The choice of Gd is explained by its seven unpaired electrons which makes it the most paramagnetic stable metal ion. Gd complexes induce an increase of both the longitudinal and transverse relaxation rates,  $R_1=1/T_1$  and  $R_2=1/T_2$  respectively, of the solvent nuclei. The observed solvent relaxation rate,  $1/T_{i,obs}$ , is the sum of the diamagnetic ( $1/T_{i,d}$ ) and paramagnetic ( $1/T_{i,p}$ ) relaxation rates. The diamagnetic term,  $1/T_{i,d}$ , corresponds to the relaxation rate of the solvent (water) nuclei in the absence of a paramagnetic solute. The paramagnetic term,  $1/T_{i,p}$ , gives the relaxation rate enhancement caused by the paramagnetic substance which is linearly proportional to the concentration of the paramagnetic species, [Gd]:

$$\frac{1}{T_{i,obs}} = \frac{1}{T_{i,d}} + r_i [Gd], \text{ where } i = 1, 2$$

In the above equation for nondilute systems the linear relationship is valid only if the concentration is given in millimoles per kilogram solvent (mmol/kg; millimolality). According to this equation, a plot of the observed relaxation rates versus the concentration of the paramagnetic species gives a straight line and its slope defines the relaxivity,  $r_i$  ( $r_i=1/T_{i,p}$ , in units of  $\text{mM}^{-1}\text{s}^{-1}$ ). If we consider the relaxation of water protons, which is the basis of imaging by MRI, the corresponding term proton relaxivity can be introduced. Proton relaxivity directly refers to the efficiency of a paramagnetic substance to enhance the relaxation rate of water protons, and thus to its efficiency to act as a contrast agent. It has to be noted that the simple term “relaxivity” is often used in the context of MRI contrast agents and refers to “longitudinal proton relaxivity enhancement”.

### **Dendrimer-based Gd CA and their effect on proton/water exchange**

For the molecular MRI, a main challenge for the  $T_1$  agents is represented by low accumulation and sensitivity. This insufficient accumulation can be compensated by attaching multiple MRI labels to a single multivalent scaffold. One of the first reported dendrimer-contrast agent systems was based on PAMAM dendrimers functionalized with isothiolcyanobenzyl-DTPA ligands to be labeled with Gd.<sup>40</sup> This initial study directly compared PAMAM G2 and G6 dendrimers. The G6 dendrimer had 170 Gd sites per molecule and a very high ‘per Gd’ relaxivity of  $34 \text{ mM}^{-1} \text{ s}^{-1}$ , which was higher than that of G2 ( $r_1= 21.3 \text{ mM}^{-1} \text{ s}^{-1}$ ) at 0.6T. The authors later described that this difference was directly related to gains in rotational correlation time.<sup>41</sup> They

## General Introduction

---

demonstrated that the blood circulation half-lives ( $t_{1/2}$ ) depended on the molecular weight of the dendrimer used.

Another interesting feature is that differences in the dendrimer molecular shape, in aqueous solution, can affect their relaxivity properties. CA based on PPI dendrimers have higher relaxivity than the corresponding PAMAM dendrimers, and thus are more efficient.<sup>42</sup> The PPI dendrimers are more ellipsoid shaped than PAMAM dendrimers. This shape has been claimed to lead to a higher  $T_1$  relaxivity.<sup>42</sup> The first commercial dendrimer-based CA was Gadomer-17, which was developed by Schering AG. It is based on a polylysine core substituted with 24 Gd-DOTA groups at the surface and is presumably marketed as a contrast agent for dynamic contrast enhanced MRI applications.

The overall proton exchange rate in a neutral pH is generally equal to the exchange rate of the entire water molecules, meaning that each proton exchanges with the bulk in the form of intact H<sub>2</sub>O molecules. On increasing the acidity or basicity of the solution, the proton exchange may become considerably faster than the water exchange due to acid- or base-catalyzed pathways.<sup>43</sup> The exchange of coordinated water protons can occur in two ways: independently of the exchange of the entire water molecule on which it resides, or via the exchange of the water molecule itself. In any case, the water exchange rate represents a lower limit for the proton exchange rate. Since the water exchange rate on DOTA- and DTPA-type complexes is lower than the optimal values to attain maximum relaxivities, there has been a continuous effort to design novel ligands that ensure stable Gd complexes with accelerated water exchange.

The negative charge of the complex and an increased steric crowding around the water binding site were identified as the two main factors, contributing to the acceleration of the water

exchange. While increasing the negative charge on the complex is not always a viable route to optimize water exchange, the design of ligands ensuring steric compression has proved to be a successful strategy. The steric compression has been induced in DTPA- or DOTA-derivative complexes, either by the addition of a CH<sub>2</sub> group in the amine backbone of the ligand or in the carboxylate arm. The introduction of one six membered chelate ring in the complex, always increases the steric crowding. The steric crowding and the consequent acceleration of the water exchange is more important on the elongation of the amine backbone than on the elongation of the carboxylate pending arm (DTPA- DOTA-derivative complexes).

Obviously, rotation is slowed down to a smaller or higher extent when a monomer Gd chelate is attached to a macromolecule, but it is less straightforward to predict how the water exchange is affected. To confirm if the attachment of a macrocyclic unit to a large dendrimer molecule influenced the kinetics of water exchange on the Gd chelate, a pioneer study was done with three different generations of PAMAM dendrimers (G3-G5) functionalized with DO3A-monoamide Gd chelates, comparing them to the corresponding monomer chelate.<sup>44</sup> The water exchange rates of all the three generations of dendrimers were similar to that of the monomer chelate, demonstrating for the first time that the attachment of a macrocyclic unit to a large dendrimer molecule does not significantly influence the kinetics of water exchange on the Gd chelate. Similar results were obtained later on other dendrimer systems.<sup>45</sup>

However, reliable kinetic parameters can only be obtained for the proton exchange if the exchange of the entire water molecules is considerably slower than that of protons. For the Gd chelates used as MRI contrast agents, at physiological pH the proton exchange rate equals the water exchange rate. For small-molecular-weight Gd chelates, it is the rotational correlation time

## General Introduction

---

( $\tau_R$ ), that mainly determines the effective correlation time of proton relaxation. In other words, the fast rotation is the limiting factor for proton relaxivity at magnetic fields relevant to MRI. This fact led to a wide variety of approaches to slow down rotation by increasing the molecular weight of the complex. The Solomon-Bloembergen-Morgan (SBM) theory of paramagnetic relaxivity predicts that the relaxivity of a Gd complex with optimally fast water exchange rate can be drastically increased upon slowing its molecular tumbling. This general trend holds true for magnetic fields up to 3T, corresponding to proton Larmor frequencies of  $\sim 127$  MHz, but starts to decline at higher magnetic fields. For instance, as the SBM theory predicts, at proton Larmor frequencies above 200 MHz,  $r_1$  increases with the inverse rotational correlation time  $1/\tau_R$ , in contrast to lower frequencies where it is proportional to  $\tau_R$ .

The  $\tau_R$  values generally increase with increasing molecular weight, however, this relation is far from the linearity. While, the proton relaxivities attained by Gd chelates attached to dendrimers increased with molecular weight, they were lower than expected solely on the basis of the molecular weight. A part of the reason is that the linking group between the Gd chelate and the rigid dendrimer molecule has some flexibility and consequently the Gd chelate experiences a more rapid motion when compared to the rotation of the dendrimer as a whole. Since the molecules are not completely rigid, the motion which then determines proton relaxivity can be considerably faster than the motion of the whole molecule, which is itself related to the molecular weight. This phenomenon is particularly important for several types of macromolecular agents, either due to the general flexibility of the whole molecule or to the flexibility of the linking group that is used to attach the Gd chelate to the macromolecule.

## General Introduction

---

Amplifying the relaxivity via accumulation of a large number of Gd ions is particularly important in molecular imaging. Macromolecular conjugates of Gd chelates are widely investigated as MRI contrast agents. In addition to the potential increase in relaxivity due to their slower rotation, they have other advantages.

Dendrimers represent a unique class of synthetic polymers in the sense that, contrary to linear polymers, highly rigid and almost monodisperse systems can be produced. For their proton relaxivity a key issue besides the rapid water exchange, is the right choice of the linker group between the macromolecule and the Gd complex. This must be rigid enough so that the slow rotation of the rigid dendrimer molecule is transmitted to the surface chelate itself.

Among the numerous examples, PAMAM dendrimers of different generations have been loaded with DOTA<sup>46</sup> or DTPA type<sup>40</sup> chelates, most often using the p-NCS-benzyl functional group as linker. For these types of dendrimer-based Gd complexes the relaxivity was increasing with increasing generation before reaching a plateau for the high generation compounds. The relaxivity profiles showed the typical high field peak around 20 MHz which is characteristic of slow rotation. The decrease in temperature, resulted in lower relaxivities for the high generation dendrimers (G=5–10), because of the slow water exchange of bound water molecules. In such circumstances, further increases in the rotational correlation time of the macromolecules associated with higher generation of dendrimers did not result in significant improvement in proton relaxivity.

In a more recent study,<sup>47</sup> the *in vitro* and *in vivo* MRI properties of G4 PAMAM dendrimers, functionalized either with C-DOTA or 1B4M-DTPA ligands were compared at 3T. Though the *in vitro* relaxivity properties of these two agents were comparable, the shorter blood clearance

lifetime of the C-DOTA dendrimers, made them the superior choice in between both systems for *in vivo* applications after *iv* injection. The challenge is to achieve the best balance between stability of the complex and the rate of water exchange.

To conclude, the multivalent character of dendrimers has positioned these well-defined, highly branched macromolecules at the forefront in the development of new CAs for MRI. By modifying the periphery of the dendrimer with numerous Gd chelates, the relaxivity of the resulting MRI CAs is increased considerably, compared to low molecular weight Gd chelates. Furthermore, dendrimers demonstrate increased relaxivity as a result of slower particle tumbling rates in solution, which minimizes the total dose of Gd ions needed without compromising image quality, thus reducing risks of toxicity. Research in the field suggests that the flexibility of the macromolecule can also affect its relaxivity. The monodisperse character of dendrimers creates a unique opportunity to introduce dendritic MRI contrast agents into clinics.

### 1.2. Glioblastoma treatment

The standard of care for glioblastoma patients is surgical resection, with the goal of maximal tumor removal, followed by external beam radiotherapy (EBRT) and adjuvant temozolomide (TMZ), usually before radiation.<sup>48-50</sup> TMZ is an oral alkylating agent that leads to cells death by alkylation of the O6 position of guanine and subsequent disturbance of DNA replication.<sup>51</sup> However, the DNA repair protein O6-methylguanine-DNA-methyltransferase (MGMT), which is present in gliomas, has been reported to aid the resistance of tumor cells to alkylating agents, making TMZ not sufficient for therapy. Surgical complete tumor resection is yet impossible due to the infiltrative nature of malignant gliomas and recurrences are inevitable. Furthermore, the

## General Introduction

---

non-specific nature of EBRT often results in damage to adjacent areas of brain. Hence, administration of curative doses to tumor is limited because of the toxicity to normal brain, which reduces the quality of life for the few patients with significant survival prolongation.<sup>52-53</sup> Systemic chemotherapy is not a good treatment option either.<sup>54</sup> The failure of chemotherapy is mostly due to the BBB that prevents the penetration of drugs from the blood into the CNS, making the injection of chemotherapeutic agents intravenously ineffective.<sup>55-56</sup>

Moreover, systemic delivery of drugs capable of crossing the BBB can lead to significant toxicity. In view of the disadvantages of current therapies, delivery techniques which bypass the BBB and administer therapeutics directly within the tumor have been developed. The stereotactic radiosurgery (SRS) is one of these methods applied to bypass BBB and improve the prognosis of gliomas. A number of retrospective reports have demonstrated the effectiveness of SRS as salvage therapy for high grade glioma including glioblastoma.<sup>57-60</sup> SRS has been well tolerated in a series of patients, with only 5.5% incidence of treatment related necrosis.<sup>61</sup> Locoregional therapies are considered as promising approaches due to their ability to circumvent the BBB, minimize systemic toxicity, and their ability to deliver high dose of radiation to a focal target.<sup>62</sup> The first approved locoregional therapy for malignant gliomas was Gliadel<sup>®</sup>, a controlled release, biodegradable polymer releasing carmustine (BCNU). Results were encouraging but only demonstrate an increase in median survival up to 2-3 months.<sup>63</sup> This can be explained by the low chemosensitivity of glioma tumor cells and their high predisposition to be prone to multidrug resistance. Due to extensive research in the field, new modalities in locoregional therapy have been researched for a localized irradiation to glioma tumor cells. As such, the three most promising modalities in terms of locoregional internal targeted radiotherapy are radiolabeled peptide receptor therapies,

radioimmunotherapy (RIT) and radionuclide delivery systems.<sup>64</sup> To avoid the BBB, the administration technique for these three managements is often by stereotactic neurosurgery. Intra-compartmental injections seem to be more effective than systemic injections because there is more effective targeting to the tumor, with typical radiation-absorbed doses approximately tenfold the dose that is typically achieved with intravenous injection.

Indeed, five criteria are important for a successful internal radiotherapy using a radiolabeled vector:

1. High and frequent expression of tumor-associated markers as a specific target.
2. Availability of a high affinity targeting agents to reach all the distant sites of tumor cell infiltration.
3. Efficient radionuclide labeling of the targeting agent, without compromising its binding properties.
4. *In vivo* stability of the radio-conjugate yielding long residence time on targeted tumor cells.
5. The radionuclide has to specifically destroy tumor cells without irradiating adjacent normal brain areas.

Among all available radionuclides for radiolabeling, only few have been developed as radiopharmaceuticals up to date.<sup>65</sup> Three are the main reasons for this:

1. The availability of radionuclides with appropriate physical properties.
2. The interaction between the radionuclide and its biologic environment, i.e., the radiation biology of the decaying moiety.
3. The identification of nontoxic carrier molecules with which to target such radionuclides to tumors.

## General Introduction

---

In the case of the radionuclide, its mode of decay, including the nature of the particulate radiations and their energies, its physical half-life, and its chemistry in relation to the carrier molecule must be considered. Radionuclide half-life should correspond to pharmacokinetics of the carrier *in vivo*. This means that the half-life must be longer than the time required for the preparation of pharmaceutical, its delivery to clinic, injection, and localization in a tumor.<sup>66</sup> In the case of the carrier, its stability and immunogenicity must be defined. The production of carrier molecules ought to be reproducible, simple, cost effective and with sufficient chemical purity.<sup>65-66</sup> It is of critical importance to avoid release of the therapeutic radioisotopes from the conjugate into circulation to avoid bone marrow and other organ toxicity. The smaller the number of radioactive decays, needed to be sustained by the chelator, the lower the toxicity risk. The selection of the radionuclide with an appropriate half-life is the key factor to obtain this objective.<sup>67</sup>

Following the same approach, RIT exploits the immune protein as a carrier for radioactivity, as a tracer or as a targeted therapeutic. The radio-antibody is formulated as a drug in sterile and pyrogen-free form and is intravenously injected directly into the tumor or compartmentally into a body cavity such as the peritoneum, pleura or intrathecal space. Once injected, the radio-antibody is distributed by blood flow, diffusion or convection to its natural target: an antigen-binding site on tumor cells. The radioactive cargo, in the form of a radionuclide that emits therapeutic quantities of particulate radiation, delivers the tumoricidal dose to the tumor mass. The radiation effects are due to the enormous energy release that occurs during radioactive decay. Many Phase I-III clinical trials have supported the use of locoregional delivery for RIT with promising results in patients with brain tumors.<sup>68</sup>

### Radionuclides for the therapy of malignant gliomas

The most common radionuclides used for locoregional therapy of malignant gliomas are, yttrium-90 ( $^{90}\text{Y}$ ), iodine-131 ( $^{131}\text{I}$ ), iodine-125 ( $^{125}\text{I}$ ) and rhenium-188 ( $^{188}\text{Re}$ ), with  $^{131}\text{I}$  and  $^{90}\text{Y}$  used in more than 95% of clinical trials.<sup>66</sup> The main physical properties of these radionuclides are given in Table 1.2.  $^{131}\text{I}$  and  $^{90}\text{Y}$  represent the current standard to which all other radionuclides are compared.<sup>69-70</sup>  $^{131}\text{I}$  has a long successful history of treating several malignancies, is relatively inexpensive, and can be used for both imaging and therapy. However,  $^{131}\text{I}$ -labelled proteins degrade rapidly if internalized into tumor cells, resulting in the release of free  $^{131}\text{I}$  into the bloodstream.<sup>71-72</sup> In addition, the  $\gamma$ -rays emitted by  $^{131}\text{I}$  may pose a radiation risk to family members and healthcare personnel, therefore patient hospitalization for radiation isolation may be required if large doses are injected.  $^{90}\text{Y}$  is a reasonable alternative radionuclide for therapeutic studies, as it emits  $\beta$ -particles almost exclusively. Since, this form of radiation does not leave the patient's body, caregivers and family members are exposed to lower levels of radiation. The  $\beta$ -radiation emitted from  $^{90}\text{Y}$  is five-fold more energetic than that of  $^{131}\text{I}$ .  $^{90}\text{Y}$  in contrast with  $^{131}\text{I}$  is stably retained by tumor cells, even after internalization. For both  $^{131}\text{I}$  and  $^{90}\text{Y}$ , dose-limiting myelosuppression at conventional doses<sup>73-74</sup> and cardiopulmonary toxicities at high doses, may be observed.<sup>75-76</sup>

$^{188}\text{Re}$  is one of the most readily available generator derived and useful radionuclides for therapy emitting  $\beta^-$  particles (2.12 MeV, 71.1% and 1.965 MeV, 25.6%) and imageable gammas (155 keV, 15.1%). It is chemically similar to technetium and many biological results already obtained for the latter could be exploited. However, the reduction potential for  $^{188}\text{Re}$  is substantially larger and therefore a much greater quantity of reducing agent is required. Given that its chemical reactions

## General Introduction

are mostly redox,  $^{188}\text{Re}$  resolves as anion  $\text{ReO}_4^{-1}$ , resulting in rapid secretion from vital organs.<sup>77</sup> From a radio-biologic point of view, higher dose rates delivered over shorter treatment times are more effective than lower dose rates delivered over longer periods. Thus, a radionuclide with a shorter half-life will tend to be biologically more effective than one with a similar emission energy but longer half-life.<sup>65</sup>

**Table 1.2 General characteristic of therapeutic radionuclides used for malignant gliomas treatment.**<sup>78</sup>

Radionuclide	$t_{1/2}$ (h)	Energy of the main $\gamma$ emission (MeV) [Abundance (%)]	Mean energy of $\beta$ particles/ disintegration (MeV)	Max. energy of $\beta$ particles/ disintegration (MeV)	Mean $\beta$ particle range in soft tissue (mm)	Max. $\beta$ particle range in soft tissue (mm)
$^{188}\text{Re}$	16.9	0.155 [15]	0.764	2.12	3.1	10.4
$^{90}\text{Y}$	64.1	-	0.935	2.28	4	11.3
$^{131}\text{I}$	192	0.208 [6.1]	0.133	0.497	0.23	1.8
$^{125}\text{I}$	1425.6	0.0355 [6.7]	-	-	-	-

So,  $^{188}\text{Re}$  has the advantage over  $^{131}\text{I}$  and  $^{90}\text{Y}$  during the first day of treatment. Even though  $^{188}\text{Re}$  has more favorable characteristics,  $^{131}\text{I}$  and  $^{90}\text{Y}$  present a simpler radiolabeling chemistry, making  $^{188}\text{Re}$  less used in clinical practice.

Radionuclides emitting  $\alpha$ -particles have very high potency, making them attractive alternatives, or adjuncts, to  $\beta$ -emitters in RIT.<sup>79-80</sup> This higher potency is due to the fact that an  $\alpha$ -emission releases a large amount of energy in a linear manner within a few cell diameters (50–90  $\mu\text{m}$ ). The high linear energy transfer (LET) of  $\alpha$ -emitters ( $\sim 100$  keV per  $\mu\text{m}$ ) confers a high relative biological effectiveness for cell killing, leading to apoptosis or necrosis.<sup>81-83</sup> Furthermore, unlike  $\beta$ -emitting radionuclides, effective cell killing can be expected even in hypoxic tumor areas.<sup>81, 83</sup>

Owing to availability and decay properties, only a few  $\alpha$ -emitting radionuclides are considered suitable for *in vivo* applications, including  $^{213}\text{Bi}$  (biological half-life ( $t_{1/2}$ ) = 45.6 min),  $^{211}\text{At}$  ( $t_{1/2}$  = 7.2 h),  $^{225}\text{Ac}$  ( $t_{1/2}$  = 10 d),<sup>82, 84</sup>  $^{223}\text{Ra}$  ( $t_{1/2}$  = 11.4 d) and  $^{212}\text{Pb}$  ( $t_{1/2}$  = 10.6 h).

### **Vectors for internal radiotherapy of glioblastoma**

Promising approaches based on the design of novel nanovectors for the improvement of the quality of diagnosis and the outcome of cancer radiotherapy, have been recently developed.<sup>85</sup> There are three generations of nanovectors for radionuclide delivery. The first generation of nanovectors, primarily based on passively targeted liposomes and polymer–drug conjugates, is rapidly trapped in the reticuloendothelial system (RES) organs (*e.g.* liver and/or spleen). To reduce the toxicity, overcome the RES capture and prolong the blood circulation time, the surface properties of these nanovectors were modified by covalently binding hydrophilic poly(ethylene glycol) (PEG) chains, leading to the creation of the second generation, known as the PEGylated nanovectors.<sup>86</sup> An enhancement of the brain tumor uptake of PEGylated nanoparticles was reported when compared with conventional nanocarriers.<sup>87</sup>

The second generation nanocarriers were further updated by the binding of specific recognition ligands, such as antibodies, or folic acid to their surface, to actively targeted specific tumor or tissues.<sup>88-89</sup>

The third generation targeted vectors typically have an architecture comprised of a building polymeric or lipidic matrix, a targeting moiety being any molecule that selectively recognizes and binds to ligands on target cells, and a loaded diagnostic or therapeutic agent. The pharmacokinetics and bioavailability of drugs and radionuclides delivered by the third generation of nanovectors

## General Introduction

---

were much improved. Cotara<sup>®</sup> (<sup>131</sup>I-chTNT-1/B), is up to date the only radiopharmaceutical in phase III of clinical trials against anaplastic astrocytoma, brain glioblastoma, and glioma.<sup>90</sup> It is based on a chimeric monoclonal antibody as a targeted vector and <sup>131</sup>I as the radionuclide component delivered to the tumor site through convection-enhanced delivery (CED).

CED is a method in which therapeutic compounds are forced directly into the region of interest through a needle or cannula by applying a low-pressure gradient. CED was developed to homogeneously distribute small- to large-MW therapeutic agents with an effective volume of distribution ( $V_d$ ) that is linearly proportional to the volume of infusion ( $V_i$ ).<sup>91</sup> Direct injection of a therapeutic actually relies on the intact BBB to partially confine the therapeutic agent within the tumor rather than exclude it as is the case with intravascular drugs.

Factors affecting CED and the resultant distribution of the drug are: (a) target location (gray vs white matter); (b) tissue density; (c) tumor permeability; (d) interstitial pressure; (e) the agent's inherent properties such as molecular weight, viscosity, polarity and target avidity; and (f) volume of infusion.<sup>56,91</sup> However, bulk flow fluid dynamics within tumor tissue are substantially different from that of normal brain and consequentially less predictable. Because of the unpredictability of the fate of infusate in the brain, there is a need to monitor the distribution of CED-administered agents.

Imaging contrast agents can be mixed with the infusate during CED to monitor the distribution of a size-matched drug provided they have similar convective properties. It is known that the CSF flows in one direction and renews about four times every 24 hours, providing a built-in washout step for all unbound radiotherapeutics.<sup>92</sup> The apparent absence of an anatomical barrier could also facilitate the movement of nanovectors between the CSF and the extracellular space of

## General Introduction

---

the brain, especially if there is damage to the meninges either by tumor or by surgery. The targeted delivery of radionuclides to the tumor cells by specific receptor binding may be important to avoid this washout and aid cell internalization.

There are two main materials featuring nanoparticle formulations for glioma treatment: gold,<sup>93-94</sup> and lipids.<sup>95-98</sup> It has been recently suggested that following near-infrared (NIR) exposure of brain tumors containing gold-nanoshell-loaded macrophages, sufficient hyperthermia could be generated to suppress tumor growth. As such, gold nanoparticles-loaded macrophages, were injected stereotactically in an orthotopic rat glioma model.<sup>99</sup> After near-infrared exposure sufficient hyperthermia could be generated to delay tumor growth. Gold nanoparticles have also been used to increase the effectiveness of radiotherapy.<sup>100</sup> This in part depends on the Auger effect, a physical phenomenon in which the filling of an inner-shell vacancy of a gold atom is accompanied by the emission of a cytotoxic electron from the same atom. Since this effect is much localized, it is important to place the gold nanoparticles on or in the cancer cells.

Lipids are another basic material for many types of nanovectors, which may be hollow (lipid shells) as in liposomes or solid (lipid dots) as in lipid nanocapsules (LNCs). Reports show promising results in the use of CED administered <sup>186</sup>Re-liposomes for the treatment of glioblastoma in U87 rat glioma model and in the more aggressive U251 rat glioma model.<sup>101-102</sup>

Another <sup>188</sup>Re-labeled PEGylated nanoliposome (<sup>188</sup>Re-liposome) formulation has been developed more recently for glioma treatment.<sup>103</sup> The progression of tumor growth in terms of tumor volume and/or tumor weight was slower for the <sup>188</sup>Re-liposome-treated group than the control group and the lifespan of glioma tumors-bearing rats treated with <sup>188</sup>Re-liposome was slightly prolonged. Another study using <sup>188</sup>Re-labeled LNCs, demonstrated that fractionated

internal radiation by combining a simple stereotactic injection with CED triggered remarkable survival responses in a rat orthotropic glioma model (cure rates of 83%).<sup>104</sup> During the last decades, many nanovectors have been designed, but clinical studies are yet to be performed for malignant gliomas treatment.

### Dendrimers as the vectors of choice

Nature often uses dendritic structures to exhibit or enhance a specific function. As a vivid example, the CNS and brain consist of a large amount of cells growing into dendritic structures with the aim to exchange the largest possible amount of material and information with the surrounding tissue.<sup>105</sup> Microglia cells, which serve as multifunctional helper cells in the brain, when activated during pathological or degenerative states in the brain, expand into dendritic structures (Figure 1.8). The main objective of this newly formed dendritic structure is the maximum delivery of anti-inflammatory interleukins to the diseased brain tissue.<sup>105</sup>

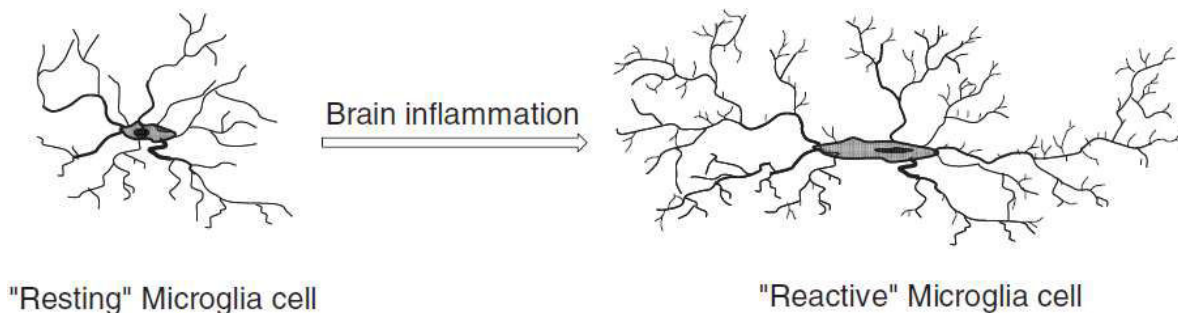


**Figure 1.8** Activation of a Microglia cell during a pathological state in the brain.<sup>105</sup>

Indeed, synthetic dendrimers, similarly to the dendritic structures in nature, can be used directly as high-loading platforms for different applications. Because of their unique cascade architecture, dendrimers can coordinate with substrates, metal ions and reagents selectively on

## General Introduction

different structural locations such as the surface, core, or branching focal point. This distinct feature has attracted great attention among scientists in many disciplines including organic, inorganic, organometallic, polymer, physical and biochemistry as well as materials and life sciences. Unique magnetic, electronic and optical properties have been intensively explored in dendritic materials. Dendrimer research has indeed become an interdisciplinary topic with a great influence on wide fields of science and technology.<sup>106-115</sup>

Dendrimers are highly branched and monodisperse macromolecules that display an exact and large number of functional groups distributed with unprecedented control within their structure or architecture.<sup>116-118</sup> Dendrimers theoretically are monodisperse, meaning that all the molecules have the exact same molecular weight and structure.<sup>119</sup> The intrinsic viscosity of dendrimers has a peculiar behavior, as it increases with increasing molecular weight (number of generations).<sup>120</sup> The dendrimer structure may be divided into three parts, namely the core, the interior and the periphery (Figure 1.9).<sup>121</sup>

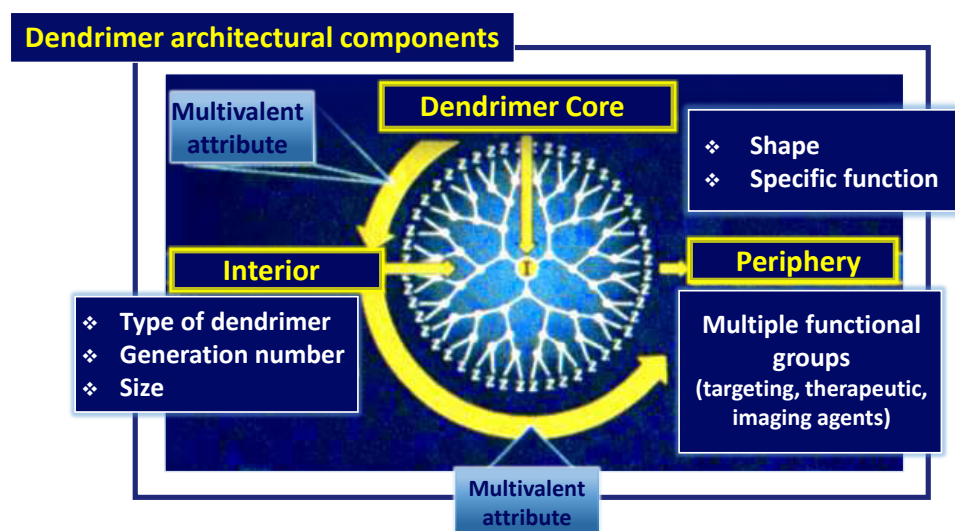


**Figure 1.9** Schematic of three main architectural components of dendrimers. Adapted from ref. <sup>121</sup>.

## General Introduction

---

The core is the primary template from where the dendritic branches originate. These branches are made of repeating units, forming the interior of the dendrimer. The interior defines the type, the size and the generation of the dendrimer. The periphery is the third component and it is composed of terminal functional groups that determine the physicochemical properties of the dendrimers. The number of terminal functional groups in dendrimers increases exponentially with the increasing number of generation (Figure 1.10.).

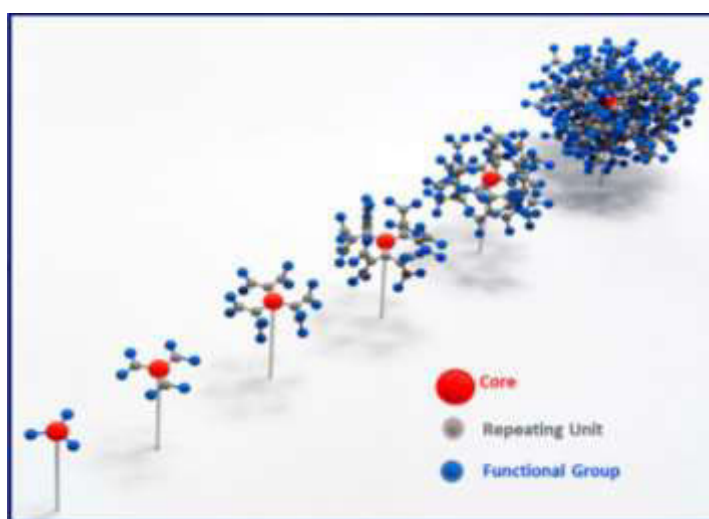


**Figure 1.10** Schematic depicting the building blocks of the dendrimer and generation growth.

As the dendrimer grows the different compartments of the dendritic structure begin to show distinct features.<sup>122-124</sup> This characteristic is crucial for their multivalent attribute. The very high number of functionalities located on the surface and the outer shell are well-suited for host–guest interactions and catalysis where the close proximity of the functional motifs is important. The core, which as the dendrimer generation increases, gets increasingly shielded off from the surroundings by the dendritic wedges.

Dendrimers are generally prepared using either a divergent method or a convergent one (Figure 1.11).<sup>125</sup> With the divergent strategy the dendrimers grow from the core to the periphery.

# General Introduction

In the convergent method the branches of the dendrimer, known as dendrons, grow from the periphery to the interior and in a final step they are coupled with the core.

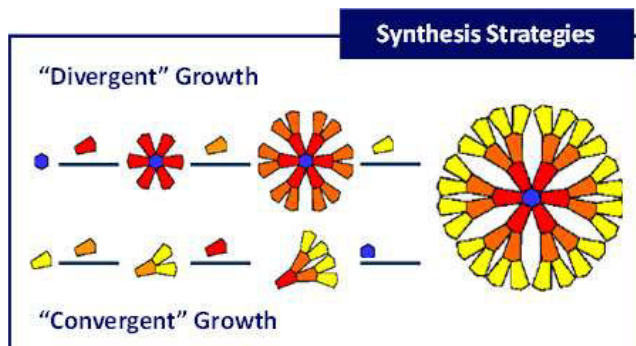


**Figure 1.11** Schematic resuming the divergent and convergent growth of dendrimers.<sup>116, 118</sup>

In both strategies the synthesis process is an iterative sequence of reactions involving coupling and activation steps (Figure 1.12). The convergent approach does not allow the formation of high generations, because steric problems occur in the reactions of the dendrons and the core molecule.<sup>126</sup>

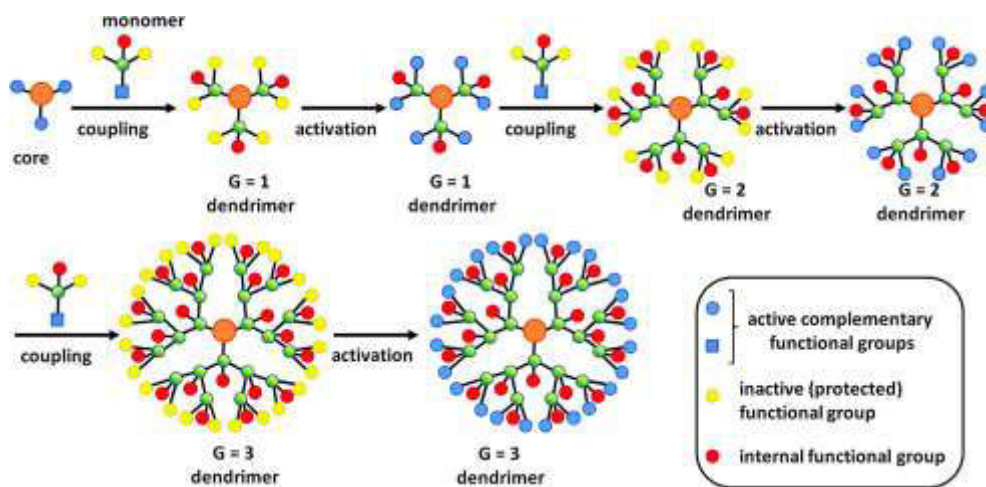


**Figure 1.12** Schematic of the iterative sequence of reactions, needed for the generation growth of the dendrimers.

Adapted from ref. <sup>116, 118</sup>.

## General Introduction

---

In flexible dendrimer structures, back-folding may occur as a consequence of weak forces between the surface functionalities or dendrons leading to a more disordered conformation. However, back-folding may also be a result of attractive forces (ion-pairing, hydrogen bonding,  $\pi$ -interactions, etc.) between functional groups at the inner part of the dendrons and the surface functional groups. The degree of back-folding is to a large extent determined by the surroundings (solvent polarity, ionic strength), thereby constituting a delicate balance between intramolecular forces and forces applied by the surroundings.<sup>105</sup> Interestingly, dendrimers having polar surface groups to some extent resemble proteins in their conformational behavior when subjecting these structures to more apolar conditions. Thus, back-folding of the polar surface groups may expose the more hydrophobic dendrimer parts to the surroundings leading to a decreased surface polarity of the back-folded dendrimer.<sup>127</sup>

When looking at the molecular size and properties of dendrimers, one soon observes that the molecular dimension of high generation dendrimers is comparable to medium-sized proteins.<sup>128</sup> Therefore, it was early suggested that these nanoscale polymers would serve as synthetic mimics of proteins.<sup>129</sup> Being nanosized structures, dendrimers may respond to stimuli from the surroundings and can, like proteins, adapt a tight-packed conformation (“native”) or an extended (“denaturated”) conformation, depending on solvent, pH, ionic strength and temperature.

However, there are some major differences in the molecular structures of dendrimers in comparison to proteins, resulting in a different physicochemical response of dendrimers compared to proteins.<sup>130</sup> The hyperbranched structure of the dendrimer creates a highly multivalent surface, exposing a much higher number of functional groups on the surface compared to proteins of similar

molecular size. The dendrimer architecture consists of a network of covalent bonds, which results in a somewhat less flexible structure than found in proteins.

Another fascinating and rapidly developing area of chemistry, that of self-assembly, has been successfully exploited with dendritic structures.<sup>131-132</sup> Self-assembly is the spontaneous, precise association of chemical species by specific, complementary intermolecular forces.

### **The role of dendrimers in biomedical applications**

Dendrimers constitute a versatile platform, whose inherent parameters can be controlled and set on demand. Dendrimer surfaces provide an excellent mean for the attachment and presentation of cell-specific targeting groups, solubility modifiers, stealth moieties that reduce immunological interactions and imaging tags. The ability to attach any or all of these molecules in a well-defined and controllable manner on to a robust dendritic surface clearly differentiates dendrimers from other vectors, such as micelles, liposomes, emulsion droplets or engineered particles.

Due to their unique physicochemical properties, dendrimers have wide ranges of potential applications, from adhesives and coatings, high-performance polymers, catalysts and chemical sensors, to medical diagnostics, drug/gene-delivery systems, and many more (Figure 1.13).<sup>133-139</sup> The use of dendrimers as targeting vectors for diagnostic imaging, drug delivery and gene transfection had been proposed in the patent literature two decades ago.<sup>121, 140-141</sup> Historically, the first *in vivo* diagnostic imaging applications using dendrimer-based MRI contrast agents were demonstrated in the early 1990s.<sup>40</sup>

## General Introduction

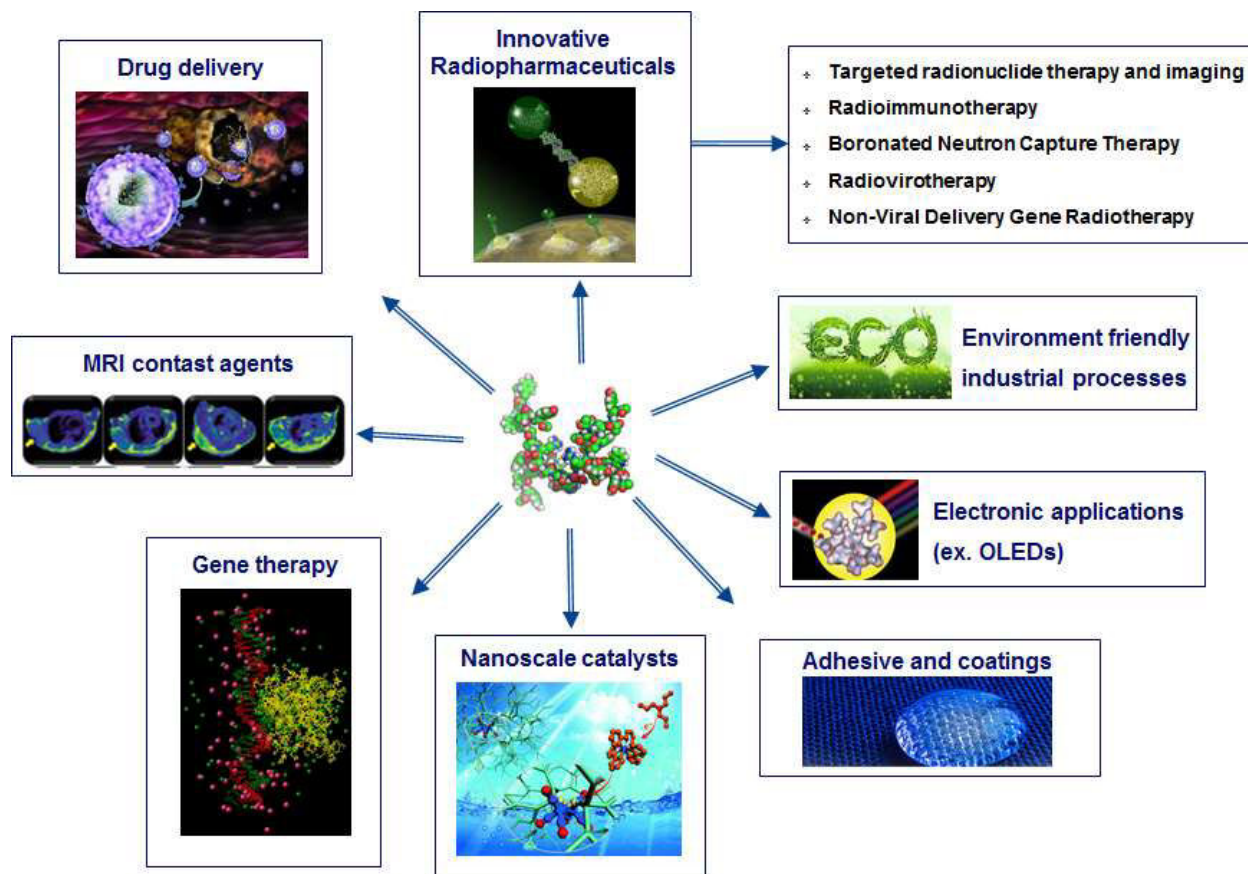


**Figure 1.13** Applications of dendrimers with high potential.

In contrast with the commercial small-molecule agent (Magnevist<sup>®</sup>, Schering, AG), the dendrimer-based reagents exhibited blood pool properties and extraordinary relaxivity values when chelated gadolinium groups were attached to PAMAM dendrimer surfaces. The generation dependent, dramatic enhancements of MRI contrast properties were some of the first examples of a ‘dendritic effect’.

The term “dendritic effect” is widely used to describe unusual physico-chemical trends observed for both dendrons and dendrimers as a function of their generation level.<sup>142</sup> The origin of the dendritic effect is not always fully understood, even if some constants can be identified.<sup>143</sup> It has been examined based on functional group multiplicity, steric shielding or blocking effects and

## General Introduction

---

so-called changes in the nature of internal micro-environment. When the function is located at the core, the dendritic effect originates from the influence of the branches towards the core, modifying the polarity of the environment, or shielding the effect of the solvent, in particular water. However, most of the dendritic effects are observed with functions located at the surface of the dendrimers. In those cases, a high local concentration of functions within well-defined nanoscopic reaction volumes can be attained. Such behaviour affects the molecular interactions between the dendrimers and their surroundings at the interface (substrates for catalysis, receptors or biological entities), which in turn affects the activity and selectivity.

As for nuclear medicine imaging, the majority of research on the use of dendrimers in this field has concentrated less on the primary diagnosis of tumors, and more on their treatment, such as dendrimers delivering cytotoxic radiation *via* radioimmunotherapy, which will be discussed later. The main reason for this is that depending on the efficiency of targeting, low signal-to-noise ratios may make it difficult to distinguish targets from the background. Each imaging modality has its own distinct advantages and limitations.

The simultaneous use of two or more modalities may help to overcome the disadvantages of the individual techniques, improving the information obtained during a single session. The combined use of PET and CT is a successful example of multi-modal imaging, as the two modalities combined can help identify and localize functional abnormalities.<sup>144</sup> However, conventional imaging agents can only be detected by one particular modality, and the use of two separate agents concurrently is rarely attempted. For instance, PET-CT scans are acquired with a PET agent alone; thus, depending on the clinical indication, the unenhanced CT images may be not so optimal. Dendrimers have multiple binding sites and have the potential to be loaded with

## General Introduction

---

multiple, separate imaging agents, thus enabling their detection by two, or more, modalities. Such probes may further improve the information derived from multi-modality scans.

The group of Brechbiel was the first one to develop dendrimers for the purpose of incorporating separate imaging moieties.<sup>145</sup> A G6-PAMAM dendrimer nanoprobe was complexed to Gd ions and Cy5.5 molecules to allow dual modality recognition by both magnetic resonance and near infrared fluorescence imaging. The dendrimer-based dual modality probe was successfully used *in-vivo* to visualize sentinel lymph nodes (SLNs) in murine models by both modalities.

Preliminary results show the potential of dendrimer-based nanocarriers in chemotherapy.<sup>119</sup> Dendrimer properties that were already tested for therapeutic purposes include their stability, spherical shape, size, hollow structure, and multivalency. The drug-loaded dendrimer nanocarriers could reduce drug's toxicity and maintain substantial anti-proliferative activity toward cancer cells *in vitro* and *in vivo*. Since dendrimers are inert and stable, they are nontoxic to human. It was shown that dendrimers could eliminate through the kidneys via urine.<sup>121 146</sup> The idea of dendrimers serving as host for foreign molecules was first stumbled upon by Meijer.<sup>147</sup> He trapped several small molecules in the cavities of water soluble dendrimer molecules, with a diameter about 5 nm. This "dendritic box", a fifth generation PPI dendrimer consisting of 64 functional groups at the periphery, trapped foreign molecules, which could not diffuse out of the box. Only upon prolonged heating, the trapped molecules were able to escape. The "dendritic box" could be used as a vehicle for drug delivery, able to be opened by enzymatic or photochemical changes. This unique feature was also explored by Tomalia's group.<sup>148</sup>

## General Introduction

---

The capability of hosting small organic molecules in water is the key to transport biological molecules. Frechet's group<sup>146</sup> used a chemotherapeutic drug, weakly bonded to the periphery of a dendrimer, which was functionalized with other functional groups to increase its water solubility. The bond between the drug and the dendrimer was designed to be cleaved (enzymatically or photochemically), once the dendrimer reached its target.<sup>140</sup> Furthermore, the mathematically defined number density of surface groups, allows rational attachment of desired ratios of drugs, targeting groups or functionality that may be required to obtain optimum solution, stealth, targeting or release properties with minimal dendrimer toxicity. Concurrently it was observed that appropriate surface-modified dendrimers themselves may act as nanodrugs against viruses, bacteria or tumors. Based on their now recognized 'multivalency' properties, a dendrimer-derived microbicide VivaGel<sup>®</sup> (Starpharma) for HIV or genital herpes is in its final stage of approval by the U.S. Food and Drug Administration (FDA), while the EU and Canada marketing approval has been granted in October 2015 and September 2016 respectively. .

Although still largely at an experimental stage, it is clear that dendrimers have a vital role to play in the rapidly developing field of medical nanotechnology and in both the diagnosis and treatment of tumors. The road to the clinical application of dendrimer-based macromolecular imaging/therapeutic agents has become a hot topic, which remains to be investigated further regarding synthesis, purity of agents, toxicity, pharmacokinetics, excretion, and immunogenicity. In summary, dendrimers present the following advantages compared to traditional transport molecules: (1) multipurpose control over surface groups; (2) excellent cell uptake, which provides high drug bioavailability; (3) monodispersity and manageable size, which facilitates biomedical applications; (4) globular architecture that resembles a protein, which enables application without

an immunoreaction<sup>149</sup>; and (5) high nucleic acid affinity and the ability to release drugs, which prevents complications during cancer therapy<sup>150</sup>.

### **1.3. Review Article: Dendrimers as innovative radiopharmaceuticals in cancer radionanotherapy.**

Radiotherapy is nowadays one of the most commonly used cancer treatments in clinics. It is of extreme importance an efficient targeting of the radiation and sufficient confinement of the radiotherapeutic at the tumor site, avoiding side effects, such as tumor resistance and radiation toxicity. In this context, nuclear medicine has recently turned the attention to new oncologic strategies based on nanovectorized radiotherapy, creating the concept of radionanomedicine.<sup>151</sup>

The core of radionanomedicine relies on the labeling of multifunctional nanomaterials with radionuclides and using ‘trace’ amounts, much less than pharmacologic amounts, for *in vivo* theranostic purposes.<sup>152</sup> Since *in vivo* toxicity of nanomaterials is dose dependent, the use of trace amounts of nanomaterials minimizes the toxicity risk itself.<sup>153</sup>

Multifunctional radionanomedicine can also be used for a multiradioisotope or multitargeting approach. The distribution study of nanomaterials can provide important information for their clinical translation, nuclear imaging monitoring and can elucidate the *in vivo* fate of nanomaterials by giving information if they are properly retained in the specific tissues.

EPR based accumulation is the basis for most tumor targeted nanomedicines. However, the therapeutic benefit over small probes is often only moderate since EPR is variable among patients and even heterogeneous within the same tumor. Here, theranostic agents and companion diagnostics can help to preselect patients and to individualize therapy. In addition, in tumors larger

## General Introduction

---

nanoparticles tend to accumulate just outside the vasculature, do hardly penetrate the stroma and thus do not reach the cancer cells. Thus, a refined balance between accumulation and penetration may be therapeutically superior over just maximal accumulation. In this context, active targeting does only marginally help since it does not improve nanoparticle distribution and accumulation but just retention.<sup>154</sup>

For example, it was shown for targeted polymers that the overall accumulation can even decrease after adding targeting ligands since increasing recognition of the nanoparticles by the RES lead to faster clearance, lower blood half-life and thus, reduction of EPR based accumulation. The principle of target-specific radionuclide theranostic is derived from nuclear medicine therapy. Classically used  $^{131}\text{I}$  for thyroid cancer is the best example, which enables both internal radiotherapy for thyroid cancer tissues and post-therapy scans to find residual thyroid tissues of metastasis.<sup>155</sup> Active targeting becomes more evident for small nanoparticles with good penetration and rapid exchange between the tissue compartments but insufficient retention, which mostly are nanoparticles below 5 nm in size.<sup>156</sup> These are the ones that are most suited for molecular imaging purposes as well. Thus, the intended medical application should route the decisions about design of nanoparticles and all aspects relevant to its *in vivo* application including the expected superiority over existing clinical gold standards should be considered from beginning on. Following this conduct, many failures in the transition from *in vitro* to *in vivo* application can be avoided.

In recent years, there has been an unprecedented expansion in the field of nanomedicine with the development of new nanometric systems for better therapeutic efficacy and imaging quality of cancer.<sup>85</sup> Various kinds of nanosystems have been described for this purpose, but among them

## General Introduction

---

dendrimers are especially appealing, because of their multifunctionality and modifiable physicochemical properties. Different approaches have been developed to conjugate dendrimers to paramagnetic or radionuclide chelators for MRI, fluorescence, CT, or radionuclide-based imaging, which are described in other specialized reviews.<sup>157-165</sup>

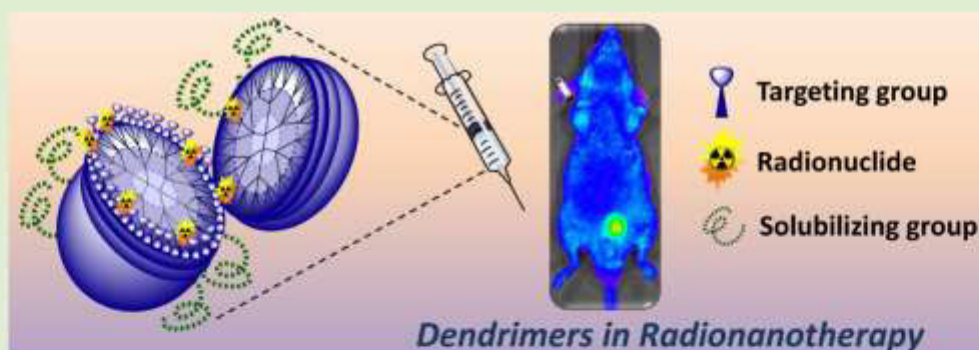
This review is focused on the use of dendrimers in radiotherapy, an emerging area which, to the best of our knowledge, has not been revised yet. Important milestones have been reached in the research with dendrimers for nanovectorized radiotherapy. Dendrimers have been functionalized with ligands for radiolabeling, targeting agents and stealth functional groups to potentially improve the biodistribution and elongate the circulation time of the conjugates with a good *in vivo* stability. Taking advantage of their numerous peripheral functionalities, dendrimers with a large number of covalently attached boron atoms have been tested with preliminary positive results in Boron Neutron Capture Therapy, when targeted to the tumors. For efficient targeting, conjugation of dendrimers to monoclonal antibodies (moAbs), resulted in a higher loading capacity of internal radiation dose, without significant loss of the moAbs immunoreactivity. Coating of the adenoviral vectors with synthetic dendrimers was effective for avoiding the liver sequestration of the adenovirus and improving the tumor targeting properties. Similarly, dendrimers were used as a vector for coexpression gene therapy to increase the radiosensitivity of the tumors, followed by exposure to radiotherapy after transfection with promising results, as described below.

# Dendrimers as Innovative Radiopharmaceuticals in Cancer Radionanotherapy

Flonja Liko,<sup>†,‡</sup> François Hindré,<sup>\*,†</sup> and Eduardo Fernandez-Megia<sup>\*,‡</sup>

<sup>†</sup>INSERM U 1066, 'Micro et Nanomédecines biomimétiques – MINT', and Plateforme de Radiobiologie et d'Imagerie Expérimentale, PRIMEX, SFR ICAT 4208, Université Angers, UMR-S1066, 49933 Angers, Cedex 9, France

<sup>‡</sup>Centro Singular de Investigación en Química Biolóxica e Materiais Moleculares (CIQUS) and Departamento de Química Orgánica, Universidade de Santiago de Compostela, Jenaro de la Fuente s/n, 15782 Santiago de Compostela, Spain



**ABSTRACT:** Radiotherapy is one of the most commonly used cancer treatments, with an estimate of 40% success that could be improved further if more efficient targeting and retention of radiation at the tumor site were achieved. This review focuses on the use of dendrimers in radionanotherapy, an emerging technology aimed to improve the efficiency of radiotherapy by implementing nanovectorization, an already established praxis in drug delivery and diagnosis. The labeling of dendrimers with radionuclides also aims to reduce the dose of radiolabeled materials and, hence, their toxicity and tumor resistance. Examples of radiolabeled dendrimers with alpha, beta, and Auger electron emitters are commented, along with the use of dendrimers in boron neutron capture therapy (BNCT). The conjugation of radiolabeled dendrimers to monoclonal antibodies for a more efficient targeting and the application of dendrimers in gene delivery radiotherapy are also covered.

## 1. INTRODUCTION

Since the discovery of X-rays and radioactivity at the end of the 19th century, and their introduction into clinical practice, radiotherapy has been used, along with surgery and chemotherapy, as a key modality in cancer treatment. Its powerful ability to cause tumor cell death lays mainly in the induction of irreparable DNA damage and cell cycle arrest.<sup>1</sup> Approximately 50% of all cancer patients receive radiotherapy during the course of their illness<sup>2</sup> with an estimated 40% success.<sup>3</sup> There are two ways to deliver radiation to the tumor sites. The most common approach in the clinical practice is external beam radiation, which delivers high-energy radiation (photons, protons, or particle radiation) from outside the body to the tumor location. The second type is internal radiation, which is delivered by radionuclides into the tumor site. Radionuclide internal therapy can therefore reduce irradiation of healthy tissues with relatively low toxicity, in comparison to conventional chemotherapy and external beam radiotherapy.

The therapeutic effect of internal radiotherapy is due to the delivery of alpha ( $\alpha$ ), beta ( $\beta^-$ ), or Auger electron emitters (Table 1) to the tumor site, resulting in tumor shrinkage or its total elimination, depending on the Linear Energy Transfer

(LET) of the emitter (Table 2). As alpha particles are positively charged monoenergetic helium nuclei with the highest energy among particle emissions (LET  $\sim 80$  keV/ $\mu$ m), they will interact in a range of penetration in tissue from 40 to 100  $\mu$ m. This is consistent with the dimension of micrometastatic lesions, so they are especially suited for localized irradiation of target cells with minimal toxicity to the surrounding normal cells. This radiation is particularly effective in killing cells,<sup>4</sup> independently of their oxygenation state or cell cycle phase.<sup>5</sup> Although human cancer cells can be eradicated *in vitro* after being hit by only a few alpha particles,<sup>6</sup> these must reach the tumor cell nuclei to show an efficient cytotoxic effect, not just the cell cytoplasm.<sup>7</sup>

Physico-chemical characteristics of Auger electrons are close with alpha particles with a tissue penetration from nanometers to a few micrometers. In comparison,  $\beta^-$  particles (high energy electrons from  $\beta^-$  decay) have the longest penetration range in tissue (1–12 mm). This is an important factor to consider

Received: June 22, 2016

Revised: September 5, 2016

Published: September 8, 2016

**Table 1. Radionuclides for Tumor Radiotherapy**<sup>13–17</sup>

radionuclide	half-life	decay mode	energy max (keV)	max range in tissue
<sup>82m</sup> Br	4.42 h	Auger	3092.6	<10 nm
<sup>125</sup> I	60 h	Auger	185.77	10 nm
<sup>225</sup> Ac	10 d	$\alpha$	5830, 5792, 5790, 5732	40–80 $\mu$ m
<sup>213</sup> Bi	45.7 min	$\alpha$	5869	50–80 $\mu$ m
<sup>211</sup> At	7.2 h	$\alpha$	5870	60–80 $\mu$ m
<sup>212</sup> Bi	1 h	$\alpha, \beta$	( $\alpha$ ): 6050; ( $\beta$ ): 2270	90 $\mu$ m
<sup>223</sup> Ra	11.43 d	$\alpha$	5850	<100 $\mu$ m
<sup>160</sup> Er	9.5 d	$\beta$	( $\beta$ ): 351	1 mm
<sup>177</sup> Lu	6.7 d	$\beta, \gamma$	( $\beta$ ): 500	1.6 mm
<sup>67</sup> Cu	2.58 d	$\beta, \gamma$	( $\beta$ ): 577	2.2 mm
<sup>131</sup> I	8.04 d	$\beta, \gamma$	( $\beta$ ): 807	2.4 mm
<sup>89</sup> Sr	50.53 d	$\beta$	1463	<3 mm
<sup>153</sup> Sm	1.95 d	$\beta, \gamma$	( $\beta$ ): 233	3 mm
<sup>198</sup> Au	2.69 d	$\beta, \gamma$	( $\beta$ ): 1372.8	4.4 mm
<sup>186</sup> Re	3.77 d	$\beta, \gamma$	( $\beta$ ): 1069	5 mm
<sup>169</sup> Dy	2.33 d	$\beta, \gamma$	( $\beta$ ): 1286.1	6.4 mm
<sup>32</sup> P	14.3 d	$\beta$	1710	8.7 mm
<sup>166</sup> Ho	26.9 h	$\beta, \gamma$	( $\beta$ ): 1853	10.2 mm
<sup>188</sup> Re	17 h	$\beta, \gamma$	( $\beta$ ): 2120	11 mm
<sup>90</sup> Y	64.1 h	$\beta$	2280	12 mm

**Table 2. Linear Energy Transfer (LET) of Therapeutic Radionuclides**<sup>18</sup>

particle decay	range in tissue	LET (keV/ $\mu$ m)
$\alpha^{++}$	(cellular) 40–100 $\mu$ m	~80 (high)
$\beta^-$	(multicellular) 0.05–12 mm	~0.2 (low)
EC/IC <sup>a</sup>	(subcellular) 2–500 nm	~4–26

<sup>a</sup>EC/IC: Electron Capture/Internal Conversion.

regarding the size of the tumors potentially treated, as well as the targeting ligands and carriers for the  $\beta^-$  radionuclide.<sup>8</sup> The  $\beta^-$  particle irradiation also leads to the generation of harmful free radical species in the presence of oxygen in tumor cells. Due to their lower LET compared to alpha particles,  $\beta^-$  particles have a lower killing efficacy, so higher concentrations of emitters are required for a comparable effect.<sup>9</sup> Conversely, since the long path of  $\beta^-$  particles crosses multiple cells, a cross-fire effect is achieved that not only avoids the need to target every cancer cell with a radionuclide emitter, but also reduces the hurdle of an heterogeneous uptake in large tumors.

Finally, Auger electrons are low energy atomic orbital electrons emitted after electron capture (EC).<sup>10</sup> Studies in vitro have shown Auger electrons as highly effective and specific in tumor cell killing when used in tandem with targeting vehicles that can direct them in close proximity to cellular DNA.<sup>11,12</sup>

With the actual improvement in the clinical outcome of cancer treatment, the reduction of the toxicity related to radiation has become a priority, together with the overcoming of some primary limitations of radiotherapy, that is, injury in surrounding tissues and tumor resistance.<sup>19,20</sup> In this context, nuclear medicine has recently turned the attention to new oncologic strategies based on the nanovectorization of radiotherapy, generating the concept of radionanomedicine.<sup>21</sup> The core of radionanomedicine relies on the labeling of nanomaterials with radionuclides to reduce the amounts of

radiolabeled materials in vivo.<sup>22</sup> Indeed, nanomedicine has traditionally been a major focus of nanotechnology.<sup>6</sup> According to the U.S. National Science Foundation, by 2020, nearly half of future pharmaceuticals will have some nanotechnology components.<sup>23,24</sup> In recent years, there has been an unprecedented expansion in the field of nanomedicine with the development of new nanometric systems for better therapeutic efficacy and imaging quality of cancer.<sup>25</sup> Nanosystems, compared to conventional medicines, have many benefits, given their nanometric size and large surface area-to-volume ratio, improved bioavailability, reduced toxicity, greater dose response, and enhanced solubility.<sup>26</sup>

Nanosystems with long circulation times can get internalized into tumors through the leaky tumor vasculature and be retained in the tumor due to abnormal lymphatic drainage. This process is known as the enhanced permeability and retention (EPR) effect.<sup>27</sup> However, for an efficient EPR effect, the physicochemical properties of the nanosystems are as important as the tumor biology. While, EPR effect is quite helpful to passively target nanosystems in animal models, a full understanding of the differences in tumor biology and clearance mechanisms between individual human patients has yet to be established.<sup>28</sup>

Accordingly, innovative radionanopharmaceuticals are much awaited for targeting cancer, with therapeutic doses of internal radiation. Their efficacy is determined by the two constituting elements, the carrier and the trace amount of a radionuclide with a defined radiation type, but also by the injection modalities (intravenous or loco-regional injection). Ideal radiopharmaceuticals should transport the radioactive nuclide quantitatively to the tumor tissue while protecting healthy tissues from radiation. Various kinds of carriers have been described for this purpose, including liposomes, carbon nanotubes, polymeric nanoparticles, nanocapsules, and so on. Among them, dendrimers are especially appealing. Their controlled synthesis allows the preparation of well-defined monodisperse and globular nanovectors, characterized by a tunable size and precise number of peripheral groups, which determine their physicochemical properties and function (Figure 1). The number of peripheral groups in dendrimers increases exponentially with the generation number. Several approaches have been developed to conjugate dendrimers to paramagnetic or radionuclide chelators for MRI, fluorescence, CT, and radionuclide-based imaging. In addition, multimodal imaging agents with improved diagnosis accuracy have been described exploiting the unique structural characteristics of

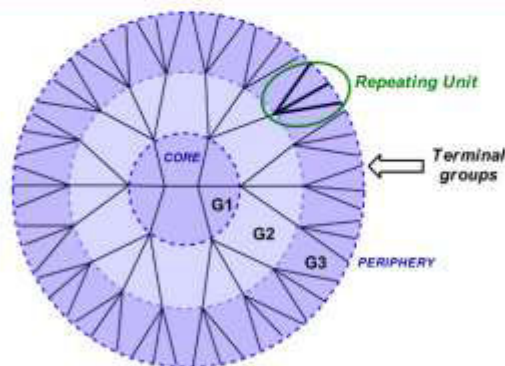


**Figure 1.** Schematic representation of a third generation (G3) dendrimer.

Table 3. Radioimmunotherapy Drugs

generic name	antigen/radionuclide	disease	clinical trial status
$^{90}\text{Y}$ -ibritumomab tiuxetan	CD20/ $^{90}\text{Y}$	non-Hodgkin's lymphoma	approved by FDA
$^{131}\text{I}$ -tositumomab	CD20/ $^{131}\text{I}$	non-Hodgkin's lymphoma	approved by FDA
$^{131}\text{I}$ -Lym 1	HLA-DR10/ $^{131}\text{I}$	non-Hodgkin's lymphoma, chronic lymphocytic leukemia	phase III
epratuzumab	CD22/ $^{90}\text{Y}$	non-Hodgkin's lymphoma, chronic lymphocytic leukemia, immune diseases	phase III
$^{131}\text{I}$ -chTNT-1/B	DNA/ $^{131}\text{I}$	glioblastoma, anaplastic astrocytoma	phase III
CEA-Cide	CEA/ $^{90}\text{Y}$ or $^{131}\text{I}$	breast, lung, pancreatic, stomach, colorectal carcinoma	phase III
pentumomab	PEM/ $^{90}\text{Y}$	ovarian, gastric carcinoma	phase III
$^{131}\text{I}$ -metuximab	(Hab18G/CD147)/ $^{131}\text{I}$	hepatocellular carcinoma	phase II
$^{131}\text{I}$ -L19	fibronectin/ $^{131}\text{I}$	hepatological malignancy, refractory Hodgkin's lymphoma, nonsmall cell lung cancer, melanoma, head and neck carcinoma	phase II
$^{90}\text{Y}$ -clivatuzumab tetraxetan	MUC1/ $^{90}\text{Y}$	pancreatic adenocarcinoma	phase III
$^{223}\text{Ra}$ dichloride	-/ $^{223}\text{Ra}$	metastatic castration-resistant prostate cancer	approved by FDA
$^{177}\text{Lu}$ -DOTA-Tyr3-octreotate <sup>a</sup>	SST/ $^{177}\text{Lu}$	metastatic gastro-entero-pancreatic neuroendocrine tumors	phase III
$^{131}\text{I}$ -MIBG	norepinephrine (NE)/ $^{131}\text{I}$	neuroblastoma, pheochromocytoma, paraganglioma	phase III

<sup>a</sup>DOTA refers to 1,4,7,10-tetraazacyclododecane-1,4,7,10-tetraacetic acid.

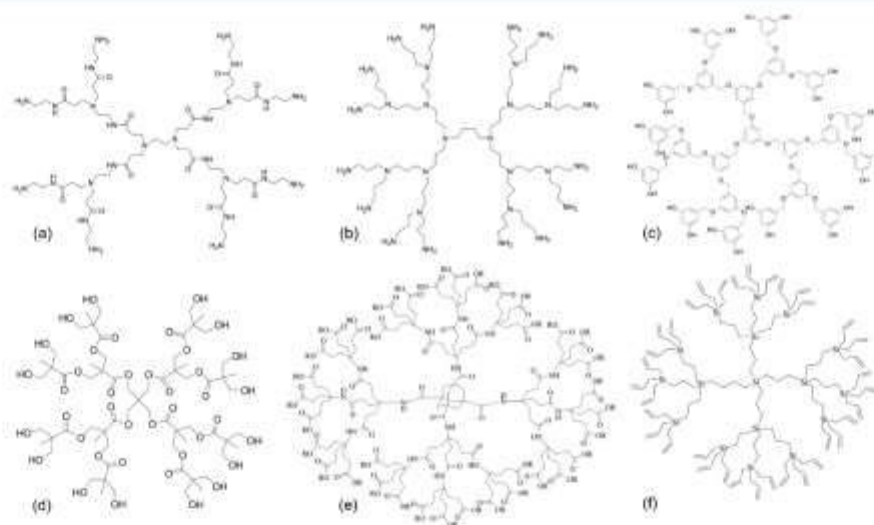


Figure 2. Structures of common dendrimers: (a) PAMAM; (b) PPI; (c) polybenzyl ether; (d) polyaliphatic ester; (e) polyesteramide; (f) polycarbosilane.<sup>51</sup>

dendrimers. As an exhaustive analysis of all this literature falls outside the scope of this review, interested readers on the use of dendrimers in cancer imaging and chemotherapy are referred to specialized reviews.<sup>29–37</sup> Herein, we will focus on the use of dendrimers in radiotherapy, including state of the art examples up to December 2015 and perspectives in an emerging field, which to the best of our knowledge has not been revised yet.

**1.1. Nanovectorized Radiotherapy Drugs Approved or under Clinical Trials.** During the past decade, alpha ( $\alpha$ ), beta minus ( $\beta^-$ ), and Auger electron-emitting radionuclides have been investigated for targeted and nanovectorized radiotherapy. Fortunately, these efforts have resulted in four targeted  $\beta^-$  emitters approved by FDA:  $^{153}\text{Sm}$ -EDTMP (Quadramet) and  $^{89}\text{Sr}$ -chloride (Metastron) for palliation of bone metastases; and  $^{90}\text{Y}$ -ibritumomab (Zevalin) and  $^{131}\text{I}$ -tositumomab (Bexxar), for the treatment of B-cell non-Hodgkin's lymphoma. While Quadramet and Metastron consist of radioactive samarium ( $^{153}\text{Sm}$ ) complexed to a tetraphosphonate chelator and a strontium-89 chloride ( $^{89}\text{SrCl}_2$ ) injection,

respectively, Zevalin and Bexxar are radiolabeled murine antibodies, directed against the CD20 antigen expressed on the surface of normal and malignant B-lymphocytes.<sup>38</sup> The latter two are good examples of the potential benefit of antibody-guided systemic radionuclide-targeted therapy.<sup>39–46</sup> In addition, several other radiopharmaceuticals for radioimmunotherapy of tumors have been introduced into clinical trials. More detailed information on these clinical trials is presented in the review of Gudkov and co-workers (Table 3).<sup>47</sup>

## 2. DENDRIMERS AS INNOVATIVE RADIOPHARMACEUTICALS

The history of dendrimers goes back to the late 1970s and early 1980s, when the groups of Vögtle,<sup>48</sup> Newkome,<sup>49</sup> and Tomalia<sup>50</sup> independently published the first contributions in the area. Since then, more than 100 dendritic structures have been described in the search of improved properties and innovative applications in fields like bio- and nanotechnology, catalysis, or materials science.<sup>51–59</sup> Nowadays, some of the

most recognized dendritic families include polyamidoamine (PAMAM),<sup>60</sup> polypropyleneimine (PPI),<sup>61</sup> and others based on polyamide,<sup>49</sup> polyether,<sup>62</sup> polyester,<sup>63,64</sup> and phosphorus-based scaffolds<sup>65</sup> (Figure 2).

Dendrimers are unique among nanomaterials since their stepwise synthesis allows creating well-defined and monodisperse structures with tunable size and number of terminal units. They have three main structural components: (i) an internal core, from which the dendritic branches grow, (ii) the layers of branches that define the dendrimer generation, and (iii) a multivalent peripheral shell. The number of terminal groups in dendrimers increases exponentially with the generation number. This characteristic is crucial to modulate the dendrimer solubility, making possible to overcome some fundamental issues in radiotherapy, such as solubility and dose delivery. The controlled architecture of dendrimers allows multiple possibilities for the simultaneous attachment of radionuclide chelators and targeting moieties.<sup>66</sup>

Historically, dendrimers have been synthesized following multiple reaction steps that involve long reaction times, tedious purifications, and sometimes reversible reactions potentially leading to structural defects. This could have led to an outdated perception that dendrimer synthesis is complex, slow, and costly.<sup>67</sup> Several improvements, however, have been done recently that simplify and fasten up the synthesis of dendrimers, including the use of (i) orthogonal chemistries to avoid the need of protecting groups and so reduce the number of reaction steps;<sup>68</sup> (ii) "click" chemistry for irreversible, fast, and high yield reactions;<sup>69</sup> (iii) hypercores and hypermonomers for the accelerated increase of size while preserving dendrimer properties; or (iv) various types of heterofunctional dendrimers.<sup>70</sup> The design principle of dendrimers has been thoroughly reviewed elsewhere according to the surface/interior chemistry, generation size, shape, flexibility/rigidity, and composition.<sup>55,71</sup>

**2.1. Radiolabeled Dendrimers in Radiotherapy.** The first successful evidence of the therapeutic use of radioactive dendrimers came from a study with radioactive gold-dendrimer based nanoparticles of various sizes (Figure 3).<sup>72</sup> In this report,

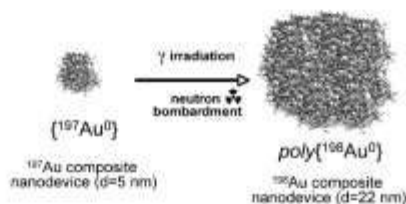


**Figure 3.** Polymerized composite nanoparticle formed by radiation of a dendrimer network with simultaneous neutron activation of  $^{197}\text{Au}$  in the composite nanoparticles into  $^{198}\text{Au}$ . Dark dots represent gold atoms, the organic network is gray. Reprinted with permission from ref 72. Copyright 2008 Elsevier.

PAMAM dendrimers were used for the targeted delivery of the radiopharmaceutical to tumors in vivo. Poly- $^{198}\text{Au}^0$  nanoparticles were synthesized from nonradioactive  $^{197}\text{Au}^0$ -PAMAM complexes using both gamma-radiation and neutron radiation components in a reactor.

The increase in size of the resulting nanoparticles was due to partial cross-linking of the PAMAM dendrimers by the combined effect of  $\gamma$  radiation and heat, while absorption of neutrons activated the gold component to  $^{198}\text{Au}$ . Biodistribu-

tion studies of both the template PAMAM dendrimers and the gold composites showed that positively charged nanoparticles were more retained in tissues than neutral or negatively charged ones. A single injection of  $^{198}\text{Au}$ -PAMAM complexes (29 nm in size) directly into a melanoma tumor mouse model resulted in more than a 45% decrease in tumor growth within 8 days.

**2.1.1. Dendrimer- $\beta^-$  Emitter Conjugates.** The preclinical and clinical research in the field of dendrimer- $\beta^-$  emitters has focused on at least 12 radionuclides: yttrium-90 ( $^{90}\text{Y}$ ), iodine-131 ( $^{131}\text{I}$ ), lutetium-177 ( $^{177}\text{Lu}$ ), samarium-153 ( $^{153}\text{Sm}$ ), strontium-89 ( $^{89}\text{Sr}$ ), holmium-166 ( $^{166}\text{Ho}$ ), rhenium-186 ( $^{186}\text{Re}$ ), rhenium-188 ( $^{188}\text{Re}$ ), copper-67 ( $^{67}\text{Cu}$ ), promethium-149 ( $^{149}\text{Pm}$ ), gold-199 ( $^{199}\text{Au}$ ), and rhodium-105 ( $^{105}\text{Rh}$ ).<sup>73</sup> In addition, many radiotherapeutic  $\beta^-$  emitters also emit a low ratio of gamma photons ( $\gamma$ ) with energy in the ideal range for nuclear imaging (80–200 keV). Therefore, these radionuclides have theranostic properties, which are valuable in clinical radiotherapeutic applications with nanometric systems.

A radionuclide with excellent theranostic properties is  $^{188}\text{Re}$  with a ratio of 85% for  $\beta^-$  emission ( $E_M = 2.12$  MeV) and 15% for  $\gamma$  emission ( $E = 155$  keV). Yu-Mei Shen and co-workers<sup>74</sup> used  $^{188}\text{Re}$  to radiolabel G5 PAMAM dendrimers conjugated with 2-(4-isothiocyanatobenzyl)-6-methyldiethylene-triamine-pentaacetic acid (1B4M-DTPA) as a bifunctional ligand and folic acid (FA) for active targeting. The labeling yield of the conjugate G5-FA-DTPA- $^{188}\text{Re}$  (percentage of incorporated radionuclide) was 67% and its radiochemical purity (the fraction of incorporated radioactivity that is present in the desired radiochemical form) exceeded 95%. Even though the conjugate showed high in vitro stability when incubated for 6 h at 37 °C in phosphate buffer saline (PBS, pH 7.4) or in newborn calf serum, a weak in vivo stability in mice revealed that further structural improvements were needed in the system.

In a preclinical study published in 2014,<sup>75</sup> G1 and G4 PAMAM dendrimers conjugated with 10-[(4-carboxy-1-oxido-pyridin-2-yl)methyl]-1,4,7,10-tetraazacyclododecane-1,4,7-triacetic acid (DO3A-py<sup>NO-C</sup>, a DOTA-like bifunctional chelator with one methylene pyridine-N-oxide pendant arm) were radiolabeled with  $^{177}\text{Lu}$  with high radiochemical purity. Both radiolabeled dendrimers were stable for at least 24 h. As already seen in previous studies,<sup>76</sup> the distribution profile of the G1 conjugate in organs and tissues of rats was more favorable than for G4. Conversely, the G4 conjugate with a considerably higher number of chelating ligands per molecule enables the binding of a larger number of radiometals. These results showed that dendrimer-radiometal chelates might constitute a prospective way to radiolabel targeting agents, such as antibodies or their fragments, with markedly high specific activity and minimal loss of their immunoreactivity.

In a more recent study,<sup>77</sup> theranostic dendrimers for targeted single-photon emission computed tomography (SPECT) imaging and radiotherapy of a MMP2-overexpressing xenografted glioma model in vivo (Figure 4) were successfully constructed by the conjugation of a G5 PAMAM dendrimer with polyethylene glycol (PEG) and the targeting agents chlorotoxin (CTX) and 3-(4'-hydroxyphenyl)propionic acid-OSu (HPAO). The dendrimer conjugates showed excellent cytocompatibility and could be effectively labeled with radioactive  $^{131}\text{I}$  with good stability and high radiochemical purity. For in vivo imaging experiments, 6-week-old BALB/c female nude mice were inoculated subcutaneously with  $2 \times 10^6$  C6 cells/mouse in the right side of flank. At approximately 3 weeks postinjection, the tumors reached a volume of 0.5–1.0

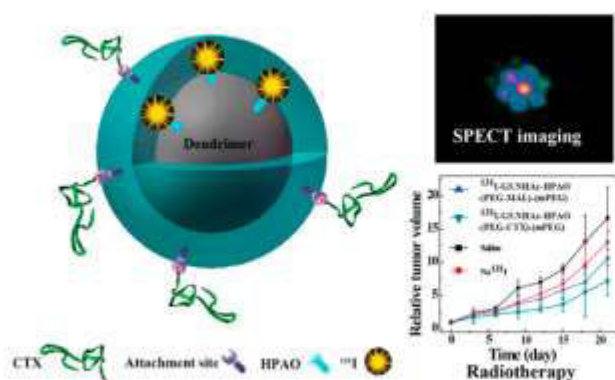


**Figure 4.** Chlorotoxin-conjugated multifunctional dendrimers labeled with radionuclide  $^{131}\text{I}$  for imaging and radiotherapy. Reprinted with permission from ref 77. Copyright 2015 American Chemical Society.

$\text{cm}^3$ . The specific targeting role mediated by the attached CTX moiety onto the dendrimers was confirmed by the relatively higher tumor uptake of  $^{131}\text{I}$ -G5 NHAc-HPAO-(PEG-CTX)-(mPEG) dendrimers in comparison with nontargeted  $^{131}\text{I}$ -G5 NHAc-HPAO-(PEG-MAL)-(mPEG) dendrimers. It was seen that after treatment with  $^{131}\text{I}$ -G5 NHAc-HPAO-(PEG-CTX)-(mPEG), the tumor grew more slowly than in mice treated with saline,  $\text{Na}^{131}\text{I}$ , or nontargeted  $^{131}\text{I}$ -G5 NHAc-HPAO-(PEG-MAL)-(mPEG). The biodistribution study of the multifunctional dendrimers, investigated by SPECT imaging, showed that the majority of the  $^{131}\text{I}$ -G5 NHAc-HPAO-(PEG-CTX)-(mPEG) or  $^{131}\text{I}$ -G5 NHAc-HPAO-(PEGMAL)-(mPEG) dendrimers accumulated in the liver at 15 h postinjection, while the heart, lung, tumor, kidney, spleen, intestines, stomach, and soft tissue had a relatively low accumulation of the nanosystems. In spite of the high nonspecific binding to normal tissue, CTX enhanced the accumulation of dendrimers in tumor compared to nontargeted dendrimers. At 24 h postinjection, the tumor SPECT signal descended for both targeted and nontargeted groups, indicating the dendrimer could be metabolized. Nevertheless, the SPECT signal intensity of tumors treated with the CTX-targeted dendrimer was still much higher than when treated with the nontargeted dendrimer.

Similar multifunctional dendrimers have been synthesized by modifying G5 PAMAM dendrimers with HPAO and FA linked to PEG.<sup>78</sup> After radiolabeling with  $^{131}\text{I}$  ( $^{131}\text{I}$ -G5-NHAc-HPAO-PEG-FA) the system was assayed for targeted SPECT imaging and radiotherapy, using a FA receptor-overexpressing xenografted tumor model *in vivo*. The radiolabeling of the dendrimer with  $^{131}\text{I}$  was done via the chloramine T method with a radiochemical purity exceeding 97%.  $^{131}\text{I}$ -G5-NHAc-HPAO-PEG-FA dendrimer displayed acceptable stability *in vitro* for at least 27 h when stored at room temperature in PBS. The relative SPECT signal intensity of different organs at 6 and 24 h postinjection of  $^{131}\text{I}$ -G5-NHAc-HPAO-PEG-FA and  $^{131}\text{I}$ -G5-NHAc-HPAO-mPEG dendrimers revealed that liver was the organ with the highest uptake, and a relatively low uptake from the other organs. Again, the tumor growth rate of mice injected with  $^{131}\text{I}$ -G5-NHAc-HPAO-PEG-FA dendrimers was significantly slower than that of mice treated with saline,  $\text{Na}^{131}\text{I}$ , and control  $^{131}\text{I}$ -G5-NHAc-HPAO-mPEG dendrimers without FA. This result underlines the importance of the effective FA targeting, also proven by the SPECT image at the tumor site.

Despite numerous investigations with dendrimers as conjugates for cancer drug therapy and imaging,<sup>29,32,79–85</sup> there have been limited efforts in the development of radiotherapeutic dendrimers for image-guided radionuclide therapies. Current results are encouraging and point to a fruitful progress of dendrimer–chelate conjugates with bound  $\beta^-$  emitters and target-specific ligands in the area. Another new axis of research could be based on loco-regional injection of dendrimers, especially for glioma or hepatocarcinoma treatment, as confinement of the radiopharmaceuticals is expected, avoiding radiotoxicity to healthy tissues.

**2.1.2. Dendrimer- $\alpha$  Emitter Conjugates.** Medically relevant  $\alpha$ -emitting radionuclides currently available for potential therapeutic application are astatine-211 ( $^{211}\text{At}$ ), bismuth-212 ( $^{212}\text{Bi}$ ), bismuth-213 ( $^{213}\text{Bi}$ ), actinium-225 ( $^{225}\text{Ac}$ ), radium-223 ( $^{223}\text{Ra}$ ), lead-212 ( $^{212}\text{Pb}$ ), thorium-227 ( $^{227}\text{Th}$ ), and terbium-149 ( $^{149}\text{Tb}$ ).<sup>86</sup> Recently, a pharmaceutical grade  $^{223}\text{Ra}$  chloride solution was the first  $\alpha$ -emitting radiopharmaceutical to be approved for clinical use in the treatment of metastatic bone disease.<sup>87</sup>

Most approaches to target  $\alpha$  particle emitters in the past relied on conjugation with antibodies through chelators. The efforts to integrate dendrimers in radiotherapy with  $\alpha$  particles are limited to an early report from Wu, Gansow, and co-workers,<sup>88</sup> who described a route to modify moAbs with a high number of chelating agents by conventional direct ligand attachment for use in radioimmunotherapy. This group successfully coupled with minimal loss of immunoreactivity a moAb with a single G2 PAMAM dendrimer carrying 10.2 of the available 12 surface primary amines decorated with 1,4,7,10-tetraazacyclododecane-1,4,7,10-tetraacetic acid (DOTA) or diethylenetriaminepentaacetic acid (DTPA) bifunctional ligands. Labeling the moAb-DTPA complex with  $^{213}\text{Bi}$  resulted in at least four times greater specific activity than the previously obtained with a single DTPA conjugated to the moAb. In addition, radioyttrium labeling did not alter the immunoreactivity of the moAb-PAMAM-DOTA complex. Cold Gd(III) complexes also readily formed with the DOTA and DTPA-dendrimer-moAb conjugates. These positive results pave the way for the construction of successful dendrimer- $\alpha$  emitter conjugates for use in radiotherapy.

**2.1.3. Dendrimer-Auger Electron Emitter Conjugates.** Auger electron emitters under investigation in therapy include bromine-77 ( $^{77}\text{Br}$ ), indium-111 ( $^{111}\text{In}$ ), iodine-123 ( $^{123}\text{I}$ ), and iodine-125 ( $^{125}\text{I}$ ).<sup>89</sup> As for  $\alpha$  particles, the precise subcellular localization of Auger emitters can dramatically affect their killing efficacy, with nuclear internalization resulting in significant efficiency compared to localization at the cell surface.<sup>90</sup> For instance, Auger electrons from neutron-activated Gd(III) are strongly cytotoxic, but only when Gd(III) ions have been internalized into cells. The group of Kobayashi<sup>91</sup> used G6 PAMAM dendrimers conjugated with a DTPA derivative and avidin (Av-G6Gd), for targeted delivery of large quantities of Gd(III) into peritoneal carcinomatosis tumor cells with the aim of generating Auger emission with an external neutron beam. Av-G6Gd significantly accumulated and internalized into tumor cells both *in vitro* and *in vivo*, and the cytotoxic effect of the external irradiation with appropriate neutron beam was monitored with MRI (Figure 5).

In another example by the same group, an Av-G4 PAMAM-1B4M chelate complex radiolabeled with  $^{111}\text{In}$ , which emits Auger and conversion electrons, was synthesized for internal radiation therapy in intraperitoneal (i.p.) disseminated

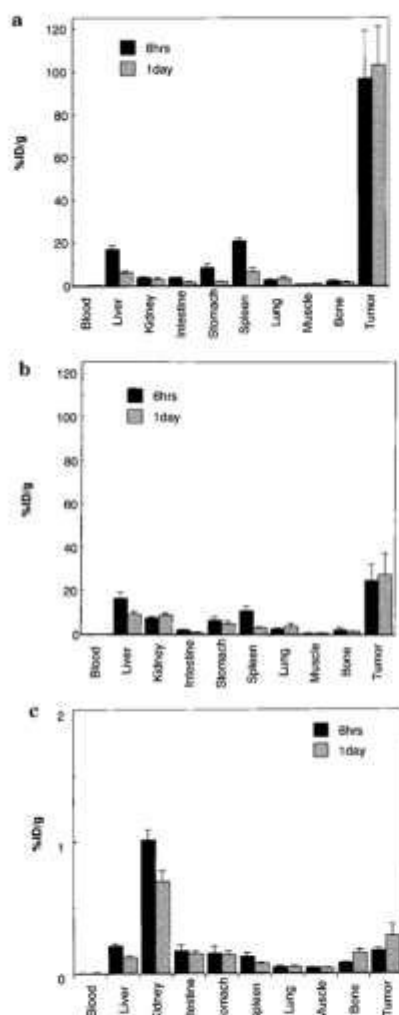


**Figure 5.** Biodistribution of  $^{153}\text{Gd}$ -labeled Av-G6Gd (a), G6Gd (b), and Gd-DTPA (c) at 6 h (black bars) and 1 day (hatched bars) after i.p. injection in nude mice bearing SHIN3 intraperitoneal disseminated tumors. The data are expressed as the mean percentages of injected dose per gram of normal tissues and standard deviation ( $n = 4-6$ ). All data show significant differences ( $p < 0.01$ ) compared with the appropriate group of data with Gd-DTPA. Reprinted with permission from ref 91. Copyright 2001 American Chemical Society.

tumors.<sup>92</sup> The chelating sites on Av-G4-(1B4M)<sub>52</sub> were saturated with either radioactive or nonradioactive In(III). The results of this work clearly show the capability of Av-Bt-G4-(1B4M)<sub>52</sub> to specifically internalize cancer cells. The

biodistribution studies of both  $^{111}\text{In}$  saturated and unsaturated dendrimers in nude mice demonstrated high dendrimer concentration in i.p. disseminated tumors with high tumor/background ratios.

In a more recent study,<sup>76</sup> G1 and G4 PAMAM dendrimers were conjugated with a bifunctional pyridine-*N*-oxide DOTA analog and radiolabeled with  $^{111}\text{In}$ . The conjugate displayed a good kinetic stability for at least 48 h after preparation. Biodistribution and elimination in rats was more favorable for the G1- $^{111}\text{In}$  conjugate than for G4. Thus, while G1- $^{111}\text{In}$  conjugate was rapidly eliminated from the body, mainly through urine, significant, and long-term radioactivity uptake in the liver and kidney was observed for G4- $^{111}\text{In}$ .

**2.1.4. Dendrimers in Boron Neutron Capture Therapy.** Boron neutron capture therapy (BNCT) is a radiation therapy modality accomplished in two stages. First, a patient is injected with a nonradioactive pharmaceutical containing a stable isotope of boron ( $^{10}\text{B}$ ), which selectively migrates to cancer cells. Next, upon irradiation with a neutral beam of low-energy or thermal neutrons boron atoms generate  $\alpha$  particles that destroy the tumor, leaving normal cells unaffected. In order to sustain a lethal effect a large number of  $^{10}\text{B}$  atoms must be delivered to each cancer cell.<sup>93,94</sup>

The high cargo loading of dendrimers has been exploited to this end. Various dendrimers covalently attached to boron have been prepared and tested with preliminary positive results. A methodology was developed to heavily boronate a moAb by coupling to a boronated PAMAM dendrimer by means of heterobifunctional reagents.<sup>95</sup> These conjugates retained the high in vitro immunoreactivity of the moAb, but after intravenous injection they accumulated in the liver. This way of injection resulted in a decrease of the in vivo tumor targeting properties of the conjugates. In order to avoid this biodistribution hurdle, an intratumoral injection of the boronated dendrimers was investigated with encouraging results. Later on, the same group<sup>96</sup> has conjugated a heavily boronated G5 PAMAM dendrimer (G5-B<sub>1100</sub>) to the Cetuximab moAb, as a boron delivery agent for BNCT to brain tumor. When injected intracerebrally, the complex showed specific molecular targeting of the epidermal growth factor receptor (EGFR), which is often amplified in human gliomas.

In an effort to improve the biodistribution and decrease reticulo-endothelial system (RES) uptake, various studies have focused on the modification of boronated PAMAM dendrimers with PEG. Since the expression of the folate receptor is amplified in a variety of human tumors, FA is frequently used to enhance the tumoral uptake of dendrimers and other

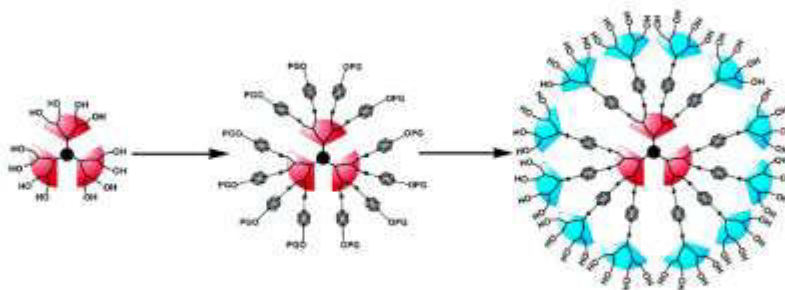


**Figure 6.** Schematic representation of the incorporation of carboranes into polyester dendrimers. Reprinted with permission from ref 98. Copyright 2005 American Chemical Society.

nanosystems. In this context, the group of Tjarks and co-workers<sup>97</sup> evaluated a series of boronated G3 PAMAM dendrimers containing 12–15 decaborate clusters, along with PEG chains to minimize hepatic uptake and FA for folate receptor targeting. One of the conjugates having an average of one PEG<sub>2000</sub> chain and one FA-PEG<sub>800</sub> resulted in selective tumor uptake (6.0% ID/g tumor) in C57BL/6 mice bearing folate receptor (+) murine 24JK-FBP sarcomas. In spite of this result, high hepatic (38.8% ID/g) and renal (62.8% ID/g) uptakes were also revealed. The authors concluded that even though the strategy was successful in increasing tumor selectivity, further improvements were necessary to optimize biodistribution.

An alternative strategy to optimize the delivery of boronated dendrimers to tumor cells is the incorporation of carborane cages within the dendritic structure (Figure 6). The group of Adronov<sup>98</sup> synthesized a family of biocompatible water-soluble, aliphatic polyester dendrimers that incorporate as many as 16 p-carboranes in their interior, as possible candidates for use in BNCT. In another example, phenylene-cored carborane dendrimers have been synthesized for BNCT.<sup>99</sup> In vitro studies with these dendrimers in human liver cancer cells showed a concentration-dependent accumulation of the dendrimer conjugates. Similarly, biocompatible Au nanoparticles containing carborane clusters and PEG chains attached to dendrons were engineered to provide a BNCT platform with potential simultaneous use in photothermotherapy, imaging, and drug vectorization.<sup>100</sup>

The photoluminescence of different generations of porphyrin-cored aryl ether dendrimers functionalized with carborane clusters has been investigated.<sup>101</sup> It was concluded that the photoluminescence properties of these dendrimers were not largely affected by the carboranes, opening the door for further investigations of these systems for theranostic use in nanomedicine. More recently,<sup>102</sup> a dendritic wedge with high boron content for BNCT or boron MRI was combined with a monomethine cyanine dye for visible-light fluorescent imaging, and an integrin ligand for efficient tumor targeting. This conjugate resulted in a rapid intratumoral accumulation and prolonged retention when analyzed in fully established animal models of human melanoma and murine mammary adenocarcinoma (Figure 7).

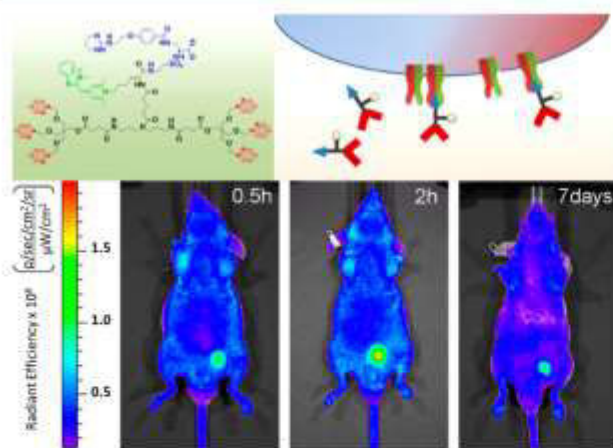


**Figure 7.** Representative fluorescence images of the in vivo tumor uptake of a trifunctional dendritic theranostic agent. Adapted with permission from ref 102. Copyright 2014 American Chemical Society.

**2.2. Dendrimer–Antibody Conjugates in Radioimmunotherapy.** Antibodies have the unique property to bind their targets in a highly selective manner, which makes them attractive for the delivery of radiotherapeutics. Phase I clinical trials have been performed with monoclonal antibodies (moAbs) radiolabeled with  $\alpha$  emitters <sup>213</sup>Bi and <sup>211</sup>At. These systems were evaluated in patients with leukemia and brain tumors,<sup>5</sup> respectively, with encouraging responses and acceptable levels of toxicity in normal tissues.

The first bifunctional chelate used to bind <sup>213</sup>Bi to moAbs was *trans*-cyclohexyl diethylene triamine pentaacetic acid (CHX-A-DTPA), with a procedure requiring 0.5 h.<sup>103</sup> Other ligands derived from DTPA were later on synthesized for the same purpose, including the cyclic anhydride of diethylene triamine penta-acetic acid (cDTPAa)<sup>104</sup> and *p*-isothiocyanatobenzyl-DTPA (CITC-DTPA).<sup>105</sup> Zalutsky and co-workers<sup>106,107</sup> developed a two-step method for the radiolabeling of intact or fragments of chimeric moAbs with <sup>211</sup>At using two similar bifunctional chelating agents [N-succinimidyl 3-(tri-n-butylstannyl) benzoate (m-BuATE) and N-succinimidyl 3-(tri-n-methylstannyl) benzoate (m-MeATE)] in a procedure lasting 1.5 h.

Tumor targeting studies with these radiolabeled moAbs showed, however, some limitations, such as insufficient targeting, low accumulation in tumor sites, and undesired irradiation of normal tissues associated with low clearance rates of IgG-based radioimmunoconjugates (days to weeks).<sup>108</sup> Also, the introduction of more than one radionuclide per moAbs, to enhance the radioactive dose, caused a drastic decrease in immunoreactivity. The attachment of any therapeutic moiety to antibodies influences their clearance kinetics, biodistribution, and side effects of radio-immunoconjugates.<sup>109</sup> Another important issue in the use of moAbs for targeted radiotherapy was the slow reaction kinetics in the formation of the ligand–metal complex, when macrocyclic bifunctional chelating ligands, such as DOTA or DTPA derivatives, were attached to them.<sup>110,111</sup> When the number of chelating groups into the structure of moAbs was increased to speed up complexation, a substantial loss in immunoreactivity was observed.<sup>112</sup> The extent of antibody loading is a critical issue for the design of highly effective immunoconjugates and still largely a subject of empirical evaluation. Indeed, amino acids amenable to modification are found along all regions of antibodies. Since most modification methods are not site-specific, there is no control over which amino acids are modified. This frequently results in immunoconjugates modified at positions weakening the binding to the antigen which, in turn, decreases the efficacy of the targeting system.<sup>108</sup> So, one of the actual challenges of immunoconjugation is product homogeneity with regard to site-specificity and stoichiometry of antibody modification.<sup>113,114</sup> Site-specifically conjugated tumor-targeting antibodies have been shown to exhibit a greater uptake at the cancerous site and less nonspecific uptake compared to heterogeneous immunoconjugates.<sup>115</sup> The most challenging issue for radioimmunotherapy (RIT) is to find the correct balance between the dose delivered to the tumor and exposure of normal organs and tissues to radiation.<sup>116</sup>

Also, in order to improve tumor/blood ratios, antibody fragments lacking the Fc part have been tested for radio-immunoconjugation.<sup>117</sup> Invariably, however, only a small fraction of the administered dose localizes in the tumor, rendering doses delivered to the tumor low for therapeutic applications.

In recent years, to solve these problems, dendritic systems have been conjugated to antibodies to preserve their immunoreactivity, while providing high specific activities and efficient radiolabeling.<sup>88,96,118</sup> Indeed, the branched structure of dendrimers creates a multivalent surface with a high number of peripheral groups, which makes them unique candidates for conjugating to antibodies to afford log-fold higher radioactivities than current antibodies with promising results.<sup>119</sup>

The use of dendrimers for potentially improving delivery of radioimmunotherapy conjugates is in its early phases of development. One of the first reports in this area came from Roberts and co-workers,<sup>120</sup> who conjugated PAMAM dendrimers to IgG-antibodies in a two-step process and demonstrated for the first time that their immunoreactivity remained largely unaffected after dendrimer conjugation using sensitive enzyme linked immunoassays (ELISA).

In 1999, the group of Kobayashi<sup>121</sup> described the biodistribution of <sup>111</sup>In- and <sup>88</sup>Y-labeled G2 PAMAM dendrimers conjugated to IB4M and an anti-Tac IgG antibody. Tumor xenografts were generated in 5–6-week-old female athymic nude mice, with ATAC4 cell line. High tumor absorption of the conjugates was observed, although accompanied by high accumulation in liver, kidney and spleen that could be decreased by saturating the chelates with cold metals. Interestingly, saturation of the IB4M chelates with Y(III) was shown to be more effective to decrease liver and spleen accumulation, in comparison with In(III). This fact probably relates a lower stability of the In(III) chelates in vivo that results in free IB4M ligands and concomitant faster opsonization and uptake by RES.

In a more recent study by the same group,<sup>122</sup> G4 PAMAM dendrimers conjugated to IB4M and OST7, a murine monoclonal IgG1, were labeled with <sup>111</sup>In and <sup>153</sup>Gd. The radiometal labeling was achieved with very high specific radioactivity and minimal loss of immunoreactivity. Biodistribution studies in a mice model with KT005-specific tumors, showed specific tumor accumulation and rapid blood clearance. Again, the saturation of the IB4M ligands with Gd(III) was more effective in decreasing liver and spleen accumulation than with In(III). Additionally, clearance times of unsaturated preparations were significantly slower than those of the saturated ones. As a result, it can be concluded that charge and molecular weight are not the only factors affecting biodistribution, and that the surface functionalization of dendrimers is critical to reduce their liver and spleen uptake.

The tumor selectivity of dendrimer-antibody conjugates has been investigated by Baker and co-workers.<sup>118</sup> PAMAM dendrimers were conjugated to two different antibodies, 60bca and J591, which bind to CD14 and prostate-specific membrane antigen (PSMA), respectively. It was revealed that the antibody-conjugated dendrimers specifically bind to the antigen-expressing cells in a time- and dose-dependent manner, with affinity similar to that of the free antibodies.

To study the effect of dendrimer size and number on the immunoreactivity of moAbs, several DOTA-containing PAMAM dendrimers of different generations were synthesized and conjugated to antibodies for radioimmunotherapy and clinical diagnostics (Figure 8).<sup>123</sup> It was concluded that the dendrimer size does not significantly influence the immunoreactivity of the conjugated antibody over a wide range of molecular weights, whereas increasing the number of conjugation sites has a clear detrimental effect. Therefore, to obtain conjugates that result in a minor compromise of

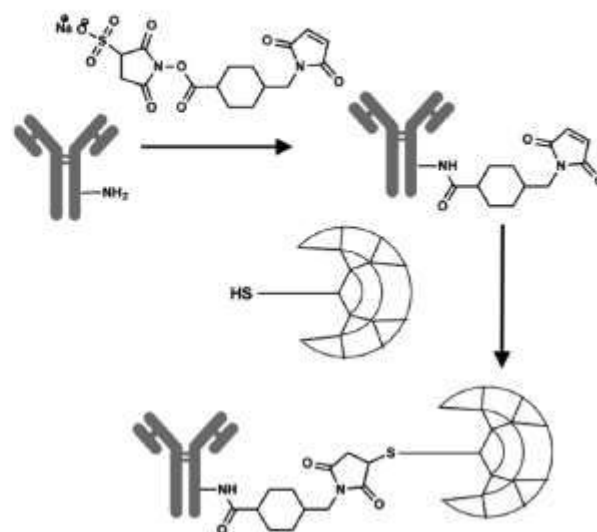


Figure 8. Scheme of the conjugation of DOTA-dendrimers to an antibody. Adapted with permission from ref 123. Copyright 2008 American Chemical Society.

immunoreactivity, antibodies should be functionalized with few large dendritic systems. Further studies are necessary to establish the clinical usefulness of dendrimer-conjugates for radioimmunotherapy.

### 2.3. Dendrimers in Gene Delivery Radiotherapy.

**2.3.1. Dendrimers in Radiovirotherapy.** Radiovirotherapy is an innovative strategy for radioisotopic therapy that uses oncolytic viruses able to selectively target and kill cancer cells.<sup>124</sup> The combination of oncolytic viruses and radiation can have synergistic antitumor properties by selectively delivering radiation therapy to tumor cells.

The sodium/iodide symporter (NIS) is the main transgene that has been studied with this aim.<sup>125</sup> NIS, is a transmembrane glycoprotein that has a crucial role in the biosynthesis of thyroid hormones<sup>126</sup> that is also known to be able to mediate the uptake of radionuclides, such as <sup>131</sup>I, <sup>188</sup>Re, or <sup>211</sup>At. While NIS expression in thyroid cancers decreases as the cancer cell differentiation decreases,<sup>127</sup> NIS expression is found in a number of other nonthyroid cancers, like breast and liver.<sup>128–130</sup> While, NIS expression in breast cancer cells is stimulated by retinoic acid (RA), estrogen, and glucocorticoids, in the stomach the expression is generally suppressed during carcinogenesis. In liver cancers, NIS is expressed in all cholangiocarcinomas (CCA) and in a small proportion of hepatocellular carcinomas (HCC).

Accordingly, the use of a viral vector for NIS gene transfer to infected tumor cells is envisaged as a means to improve the delivery of radioisotopes. Among the oncolytic viruses for this purpose, adenoviruses are the preferred vectors, as they are known to selectively infect and replicate in cancer cells. Adenovirus-mediated gene therapy has nevertheless some limitations, such as high prevalence of neutralizing antibodies, widespread expression of the coxsackie-adenovirus receptor (CAR), and unexpected interactions with host proteins in vivo. In addition, targeting adenoviruses to receptors on hepatocytes results in vector sequestration in liver.<sup>131</sup> Therefore, with the aim of improving an efficacious targeting to tumor sites and limit nonspecific uptake of viruses to nontarget tissues (mainly liver and spleen), it has been necessary to develop suitable

strategies to modify the capsid proteins on the virus shell, including the use of dendrimer coatings.

With the aim of developing adenoviral vectors for a combined systemic oncolytic virotherapy and NIS-mediated radiotherapy, the groups of Spitzweg and Ogris<sup>132</sup> in collaboration recently used PAMAM dendrimers with positively charged terminal amines to coat the negatively charged adenoviral capsid of Ad5-E1/AFP-E3/NIS by electrostatic interactions. NIS expression was followed with noninvasive imaging by <sup>125</sup>I scintigraphy. In vivo tests in a liver cancer xenograft mouse model (Figure 9) showed significantly lower

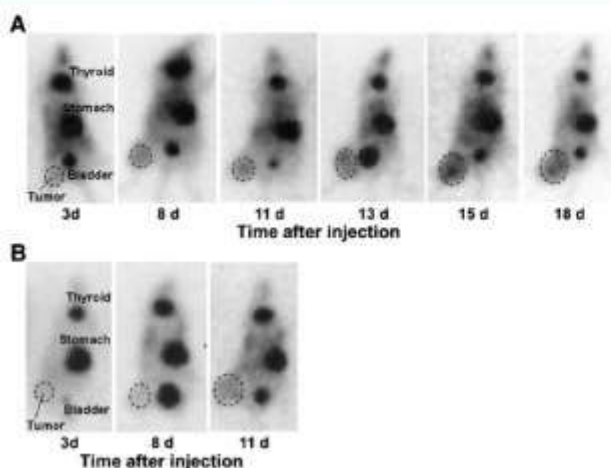


**Figure 9.** <sup>125</sup>I scintigraphy confirms significantly increased levels of tumor-specific iodide accumulation after application of coated adenovirus (A) as compared with injection of uncoated virus (B). Reprinted with permission from ref 132. Copyright 2013 Society of Nuclear Medicine and Molecular Imaging, Inc.

hepatic accumulation of <sup>125</sup>I after systemic application. More importantly, the combined radiovirotherapy using the dendrimer-coated Ad5-E1/AFP-E3/NIS (dc300Ad5-E1/AFP-E3/NIS), followed by a single application of a therapeutic dose of <sup>131</sup>I, resulted in a stronger stimulation of the therapeutic effect, as observed by an extensively delayed tumor growth and prolonged survival in comparison with virotherapy alone or with control groups using the uncoated vector.

In another study from the same group,<sup>133</sup> tumor-selective iodide uptake and therapeutic efficacy of combined radiovirotherapy was reported after systemic delivery of a theranostic NIS gene using a dendrimer-coated adenovirus. In this case the dendritic coating consisted of PAMAM dendrimers linked to an EGFR specific peptide ligand (GE11). As above, injection of the uncoated adenovirus in a liver cancer xenograft mouse model led to high levels of NIS expression in the liver due to hepatic sequestration, which were significantly reduced after dendrimer coating as demonstrated by <sup>125</sup>I-scintigraphy. The EGFR targeting specificity was confirmed by <sup>124</sup>I-PET-imaging (Figure 10), showing a significantly lower tumoral radioiodine accumulation after pretreatment with the EGFR-specific antibody cetuximab. The enhanced oncolytic effect following systemic application of the dendrimer-coated adenovirus was further increased by additional treatment with a therapeutic dose of <sup>131</sup>I (Figure 10).

Altogether, these results show that coating of adenoviral vectors with synthetic dendrimers is a promising strategy for effective adenovirus liver detargeting and tumor retargeting,

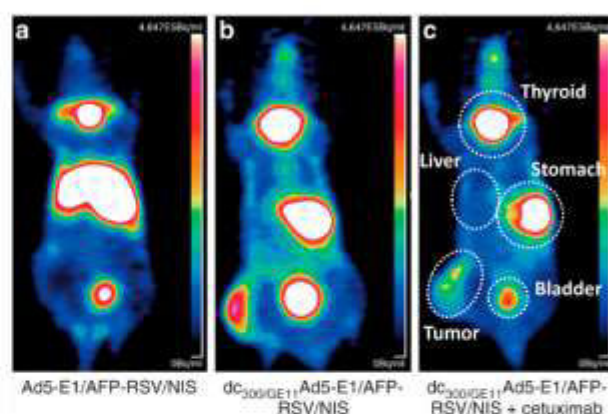


**Figure 10.** <sup>124</sup>I-PET-imaging shows that the strong hepatic transduction after i.v. injection of an uncoated adenoviral vector (Ad5-E1/AFP-RSV/NIS) (a) is significantly reduced by coating with PAMAM-G2 linked to peptide GE11 (dc<sub>300</sub>/GE11-Ad5-E1/AFP-RSV/NIS) (b), even when mice are treated with the monoclonal anti-EGFR antibody cetuximab before systemic administration (c). Significantly higher transduction of tumor xenografts was observed in (b) than (c). Adapted with permission from ref 133. Copyright 2013 Macmillan Publishers Ltd.: <http://www.nature.com/mtna/journal/v2/n11/full/mtna201358a.html>.

taking advantage of the merging of nonviral and viral vector technologies.

**2.3.2. Dendrimers in Combined Nonviral Gene Delivery and Radiotherapy.** Since dendrimers on their own provide efficient and safe nonviral vectors for the delivery of genes into target cells,<sup>134</sup> they have been also assayed for gene delivery radiotherapy. In a preclinical study, the groups of Spitzweg and Ogris<sup>135</sup> used G2 oligoethylenimine (OEI)-grafted polypropylene dendrimers (PPI) as novel and highly efficient nonviral gene delivery vehicles for systemic NIS gene transfer (G2-HD-OEI/NIS) in a syngeneic neuroblastoma mouse model. Based on its dual function as reporter and gene therapy, NIS was used for noninvasive imaging of the biodistribution of the dendrimer conjugates by <sup>125</sup>I-scintigraphy, followed by assessment of the therapy response after application of <sup>131</sup>I. Tumor-specific iodide accumulation was shown to be sufficiently high for a significant delay of tumor growth, as observed by an increased survival rate after application of two cycles of NIS-dendrimer conjugates followed by <sup>131</sup>I radiotherapy.

In a more recent contribution,<sup>136</sup> the radiosensitivity of human uveal primary tumor, which is the most common primary intraocular tumor, was efficiently improved in vitro, when dendrimers were used as a vector to produce coexpression gene therapy of TNF $\alpha$  and HSV-TK, followed by exposure to <sup>125</sup>I after transfection.

### 3. CONCLUSIONS AND FUTURE PERSPECTIVES

In order to improve the efficacy of internal radiotherapy as one of the most commonly used cancer treatments, nuclear medicine has recently turned the attention to new oncologic strategies based on nanovectorization, often referred to as radionanomedicine. The ultimate aim is to efficiently target and retain radiation at the tumor site, avoiding side effects such as toxicity and tumor resistance process. Thus, it is known that nanosystems with long circulation times in the bloodstream can get internalized and retained into tumors thanks to a leaky

vasculature and an abnormal lymphatic drainage. This effect, known as EPR, can be further assisted by the use of targeting agents. The objective of radionanotherapy is the labeling of nanosystems with radionuclides to improve the efficiency of the treatment, while reducing the dose of radiolabeled materials *in vivo*. Among the nanosystems described for this purpose, dendrimers are especially appealing because of their multivalency, tunable size and physicochemical properties as a function of the generation. Milestones in the development of dendrimers for nanovectorized radiotherapy include their functionalization with ligands for radiolabeling, targeting agents, and stealth functional groups to potentially improve their biodistribution, circulation times, and stability *in vivo*.

The active role of dendrimers as innovative radiopharmaceuticals is reviewed with a special focus on critical challenges encountered in the advance of targeted radiotherapy. As discussed, the radiolabeling of dendrimers with therapeutic radionuclides has resulted in tumor regression and longer survival. The biodistribution of dendritic conjugates can be improved by PEGylation, intratumoral application, saturation with cold metals, or by modulating their charge and molecular weight. In addition, the multifunctionality of dendrimers makes them excellent candidates for theranostics. For instance, optimized delivery of boron compounds to tumor cells was achieved by incorporating carborane cages within biodegradable dendrimers, which proved useful as theranostic agents in a combined use of BNCT, photothermotherapy, imaging, and drug vectorization. The development of radiotherapeutic dendrimers for image-guided radionuclide therapies is also a work in progress. The multivalency and precise architecture of dendrimers can be exploited for radiotherapy in combination with mAbs, a strategy that pursues minor changes in immunoreactivity. Finally, dendrimers have been investigated in radiotherapy as coatings of adenoviral vectors for effective liver detargeting and tumor retargeting, as well as nonviral gene delivery vectors for NIS-targeted radionuclide therapy of metastatic cancer.

Although issues associated with *in vivo* properties and the toxicity of dendrimer conjugates are challenges to be addressed individually, as a whole there are considerable promise and benefits on current applications of dendrimers for radionanotherapy. A proper evaluation of dendrimer-based radiopharmaceuticals must be appreciated according to three criteria: the choice of radionuclide, the vector used, and the modalities of administration. Relatively recent results on dendrimer-based radiopharmaceuticals in preclinical models do not permit such a comparison yet. As discussed in this review, the physicochemical properties of the radionuclide are crucial, but differences between vectors (untargeted vs targeted dendrimer, different dendrimer generations) are appreciated after intravenous injections with the aim of qualifying the targeting rather than the efficacy. In fact, for medical applications with radiopharmaceuticals, loco-regional injection could be a preferred way, where dendrimers play the role of confining agent at the injection site, in order to reduce the associated radio toxicity on healthy tissues or organs. Targeting will increase this confining action as needed for alpha-emitter and Auger-emitter.

## AUTHOR INFORMATION

### Corresponding Authors

\*Tel.: +33 244 68 85 29. Fax: +33 244 68 85 46. E-mail: francois.hindre@univ-angers.fr.

\*Tel.: +34 881 815 727. Fax: +34 881 815 704. E-mail: ef.megia@usc.es.

### Notes

The authors declare no competing financial interest.

## ACKNOWLEDGMENTS

This work was financially supported by the Spanish Government (CTQ2015-69021-R, CTQ2012-34790) and the Xunta de Galicia (GRC2014/040) and by the "Institut National de la Santé et de la Recherche Médicale" (INSERM), by the "Axe Vectorisation and Radiothérapies" and the "Réseau Gliome Grand Ouest" (ReGGO) of the "Cancéropôle Grand-Ouest". The coauthors of this manuscript are also members of the LabEx IRON "Innovative Radiopharmaceuticals in Oncology and Neurology" as part of the french government program "Investissements d'Avenir". F.L. thanks the European Commission, Education, Audiovisual and Cultural Executive Agency (EACEA) for an Erasmus Mundus Grant under the NanoFar Joint Doctoral Program.

## REFERENCES

- Bernier, J.; Hall, E. J.; Giaccia, A. *Nat. Rev. Cancer* **2004**, *4*, 737.
- Begg, A. C.; Stewart, F. A.; Vens, C. *Nat. Rev. Cancer* **2011**, *11*, 239.
- West, C. M.; Barnett, G. C. *Genome Med.* **2011**, *3*, 52.
- McDevitt, M. R.; Ma, D. S.; Lai, L. T.; Simon, J.; Borchardt, P.; Frank, R. K.; Wu, K.; Pellegrini, V.; Curcio, M. J.; Miederer, M.; Bander, N. H.; Scheimberg, D. A. *Science* **2001**, *294*, 1537.
- Couturier, O.; Supiot, S.; Degraef-Mougin, M.; Faivre-Chauvet, A.; Carlier, T.; Chatal, J.-F.; Davodeau, F.; Cherel, M. *Eur. J. Nucl. Med. Mol. Imaging* **2005**, *32*, 601.
- Akabani, G.; Carlin, S.; Welsh, P.; Zalutsky, M. R. *Nucl. Med. Biol.* **2006**, *33*, 333.
- Hassfjell, C. S. S. P. *Int. J. Radiat. Biol.* **2000**, *76*, 1315.
- Wheldon, T. E.; O'Donoghue, J. A. *Int. J. Radiat. Biol.* **1990**, *58*, 1.
- Zaidi, H.; Sgouros, G. *Therapeutic Applications of Monte Carlo Calculations in Nuclear Medicine*; CRC Press, 2002.
- Kassis, A. I. *Int. J. Radiat. Biol.* **2004**, *80*, 789.
- Chen, P.; Wang, J.; Hope, K.; Jin, L.; Dick, J.; Cameron, R.; Brandwein, J.; Minden, M.; Reilly, R. M. *J. Nucl. Med.* **2006**, *47*, 827.
- Adelstein, S. J.; Kassis, A. I.; Bodei, L.; Mariani, G. *Cancer Biother. Radiopharm.* **2003**, *18*, 301.
- Unak, P. *Braz. Arch. Biol. Technol.* **2002**, *45*, 97.
- Hamoudeh, M.; Kamleh, M. A.; Diab, R.; Fessi, H. *Adv. Drug Delivery Rev.* **2008**, *60*, 1329.
- Tamblyn, M. *Cancer Control* **2012**, *19*, 137.
- Speer, T. W. *Targeted Radionuclide Therapy*; Lippincott Williams & Wilkins, 2012.
- Audi, G.; Wapstra, A. *Nucl. Phys. A* **1995**, *595*, 409.
- Kassis, A. I. *Semin. Nucl. Med.* **2008**, *38*, 358.
- Korkolis, D. P.; Plataniotis, G. D.; Gondikakis, E.; Xinopoulos, D.; Koulaxouzidis, G. V.; Katsilieris, J.; Vassilopoulos, P. P. *Int. J. Colorectal Dis.* **2006**, *21*, 1.
- Pajonk, F.; Vlaski, E.; McBride, W. H. *Stem Cells* **2010**, *28*, 639.
- Vanpouille-Box, C.; Hindré, F. *Front. Oncol.* **2012**, *2*, 136.
- Lee, D. S.; Im, H.-J.; Lee, Y.-S. *Nanomedicine* **2015**, *11*, 795.
- McGrady, E.; Conger, S.; Blanke, S.; Landry, B. J. *J. Healthc. Manag.* **2010**, *55*, 353.
- Bharali, D. J.; Mousa, S. A. *Pharmacol. Ther.* **2010**, *128*, 324.
- Panchapakesan, B.; Wickstrom, E. *Surg. Oncol. Clin. N. Am.* **2007**, *16*, 293.
- Bawa, R. *Curr. Drug Deliv.* **2011**, *8*, 227.
- Maeda, H. *Bioconjugate Chem.* **2010**, *21*, 797.
- Prabhakar, U.; Maeda, H.; Jain, R. K.; Sevick-Muraca, E. M.; Zamboni, W.; Farokhzad, O. C.; Barry, S. T.; Gabizon, A.; Grodzinski, P.; Blakey, D. C. *Cancer Res.* **2013**, *73*, 2412.

- (29) Khan, M. K.; Nigavekar, S. S.; Minc, L. D.; Kariapper, M. S. T.; Nair, B. M.; Lesniak, W. G.; Balogh, L. P. *Technol. Cancer Res. Treat.* **2005**, *4*, 603.
- (30) Qiao, Z.; Shi, X. *Prog. Polym. Sci.* **2015**, *44*, 1.
- (31) Liu, K.; Xu, Z.; Yin, M. *Prog. Polym. Sci.* **2015**, *46*, 25.
- (32) Tomalia, D. A. *Nanomedicine* **2006**, *2*, 309.
- (33) Svenson, S.; Tomalia, D. A. *Adv. Drug Delivery Rev.* **2005**, *57*, 2106.
- (34) Koo, O. M.; Rubinstein, I.; Onyukel, H. *Nanomedicine* **2005**, *1*, 193.
- (35) Wolinsky, J. B.; Grinstaff, M. W. *Adv. Drug Delivery Rev.* **2008**, *60*, 1037.
- (36) Menjoge, A. R.; Kannan, R. M.; Tomalia, D. A. *Drug Discovery Today* **2010**, *15*, 171.
- (37) Kesharwani, P.; Iyer, A. K. *Drug Discovery Today* **2015**, *20*, 536.
- (38) Goldenberg, D. *Crit. Rev. Oncol. Hemat.* **2001**, *39*, 195.
- (39) Macklis, R. M.; Pohlman, B. *Int. J. Radiat. Oncol., Biol., Phys.* **2006**, *66*, 833.
- (40) Davies, A. J. *Oncogene* **2007**, *26*, 3614.
- (41) Jacene, H. A.; Filice, R.; Kasecamp, W.; Wahl, R. L. *J. Nucl. Med.* **2007**, *48*, 1767.
- (42) Lang, J.; Lan, X.; Liu, Y.; Jin, X.; Wu, T.; Sun, X.; Wen, Q.; An, R. *Nucl. Med. Biol.* **2015**, *42*, 505.
- (43) Kim, M.-k.; Jeong, H.-j.; Kao, C.-H. K.; Yao, Z.; Paik, D. S.; Pie, J. E.; Kobayashi, H.; Waldmann, T. A.; Carrasquillo, J. A.; Paik, C. H. *Nucl. Med. Biol.* **2002**, *29*, 139.
- (44) Brady, L. W.; Woo, D. V.; Heindel, N. D.; Markoe, A. M.; Koprowski, H. *Int. J. Radiat. Oncol., Biol., Phys.* **1987**, *13*, 1535.
- (45) Lavie, E.; Boazi, M.; Weininger, J.; Bitton, M.; Yosilevski, G.; Front, D.; Hirshaut, Y.; Robinson, E.; Bartal, A. H. *Radiother. Oncol.* **1987**, *8*, 129.
- (46) Epenetos, A. A.; Snook, D.; Hooker, G.; Lavender, J. P.; Halnan, K. E. *Lancet* **1984**, *324*, 169.
- (47) Gudkov, S.; Shilyagina, N.; Vodeneev, V.; Zvyagin, A. *Int. J. Mol. Sci.* **2016**, *17*, 33.
- (48) Buhleier, E.; Wehner, W.; Vogtle, F. *Synthesis* **1978**, *1978*, 155.
- (49) Newkome, G. R.; Yao, Z.; Baker, G. R.; Gupta, V. K. *J. Org. Chem.* **1985**, *50*, 2003.
- (50) Tomalia, D. A.; Baker, H.; Dewald, J.; Hall, M.; Kallos, G.; Martin, S.; Roeck, J.; Ryder, J.; Smith, P. *Polym. J.* **1985**, *17*, 117.
- (51) Wang, D.; Astruc, D. *Coord. Chem. Rev.* **2013**, *257*, 2317.
- (52) Mintzer, M. A.; Grinstaff, M. W. *Chem. Soc. Rev.* **2011**, *40*, 173.
- (53) Tekade, R. K.; Kumar, P. V.; Jain, N. K. *Chem. Rev.* **2009**, *109*, 49.
- (54) Medina, S. H.; El-Sayed, M. E. *Chem. Rev.* **2009**, *109*, 3141.
- (55) Dufes, C.; Ucheqbu, I. F.; Schatzlein, A. G. *Adv. Drug Delivery Rev.* **2005**, *57*, 2177.
- (56) Rolland, O.; Turrin, C.-O.; Caminade, A.-M.; Majoral, J.-P. *New J. Chem.* **2009**, *33*, 1809.
- (57) Astruc, D.; Boisselier, E.; Ornelas, C. *Chem. Rev.* **2010**, *110*, 1857.
- (58) Reek, J. N. H.; Arévalo, S.; van Heerbeek, R.; Kamer, P. C. J.; van Leeuwen, P. W. N. M. In *Adv. Catal.*; Bruce, C. G., Helmut, K., Eds.; Academic Press, 2006; Vol. 49, p 71.
- (59) Rosen, B. M.; Wilson, C. J.; Wilson, D. A.; Peterca, M.; Imam, M. R.; Percec, V. *Chem. Rev.* **2009**, *109*, 6275.
- (60) Esfand, R.; Tomalia, D. A. *Drug Discovery Today* **2001**, *6*, 427.
- (61) de Brabander-van den Berg, E. M. M.; Meijer, E. W. *Angew. Chem., Int. Ed. Engl.* **1993**, *32*, 1308.
- (62) Hawker, C. J.; Fréchet, J. M. J. *J. Am. Chem. Soc.* **1990**, *112*, 7638.
- (63) Carnahan, M. A.; Grinstaff, M. W. *Macromolecules* **2006**, *39*, 609.
- (64) Ihre, H.; Padilla De Jesús, O. L.; Fréchet, J. M. J. *J. Am. Chem. Soc.* **2001**, *123*, 5908.
- (65) Majoral, J. P.; Caminade, A. M. *Chem. Rev.* **1999**, *99*, 845.
- (66) Patri, A. K.; Kukowska-Latallo, J. F.; Baker, J., Jr. *Adv. Drug Delivery Rev.* **2005**, *57*, 2203.
- (67) Svenson, S. *Chem. Soc. Rev.* **2015**, *44*, 4131.
- (68) Wong, C.-H.; Zimmerman, S. C. *Chem. Commun.* **2013**, *49*, 1679.
- (69) Lallana, E.; Fernandez-Trillo, F.; Sousa-Herves, A.; Riguera, R.; Fernandez-Megia, E. *Pharm. Res.* **2012**, *29*, 902.
- (70) Boas, U.; Heegaard, P. M. H. *Chem. Soc. Rev.* **2004**, *33*, 43.
- (71) Kannan, R. M.; Nance, E.; Kannan, S.; Tomalia, D. A. *J. Intern. Med.* **2014**, *276*, 579.
- (72) Khan, M. K.; Minc, L. D.; Nigavekar, S. S.; Kariapper, M. S. T.; Nair, B. M.; Schipper, M.; Cook, A. C.; Lesniak, W. G.; Balogh, L. P. *Nanomedicine* **2008**, *4*, 57.
- (73) Zalutsky, M. R. In *Handbook of Nuclear Chemistry*; Vértes, A., Nagy, S., Klencsár, Z., Lovas, R., Rösch, F., Eds.; Springer, 2011; p 2179.
- (74) Wei Cui, Y. Z.; Xu, X.; Shen, Y.-M. *Med. Chem.* **2012**, *8*, 727.
- (75) Laznickova, A.; Biricova, V.; Laznicek, M.; Hermann, P. *Appl. Radiat. Isot.* **2014**, *84*, 70.
- (76) Biricová, V.; Lázníčková, A.; Lázníček, M.; Polásek, M.; Hermann, P. *J. Pharm. Biomed. Anal.* **2011**, *56*, 505.
- (77) Zhao, L.; Zhu, J.; Cheng, Y.; Xiong, Z.; Tang, Y.; Guo, L.; Shi, X.; Zhao, J. *ACS Appl. Mater. Interfaces* **2015**, *7*, 19798.
- (78) Zhu, J.; Zhao, L.; Cheng, Y.; Xiong, Z.; Tang, Y.; Shen, M.; Zhao, J.; Shi, X. *Nanoscale* **2015**, *7*, 18169.
- (79) Leiro, V.; García, J. P.; Tomás, H.; Pêgo, A. P. *Bioconjugate Chem.* **2015**, *26*, 1182.
- (80) Cheng, Y.; Zhao, L.; Li, Y.; Xu, T. *Chem. Soc. Rev.* **2011**, *40*, 2673.
- (81) Majoros, I. J.; Myc, A.; Thomas, T.; Mehta, C. B.; Baker, J. R. *Biomacromolecules* **2006**, *7*, 572.
- (82) Venditto, V. J.; Regino, C. A. S.; Brechbiel, M. W. *Mol. Pharmaceutics* **2005**, *2*, 302.
- (83) Xu, X.; Zhang, Y.; Wang, X.; Guo, X.; Zhang, X.; Qi, Y.; Shen, Y.-M. *Bioorg. Med. Chem.* **2011**, *19*, 1643.
- (84) Zhang, Y.; Sun, Y.; Xu, X.; Zhang, X.; Zhu, H.; Huang, L.; Qi, Y.; Shen, Y.-M. *J. Med. Chem.* **2010**, *53*, 3262.
- (85) Agashe, H. B.; Babbar, A. K.; Jain, S.; Sharma, R. K.; Mishra, A. K.; Asthana, A.; Garg, M.; Dutta, T.; Jain, N. K. *Nanomedicine* **2007**, *3*, 120.
- (86) Fisher, D. R. *Curr. Radiopharm.* **2008**, *1*, 127.
- (87) Colletti, P. M. *Clin. Nucl. Med.* **2013**, *38*, 724.
- (88) Wu, C.; Brechbiel, M. W.; Kozak, R. W.; Gansow, O. A. *Bioorg. Med. Chem. Lett.* **1994**, *4*, 449.
- (89) Humm, J. L.; Howell, R. W.; Rao, D. V. *Med. Phys.* **1994**, *21*, 1901.
- (90) Boswell, C. A.; Brechbiel, M. W. *J. Nucl. Med.* **2005**, *46*, 1946.
- (91) Kobayashi, H.; Kawamoto, S.; Saga, T.; Sato, N.; Ishimori, T.; Konishi, J.; Ono, K.; Togashi, K.; Brechbiel, M. W. *Bioconjugate Chem.* **2001**, *12*, 587.
- (92) Mamede, M.; Saga, T.; Kobayashi, H.; Ishimori, T.; Higashi, T.; Sato, N.; Brechbiel, M. W.; Konishi, J. *Clin. Cancer Res.* **2003**, *9*, 3756.
- (93) Barth, R. F.; Coderre, J. A.; Vicente, M. G. H.; Blue, T. E. *Clin. Cancer Res.* **2005**, *11*, 3987.
- (94) Moss, R. L. *Appl. Radiat. Isot.* **2014**, *88*, 2.
- (95) Barth, R.; Soloway, A. *Mol. Chem. Neuropathol.* **1994**, *21*, 139.
- (96) Wu, G.; Barth, R. F.; Yang, W.; Chatterjee, M.; Tjarks, W.; Ciesielski, M. J.; Fenstermaker, R. A. *Bioconjugate Chem.* **2004**, *15*, 185.
- (97) Shukla, S.; Wu, G.; Chatterjee, M.; Yang, W.; Sekido, M.; Diop, L. A.; Müller, R.; Sudimack, J. J.; Lee, R. J.; Barth, R. F.; Tjarks, W. *Bioconjugate Chem.* **2003**, *14*, 158.
- (98) Parrott, M. C.; Marchington, E. B.; Valliant, J. F.; Adronov, A. J. *Am. Chem. Soc.* **2005**, *127*, 12081.
- (99) Dash, B. P.; Satapathy, R.; Bode, B. P.; Reidl, C. T.; Sawicki, J. W.; Mason, A. J.; Maguire, J. A.; Hosmane, N. S. *Organometallics* **2012**, *31*, 2931.
- (100) Li, N.; Zhao, P.; Salmon, L.; Ruiz, J.; Zabawa, M.; Hosmane, N. S.; Astruc, D. *Inorg. Chem.* **2013**, *52*, 11146.
- (101) Cabrera-González, J.; Xochitiotzi-Flores, E.; Viñas, C.; Teixidor, F.; García-Ortega, H.; Farfán, N.; Santillan, R.; Parella, T.; Núñez, R. *Inorg. Chem.* **2015**, *54*, 5021.

- (102) Dubey, R.; Kushal, S.; Mollard, A.; Vojtovich, L.; Oh, P.; Levin, M. D.; Schnitzer, J. E.; Zharov, I.; Olenyuk, B. Z. *Bioconjugate Chem.* **2015**, *26*, 78.
- (103) Brechbiel, M. W.; Gansow, O. A. *J. Chem. Soc., Perkin Trans. 1* **1992**, 1173.
- (104) Abbas Rizvi, S. M.; Henniker, A. J.; Goozee, G.; Allen, B. J. *Leuk. Res.* **2002**, *26*, 37.
- (105) Mishra, A. K.; Iznaga-Escobar, N.; Figueredo, R.; Jain, V. K.; Dwarakanath, B. S.; Perez-Rodriguez, R.; Sharma, R. K.; Mathew, T. L. *Methods Find. Exp. Clin. Pharmacol.* **2002**, *24*, 653.
- (106) Zalutsky, M. R.; Narula, A. S. *Int. J. Rad. Appl. Instrum. A* **1988**, *39*, 227.
- (107) Zalutsky, M. R.; Garg, P. K.; Friedman, H. S.; Bigner, D. D. *Proc. Natl. Acad. Sci. U. S. A.* **1989**, *86*, 7149.
- (108) Garnett, M. C. *Adv. Drug Delivery Rev.* **2001**, *53*, 171.
- (109) Allen, T. M. *Nat. Rev. Cancer* **2002**, *2*, 750.
- (110) Broan, C. J.; Cox, J. P. L.; Craig, A. S.; Katakly, R.; Parker, D.; Harrison, A.; Randall, A. M.; Ferguson, G. J. *Chem. Soc., Perkin Trans. 2* **1991**, 87.
- (111) Rugg, C. L.; Anderson-Berg, W. T.; Brechbiel, M. W.; Mirzadeh, S.; Gansow, O. A.; Strand, M. *Cancer Res.* **1990**, *50*, 4221.
- (112) Brechbiel, M. W.; Gansow, O. A.; Atcher, R. W.; Schlom, J.; Esteban, J.; Simpson, D.; Colcher, D. *Inorg. Chem.* **1986**, *25*, 2772.
- (113) Carter, P. J.; Senter, P. D. *Cancer J.* **2008**, *14*, 154.
- (114) Junutula, J. R.; Bhakta, S.; Raab, H.; Ervin, K. E.; Eigenbrot, C.; Vandlen, R.; Scheller, R. H.; Lowman, H. B. *J. Immunol. Methods* **2008**, *332*, 41.
- (115) Jeger, S.; Zimmermann, K.; Blanc, A.; Grunberg, J.; Honer, M.; Hunziker, P.; Struthers, H.; Schibli, R. *Angew. Chem., Int. Ed.* **2010**, *49*, 9995.
- (116) Wu, A. M.; Senter, P. D. *Nat. Biotechnol.* **2005**, *23*, 1137.
- (117) Sharkey, R. M.; Goldenberg, D. M. *Adv. Drug Delivery Rev.* **2008**, *60*, 1407.
- (118) Thomas, T. P.; Patri, A. K.; Myc, A.; Myaing, M. T.; Ye, J. Y.; Norris, T. B.; Baker, J. R. *Biomacromolecules* **2004**, *5*, 2269.
- (119) Gröhn, F.; Bauer, B. J.; Akpalu, Y. A.; Jackson, C. L.; Amis, E. J. *Macromolecules* **2000**, *33*, 6042.
- (120) Roberts, J. C.; Adams, Y. E.; Tomalia, D.; Mercer-Smith, J. A.; Lavalley, D. K. *Bioconjugate Chem.* **1990**, *1*, 305.
- (121) Kobayashi, H.; Wu, C.; Kim, M.-K.; Paik, C. H.; Carrasquillo, J. A.; Brechbiel, M. W. *Bioconjugate Chem.* **1999**, *10*, 103.
- (122) Kobayashi, H.; Sato, N.; Saga, T.; Nakamoto, Y.; Ishimori, T.; Toyama, S.; Togashi, K.; Konishi, J.; Brechbiel, M. W. *Eur. J. Nucl. Med.* **2000**, *27*, 1334.
- (123) Wängler, C.; Moldenhauer, G.; Eisenhut, M.; Haberkorn, U.; Mier, W. *Bioconjugate Chem.* **2008**, *19*, 813.
- (124) Toucheffeu, Y.; Franken, P.; J. Harrington, K. *Curr. Pharm. Des.* **2012**, *18*, 3313.
- (125) Filetti, S.; Bidart, J.-M.; Arturi, F.; Caillou, B.; Russo, D.; Schlumberger, M. *Eur. J. Endocrinol.* **1999**, *141*, 443.
- (126) Carrasco, N. *Biochim. Biophys. Acta, Rev. Biomembr.* **1993**, *1154*, 65.
- (127) Wapnir, I. L.; van de Rijn, M.; Nowels, K.; Amenta, P. S.; Walton, K.; Montgomery, K.; Greco, R. S.; Dohan, O.; Carrasco, N. *J. Clin. Endocrinol. Metab.* **2003**, *88*, 1880.
- (128) Liu, B.; Herve, J.; Bioulac-Sage, P.; Valogne, Y.; Roux, J.; Yilmaz, F.; Boisgard, R.; Guettier, C.; Cales, P.; Tavitian, B.; Samuel, D.; Clerc, J.; Brechot, C.; Faivre, J. *Gastroenterology* **2007**, *132*, 1495.
- (129) Tazebay, U. H.; Wapnir, I. L.; Levy, O.; Dohan, O.; Zuckier, L. S.; Zhao, Q. H.; Deng, H. F.; Amenta, P. S.; Fineberg, S.; Pestell, R. G.; Carrasco, N. *Nat. Med.* **2000**, *6*, 871.
- (130) Altorjay, A.; Dohan, O.; Szilagyí, A.; Paroder, M.; Wapnir, I. L.; Carrasco, N. *BMC Cancer* **2007**, *7*, 5.
- (131) Khare, R.; Chen, C. Y.; Weaver, E. A.; Barry, M. A. *Curr. Gene Ther.* **2011**, *11*, 241.
- (132) Grünwald, G. K.; Vetter, A.; Klutz, K.; Willhauck, M. J.; Schwenk, N.; Senekowitsch-Schmidtke, R.; Schwaiger, M.; Zach, C.; Wagner, E.; Göke, B.; Holm, P. S.; Ogris, M.; Spitzweg, C. *J. Nucl. Med.* **2013**, *54*, 1450.
- (133) Grünwald, G. K.; Vetter, A.; Klutz, K.; Willhauck, M. J.; Schwenk, N.; Senekowitsch-Schmidtke, R.; Schwaiger, M.; Zach, C.; Wagner, E.; Göke, B.; Holm, P. S.; Ogris, M.; Spitzweg, C. *Mol. Ther.–Nucleic Acids* **2013**, *2*, e131.
- (134) Shcharbin, D.; Pedziwiatr, E.; Blasiak, J.; Bryszewska, M. *J. Controlled Release* **2010**, *141*, 110.
- (135) Klutz, K.; Russ, V.; Willhauck, M. J.; Wunderlich, N.; Zach, C.; Gildehaus, F. J.; Göke, B.; Wagner, E.; Ogris, M.; Spitzweg, C. *Clin. Cancer Res.* **2009**, *15*, 6079.
- (136) Wang, Y.; Mo, L.; Wei, W.; Shi, X. *Int. J. Nanomed.* **2013**, *8*, 3805.

## Conclusions

Nuclear medicine, in order to efficiently target and retain radiation at the tumor site, avoiding side effects such as toxicity and tumor resistance process, has recently turned the attention to new oncologic strategies based on nanovectorization. The main objective of this innovative approach is to label nanosystems with radionuclides for the improvement of the treatment efficacy, while reducing the dose of radiolabeled materials *in vivo*. Among the nanosystems described for this purpose, dendrimers are particularly attractive due to their multivalency, tunable size and physicochemical properties as a function of the generation. Milestones in the development of dendrimers for nanovectorized radiotherapy include their functionalization with ligands for radiolabeling, targeting agents, and stealth functional groups to potentially improve their biodistribution, circulation times, and stability *in vivo*. The active role of dendrimers as innovative radiopharmaceuticals was reviewed with a special focus on critical challenges encountered in the advance of targeted radiotherapy.

As discussed in this review, the radiolabeling of dendrimers with therapeutic radionuclides resulted in tumor regression and longer survival. The biodistribution of dendritic conjugates could be improved by PEGylation, intratumoral application, saturation with cold metals, or by modulating their charge and molecular weight.

In addition, the multifunctionality of dendrimers makes them excellent candidates for theranostics. For instance, optimized delivery of boron compounds to tumor cells was achieved by incorporating carborane cages within biodegradable dendrimers, which proved useful as theranostic agents in a combined use of BNCT, photothermotherapy, imaging, and drug vectorization. The development of radiotherapeutic dendrimers for image-guided radionuclide therapies is also a work in progress. The multivalency and precise architecture of dendrimers can

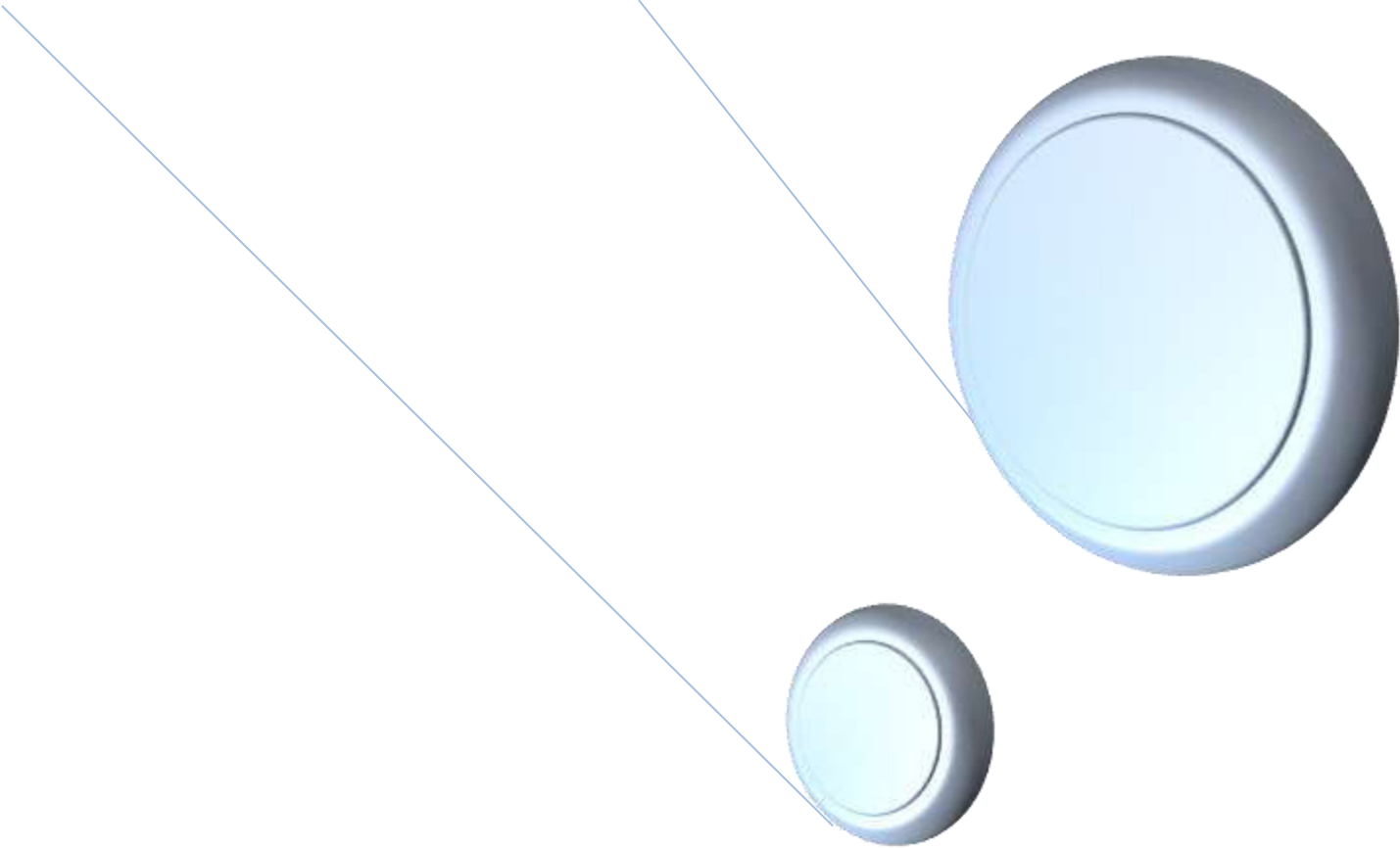
## General Introduction

---

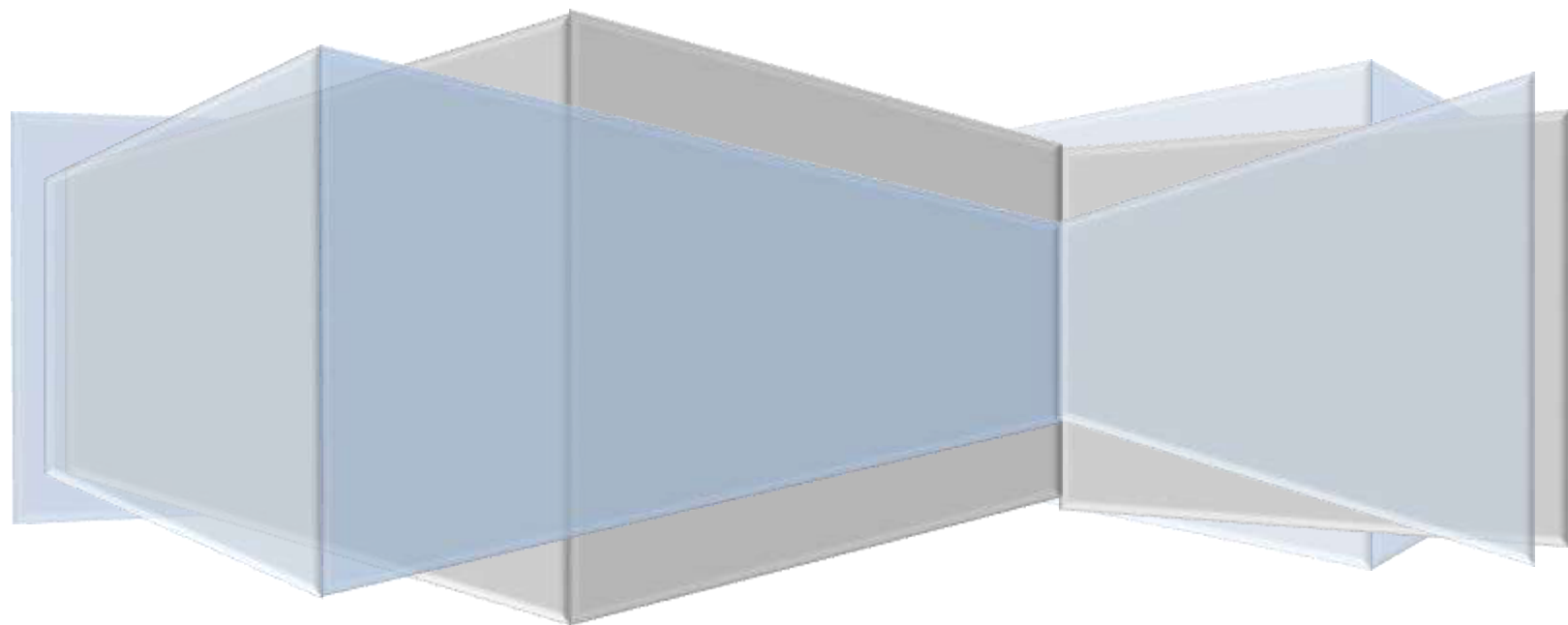
be exploited for radiotherapy in combination with moAbs, a strategy that pursues minor changes in immunoreactivity. Finally, dendrimers have been investigated in radiovirotherapy as coatings of adenoviral vectors for effective liver detargeting and tumor retargeting, as well as nonviral gene delivery vectors for NIS-targeted radionuclide therapy of metastatic cancer.

Although issues associated with *in vivo* properties and the toxicity of dendrimer conjugates are challenges to be addressed individually, as a whole there are considerable promise and benefits on current applications of dendrimers for radionanotherapy. A proper evaluation of dendrimer-based radiopharmaceuticals must be appreciated according to three criteria: the choice of radionuclide, the vector used, and the modalities of administration. Relatively recent results on dendrimer-based radiopharmaceuticals in preclinical models do not permit such a comparison yet.

As discussed in this review, the physicochemical properties of the radionuclide are crucial, but differences between vectors (untargeted vs targeted dendrimer, different dendrimer generations) are appreciated after intravenous injections with the aim of qualifying the targeting rather than the efficacy. In fact, for medical applications with radiopharmaceuticals, loco-regional injection could be a preferred way, where dendrimers play the role of confining agent at the injection site, in order to reduce the associated radio toxicity on healthy tissues or organs. Targeting will increase this confining action as needed for alpha-emitter and Auger-emitter.



## **PART 2. Strategies and Objectives**





### PART 2. Strategies and Objectives

As previously discussed in the introduction, there is a strong need for innovative regimens to improve the diagnosis and treatment of glioblastoma, one of the most deadly and aggressive malignancies ever known.

Multimodal dendrimers were evaluated for the first time, after being dual labeled with paramagnetic nuclei ( $Gd^{3+}$ ) for MRI and the  $\beta$  emitter  $^{188}Re$  for radiotherapy, following a minimally invasive stereotactic surgery, in a F98 rat glioma model. This animal model is known to mimic the behavior of human glioblastoma. Because of its wide availability, convenient half-life, and appropriate  $\gamma$  energy,  $^{99m}Tc$  was the radionuclide of choice for the further investigation of the *in vivo* behavior and properties of the dendrimers, following intravenous injection.

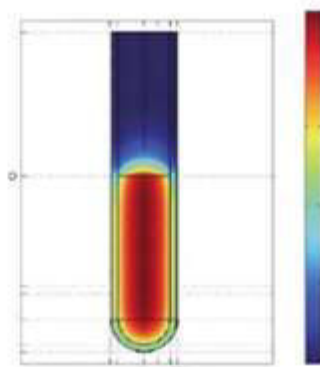
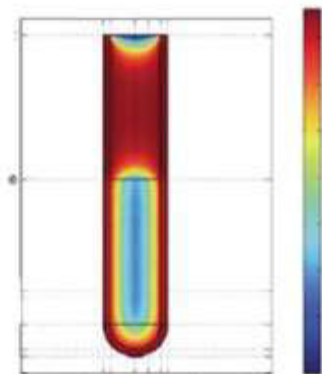
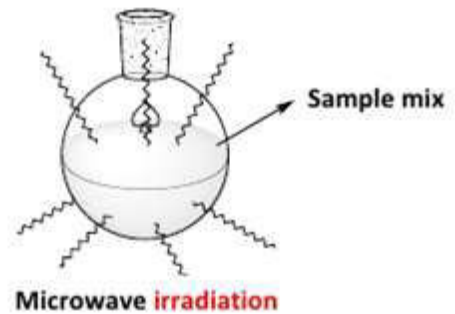
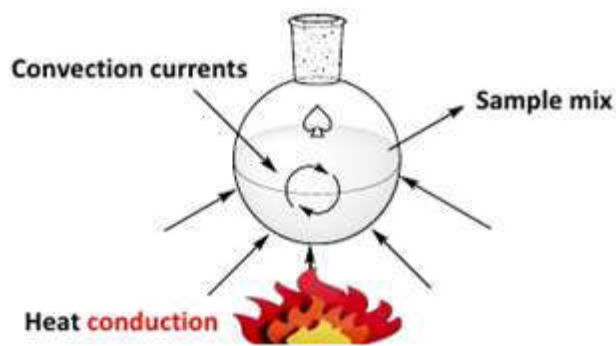
The dominant role of technetium compounds in diagnostic procedures, recommends the  $\beta$ -emitting rhenium isotope ( $^{188}Re$ ) for applications in nuclear-medical therapy, because it is possible to adopt general approaches for  $^{188}Re$  radiolabeling, from the established technetium chemistry. Moreover, parallel *in vivo* experiments, carried out with  $^{99m}Tc$  and  $^{188}Re$ , showed similar biodistribution with identical complex structures.<sup>98</sup>

To synthesize dendrimers with a high *in vivo* stability, two strategies were implemented. The first strategy aimed to create a synthetic route for a new family of dendrimers, made of carbamate groups as building blocks, which would increase the stability of the dendrimers to hydrolysis and enzymatic reactions. These dendrimers would be synthesized using microwave assisted azide-alkyne cycloaddition (AAC), avoiding the use of toxic catalyst and coupling agents. This would fasten up the synthesis process from days to hours long. However, different challenges were faced during the generation growth of these dendrimers, such as instability of the carbamate dendrimers to degradation during

microwave assisted AAC reaction, slow conversion kinetics, solubility issues, along with purification difficulties and low yield. For these reasons, the AAC-based carbamate dendrimers were replaced by Gallic Acid Triethylene Glycol (GATG) dendrimers, as the straightforward synthesis of the later ones allowed the planning of a second strategy.

Six macromolecular nanovectors were prepared, using G2, G3 and G4 GATG dendrimers (abbreviated as 2[Gn] dendrimers, where n is the generation number), fully conjugated either with bifunctional DTPA or DOTA derivatives, to evaluate their pharmacokinetics, tissue perfusion and excretion. These nanovectors were radiolabeled with either  $^{99m}\text{Tc}$  or  $^{188}\text{Re}$  and paramagnetic nuclei ( $\text{Gd}^{3+}$ ) agents with the objective of evaluating their potential for radiotherapy and MRI of glioblastoma via locoregional therapy.

# Accelerated synthesis of carbamate dendrimers





### **2.1. Modern strategies for the accelerated synthesis of dendrimers**

Both divergent and convergent strategies involve an iterative sequence of reactions with coupling and activation steps, which makes the synthesis of dendrimers tedious and time-consuming. The field of dendrimer synthesis is progressing towards faster and simpler synthetic methodologies to obtain dendrimers of high molecular weights without compromising the large number of functional groups. The accelerated synthesis of dendrimers pursues a higher branching and/or number of functional groups through faster and/or fewer reaction steps.

The copper-catalyzed azide–alkyne cycloaddition reaction (CuAAC), commonly known as “Click” reaction,<sup>166-168</sup> has become one of the most important reactions in synthetic organic chemistry.<sup>167</sup> Huisgen dipolar cycloaddition of azides and alkynes<sup>169</sup> are amongst the highest rated of cycloaddition reactions. A positive aspect of this reaction for biological purposes is that the azide and alkyne functional groups are largely inert towards biological molecules and aqueous environments. Dendrimers have been synthesized by CuAAC using both the divergent and convergent growth approaches.

In an early report,<sup>170</sup> the convergent method was utilized starting from AB<sub>2</sub>-monomers in which the A-functionality was a chloromethyl group and the B<sub>2</sub>-functionalities were acetylenes. After each CuAAC coupling, the chloride atom was easily replaced with an azide moiety, activating it for the next coupling step (Figure 2.1). As a result, the dendrons contain numerous 1,4-disubstituted 1,2,3-triazole linkages and in a final step, 4th generation dendrons were coupled to a range of different core molecules. The major achievement of this work was to demonstrate the utility of “Click” chemistry and the level of efficiency that could be achieved during a traditionally difficult synthetic process.

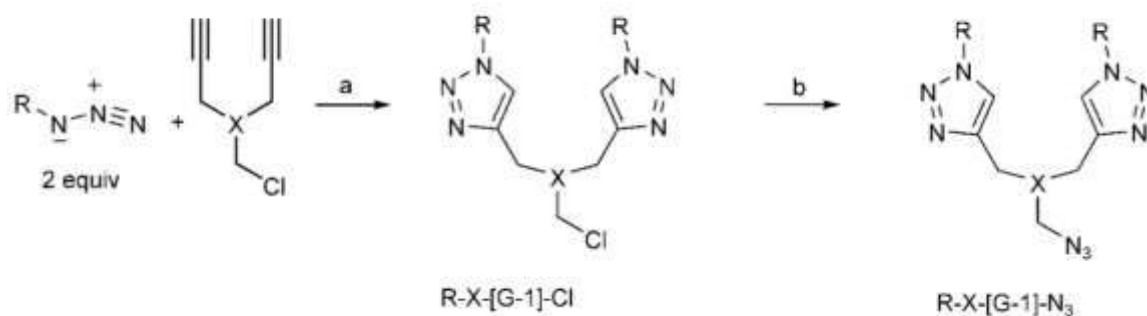


**Figure 2.1** Convergent approach toward triazole dendrimers. a)  $CuSO_4$  (5 mol%), sodium ascorbate (10 mol%),  $H_2O/tBuOH$  (1:1); b) 1.5 eq.  $NaN_3$ ,  $CH_3COCH_3/H_2O$  (4:1), 60 °C, 1–3 h. Adapted from ref. <sup>170</sup>.

Subsequently, it was reported the divergent growth approach to Fréchet-type dendrimers using “Click” chemistry, resulting in either azide or acetylene terminated dendrimers.<sup>171</sup> To date, copper stands out as the only metal for the reliable, facile, and 1,4-regiospecific catalysis of the azide–alkyne cycloaddition. Since residues originating from copper catalysis are known to create toxicity issues, the copper component may be a problem if traces remain under physiological conditions. Copper contamination can be overcome by using copper-free strategies.<sup>172</sup> Recently, Hawker and collaborators described the utilization of another Click process, the thiol–ene reaction, for the divergent synthesis of poly(thioether) dendrimers.<sup>173</sup> The synthesis was carried out under mild reaction conditions and without the use of a metal catalyst. The demand of green and sustainable synthetic methods is a significant challenge in the chemical field. This objective can be achieved through the use of aqueous synthetic protocols and microwave technique, which has been reported to reduce the reaction time and increase the product yield.<sup>174</sup> Microwave chemistry generally relies on the ability of the reaction mixture to efficiently absorb microwave energy, taking the advantage of microwave dielectric heating phenomena.<sup>175</sup>

In traditional organic synthesis using reflux conditions the boiling point of the solvent controls the reaction temperature. If a high reaction temperature is required in order for a

reaction to proceed, a solvent with a high boiling point must therefore be selected, which may be difficult to remove during work-up and purification. In contrast, using sealed vessel microwave heating, the boiling point of the solvent is less important since the solvent can be superheated above its regular boiling point under atmospheric conditions. This rapid increase in the reaction temperature, to a level typically not attainable under reflux conditions, results in a significant decrease of the reaction times, sometimes from days to minutes.

Several other parameters have been identified to accelerate the synthesis of dendrimers.<sup>176</sup> The selection of building-blocks is crucial, since the composition, number and nature of the functional groups dramatically affect the dendrimer structure. The monomers are used in excess during the synthesis and commercially available molecules are therefore preferred. Monomers that can be synthesized in a straightforward manner and on a large scale should be considered.

In conventional strategies, two iterative steps, growth and activation, are necessary for generating a new dendrimer generation. As a consequence, performing the growth without the need of any activation step would yield dendrimers in half the number of reaction steps.

One-pot chemistry is another alternative to accelerate the dendrimer synthesis, since the number of purification steps required can be severely decreased thus shortening the overall reaction time.

The initial objective of our project was to create a novel synthetic strategy for the design of a new family of carbamate dendrimers, more stable to hydrolysis and enzymatic reactions *in vivo*, using microwave assisted AAC and avoiding toxic catalysts and coupling agents. This method was previously proven to be successful by our group for the synthesis of dendrimers containing alternative functionalities, shortening the synthesis reactions times from day to hours long. Structurally, the carbamate functionality was chosen for its very good chemical and

proteolytic stabilities. During the course of this work, two types of repeating units with carbamate groups and one aliphatic core were successfully synthesized for the first time, as building blocks for the preparation of carbamate dendrimers. Other two aromatic cores, whose synthetic procedure was previously developed in our group, were tested in different combinations of repeating units and solvents, in the effort to form stable carbamate dendrimers.

Various microwave assisted AAC conditions were tried, resulting in the synthesis of two novel first generation carbamate dendrimers (G1cb4 and G1cb5), with 6 and 4 terminal groups respectively (Figure 2.2). The synthesis was based on green chemistry conditions.

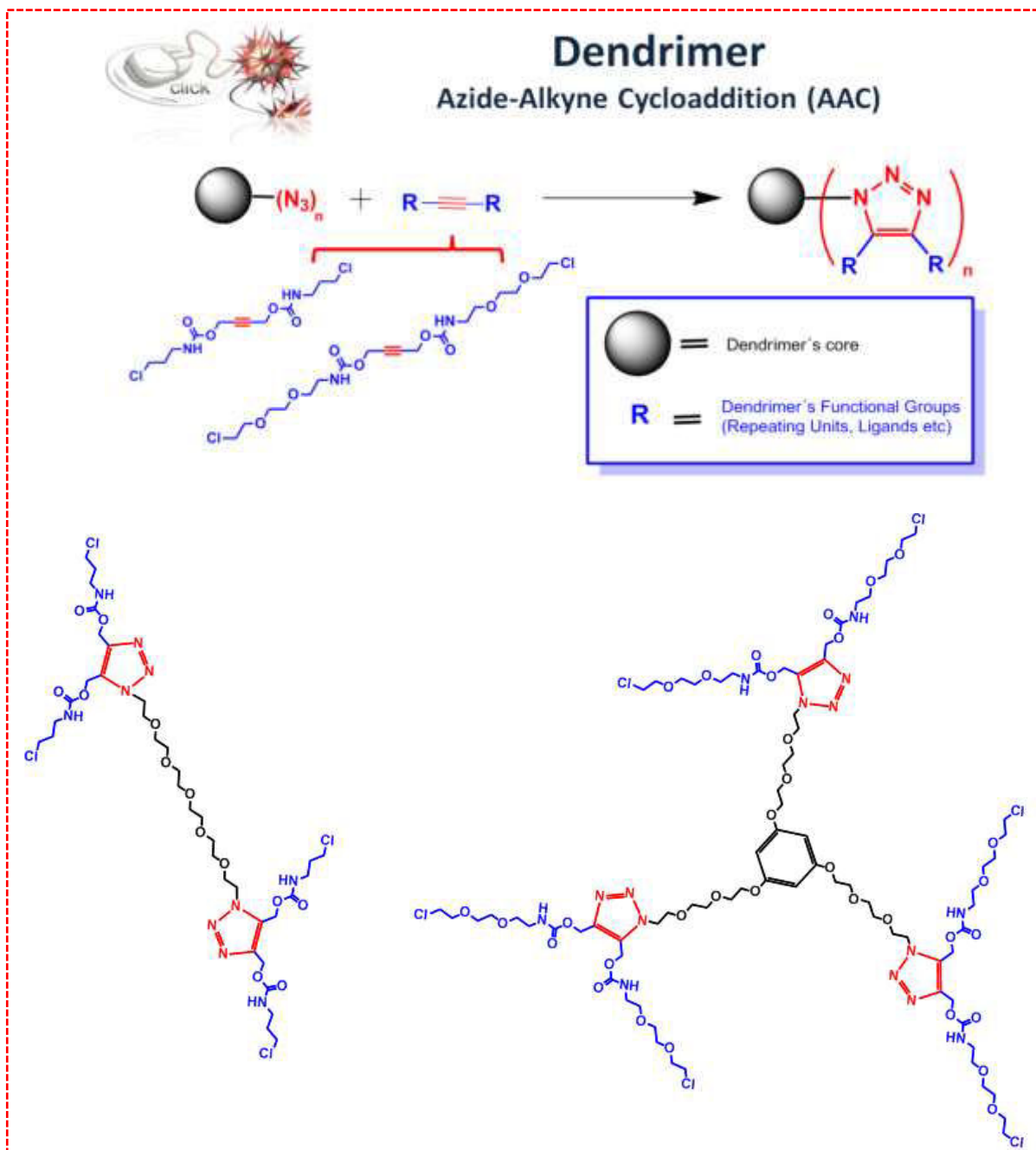


Figure 2.2 Synthetic scheme for carbamate dendrimers

## Results and Discussion

### Synthesis and characterization of novel building blocks for carbamate dendrimers

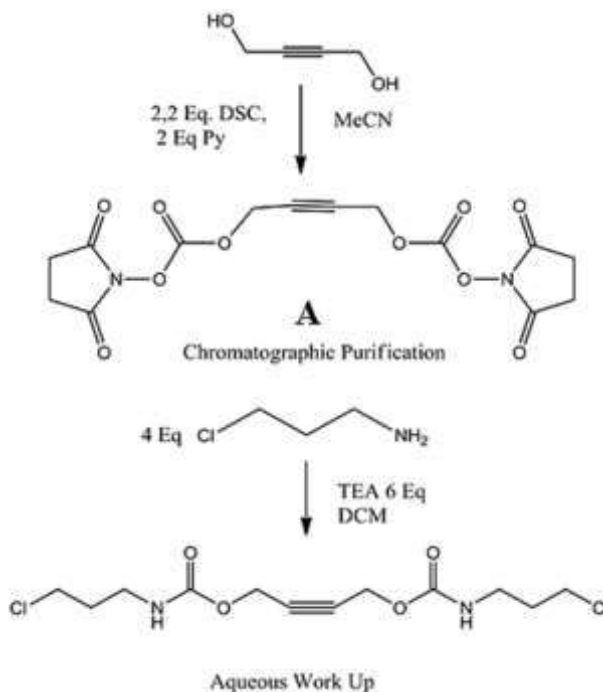


Figure 2.3. Synthetic scheme for RU-1

The synthesis of the first repeating unit (RU-1) to form the interior of the carbamate dendrimers was done according to the synthetic scheme, shown in Figure 2.3. (See EI for further details on the synthesis and characterization).

Table 2.1 Stability tests of the RU-1 in various microwave assisted AAC conditions

Solvent	Power (W)	Temp. (°C)	Time (h)	Result
<i>n</i> BuOH	120	100	2	Stable
<i>t</i> BuOH	120	100	2	Stable
<i>t</i> BuOH:H <sub>2</sub> O (2:1)	120	100	2	Stable
Butanone	300	100	2	Stable
Dioxan	80	100	2	Stable

The RU-1 resulted stable in all the tested microwave assisted AAC conditions shown in Table 2.1. In order to determine the optimal conditions for the coupling reaction of the RU-1 with the core of the carbamate dendrimers, several AAC conditions were tested with one fragment of the core (2) (Figure 2.4).



**Figure 2.4** Fragment of the core: 2

RU-1 (1.2 eq/ N<sub>3</sub>) was reacted with the core fragment 2 in a microwave tube fitted with a magnetic stirrer, while using a variety of solvents under specific microwave irradiation powers, ranging from 60-150 W (Table 2.2). The shut-off temperature was 100 °C in all cases. Solvents tested were butanone: H<sub>2</sub>O (2:1), nBuOAc: butanone (3:1) and tBuOAc, respectively. The progression of the AAC reactions was followed up by FT-IR for the disappearance of the azide stretch band at 2100 cm<sup>-1</sup>. None of the <sup>1</sup>H NMR spectra, following the MPLC purifications of these reactions' products, corresponded to the pure product, but rather to its decomposed version. The color of these end products was dark brown.

**Table 2.2** Results of the tests following the reactions of the RU-1 with core fragment 2, in various microwave assisted AAC conditions

Reaction	Eq. RU/N <sub>3</sub>	Solvent	Conc (M)	Power (W)	Temp (°C)	Time (h)	Result
AAC 1	1.2	Butanone:H <sub>2</sub> O (2:1)	1	150	100	6	<ul style="list-style-type: none"> <li>○ IR 100%</li> <li>○ No color change</li> <li>○ Unstable AAC</li> <li>○ Impure NMR</li> </ul>
AAC 2 *	1.2	<i>n</i> BuOAc: Butanone (3:1)	1	120	100	6	<ul style="list-style-type: none"> <li>○ IR 60%</li> <li>○ Unchanged color</li> <li>○ Stable AAC</li> <li>○ NMR OK</li> </ul>
AAC 3 *	1.2	<i>t</i> BuOAc	1	120	100	3	<ul style="list-style-type: none"> <li>○ IR 50%</li> <li>○ No color change</li> <li>○ Stable AAC</li> <li>○ NMR OK</li> </ul>
AAC 4	1.2	<i>t</i> BuOH: H <sub>2</sub> O (2:1)	1	120	100	3	<ul style="list-style-type: none"> <li>○ IR 100%</li> <li>○ Dark brown</li> <li>○ Unstable AAC</li> <li>○ Impure NMR</li> </ul>
AAC 5	1.2	<i>t</i> BuOH: H <sub>2</sub> O (2:1)	1	60	100	2	<ul style="list-style-type: none"> <li>○ IR 90%</li> <li>○ No color change</li> <li>○ Stable AAC</li> <li>○ Impure NMR</li> </ul>

\*: Best conditions

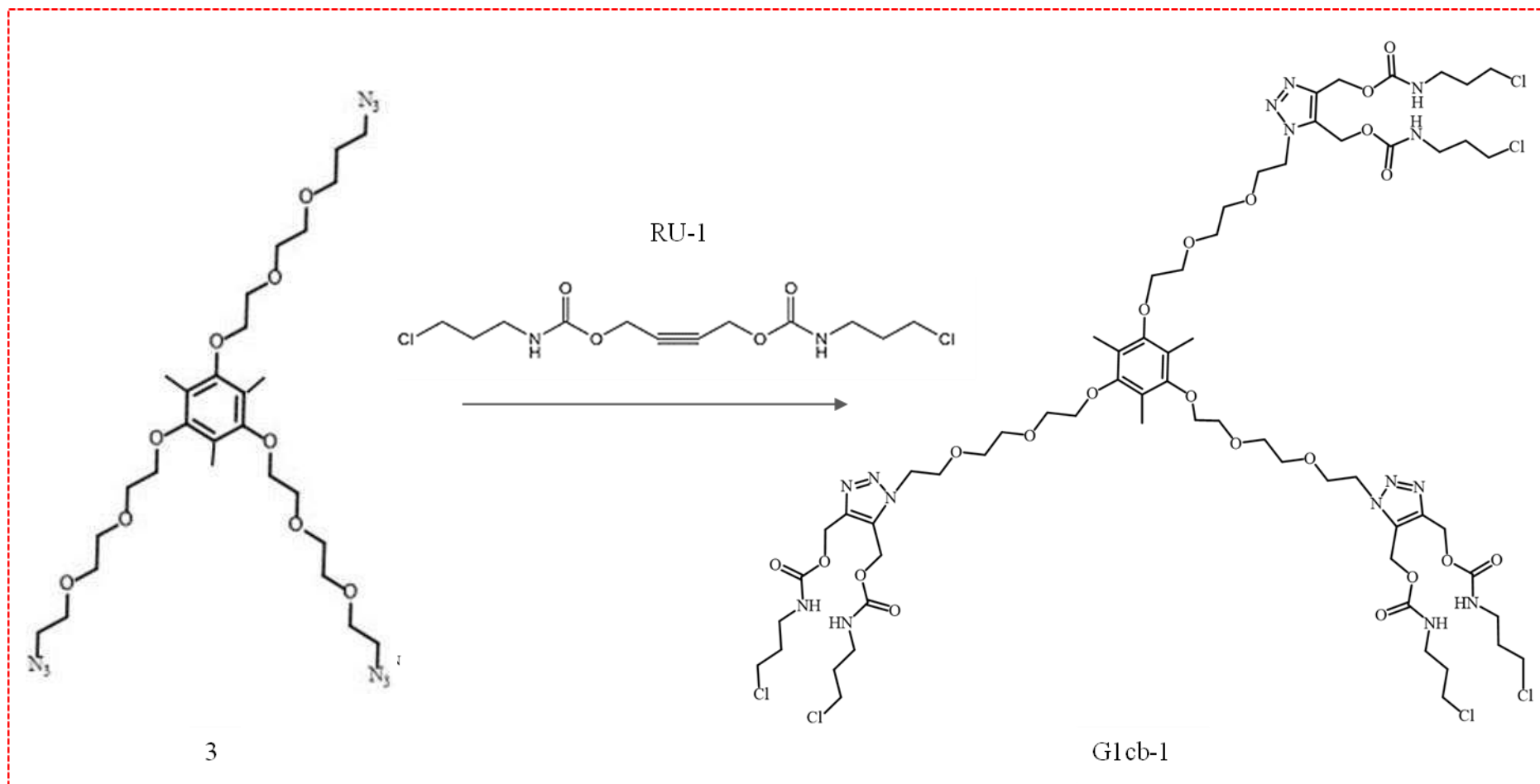


Figure 2.5 The synthetic scheme of the G1cb-1

However, in two cases, when the reaction progressed up to 60% in 2-6h, the  $^1\text{H}$  NMR spectrum corresponded to the expected product, while no color change to brown was observed. These conditions were found to be interesting to be tested for the first design of carbamate dendrimers (G1cb-1), after making several modifications to increase the reaction kinetics (Figure 2.5). These modifications included the increase of the microwave irradiation power to 300W and the change the solvents to either a mixture of ethyl acetate (EtOAc): acetone solvents (1:1), or butanone, with an increasing concentration (from 1 to 2M). The shut-off temperature of 100  $^{\circ}\text{C}$  was kept constant.

EtOAc: acetone (1:1) was substituted by butanone as a solvent, because of the higher boiling point of the latter one. In this way the evaporation of the reaction solvent, observed after 3h with ethyl acetate: acetone (1:1), would be avoided. Despite these efforts (Table 2.3), the azide stretch band at 2100  $\text{cm}^{-1}$  did not completely disappear even after 7 hours, time when the product resulted degraded.

**Table 2.3** Results of various microwave assisted AAC conditions tested for the synthesis of G1cb-1

Reaction	Eq. RU/N <sub>3</sub>	Solvent	Conc. (M)	Power (W)	Temp. ( $^{\circ}\text{C}$ )	Time (h)
AAC 6	1.05	EtOAc: Acetone (1:1)	1	300	100	3
AAC 7	1.05	Butanone	2	300	100	7
AAC 8	1.2	Butanone	2	300	100	3.5

To avoid degradation, the dendrimer core (3) was substituted with another one (4) that lacked the aromatic methyl groups and combined with RU-1 (Figure 2.6) in several AAC conditions (Table 2.4) to synthesize the second design of carbamate dendrimers (G1cb-2). The

temperature was kept constant (100 °C) in all cases. Butanone was substituted by *tert*-Butyl acetate (*t*BuOAc), known as a high-boiling solvent with moderate polarity. The equivalence of RU-1 was increased from 1.2 to 2, and the concentration of the solution was kept as 2 M. To prevent the degradation risk, the microwave irradiation power was decreased from 300 to 80 W. Even though the profile of the AAC reaction was stable, after 4 hours the reaction product suffered degradation.

**Table 2.4** Results of various microwave assisted AAC conditions tested for the synthesis of G1cb-2

Reaction	Eq. RU/N <sub>3</sub>	Solvent	Conc (M)	Power (W)	Temp (°C)	Time (h)	Result
AAC 9	2	<i>t</i> BuOAc	2	80	100	4	<ul style="list-style-type: none"> <li>○ Degraded product</li> <li>○ AAC profile stable</li> </ul>
AAC 10	2	<i>t</i> BuOAc	1	80	100	4	<ul style="list-style-type: none"> <li>○ No color change</li> <li>○ AAC profile stable</li> <li>○ NMR good</li> <li>○ G1cb-2: not soluble in <i>t</i>BuOAc</li> </ul>
AAC 11	2	Dioxan	1	175	100	6	<ul style="list-style-type: none"> <li>○ IR 100%</li> <li>○ Light orange color</li> <li>○ AAC profile stable</li> <li>○ NMR good</li> <li>○ Impure GPC</li> </ul>

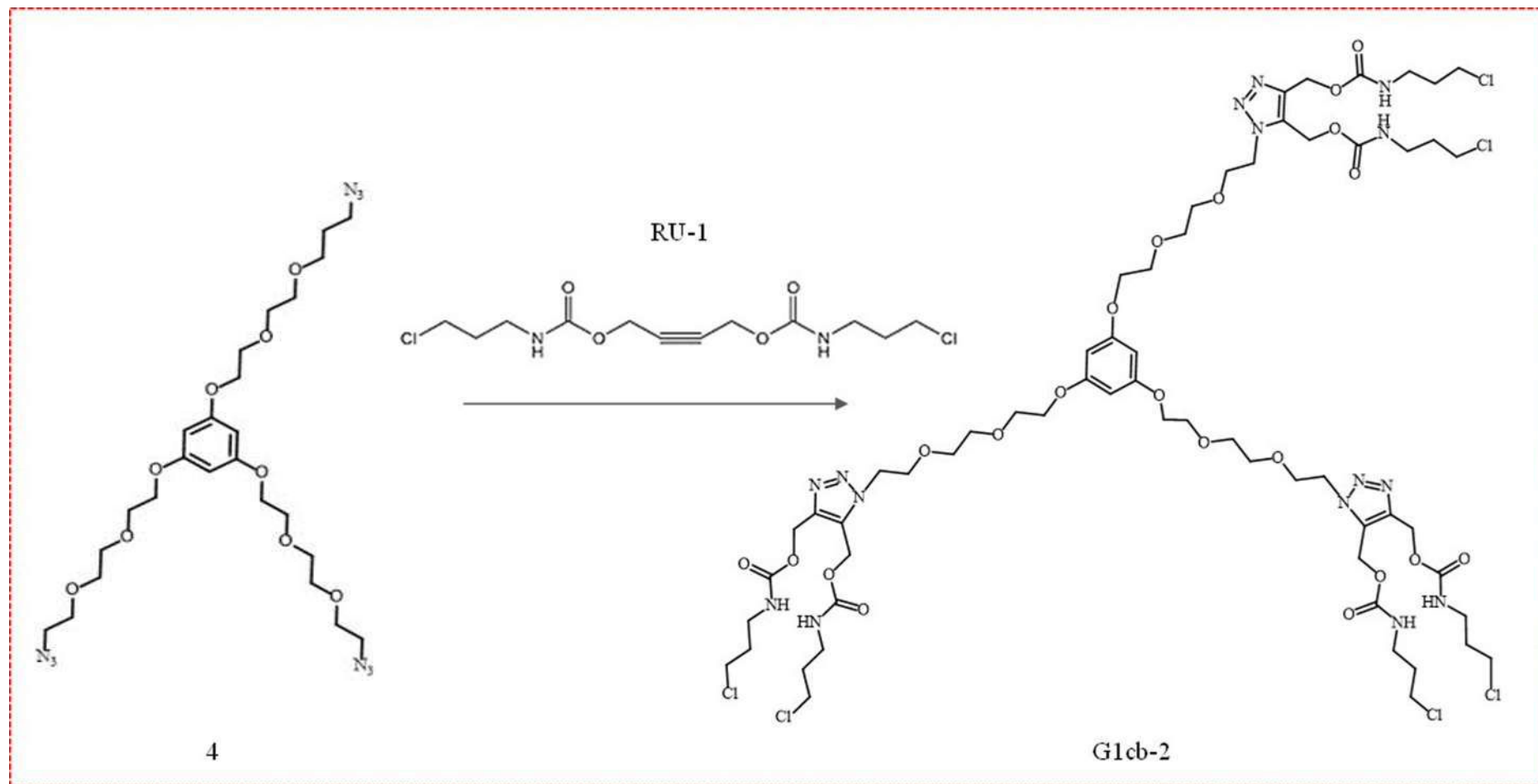
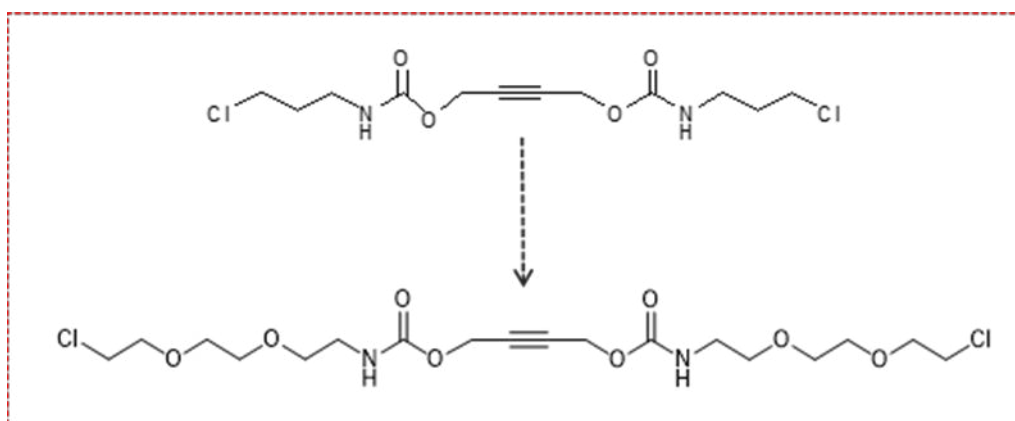


Figure 2.6 The synthetic scheme of the G1cb-2

In another effort to optimize the conditions of AAC, the concentration of the reaction was lowered from 2 to 1M. This dilution resulted successful for the progression of the reaction, except that G1cb-2 was insoluble in *t*BuOAc. After 4 h the AAC reaction was not completed. To aid with this newly detected insolubility issue, *t*BuOAc was substituted by 1,4-dioxan that is a solvent with higher polarity. The concentration of the reaction was kept the same (1 M), but the power of microwave irradiation was increased from 80 W to 175 W, with the aim of improving the reaction kinetics. Following continuous FT-IR controls, the reaction was completed in 6 hours. The  $^1\text{H}$  NMR spectrum corresponded to the expected product, but GPC revealed structural defects of the G1cb-2 dendrimers, by the observation of another specie in the chromatogram. The reason for these defects was doubted to be a possible intramolecular reaction between the terminal chloride groups of the repeating unit and the core. To prevent this undesired intramolecular reaction the RU-1 was modified by an elongation of its branches, as shown in the Figure 2.7. The synthetic scheme of the second carbamate repeating unit (RU-2) is given in Figure 2.8. (For further details on synthesis and characterization of RU-2 see EI).



**Figure 2.7** Elongation of the carbamate repeating unit from RU-1 to RU-2

## Accelerated Synthesis of Carbamate Dendrimers

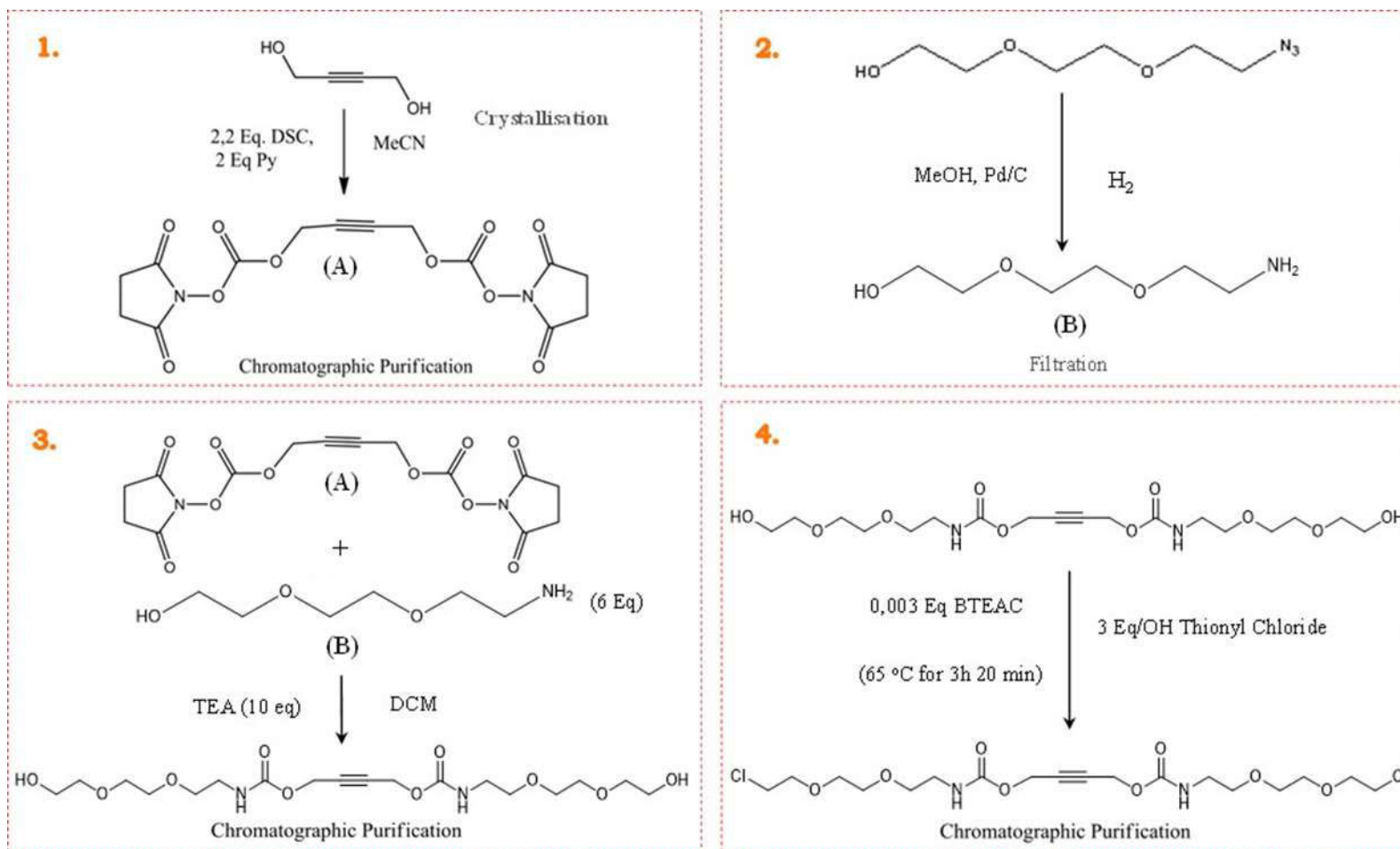


**Figure 2.8** Scheme depicting the steps for the synthesis of RU-2; 1. first step for the synthesis of product A; 2. second step for the synthesis of product B; 3. third step for the combination of A and B to give RU-2-OH; 4. fourth step resulting in RU-2.

The RU-2 resulted as stable in all the tested microwave assisted AAC conditions shown in Table 2.5.

**Table 2.5** Stability tests of the RU-2 in various microwave assisted AAC conditions

Solvent	Power (W)	Temp. (°C)	Time (h)	Result
<i>t</i> BuOH:H <sub>2</sub> O (3:1)	175	100	2	Stable
Dioxan	80	100	2	Stable

The core fragment 2 and RU-2 (2eq/ N<sub>3</sub>) were dissolved in a 3:1 mixture of *t*BuOH: H<sub>2</sub>O solution, in a microwave tube with a magnetic stirrer. The concentration of the final mixture was 2 M. Microwave irradiation with power of 175 W and temperature of 100 °C were used. The AAC reaction was completed after 3 hours with positive results.

For the accelerated synthesis of G1cb-3, core 3 and RU-2 were combined in the same AAC conditions as above, except for the ratio of the solvent mixture, which was modified from 3:1 to 2:1 *t*BuOH:H<sub>2</sub>O, increasing in this way both the boiling point and the polarity of the reaction media. The reaction was stopped after 6 hours, as the product suffered degradation.

For the next synthesis (G1cb-4), core 4 and RU-2 were combined (Figure 2.10) in various AAC conditions, as shown in Table 2.6. These conditions were chosen based on the results of the previous AAC tests. G1cb-4 was successfully synthesized in both AAC 13 and AAC 14 conditions. Taking into consideration the faster reaction kinetics of AAC 13 versus that of AAC 14 (4 h faster), it was chosen as the best one (See EI for synthesis and characterization details).

**Table 2.6** Microwave assisted AAC conditions tested for the synthesis of G1cb-4

Reaction	Eq. RU/N <sub>3</sub>	Solvent	Conc (M)	Power (W)	Temp (°C)	Time (h)	Result
AAC 12	2	<i>t</i> BuOH:H <sub>2</sub> O (3:1)	2	175	100	6	○ IR 100% ○ Impure ○ NMR
AAC 13	2	<i>t</i> BuOH:H <sub>2</sub> O (3:1)	1	150	100	6	○ IR 100% ○ NMR OK ○ GPC OK
AAC 14	2	Dioxan	1	80	100	10	○ IR 100% ○ NMR OK ○ GPC OK

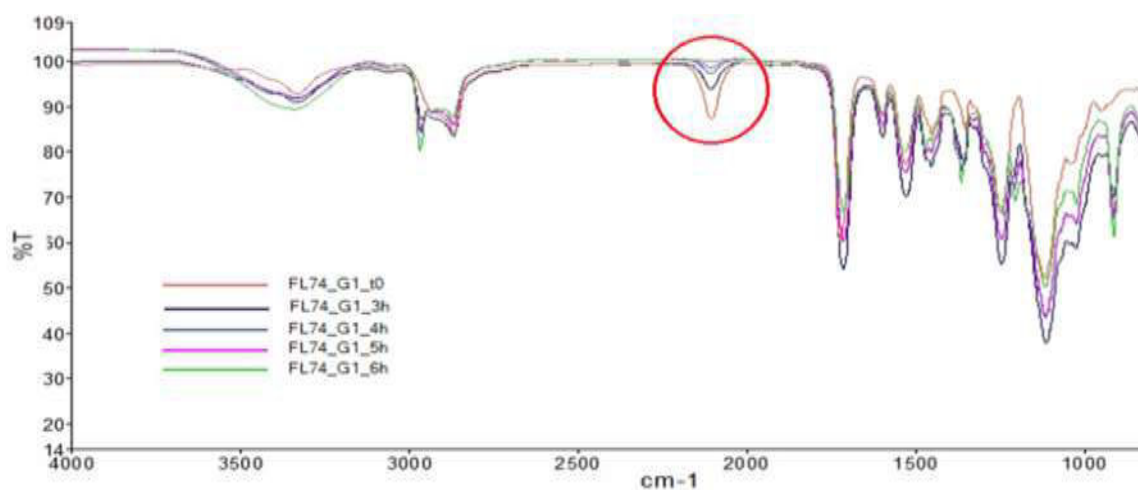


**Figure 2.9** Disappearance of the azide band during the coupling reaction

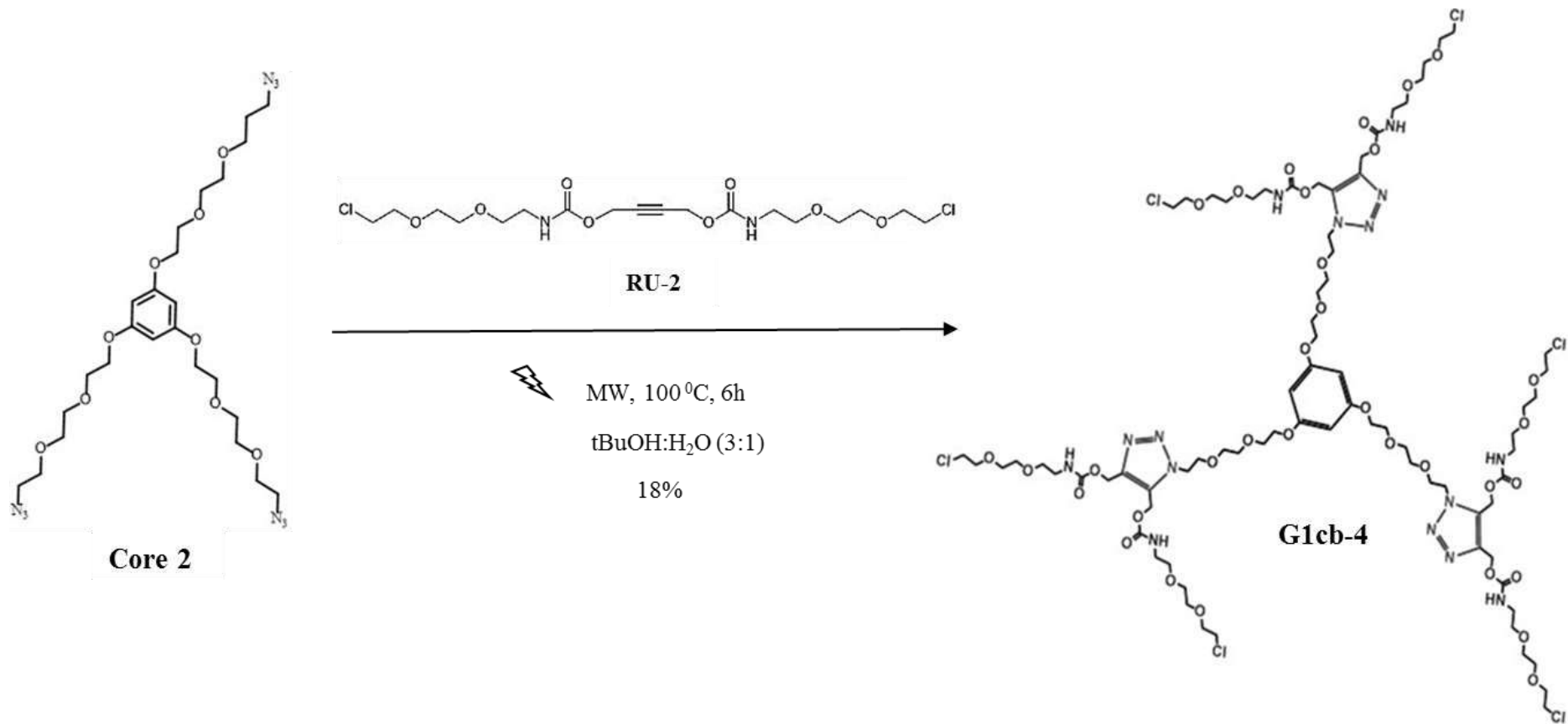
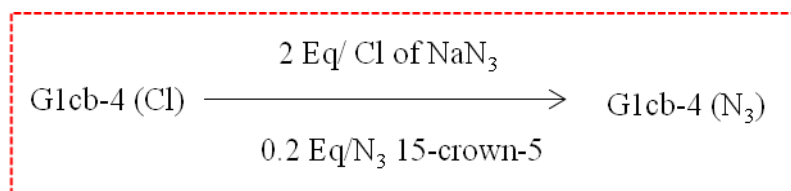


Figure 2.10 The synthetic scheme of the G1cb-4

The generation growth of G1cb-4 to G2cb-4 was done in two steps. Initially the terminal “Cl” groups of G1cb-4 were substituted with azide ( $N_3$ ) groups (Figure 2.11.), to allow the coupling of RU-2 in the second step with microwave assisted AAC.



**Figure 2.11.** Scheme for the azide substitution reaction

Dendrimer G1cb-4 and  $\text{NaN}_3$  were added to a microwave tube with a magnetic stirrer and dissolved in dry DMSO (0.5 M per Cl group). The mixture was stirred for 40 minutes at 80 °C under microwave irradiation of 20 W (Table 2.7). The reaction was followed by  $^1\text{H}$  NMR with the appearance of proton signals in the  $\alpha$  position related to the azide groups (the multiplet between 3.25 and 3.5 ppm). The purification was done by aqueous workup (3x with EtOAc: Water) to remove the excess  $\text{NaN}_3$ , 15-Crown-5 and dimethyl sulfoxide (DMSO). The solution was dried with  $\text{Na}_2\text{SO}_4$  and filtered to give a final reaction yield of 80%.

**Table 2.7** Microwave assisted AAC conditions tested for the azide substitution reaction

Reaction	Eq/ $N_3$	Solvent	Conc (M)	Power (W)	Temp. ( $^{\circ}\text{C}$ )	Time (min)	Pressure (Bar)
Azide Substitution	2	DMSO	0.5	20	80	40	17

For the generation growth to G2cb-4 (with structure as shown in Figure 2.12), G1cb-1 and the RU-2 were added in a microwave tube, following the conditions of AAC 15, given in the Table 2.8.

**Table 2.8** Microwave assisted AAC condition tested for the synthesis of G2cb-4

Reaction	Eq. RU/N <sub>3</sub>	Solvent	Conc (M)	Power (W)	Temp. (°C)	Time (h)	Result
AAC 15	2	<i>t</i> BuOH:H <sub>2</sub> O (3:1)	1	150	100	6	<ul style="list-style-type: none"><li>○ IR 100%</li><li>○ Dark Color</li><li>○ Impure NMR</li></ul>

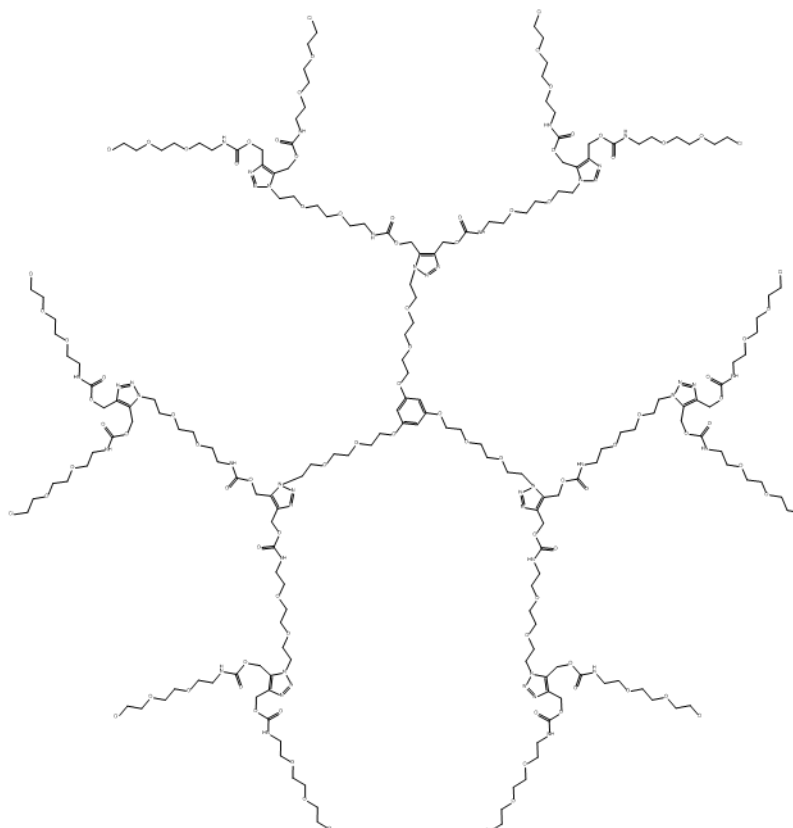


**Figure 2.12** Structure of G2cb-4

The dendrimer growth reaction was completed after 6 hours, resulting in a darker color and an impure  $^1\text{H}$  NMR, which showed decomposition of the aromatic core. Taking into account this important data, it was decided to modify the core to an aliphatic one. As a result, conditions (Table 2.9) for accelerated synthesis of aliphatic core 1 (Figure 2.13) were tested as follows.

The reaction was followed by  $^1\text{H}$  NMR with the appearance of proton signals in the  $\alpha$  of the azide groups (the multiplet between 3.3 and 3.4 ppm). (See EI for synthesis and characterization details).

**Table 2.9** Microwave assisted reaction conditions tested for the azide substitution reaction

Reaction	Eq/ $\text{N}_3$	Solvent	Conc (M)	Power (W)	Temp. ( $^\circ\text{C}$ )	Time (min)	Pressure (Bar)
Azide Substitution	2	DMSO	0.5	20	80	40	17

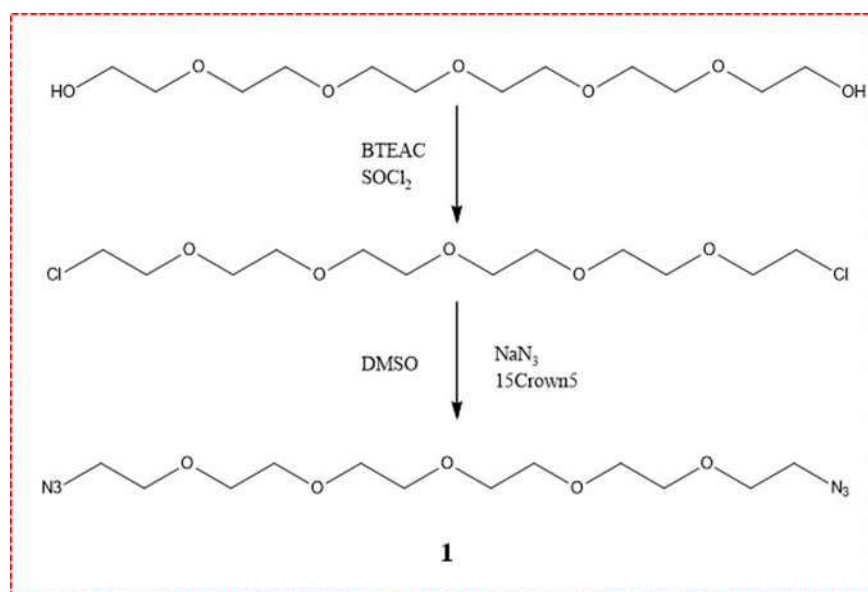


**Figure 2.13** The synthetic scheme of **1**

With the aim to synthesize G1cb-5 (Figure 2.14), core 1 and RU-1 were combined in the AAC conditions shown in Table 2.7. The synthesis was completed successfully in 4 hours (See EI for synthesis and characterization details).

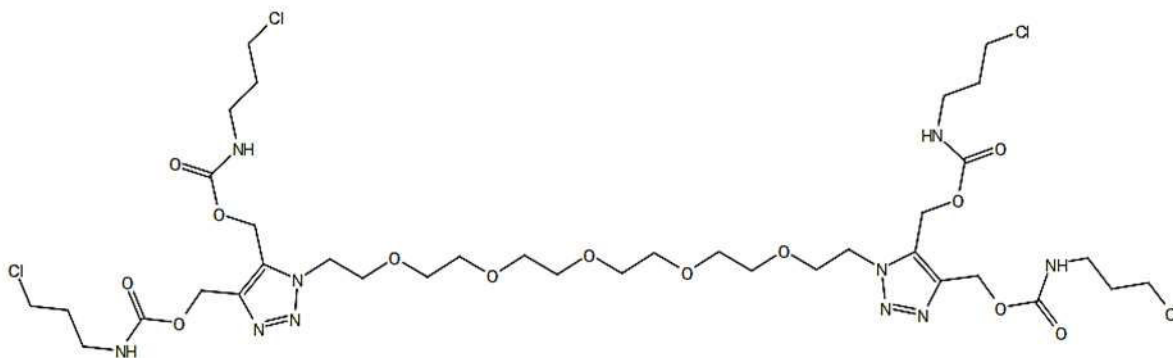


**Figure 2.14** The chemical structure of G1cb-5

To make possible the coupling reaction of the RU-1 with G1cb-5 for the generation growth (G2cb-5) of the dendrimer, initially an azide substitution (Figure 2.15) of the terminal Cl groups of G1cb-5 was done, as shown in Table 2.7-Azide substitution (See EI for details).

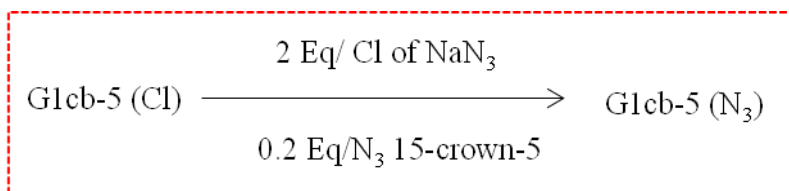


**Figure 2.15** The synthetic scheme of the azide substitution of the G1cb-5

**Table 2.10** Microwave assisted AAC conditions tested for the synthesis of G1cb-5 (AAC 16), the azide substitution reaction of G1cb-5, the synthesis of G2cb-5 (AAC 17) and the synthesis of G1cb-6 (AAC 18).

Reaction	Eq/N <sub>3</sub>	Solvent	Conc (M)	Power (W)	Temp. (°C)	Time	P (Bar)	Result
AAC 16	2	<i>t</i> BuOAc	1	120	100	4 h		<ul style="list-style-type: none"> <li>○ IR 100%</li> <li>○ Light green</li> <li>○ NMR: OK</li> <li>○ GPC: OK</li> </ul>
Azide Substitution	2	DMSO	0.5	20	80	40 min	17	
AAC 17	2	<i>t</i> BuOAc	1	120	100	4.5 h		<ul style="list-style-type: none"> <li>○ IR 100%</li> <li>○ No color</li> <li>○ Impure NMR</li> </ul>
AAC 18	2	<i>t</i> BuOH: H <sub>2</sub> O (3:1)	2	175	100	1.5 h		<ul style="list-style-type: none"> <li>○ IR 100%</li> <li>○ Brown color</li> </ul>

Afterwards, G1cb-5-N<sub>3</sub> and RU-1 were added in a microwave tube and AAC 17 test was run for the generation growth (Table 2.10). Reaction was completed in 4.5 hours, but the end product showed degradation and impurities. The newly formed G2cb-5 dendrimer (Figure 2.16) was not soluble in *t*BuOAc, as well.

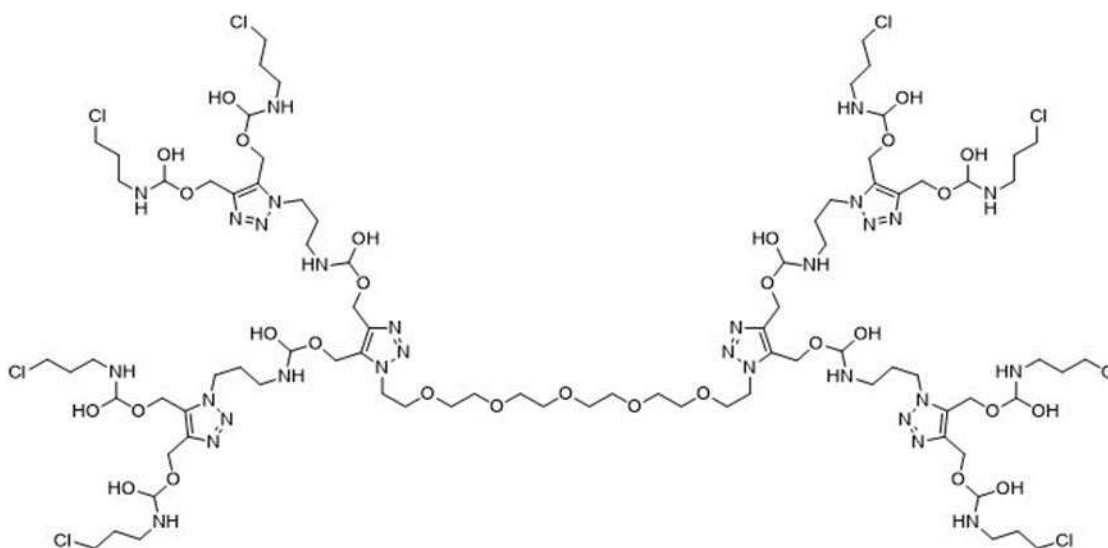


**Figure 2.16** Structure of G2cb-5

With the aim to synthesize G1cb-6 (Figure 2.17), core 1 and RU-2 were combined according to the AAC conditions shown in Table 2.10 (AAC 18). The conversion was completed in 1.5 hours, resulting in degradation of G1cb-6 dendrimer.

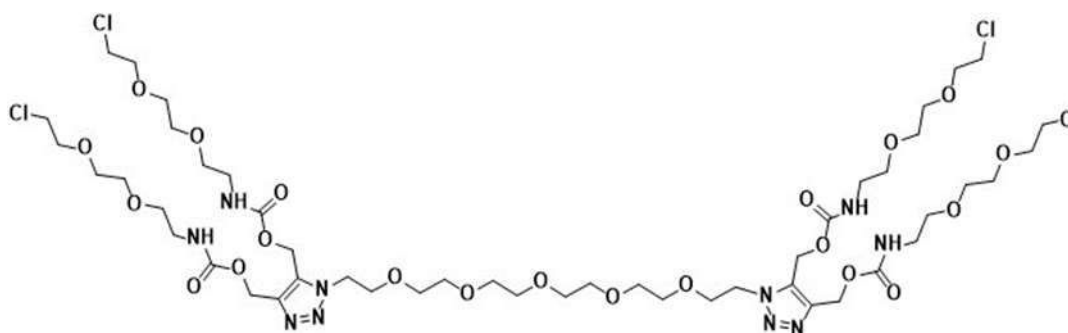


**Figure 2.17** Structure of G1cb-6

## Experimental Information

### Materials and Instrumentation

2-[2-(2-Chloroethoxy)ethoxy]ethanol and  $\text{NaN}_3$  were purchased from Wako. Thionyl chloride was purchased from Acros Organics. Hexaethylene glycol (97%), 15-crown-5 (15C5), 3-chloropropylamine hydrochloride (98%), trimethylamine (TEA), N,N'-disuccinimidyl carbonate (DSC), 2-butyne-1,4-diol (99%) (crystallized overnight in ethylacetate), phloroglucinol, 2,2-(ethylenethoxy)bis(ethylamine), benzyltriethylammonium chloride (BTEAC) were purchased from Sigma-Aldrich. Amberlite IR-120 and 10% Pd on charcoal was obtained from Fluka. The two repeating units, functionalized with carbamate groups abbreviated as RU-1 and RU-2, 1,17-dichloro-3,6,9,12,15-pentaoxaheptadecane and 3,6,9,12,15-pentaoxaheptadecane-1,17-diyl bis-azide (1), were of synthetic grade as reported here. The core used for the reactions of carbamate dendrimers, 2-[2-(2-azidoethoxy)ethoxy]ethanol (2), the azide-functionalized aromatic cores (3, 4), and 1-azido-2-[2-(2-chloroethoxy) ethoxy]ethane were prepared following previously reported procedures by our group.<sup>177-178</sup> All other reagents were of analytical grade. All solvents were HPLC grade, purchased from Sigma-Aldrich or Fisher Scientific and used without further purification. Water was of Milli-Q grade.

Microwave assisted AAC was done with a Discover SP-Microwave Synthesizer by CEM. Automated column chromatography was performed on a MPLC Teledyne ISCO CombiFlash RF – 200 psi with a RediSepRf normal-phase 12 g silica column, and disposable RediSep Rf normal-phase 4 g silica flash columns filled with silica gel 230-400 mesh from Teledyne ISCO were used for the purifications of RU-1, RU-2, G1cb-4 and G1cb-5 dendrimers. The sample was injected on solid form through a mix of silica and the crude product that was deposited into a solid cartridge.

For the method a gradient of hexane/acetone was used from 100% hexane until 100% Acetone during 15 minutes.

NMR spectra were recorded on a Varian Mercury 300 MHz and Varian Inova 500 MHz spectrometers. Chemical shifts are reported in ppm ( $\delta$  units) referenced to residual solvent peaks. FT-IR spectra were recorded on a Bruker IFS-66v using neat samples (CsI window).

Polidispersity of dendrimers was analyzed by size exclusion chromatography (SEC) on an Agilent 1100 series separation module using a PSS SDV pre-column (5 $\mu$ m, 8 $\times$ 50 mm), a PSS SDV Linear S column (5 $\mu$ m, 8 $\times$ 300 mm), a PSS SDV Lux Linear M column (5 $\mu$ m, 8 $\times$ 300 mm) with an Agilent 1100 series refractive index (RI) detector. THF was used as eluent at 1mL/min for azide dendrimers, and filtered through 0.45  $\mu$ m before injection.

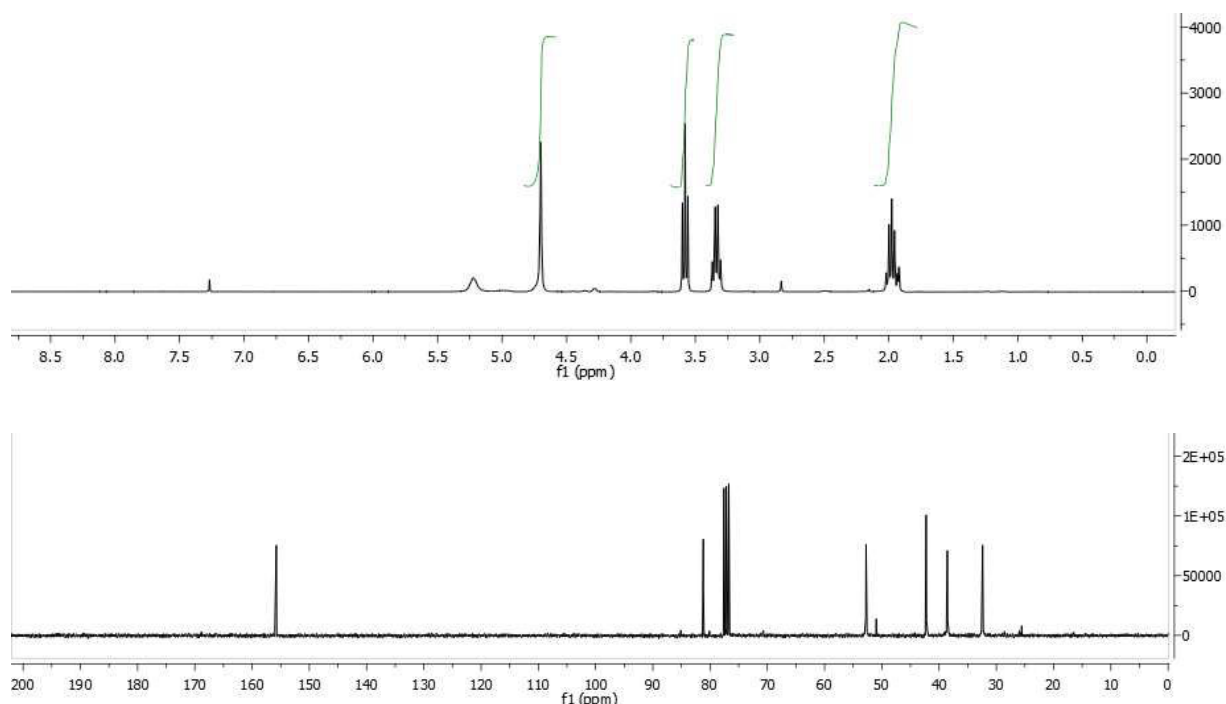
### **Warning on the use of azides<sup>178</sup>**

Since the first reports on the CuAAC reaction by the groups of Meldal, and Fokin and Sharpless in 2002, the appearance of NaN<sub>3</sub> and organic azides in synthesis has exponentially increased to the point of us forgetting a prevailing earlier azidophobia. Indeed, the success of CuAAC lays on the extraordinary stability of azides towards H<sub>2</sub>O, O<sub>2</sub>, and the majority of organic synthesis conditions. Nevertheless, one must take into consideration some general safety precautions, because of the potential explosive nature of some azides under certain conditions. Ionic azides such as NaN<sub>3</sub> are relatively stable, but organic and heavy metal azides are thermally decomposable and in part explosive classes of compounds. For organic azides to be workable or non-explosive, the “Smith’s rules” must be followed: i) the number of nitrogen atoms (NN) must not exceed that of carbon (NC), and ii)  $(NC + NO)/NN \geq 3$ . All organic azides and dendrimers in

this work follow these rules and have proven to be stable in our hands.  $\text{NaN}_3$  is toxic [LD50 oral (rats) = 27 mg/Kg] and can be absorbed through the skin. It is not explosive except when heated near its decomposition temperature (275 °C) and does not form explosive compounds when dissolved in water. However, in reaction with Brønsted acids, the highly toxic and potentially explosive hydrazoic acid ( $\text{HN}_3$ ) is released (volatile liquid, Bp 37 °C). Besides its toxicity, the danger associated with  $\text{NaN}_3$  is its ability to form highly explosive azides (under pressure or shock) when reacted with heavy metals such as Pb, Cu, Zn, Cd, or Ni. The same applies to  $\text{HN}_3$  vapors into contact with heavy metals or their salts. Accordingly,  $\text{NaN}_3$  should never be flushed down the drain to avoid incidents by reaction with Pb or Cu in drain lines. In addition, metal items used to handle  $\text{NaN}_3$ , including spatulas should be avoided. Caution must be also taken to avoid accumulation of heavy metal azides on the metal components of diverse laboratory equipment, including rotary evaporators and freeze-dryers. It has been reported that  $\text{NaN}_3$  and polymer-bound azide reagents form explosive di- and triazidomethane in contact with  $\text{CH}_2\text{Cl}_2$  and  $\text{CHCl}_3$  at rt, respectively. Therefore, contact of  $\text{NaN}_3$  with these solvents must be avoided.  $\text{NaN}_3$  reacts also vigorously with  $\text{CS}_2$ ,  $\text{Br}_2$ ,  $\text{HNO}_3$ , and dimethyl sulfate.

### Synthesis and characterization of new compounds

**RU-1.** 2-butyne-1,4-diol (500 mg, 5.81 mmol) was added to a solution of DSC (3270 mg, 12.76 mmol) and Py (1 mL) in MeCN (17.6 mL). The mixture was stirred at r.t. under Ar atmosphere for 24 h. The resulting solution was purified by MPLC (acetone: hexane, 1:1) to obtain product A (Figure 3.2) with 79% yield (1690 mg). Then, product A (500 mg, 1.36 mmol) was mixed with 3-chloropropyl amine (706 mg, 5.43 mmol) and TEA (1.13 mL, 8.16 mmol) in DCM (3 mL). The mixture was stirred at rt under Ar atmosphere for 7 h, followed by a purification with an aqueous work up (ethyl acetate: water), giving RU-1 (67% yield).  $^1\text{H}$  NMR (300 MHz,  $\text{CDCl}_3$ )  $\delta_{\text{H}}$ : 4.7 (s, 4H), 3.60-3.56 (m, 4H), 3.37-3.30 (m, 4H), 2.02-1.92 (m, 4H).  $^{13}\text{C}$  NMR (100 MHz,  $\text{CDCl}_3$ )  $\delta_{\text{C}}$ : 155.8, 81.2, 52.75, 42.3, 38.6, 32.4.



**S1.**  $^1\text{H}$  and  $^{13}\text{C}$  NMR spectra of RU-1

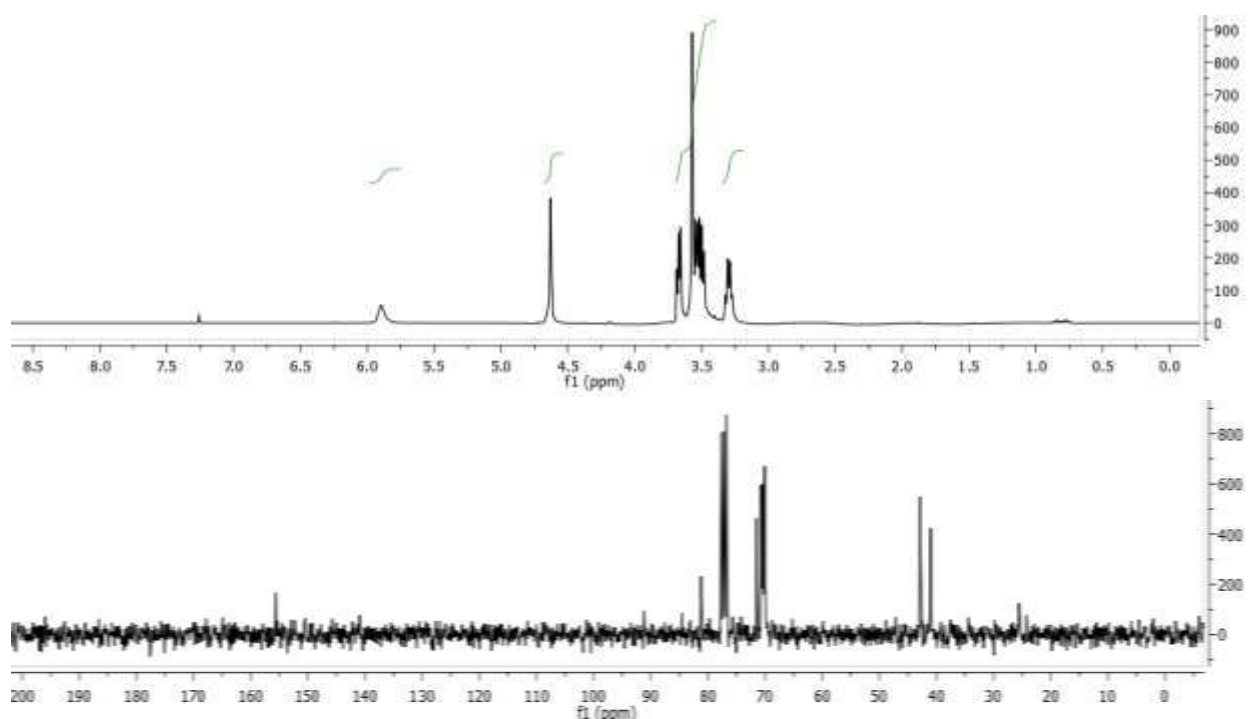
The synthesis of **RU-2** was done in a four step process. The first step was identical to that of RU-1 synthesis, as described above. 2-butyne-1,4-diol (500 mg, 5.81 mmol) was added to a solution of disuccinimidyl chloride (DSC) (3.27 g, 12.76 mmol) and pyridine (Py) (1 mL) in acetonitrile (MeCN) (17.6 mL). The mixture was stirred at rt under Ar atmosphere for 24h. The resulting solution was purified by medium pressure liquid chromatography (MPLC) (acetone: hexane, 1:1) to obtain product A (Figure 2.2) with 79% yield (1690 mg).

It was followed by the hydrogenation reaction of **2** (Figure 3.3) (680 mg, 3.7 mmol) with palladium on activated charcoal (Pd/C) (10% of the weight of **2**, 68 mg) in MeOH under hydrogen gas pressure. This reaction was completed in 6 h and the purification was done by vacuum filtration, resulting in 91% yield (product B, Figure 2.7/2).

For the third step, the product of the first reaction (A: 225 mg, 0.61 mmol) was mixed with the product of the second step (B: 360 mg, 2.42 mmol) and TEA (0.337 mL, 2.42 mmol) in dry MeCN (3.05 mL), at rt during 24 h. Purification was done by MPLC with acetone: hexane giving as a result RU-OH-2 with 75% yield.

For the last synthetic step, thionyl chloride (SOCl<sub>2</sub>) was selected as a chlorinating agent based on its easy removal by distillation. In addition, the volatility of HCl and SO<sub>2</sub> produced in the chlorination process simplifies purifications. Treatment of RU-OH-2 (100 mg, 0.22 mmol) with 2 eq. of SOCl<sub>2</sub> per hydroxyl group (0.16 mL, 0.44 mmol), in the presence of catalytic amounts of BTEAC (0.3 mol %) afforded RU-2 quantitatively after an aqueous workup to recover the catalyst. The reaction was heated at 65°C in a three-necked round-bottom flask under Ar. SOCl<sub>2</sub> was added dropwise from an addition funnel with pressure-equalization arm, and then the reaction was stirred at 65°C for 3.5 h while maintaining a continuous positive Ar flow (to remove HCl

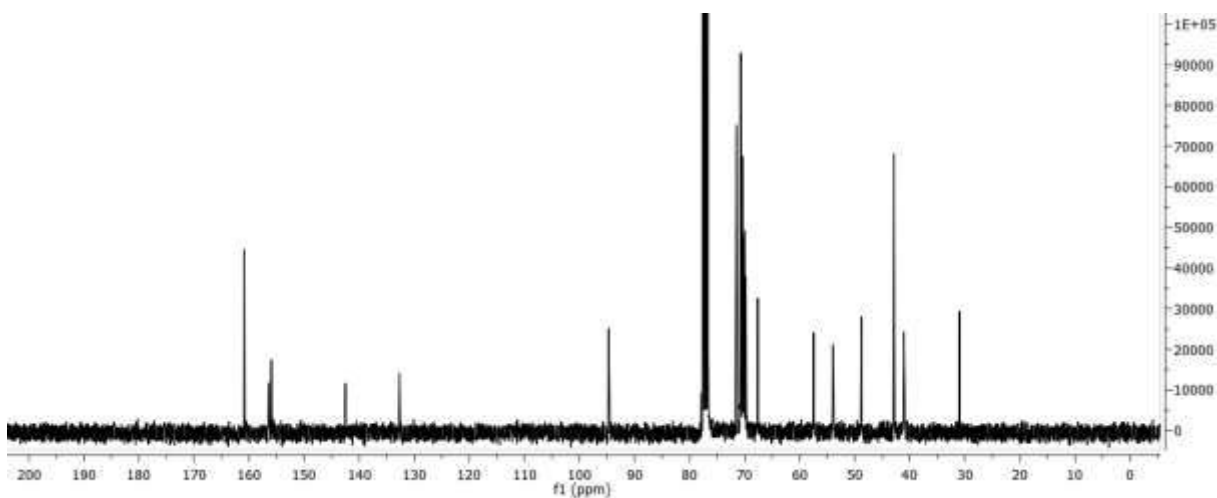
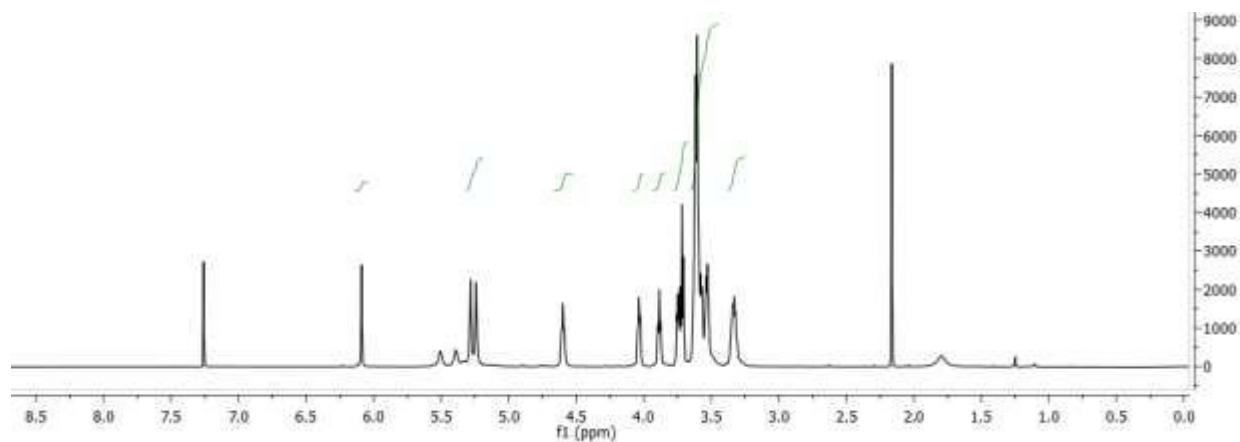
generated during the process). After cooling at rt, the excess of  $\text{SOCl}_2$  was removed at reduced pressure. The resulting crude product was suspended in phosphate buffer (50 mM, pH 7.0) and extracted with a mixture EtOAc. The organic layer was washed with phosphate buffer (50 mM, pH 7.0, 5x1.0 L), dried ( $\text{Na}_2\text{SO}_4$ ), and concentrated to give RU-2 as a yellow gel (77 mg, 70% yield).  $^1\text{H}$  NMR (300 MHz,  $\text{CDCl}_3$ )  $\delta_{\text{H}}$ : 5.9 (s, 2H), 4.63 (s, 4H), 3.69-3.48 (m, 20H), 3.32-3.27 (m, 4H).  $^{13}\text{C}$  NMR (100 MHz,  $\text{CDCl}_3$ )  $\delta_{\text{C}}$ : 155.6, 81.2, 71.8, 70.7, 70.4, 7.1, 42.8, 41.



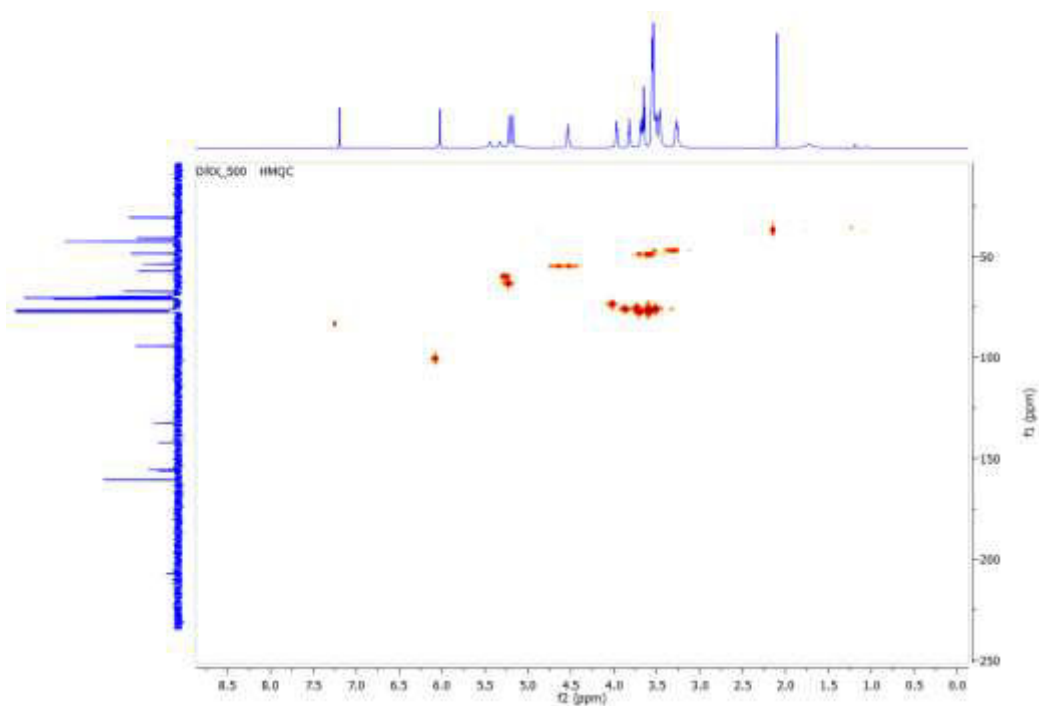
S2.  $^1\text{H}$  and  $^{13}\text{C}$  NMR spectra of RU-2

**G1cb-4.** RU-2 (111 mg, 0.23 mmol) and the core 3 (23.9 mg, 0.04 mmol) were dissolved in a solution of *t*BuOH:  $\text{H}_2\text{O}$  (0.06 mL) inside a microwave tube fitted with a magnetic stirrer. The mixture was object of microwave irradiation with an irradiation power of 150 W and a shut-off temperature of  $100^\circ\text{C}$ . Purification was done by MPLC (hexane: acetone), giving as a result G1cb-4 (14 mg, 18% yield).  $^1\text{H}$  NMR (500 MHz,  $\text{CDCl}_3$ )  $\delta_{\text{H}}$ : 6.1 (s, 3H), 5.28-5.24 (d, 9H), 5.61-5.59

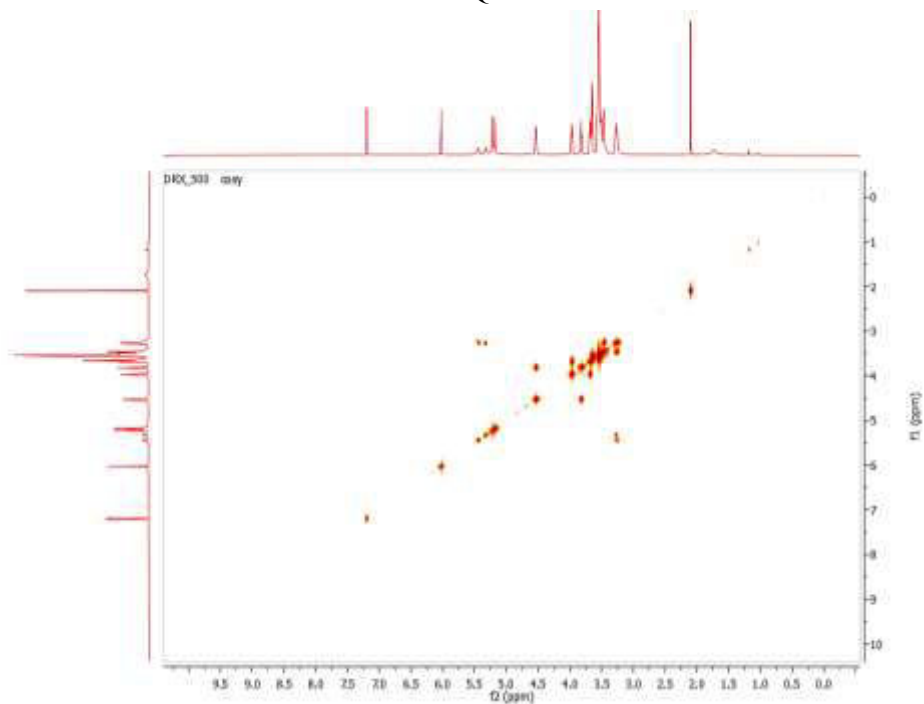
(t, 6H), 4.61-4.59 (t, 6H), 4.04-4.03 (t, 6H), 3.89-3.87 (t, 6H), 3.76-3.52 (t, 83H), 3.35-3.32 (t, 12H).  $^{13}\text{C}$  NMR (101 MHz,  $\text{CDCl}_3$ )  $\delta$ : 160.8, 156.4, 155.9, 142.5, 132.7, 94.7, 71.5, 71.4, 70.8, 70.7, 70.6, 70.4, 70.3, 70.1, 70, 69.9, 69.8, 67.6, 57.5, 54, 48.8, 42.9, 42.8, 41.1.



S3.  $^1\text{H}$  and  $^{13}\text{C}$  NMR spectra of G1cb-4

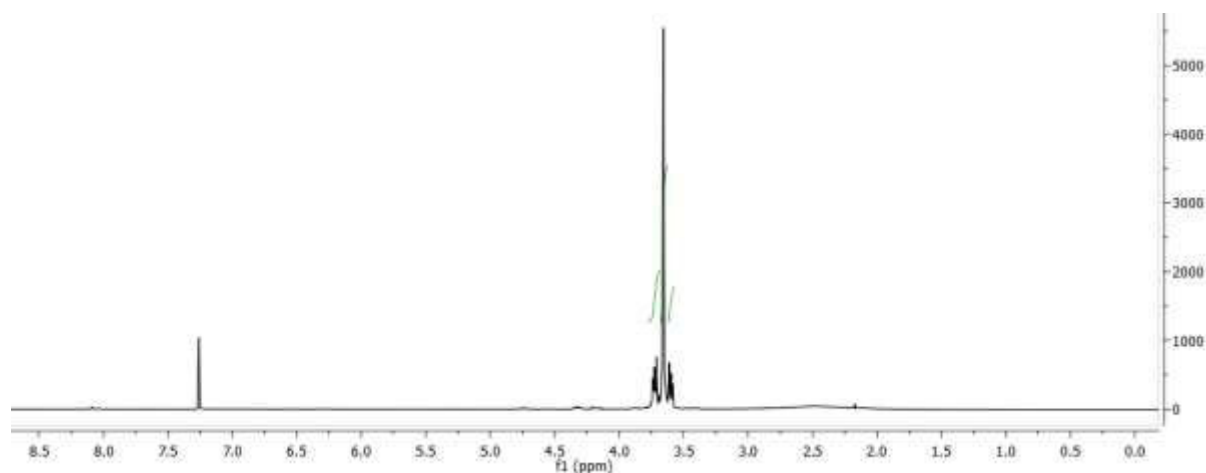


S4.  $^{13}\text{C}$ - $^{13}\text{C}$  HMQC of G1cb-4



S5.  $^1\text{H}$ - $^1\text{H}$  COSY of G1cb-4

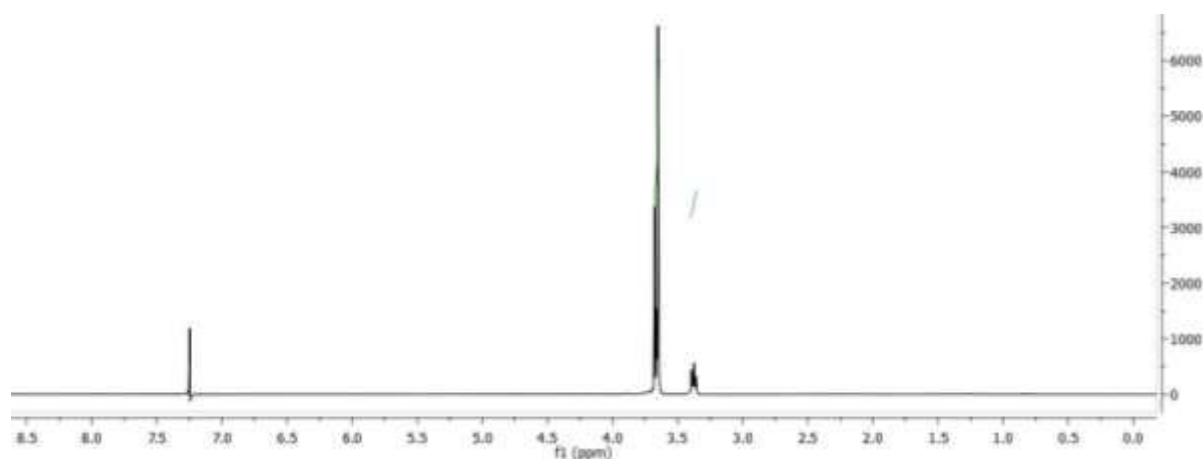
**Aliphatic Core (1).** A mixture of hexaethylene glycol (150 mg, 0.53 mmol) and BTEAC (0.8 mg,  $1.6 \times 10^{-3}$  mmol) was heated at 65 °C in a three-necked round-bottom flask under Ar atmosphere.  $\text{SOCl}_2$  (0.08 mL, 2.12 mmol) was added dropwise from an addition funnel with pressure-equalization arm, and then the reaction was stirred at 65°C for 3.5 h while maintaining a continuous positive Ar flow (to remove HCl generated during the process). After cooling at rt, the excess of  $\text{SOCl}_2$  was removed at reduced pressure. The resulting crude product was suspended in phosphate buffer (50 mM, pH 7.0) and extracted with a mixture EtOAc. The organic layer was washed with phosphate buffer (50 mM, pH 7.0, 5x1.0 L), dried ( $\text{Na}_2\text{SO}_4$ ), and concentrated to give 1,17-dichloro-3,6,9,12,15-pentaoxaheptadecane (146 mg, 86% yield) as a light yellow gel.  $^1\text{H}$  NMR (300 MHz,  $\text{CDCl}_3$ )  $\delta_{\text{H}}$ : 4.7 (s, 4H), 3.74-3.69 (m, 4H), 3.67-3.65 (m, 16H), 3.61-3.58 (m, 4H).



S6.  $^1\text{H}$  NMR spectrum of the chlorinated core 1

The chlorination reaction step was followed by the azide substitution reaction. 1,17-dichloro-3,6,9,12,15-pentaoxaheptadecane (146 mg, 0.53 mmol),  $\text{NaN}_3$  (137.8 mg, 2.12 mmol) and catalytic amounts of 15-Crown-5 (70 mg, 0.318) and were added to a microwave tube with a

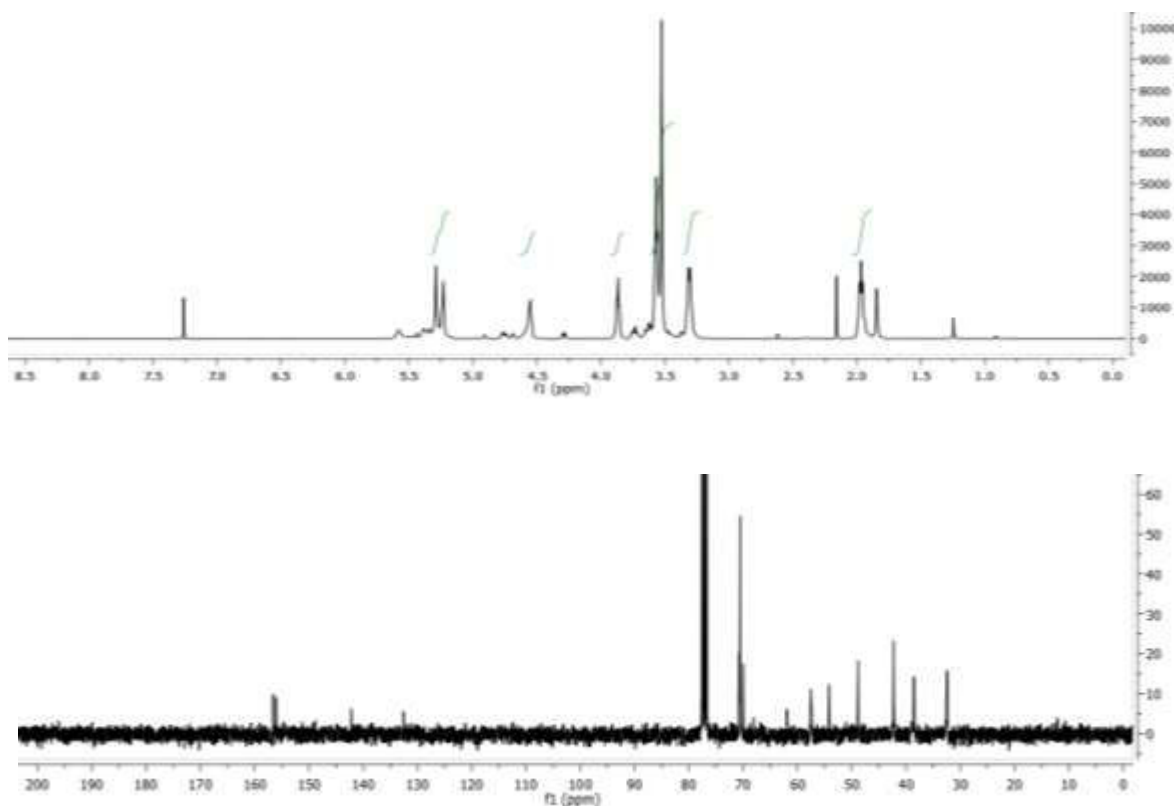
magnetic stirrer and dissolved in dry DMSO (2.12 mL). The mixture was stirred for 40 minutes at 80 °C under microwave irradiation (20 W, airflow 20 with cooling). The purification was done by aqueous workup (3x with EtOAc: Water) to remove the excess NaN<sub>3</sub>, 15-Crown-5 and DMSO. The solution was dried with Na<sub>2</sub>SO<sub>4</sub> and filtered to give a reaction core 1 as light yellow gel (163.8 mg, 93% yield). <sup>1</sup>H NMR (300 MHz, CDCl<sub>3</sub>) δ<sub>H</sub>: 3.68-3.65 (m, 23H), 3.39-3.36 (t, 4H).



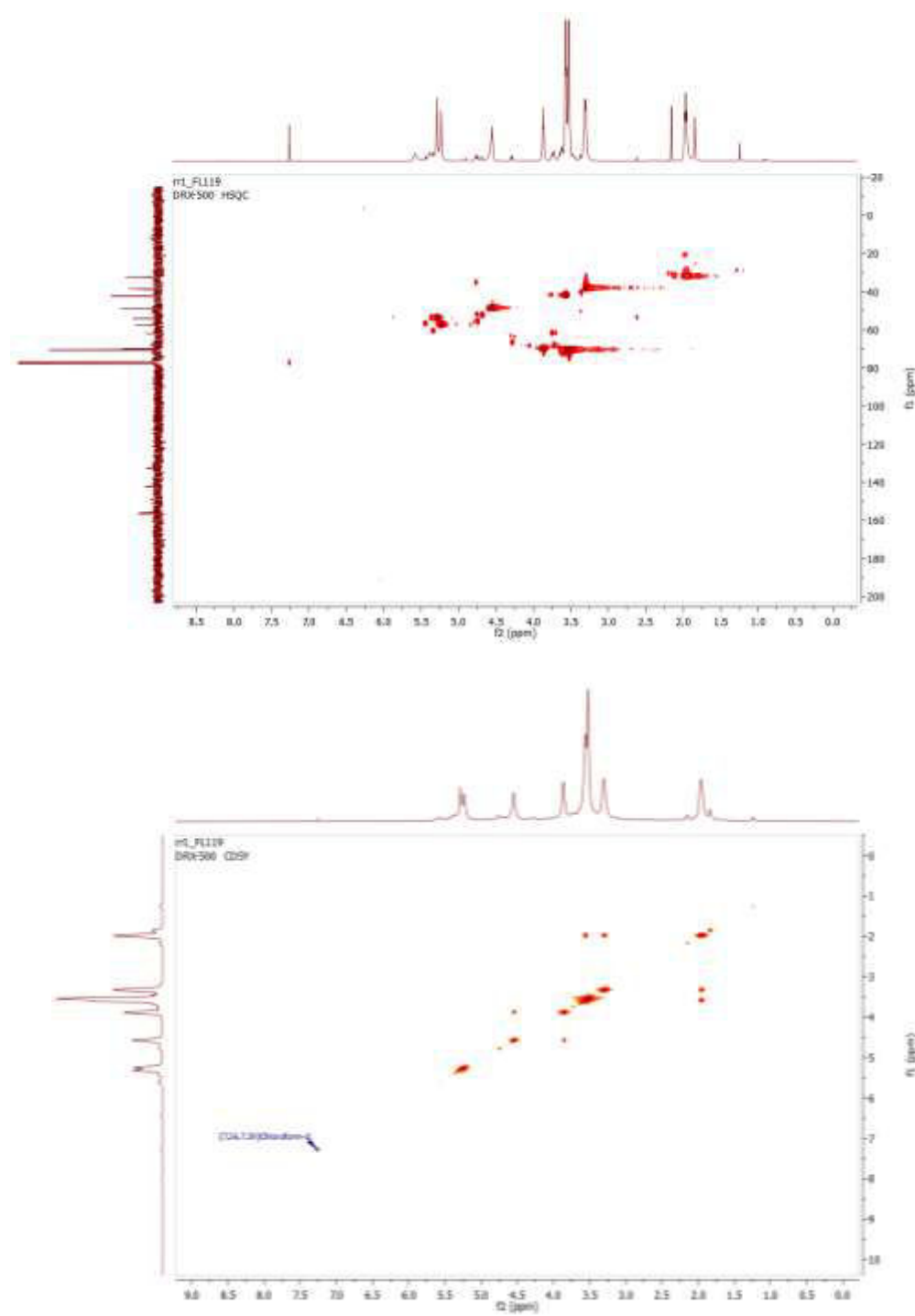
S7. <sup>1</sup>H NMR spectrum of the core 1

**G1cb-5.** RU-1 (150 mg, 0.43 mmol) and the core 1 (35 mg, 0.11 mmol) were dissolved in *t*BuOAc (0.28 mL) inside a microwave tube fitted with a magnetic stirrer. The mixture was object of microwave irradiation with an irradiation power of 120 W and a shut-off temperature of 100 °C. Purification was done by MPLC (hexane: acetone), giving as a result G1cb-5 as a light green gel (92 mg, 84% yield). <sup>1</sup>H NMR (500 MHz, CDCl<sub>3</sub>) δ<sub>H</sub>: 5.29-5.23 (d, 8H), 4.55 (s, 4H), 3.88-3.86 (t, 4H), 3.58-3.53 (m, 26H), 3.32-3.30 (t, 8H). <sup>13</sup>C NMR (101 MHz, CDCl<sub>3</sub>) δ<sub>C</sub>: 156.6, 156, 142.2, 132.5, 70.7, 70.6, 70, 62, 57.6, 57.4, 54.2, 48.8, 42.3, 42.2, 38.6, 38.5, 32.5, 32.4.

**G1cb-5-N<sub>3</sub>.** G1cb-5 (92 mg, 0.098 mmol), NaN<sub>3</sub> (51 mg, 0.78 mmol) and catalytic amounts of 15-Crown-5 (17.3 mg, 0.08 mmol) and were added to a microwave tube with a magnetic stirrer and dissolved in dry DMSO (0.784 mL). The mixture was stirred for 40 min at 80 °C under microwave irradiation (20 W, airflow 20 with cooling). The purification was done by aqueous workup (3x with EtOAc: Water) to remove the excess NaN<sub>3</sub>, 15-Crown-5 and DMSO. The solution was dried with Na<sub>2</sub>SO<sub>4</sub> and filtered to give G1cb-5-N<sub>3</sub> as light yellow gel (32 mg, 34% yield).



S8. <sup>1</sup>H and <sup>13</sup>C NMR spectra of G1cb-5



S9.  $^{13}\text{C}$ - $^{13}\text{C}$  HMQC and  $^1\text{H}$ - $^1\text{H}$  COSY of G1cb-5

### **Conclusions**

During the course of this work two first generation carbamate dendrimers, with either one aliphatic core (newly synthesized) or one aromatic core (synthesized following the procedures previously determined in our group) were constructed using microwave assisted AAC reactions. Two repeating units were newly synthesized as building blocks for these dendrimers, as well. Different challenges were faced during the synthesis and generation growth, such as instability to degradation during microwave assisted AAC reaction, slow conversion kinetics, solubility issues, along with purification difficulties and low yield. Substitution of microwave assisted AAC with one pot reactions done in thermal conditions might lead to better results in the future, for the synthesis and generation growth of structurally similar carbamate dendrimers. However, the continuation of these synthetic efforts, would need critical evaluation on the practicality and cost for the prospective implementation of these carbamate dendrimers in pharmaceutical or industrial settings.

Taking advantage of the previous experience of our group with dendrimer synthesis, this class of dendrimers was substituted with another one, known as GATG dendrimers that incorporated esters instead of carbamate groups. The synthesis of GATG dendrimers was done avoiding the use of Cu, as a catalyst. Recently, our group had good results with the synthesis of a similar family of GATG dendrimers, using microwave assisted AAC protocols, which would facilitate the passage of these dendrimers, from the research field into the industrial/pharmaceutical settings.

An abstract graphic consisting of several thin, white, parallel lines that originate from the lower-left quadrant and extend towards the upper-right quadrant, creating a sense of movement and depth against the blue background.

**GATG dendrimers for  
integrated radiotherapy and  
MRI of glioblastoma**



### 2.2. GATG dendrimers for integrated radiotherapy and MRI of glioblastoma

#### Preamble

Glioblastoma is the most common malignant brain tumor.<sup>179</sup> Despite continuous efforts to treat and prolong the overall survival of glioblastoma patients, this cancer remains incurable.<sup>180</sup> Palliative therapy includes surgical resection combined with radiotherapy and concomitant chemotherapy.<sup>181</sup> The blood-brain barrier (BBB) is the main reason for the failure of conventional systemic drug delivery to gliomas, preventing most chemotherapeutic agents from reaching the brain tumor site in therapeutic doses.<sup>182</sup> The challenge in treating glioblastoma lies on the effective delivery of therapeutic agents, not only to the tumor itself, but to diffuse infiltrative cells that are not located in the tumor bed,<sup>183</sup> avoiding systemic toxicity and healthy brain tissue damage.

Since primary brain tumors have a tendency to reappear after surgical resection within ca. 2 cm of the tumor margin, efforts have been made to prevent recurrence<sup>184</sup> by targeting internal radiation intratumorally.<sup>185-187</sup> Localized radiotherapy is considered nowadays as a promising treatment option for many unresectable solid cancerous tumors. Clinical studies have suggested a benefit to fractionated stereotactic radiosurgery for reirradiation of recurrent glioblastoma.<sup>188-190</sup> Stereotactic radiosurgery is the most precise method to target radiation, while avoiding high systemic doses associated with debilitating toxicities.<sup>191</sup>

Pressure-driven infusion through an intracranial catheter or syringe, also known as convection-enhanced delivery (CED), has the advantage of delivering therapeutic agents along a pressure gradient rather than by simple diffusion, which has shown promising results in animal glioma models.<sup>104, 192-196</sup> A limitation of localized radiotherapy *via* CED is the short biological half-lives of radionuclides that tend to disappear soon after the infusion finishes.<sup>197</sup> To improve

brain retention of therapeutically active compounds following CED, lipid-based nanovectors, such as liposomes,<sup>196, 198-200</sup> and polymers<sup>201</sup> have been studied with promising results for chemotherapy.

However, the optimal liposomal system for radiotherapy was suggested to differ from what is considered optimal for chemotherapeutic delivery.<sup>202</sup> One of the most important limitations of conventional liposomes is the poor control of sustained drug release over prolonged periods.<sup>203</sup> A controlled release profile is especially critical in the case of radionuclide delivery, to avoid radiotoxicity. In search of a stable and innovative internal radiotherapeutic regime, several research groups have explored the use of polymers as carriers of radioisotopes,<sup>204-205</sup> however the lack of precisely defined molecular weights and the characteristic polydispersity of polymers caused large pharmacokinetic variations within labeled materials. Moreover, major concerns in radiotherapy with radio-nanopharmaceuticals include a limited control over isotope release profiles, synthesis methods, carrier size and size distribution, and the number and localization of functionalized pendants that unavoidably results in undefined and so, hardly reproducible mixtures.

Thus, the choice of the nanovectors represents a crucial milestone for the success of internal radiotherapy. In this context, we have turned our attention to dendrimers, especially appealing globular macromolecules characterized by a controlled synthesis that suits well the preparation of monodisperse nanovectors, with tunable size and precise number of peripheral groups.<sup>206</sup> The exquisite control over the architecture of dendrimers provides a powerful tool towards innovative radiopharmaceuticals with well-defined structures and tunable physicochemical properties and function.<sup>207</sup> In addition, the inherent multivalency of dendrimers is envisioned to facilitate the

controlled production of multifunctional nanovectors with synergistically integrated drugs and probes.<sup>133, 208</sup>

Our strategy to a multifunctional theranostic nanovector with improved brain retention involved dendrimers combining  $^{188}\text{Re}$  radioisotopes and paramagnetic  $\text{Gd}^{3+}$  for simultaneous internal radiation and MRI of a F98 rat glioma model. There are not any previous works, in our knowledge, investigating this strategy. The choice of  $^{188}\text{Re}$  radionuclide was based on the usefulness of  $^{188}\text{Re}$ -Nimotuzumab radioimmunotherapy in glioma patients.<sup>209</sup> In addition, in a previous study from our group,  $^{188}\text{Re}$ -loaded lipid nanocapsules proved to be successful in triggering remarkable survival responses in a rat orthotropic glioma model, following different protocols involving CED and simple stereotactic delivery.<sup>104</sup>

Gd contrast-enhanced MRI is known to play a central clinical role in diagnosis, characterization, surveillance and therapeutic monitoring of gliomas. As dendritic scaffold we selected the GATG,<sup>209 210</sup> previously developed by our group for various biomedical applications, including ligand–receptor interactions,<sup>211 212</sup> drug and gene delivery,<sup>210 214</sup> clustering of bacteria,<sup>215</sup> or the preparation of inorganic nanoparticles and contrast agents for MRI.<sup>216 217</sup> Three generations (Gn, with n= 2, 3, 4) of GATG dendrimers, incorporating 18 to 162 peripheral groups were synthesized and fully functionalized with DTPA chelating groups. To directly assess the macromolecular effect of the Gd-labeled dendrimers on the quality of MRI, their relaxivity enhancement properties were compared with those of commercial Gd-DTPA (Magnevist<sup>®</sup>) at 7T. While, all dendrimer generations revealed remarkably superior relaxivity relative to Gd-DTPA, the third generation Gd-2[G3]-DTPA excelled them all and hence, it was selected to be administered *via* CED in an F98 glioma rat model and investigate its brain retention by MRI. A

complementary tissue distribution study was done to compare the brain retention properties of  $^{188}\text{Re}$ -perrhenate and 2[G3]-DTPA-( $^{188}\text{Re}$ , Gd) in F98-rats injected via the same CED procedure.

Finally, in order to mimic the behavior of dendrimers in the bloodstream following their brain clearance,  $^{99\text{m}}\text{Tc}$ -radiolabeling of 2[G2]-DTPA, 2[G3]-DTPA and 2[G4]-DTPA dendrimers was performed and their pharmacokinetics, throughout body distribution and clearance profiles, studied after intravenous (*iv*) injection. We demonstrate that molecular weight and architecture of dendrimers had an important role on their *in vivo* behavior and that the use of dendrimers prevented the fast brain clearance of the radionuclide alone.

### Abstract

A new oncologic strategy, based on the integration of nanovectorized radiotherapy and locoregional delivery, was evaluated for the treatment and imaging of glioblastomas, the most common and lethal type of primary brain tumors. Our focus was the synthesis of heterofunctional dendrimers to facilitate personalized management of glioblastoma. GATG dendrimers, fully functionalized with DTPA derivatives, were the nanovectors of choice to deliver the radiotherapeutic  $^{188}\text{Re}$  and paramagnetic nuclei  $\text{Gd}^{3+}$ , with a minimally invasive stereotactic injection, directly targeting the radiotherapeutic dose to the tumor site in a F98 rat glioma model. Intravenous injection was used to further investigate the pharmacokinetics, throughout body distribution and clearance profiles of these dendrimers. Molecular weight and architecture had an important role on the *in vivo* behavior of the dendrimers. Their use as nanovectors prevented the fast brain clearance of the radionuclide alone, and prolonged the confinement of the internal

radiation at the tumor site. The easy procedure for the dual labeling of these dendrimers opens the perspective of multimodality in therapy and imaging.

### 2.2.1. Materials and methods

#### Materials

Gadolinium (III) chloride hexahydrate, diethylenetriaminepentaacetic acid gadolinium (III) dihydrogen salt hydrate, tin (II) chloride dihydrate, phloroglucinol, 2,2-(ethylenethoxy)bis(ethylamine) and triphenyl phosphine were provided by Sigma-Aldrich. p-SCN-Bn-DTPA was purchased from Macrocyclics. Ketamine (100 mg/mL) was provided from Vétoquinol and xylazine (20 mg/mL) from Bayer. GATG dendrimer repeating unit was prepared following known procedures.<sup>178</sup> All solvents were of HPLC grade and purchased from Sigma-Aldrich or Fisher Scientific and used without further purification. All reagents were of analytical grade. Dulbecco's Phosphate Buffered Saline- 0.0095M (PO<sub>4</sub>) without Ca and Mg (DPBS) BioWhittaker<sup>®</sup> was purchased from Lonza as sterile and filtered. Deionized water was obtained from a Milli-Q plus system (Millipore). <sup>188</sup>Re as carrier-free Na[<sup>188</sup>ReO<sub>4</sub><sup>-</sup>] in physiological solution was obtained by saline elution of <sup>188</sup>W/<sup>188</sup>Re generator (PRIMEX, IBS-CHU, and University of Angers, France). <sup>99m</sup>Tc was kindly provided as carrier-free Na[<sup>99m</sup>TcO<sub>4</sub><sup>-</sup>] from the Department of Radiopharmacy, CHU- Angers, France.

### Instrumentation

Ultrafiltration was performed on Millipore<sup>®</sup> stirred cells using Ultracel<sup>®</sup> regenerated cellulose membranes discs of Mw cutoff 3000 Da (YM3) for 2[G2]-DTPA, and 5000 (YM5) for 2[G3]-DTPA and 2[G4]-DTPA. Size exclusion chromatography (SEC) was performed on an Agilent 1100 series separation module using a PSS Suprema pre-column (5 $\mu$ m 8 x 50 mm) and a PSS Suprema Lux column (5 $\mu$ m 8x300 mm) with an UV detector. A 10 mM PB pH 7.4, 150 mM LiCl solution was used as eluent at 1 mL/min. Solutions of dendrimers (1 mg/mL) were filtered through 0.45  $\mu$ m before injection.

NMR spectra were recorded on Varian Mercury 300 MHz and Varian Inova 750 MHz spectrometers. Chemical shifts are reported in ppm ( $\delta$  units) referenced to residual solvent peaks. FT-IR spectra were recorded on a Bruker IFS-66v using KBr pellets or neat samples (CsI window).

Dendrimer hydrodynamic diameters and  $\zeta$ -potentials were measured by dynamic light scattering (DLS) and laser Doppler micro-electrophoresis on a Nano-S Zetasizer (Malvern Instrument Ltd) at 25 °C. DLS of 2[Gn]-DTPA dendrimers was performed by dissolving the samples in 10 mM PB pH 7.4, 150 mM LiCl (1 mg/mL). The  $\zeta$ -potentials of 2[Gn]-DTPA and Gd-2[Gn]-DTPA were measured by dissolving the samples (1 mg/mL) in 1M PBS pH 7.4, without previous filtering.

MRI was performed with a Bruker Avance DRX 300 equipped with a magnet of 7T at the Primex platform IBS-CHU, University of Angers, France. When possible, experiments were done in triplicate. Mean values and standard deviations are reported unless otherwise stated.

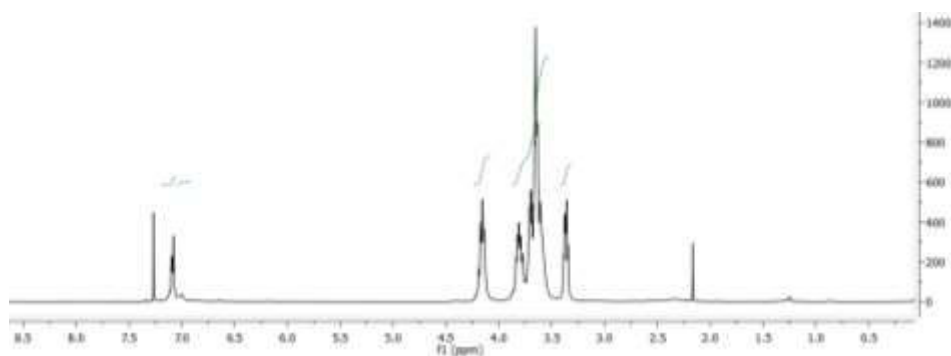
### Characterization of starting dendrimers

Three generations of GATG dendrimers 2[Gn]-N<sub>3</sub> (n = 2, 3, 4), incorporating a divalent 2,2'-(ethylenedioxy)bis(ethylamine) core were synthesized through modification of a previously published route.<sup>178, 211-212</sup>

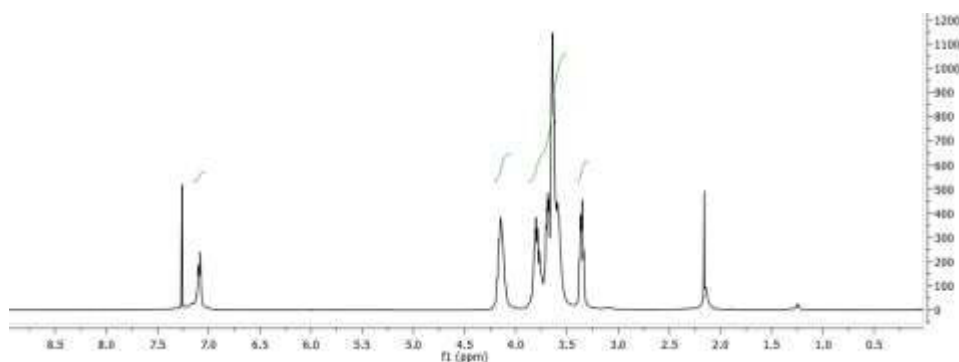
**2[G2]-N<sub>3</sub>.** <sup>1</sup>H NMR (300 MHz, CDCl<sub>3</sub>) δ<sub>H</sub>: 7.10-7.09 (m, 16H), 7.03-7.01 (s, 8H), 4.20-4.14 (m, 48H), 3.85-3.59 (m, 216H), 3.39-3.34 (m, 36H). IR (CH<sub>3</sub>Cl<sub>3</sub>, ICs) ν<sub>max</sub>: 3302, 2925, 2871, 2106, 1652, 1121 cm<sup>-1</sup>.

**2[G3]-N<sub>3</sub>.** <sup>1</sup>H NMR (300 MHz, CDCl<sub>3</sub>) δ<sub>H</sub>: 7.13-7.09 (m, 52H), 4.19-4.15 (m, 156H), 3.81-3.60 (m, 684H), 3.39-3.36 (m, 108H). IR (neat, ICs) ν<sub>max</sub>: 3295, 2926, 2871, 2106, 1652, 1121 cm<sup>-1</sup>.

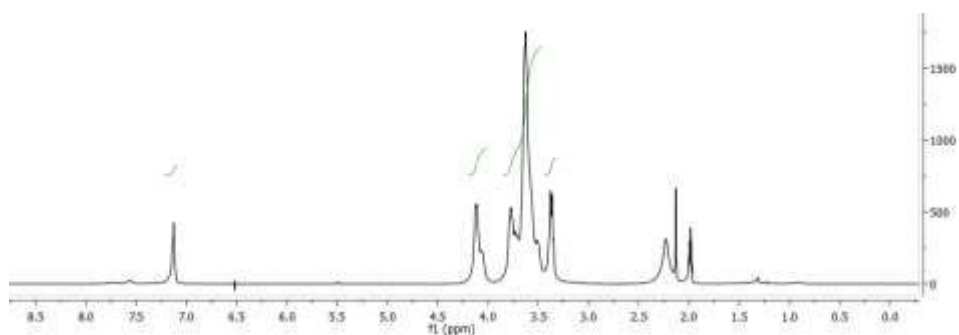
**2[G4]-N<sub>3</sub>.** <sup>1</sup>H NMR (300 MHz, CD<sub>3</sub>CN) δ<sub>H</sub>: 7.13-7.14 (m, 160H), 4.13-4.07 (m, 456H), 3.77-3.52 (m, 2223H), 3.38-3.35 (m, 301H). IR (KBr) ν<sub>max</sub>: 3294, 2927, 2871, 2105, 1652, 1119 cm<sup>-1</sup>.



S10. <sup>1</sup>H NMR spectrum of 2[G2]-N<sub>3</sub>



S11.  $^1\text{H}$  NMR spectrum of 2[G3]-N<sub>3</sub>



S12.  $^1\text{H}$  NMR spectrum of 2[G4]-N<sub>3</sub>

### Synthesis and characterization of new compounds

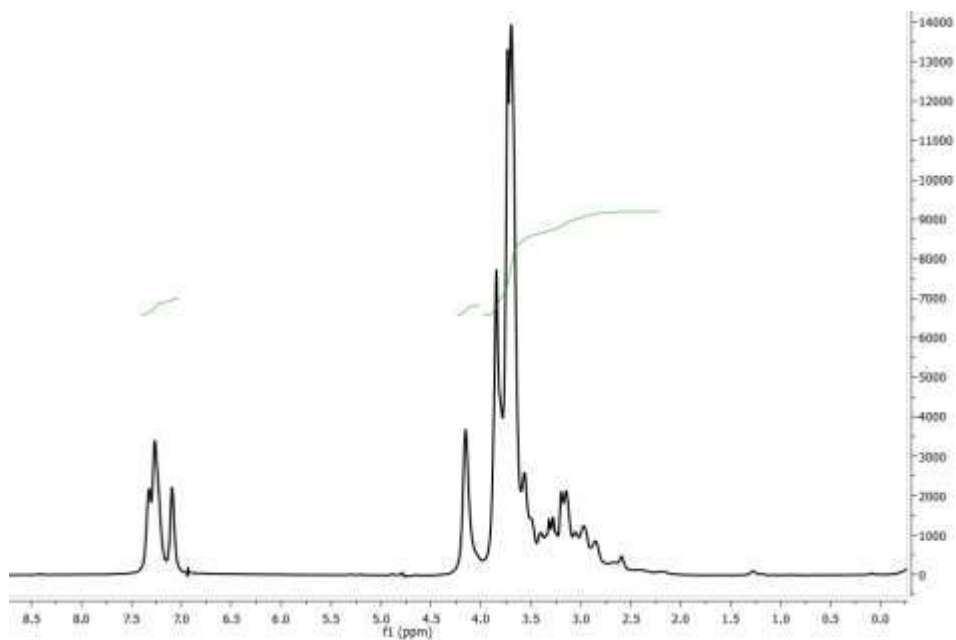
**2[G2]-DTPA.** Ph<sub>3</sub>P (32 mg, 0.12 mmol) was added to a solution of 2[G2]-N<sub>3</sub> (27 mg, 5  $\mu\text{mol}$ ) in MeOH/CHCl<sub>3</sub>/H<sub>2</sub>O 5:5:1 (1.1 mL; 0.1 M/N<sub>3</sub>). The mixture was stirred at rt under Ar until complete reduction of the terminal azides (16 h, as followed by IR). Then, 18-fold molar excess of S-2-(4-isothiocyanatobenzyl)-diethylenetriamine pentaacetic acid (65 mg, 0.10 mmol, *p*-SCN-Bn-DTPA) was added to the mixture. The reaction mixture was heated at 40 °C and the pH adjusted to 9.0 with 2.2 mL of 10 mM PB pH 9/150 mM LiCl solution. After 24 h of stirring at 40 °C, acetone (1.1 mL) was added to homogenize the mixture. A second portion of *p*-SCN-Bn-DTPA (65 mg, 0.10 mmol) was added and stirring continued at 40 °C for another 24 h, while keeping the

pH 9. The resulting solution was purified by ultrafiltration [YM3, 10 mM PB pH 9, 150 mM LiCl (5×30 mL), followed by milliQ water (2 × 30 mL)] and lyophilized to obtain 2[G2]-DTPA as a pale yellow powder (97% yield). <sup>1</sup>H NMR (750 MHz, D<sub>2</sub>O) δ<sub>H</sub>: 7.59-6.97 (m, 88H), 4.15 (br s, 48H), 3.91-2.31 (m, 548H). <sup>13</sup>C NMR (101 MHz, D<sub>2</sub>O) δ<sub>C</sub>: 206.0 185.6, 179.8, 179.5, 178.0, 177.0, 171.3, 168.5, 151.7, 151.0, 139.6, 136.6, 136.2, 135.6, 130.0, 129.0, 126.8, 125.4, 124.3, 106.1, 72.1, 69.9, 69.6, 69.1, 68.9, 68.6, 68.2, 66.4, 62.00, 57.5, 55.1, 54.0, 52.2, 49.0, 43.9, 39.7, 39.0, 32.2. IR ν<sub>max</sub>: 3266, 1586, 1404, 1100 cm<sup>-1</sup>.

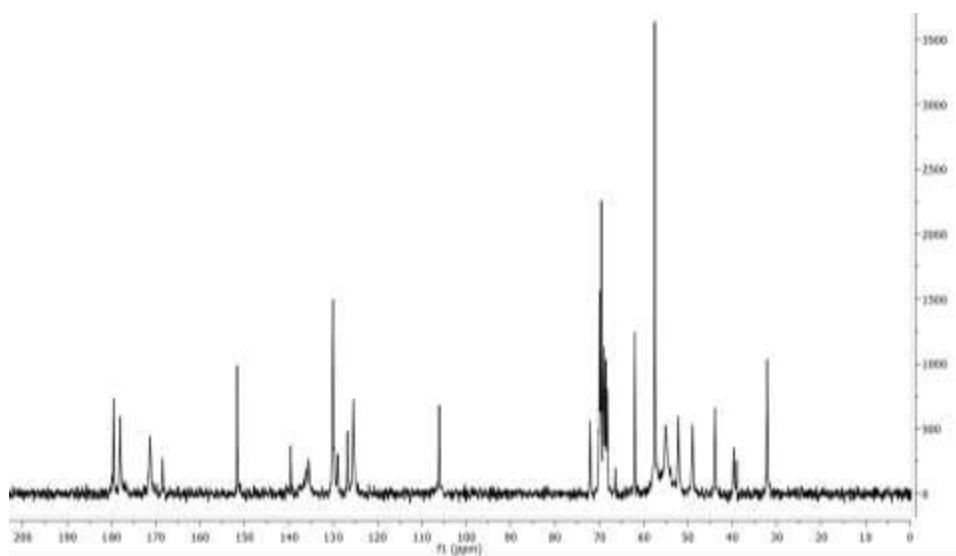
**2[G3]-DTPA.** Ph<sub>3</sub>P (68 mg, 0.26 mmol) was added to a solution of 2[G3]-N<sub>3</sub> (60 mg, 4 μmol) in MeOH/CHCl<sub>3</sub>/H<sub>2</sub>O 5:5:1 (2 mL; 0.1 M/N<sub>3</sub>). The mixture was stirred at r.t. under Ar atmosphere until complete reduction of the terminal azides (36 h, reaction followed up by FT-IR). Then, 54-fold molar excess of p-SCN-Bn-DTPA (136.5 mg, 0.21 mmol) was added to the mixture. The temperature was changed to 40 °C and the pH was adjusted to 9 with 5.4 mL of a 10 mM PB pH 9/ 150 mM LiCl solution. After 24 h of stirring at 40 °C, acetone (2 mL) was added to homogenize the mixture. A second portion of p-SCN-Bn-DTPA (136.5 mg, 0.21 mmol) was added and stirring continued at 40 °C for another 24 h, while keeping the pH 9. The resulting solution was purified by ultrafiltration [YM5, 10 mM PB pH 9/150 mM LiCl (5×30 mL) followed by milliQ water (2 × 30 mL)] and lyophilized to obtain 2[G3]-DTPA as a light yellowish powder (98% yield). <sup>1</sup>H NMR (750 MHz, D<sub>2</sub>O) δ<sub>H</sub>: 7.34-7.02 (m, 268H), 4.12 (s, 156H), 3.93-2.40 (m, 1680H). <sup>13</sup>C NMR (101 MHz, D<sub>2</sub>O) δ<sub>C</sub>: 179.5, 178.5, 168.4, 151.7, 139.6, 135.3, 130.1, 128.93, 125.4, 106.1, 72.1, 70.1, 69.9, 69.6, 69.1, 68.6, 68.3, 61.9, 57.8, 55.5, 51.8, 49.4, 43.9, 39.6, 39.1, 32.4. IR ν<sub>max</sub>: 3310, 1583, 1513, 1396, 1323, 1098, 915 cm<sup>-1</sup>.

**2[G4]-DTPA.** Ph<sub>3</sub>P (55 mg, 0.21 mmol) was added to a solution of 2[G4]-N<sub>3</sub> (50 mg, 1 μmol) in MeOH/CHCl<sub>3</sub>/H<sub>2</sub>O 5:5:1 (1.7 mL; 0.1 M/N<sub>3</sub>). The mixture was stirred at r.t. under Ar atmosphere until complete reduction of the terminal azides (48 h, reaction followed up by FT-IR). Then, it was reacted with a 162-fold molar excess of p-SCN-Bn-DTPA (110.5 mg, 0.17 mmol) at 40 °C and the pH was adjusted to 9 with 4.3 mL of a 10 mM PB pH 9/ 150 mM LiCl solution. After 24 h of stirring at 40 °C, acetone (1.7 mL) was added to homogenize the mixture. A second portion of p-SCN-Bn-DTPA (110.5 mg, 0.17 mmol) was added and stirring continued at 40 °C for another 24 h, while keeping the pH 9. The resulting solution was purified by ultrafiltration [YM5, 10 mM PB pH 9/150 mM LiCl (5×30 mL) followed by milliQ water (2 × 30 mL)] and lyophilized to obtain 2[G4]-DTPA (123 mg, 97%) as a light yellowish powder. <sup>1</sup>H NMR (750 MHz, D<sub>2</sub>O) δ<sub>H</sub>: 7.43-7.00 (m, 774H), 4.15 (s, 468H), 3.92-2.41 (m, 5196H). <sup>13</sup>C NMR (101 MHz, D<sub>2</sub>O) δ<sub>C</sub>: 180.7, 180.2, 180.1, 179.6, 168.3, 151.7, 139.6, 136.5, 129.8, 129.4, 129, 125.1, 123.2, 120.4, 106.1, 72.3, 72.1, 69.9, 69.5, 69.4, 68.9, 68.3, 61.9, 59.2, 58.6, 55.1, 52.8, 50.8, 47.1, 43.5, 39.9, 39.6, 39.2, 32.5. IR ν max: 3365, 2922, 2477, 1578, 1513, 1406, 1327, 1096 cm<sup>-1</sup>.

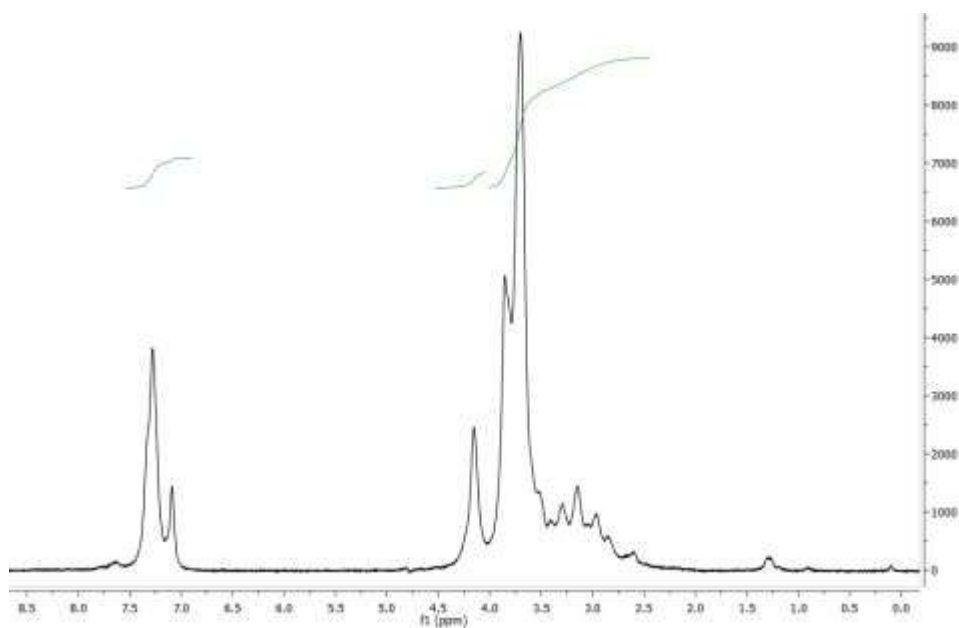
NMR spectra



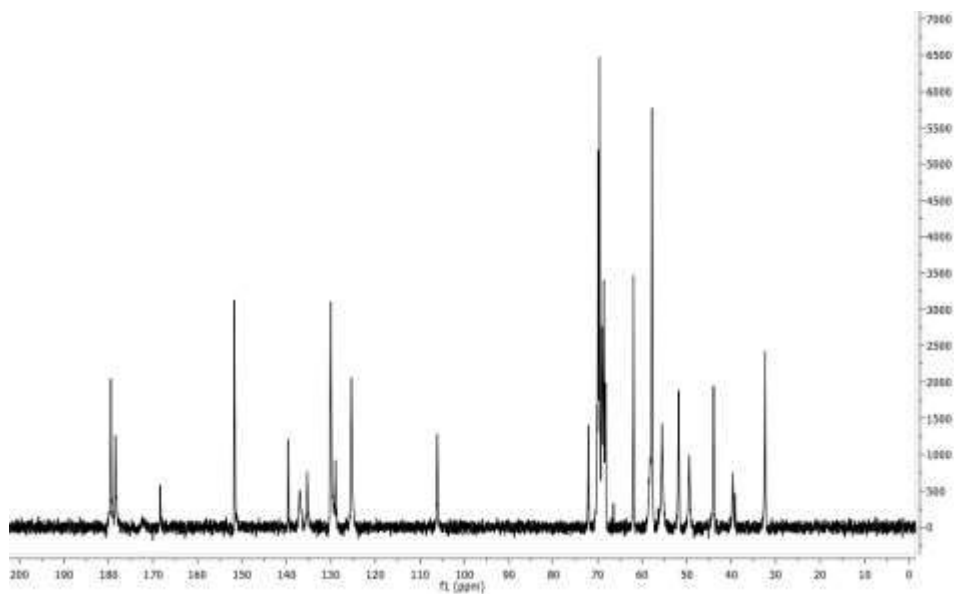
S13. <sup>1</sup>H NMR spectrum of 2[G2]-DTPA (Dfilter 50 ms)



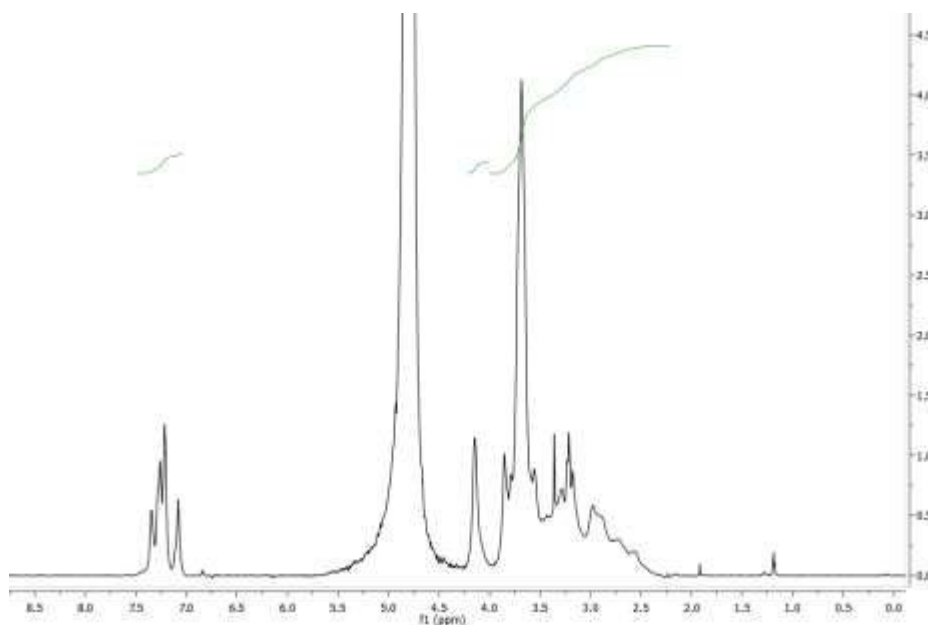
S14. <sup>13</sup>C NMR spectrum of 2[G2]-DTPA



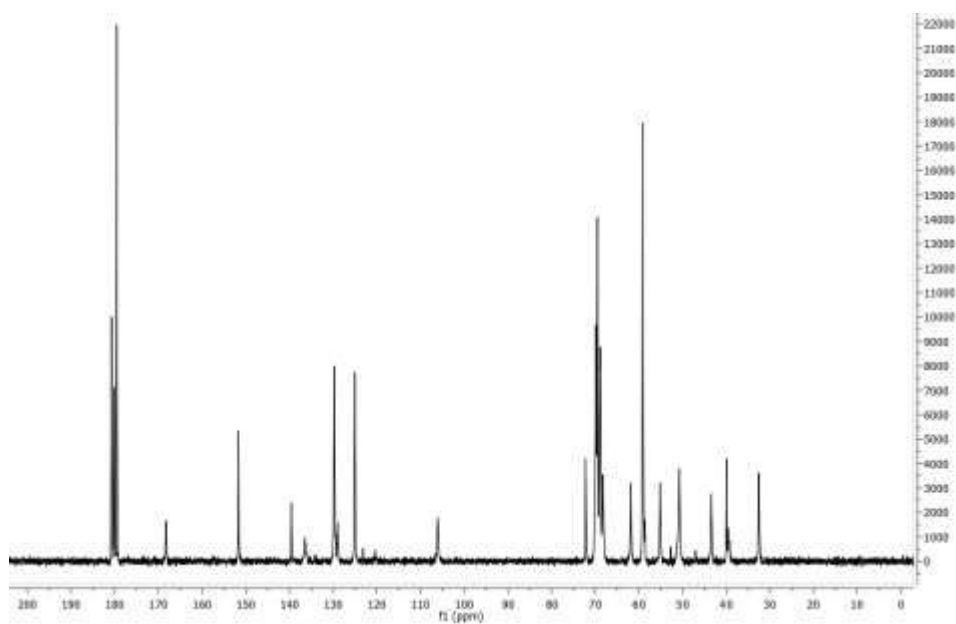
**S15.** <sup>1</sup>H NMR spectrum of 2[G3]-DTPA (Dfilter 200 ms)



**S16.** <sup>13</sup>C NMR spectrum of 2[G3]-DTPA

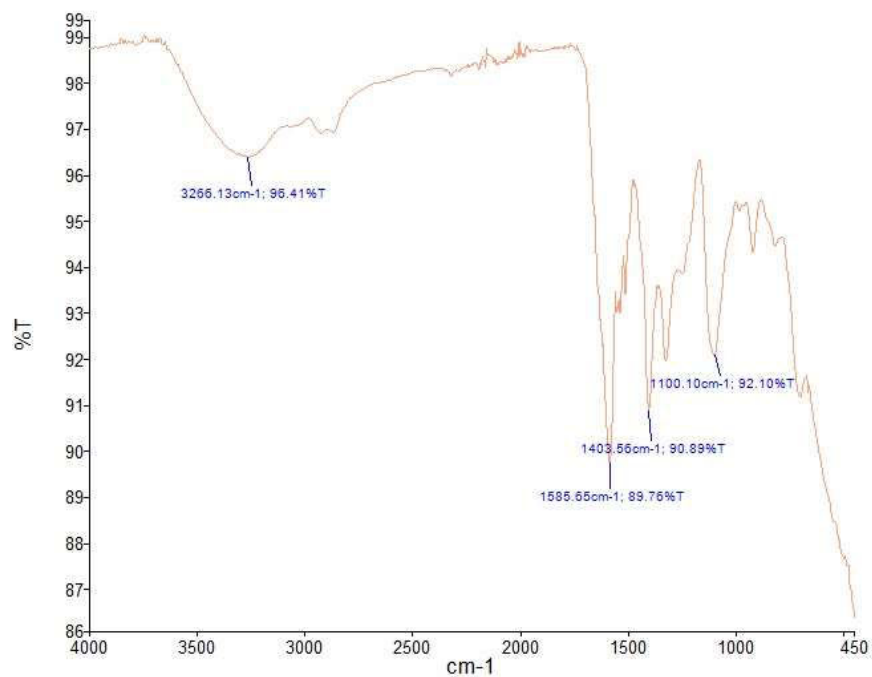


S17. <sup>1</sup>H NMR spectrum of 2[G4]-DTPA

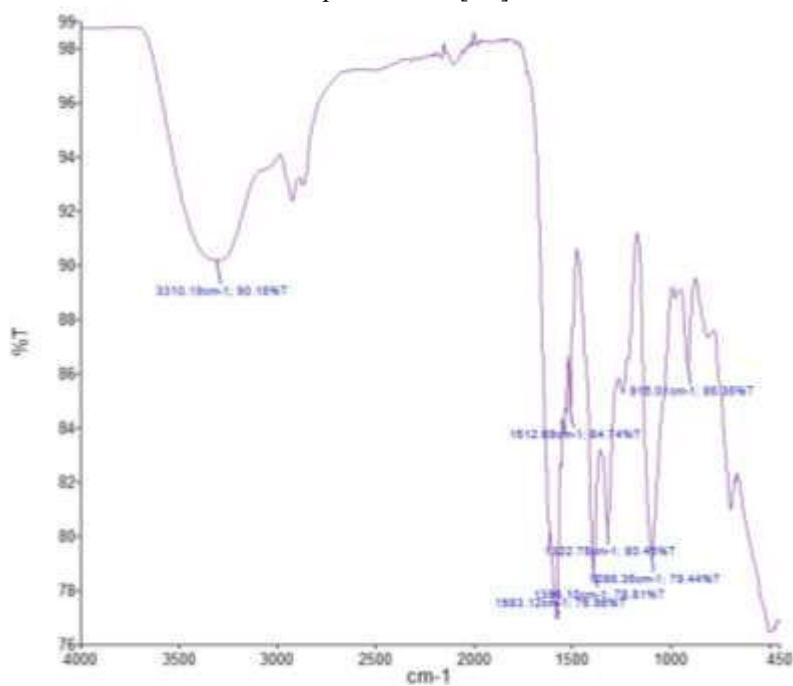


S18. <sup>13</sup>C NMR spectrum of 2[G4]-DTPA

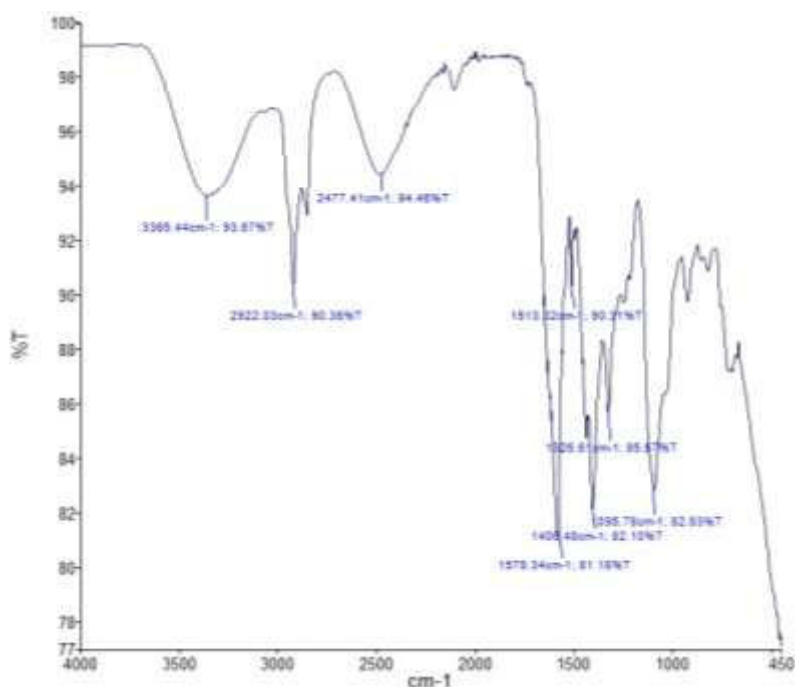
IR spectra



S19. IR spectrum of 2[G2]-DTPA



S20. IR spectrum of 2[G3]-DTPA

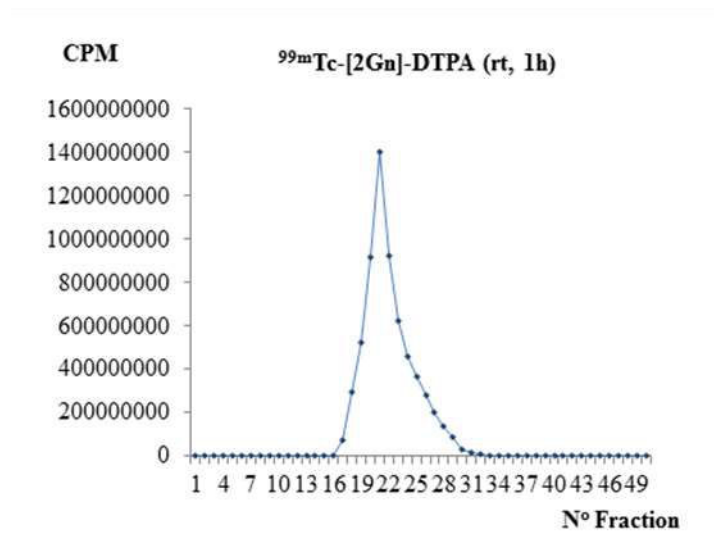


S21. IR spectrum of 2[G4]-DTPA

### Technetium radiolabeling

2[G2]-DTPA, 2[G3]-DTPA and 2[G4]-DTPA (5 mg; 0.385, 0.126, 0.041  $\mu\text{mol}$  respectively) were diluted in 0.9 mL of saline solution (0.9% NaCl). Then 0.1 mL of  $\text{SnCl}_2 \cdot 2\text{H}_2\text{O}$  (7.5 mg/mL) solution was added along with 105 MBq of sodium pertechnetate ( $\text{NaTcO}_4$ ) in 1 mL 0.9% saline solution (as eluted from the  $^{99}\text{Mo}/^{99\text{m}}\text{Tc}$ -generator). The pH of the reaction was maintained at 5.5-6 with 0.1 N NaOH or 0.1 N HCl, as necessary. The resulting mixture was left stirring for 1h at rt.  $^{99\text{m}}\text{Tc}$ -2[Gn]-DTPA dendrimers were purified with a Sephadex G-25 M PD10 column (GE Healthcare Bio- Sciences AB), followed by elution with PBS (10X). The PD10 column was saturated with 70 mL of PBS (10X), before the filtration. Then the mixture from the reactions was filtrated and collected in tubes. Each tube was counted in the gamma counter to determine the elution profile of  $^{99\text{m}}\text{Tc}$ -2[Gn]-DTPA dendrimers. The radiochemical purity of the final solutions was confirmed by ascending instant thin-layer chromatography (ITLC) reading with

a Cyclone Phosphor Imaging System (Packard Instruments) and measuring the content activity of the ITLC silica gel-coated aluminum sheets with a gamma counter (Packard Auto-Gamma 5000 series). The ITLC strips were developed in acetone. Free pertechnetate traveled to the solvent front and the radiolabeled dendrimers remained in the baseline ( $R_f = 0$ ). Free  $^{99m}\text{TcO}_4^-$  was estimated after dividing the ITLC sheet into two equal halves and checking radioactivity in each segment.



**S22.** Elution profile detected by the gamma counter following the radiolabeling reaction of 2[Gn]-DTPA dendrimers with pertechnetate in rt.

### ***In vivo* study of $^{99m}\text{Tc}$ -2[Gn]-DTPA dendrimers following *iv* injection**

In total 36 healthy, 8-10 weeks old, female Wistar rats, weighting 250-300 g were selected for this study. The animals were divided into three groups injected with  $^{99m}\text{Tc}$ -2[G2]-DTPA,  $^{99m}\text{Tc}$ -2[G3]-DTPA and  $^{99m}\text{Tc}$ -2[G4]-DTPA ( $n=12$  per each group). Each rat received a dose of 3.7 MBq of the radiolabeled  $^{99m}\text{Tc}$ -2[Gn]-DTPA dendrimers, by separate *iv* injection through the tail vein. Animals were put in individual metabolic cages directly after injection, to obtain urine and feces. The rats were humanely sacrificed at 1, 6, 24 and 48 hours after the injection ( $n=3$  per each time interval). The blood was collected by tail vein. Subsequently different organs like liver,

kidney, spleen, pancreas, small intestines, large intestines, bladder, ovaries, heart, lungs, stomach, muscle (abdominal wall), skin, bones, brain, and carcass were dissected, washed and weighted.

The content activity of urine, feces and each organ was determined using a gamma counter (Packard Auto-Gamma 5,000 series). The results were expressed as percentage of injected activity (IA) per organ (%IA).



**S23.** Rat in a metabolic cage

The blood pharmacokinetics study was performed in adult, healthy, female Wistar rats weighing 250-350 g. Animals were divided in three groups (n=3), for all the three highest dendrimer generations. Animals were injected via the tail vein with 3.7 MBq of  $^{99m}\text{Tc}$ -2[Gn]-DTPA in 0.2 mL saline. The blood was withdrawn through the tail vein at 0.5, 1, 2, 6, 24, 48 hours after injection. The weight of the blood withdrawn at each sampling point was recorded and the radioactivity measured using a gamma counter (Packard Auto-Gamma 5,000 series). The activity present in total blood was calculated by considering 7.3% of total body weight as total

blood weight.<sup>213</sup> Pharmacokinetic parameters, such as  $t_{1/2}(\alpha)$  and  $t_{1/2}(\beta)$ , were calculated using a two-compartmental model for analysis of pharmacokinetics data via PK solver 2.0, where concentration (C) is the mean % IA found in the total blood of the healthy rats at the specified time interval.<sup>214</sup> In this way, a comparison of the distribution and clearance properties of  $^{99m}\text{Tc}$ -2[G2]-DTPA,  $^{99m}\text{Tc}$ -2[G3]-DTPA and  $^{99m}\text{Tc}$ -2[G4]-DTPA dendrimers was done.

### Gadolinium labeling

5 mg of 2[Gn]-DTPA dendrimers (0.385  $\mu\text{mol}$  2[G2]-DTPA, 0.126  $\mu\text{mol}$  2[G3]-DTPA, 0.041  $\mu\text{mol}$  2[G4]-DTPA dendrimers) containing 6.933  $\mu\text{mol}$ , 6.797  $\mu\text{mol}$  and 6.664  $\mu\text{mol}$  DTPA groups respectively, were mixed with 5.547, 5.438, and 5.331  $\mu\text{mol}$  of  $\text{GdCl}_3 \cdot 6\text{H}_2\text{O}$  (for 2[G2]-DTPA, 2[G3]-DTPA and 2[G4]-DTPA correspondingly) in deionized water for 24 h, at rt (pH 6 arranged with 0.1 M HCl or 0.1 M NaOH solution as necessary). The excess gadolinium in each preparation was removed by centrifugation in a 320R Hettich centrifuge, using Amicon Ultra-4 centrifugal filters (Ultracel®) with a regenerated cellulose membrane Mw cutoff 3000 Da (Merck Millipore®), while simultaneously changing the buffer to 1X PBS. The gadolinium content in the dendrimers was determined by inductively coupled plasma-mass spectroscopy (ICP-MS) analysis at Pharmacology and Toxicology Laboratory, CHU Angers, France. In addition, the filtrate after centrifugation was checked for free  $\text{Gd}^{3+}$  ions by ICP-MS, too.

### Molar relaxivity measurements of Gd-2[Gn]-DTPA dendrimers

Stock solutions of the Gd-2[Gn]-DTPA dendrimers (1 mM in Gd), were diluted to concentrations of 0.1, 0.25, and 0.50 mM in 1X PBS (300  $\mu\text{L}$ ). Solutions of Gd-DTPA (Sigma

Aldrich) were prepared in 1X PBS (300  $\mu$ L) at the same concentration range and used as a reference standard. Relaxivity measurements were obtained at  $\sim 25^{\circ}\text{C}$  using a Bruker Biospec 70/20 system, operating at 7 Tesla. For the  $T_1$  map, a series of variable repetition times ( $T_R$ ) single slice fast spin echo images of all the solutions were acquired at the same time with an echo time ( $T_E$ ) of 7 ms, and 1 average. The total scan time was 18 min and 14 sec.  $T_1$  map parameters were as follows: Matrix (Mtx): 256 x 256; 1 axial slice with 2 mm thickness 6 repetition times:  $T_R = 200; 400; 800; 1500; 3000; 5500$  ms;  $T_E = 7$  ms; FOV= 35 mm x 35 mm. The  $T_1$  values were calculated from the mean signal in the region of interest (ROI) for each repetition time, adjusted to the equation:  $S = S_0 \times (1 - e^{-\frac{TR}{T_1}})$ .

The  $T_2$  maps were calculated from multi spin echo images with a  $T_R$  of 2 s. 25 echo images were acquired with a  $T_E$  of 8.02 ms, which was the interval time between echo images acquisitions, too.  $T_2$ - map parameters were as follows: 1 axial slice of 2 mm thickness;  $T_R = 3200$  ms;  $T_E = 8.02$  ms (25 echo times with interval of 8.02 ms in between), 1 average. Field of view (FOV): 35 x 35 mm; Mtx: 256 x 256; The  $T_2$  values were calculated from mean signal in the ROI for each echo image, adjusted according to the equation:  $S = S_0 \times e^{-\frac{TE}{T_2}}$ . The software used for the calculations was Paravision 6.0 (Bruker Software).

The molar relaxivities,  $r_1$  and  $r_2$ , were obtained from the slope of the inverse of longitudinal relaxation time ( $1/T_1$ ), or of the inverse of transverse relaxation time ( $1/T_2$ ) vs. [Gd] plots, determined from region of interest (ROI) measurements.

### Ethic statement

This study was carried out in strict accordance with the French Minister of Agriculture and the European Communities Council Directive of 24 November 1986 (86/609/EEC). The protocol was approved by the Committee on the Ethics of Animal Experiments of the “Pays de la Loire” (Permit Number: CEEA.2009.6). All surgery was performed under ketamine/xylazine anesthesia, and all efforts were made to minimize suffering.

### Preparation of the glioma animal model

**Tumor cells:** F98 American Type Culture Collection (ATCC), Catalog n° CRL-2397, a rat gliosarcoma cell line, was maintained in Dulbecco’s modified Eagle’s medium (DMEM, BioWhittaker, Verviers, Belgium) containing 10% fetal calf serum (FCS) (BioWhittaker, Verviers, Belgium) and 1% antibiotic and antimycotic solution (Sigma, St Quentin Fallavier, France) in a humidified incubator gassed with 5% CO<sub>2</sub> (37°C) until reaching 80–90% confluence. The number of F98 passages at the time of use for the experiments was between P16-P18.

**Animals:** All the experiments with F98 glioma cell animal model were done with 9 weeks old female syngeneic Fischer rats, weighting 150-180 g, obtained from Charles River. The biodistribution study after intravenous injection of the 2[Gn]-DTPA dendrimers radiolabeled with technetium was performed on 8-10 weeks old healthy female Wistar rats, weighting 250-300 g, obtained from the animal house of the Angers University Hospital. The animals were kept in polycarbonate cages in a room with controlled temperature (20-22 °C), humidity (50-70%), and light (12- hour light/dark cycles). Room air was renewed at the rate of 10 vol. / hour. Tap water and food were provided ad libitum. For biodistribution studies urine and feces were separately

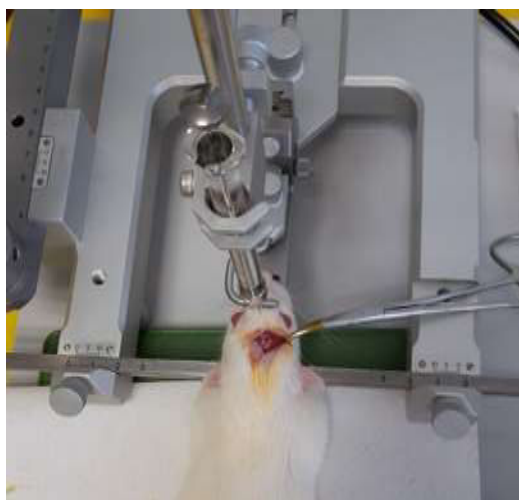
collected in individual metabolic cages, provided from the animal house of the Angers University Hospital. The experiments were conducted in line with the French Minister of Agriculture and the European Communities Council Directive of 24 November 1986 (86/609/EEC).

**Intracerebral tumor implantation:** F98 tumor cells for intracerebral implantation were trypsinized, counted, and checked for viability by trypan blue exclusion. Cells were washed twice with DMEM, (BioWhittaker, Verviers, Belgium) without FCS or antibiotics, and a final suspension of  $1 \times 10^5$  cells/mL in DMEM was obtained. Animals were anesthetized with an intraperitoneal injection of 1 mL/kg of a solution containing 2/3 of ketamine (100 mg/mL) and 1/3 xylazine (20 mg/mL). Using a stereotactic head frame and a 10 $\mu$ L Hamilton syringe 10 $\mu$ L of  $1 \times 10^3$  F98 cells were injected into the rat's right striatum. The coordinates used for the intracerebral injection were 0.8 mm posterior to the bregma, 2.5 mm lateral to the sagittal suture (right hemisphere), and 5 mm below the dura.

**CED procedure:** The animals were anesthetized with an intraperitoneal injection of 0.75 – 1.5 mL/kg of a solution containing 2/3 of ketamine (100 mg/mL; Clorketam®, Vétquinol, Lure, France) and 1/3 xylazine (20 mg/mL; Rompun®, Bayer, Puteaux, France). For the CED injection, 10 $\mu$ L were injected into the rat striatum using a 10 $\mu$ L syringe (Hamilton® glass syringe 700 series RN) with a 32-G needle (Hamilton®), connected to an osmotic pump PHD 2000 infusion (Harvard Apparatus) at a flow of 0.5 $\mu$ L/min for 20 min. For this purpose, rats were immobilized in a stereotactic head frame (Lab Standard Stereotactic; Stoelting, Chicago, IL). Coordinates were 1 mm posterior to the bregma, 3 mm lateral to the sagittal suture, and 5 mm below the dura. Following the injection, the needle was left in place for an additional 5 minutes to avoid expulsion of the injected solution from the brain during the removal of the syringe.

### **CED procedure of Gd-2[G3]-DTPA dendrimers**

The stereotactic injections of 2[G3]-DTPA-Gd dendrimers were performed with a 10 $\mu$ L Hamilton<sup>®</sup> syringe that had a 32-G needle, using an osmotic pump PHD 2000 infusion (Harvard Apparatus, Les Ulis, France), by controlling the flow rate at 0.5 mL $\cdot$ min<sup>-1</sup>. Animals were at day 12 post F98 cells implantation. The coordinates used for these injections were the same as the ones for the implantation of F98 tumor cells.



S24. CED procedure

### **MRI with Gd-2[G3]-DTPA dendrimers in F98 glioma rats, following CED**

For imaging, the animal was positioned supine, with face snugly inserted into a nose cone, centered within a transmitter 86 mm diameter volume coil and receiver 2x2 phase array surface coil. The respiration sensor was placed under the thorax and the temperature of the crib was regulated to 38°C. The anesthesia gas was adjusted between 1.5–2.5% isoflurane and an oxygen flow of 0.5 mL/min, to maintain a respiration rate of ~ 30 bpm during the acquisition of all images. 3 rats bearing F98 glioma tumor were explored by MRI at 24 hours post-CED of Gd-2[G3]-DTPA

dendrimers (1 mM with respect to Gd) to investigate their brain retention and volume of distribution. Animals were at day 12 post-F98 cells implantation. The presence of Gd-dendrimers in fitted  $T_1$ - maps was observed as darker intensity, due to the shorter  $T_1$  relaxation times present. Region of Interests (ROI) that encircled this entire darker intensity were placed with the aid of a cursor and graphic display device on an axial image. ROIs were drawn to measure the volume of distribution ( $V_d$ ) of Gd-2[G3]-DTPA dendrimers at the injection site. The *in vivo*  $V_d$  of the Gd-2[Gn]-DTPA ( $\text{mm}^3$ ) in the MRI was estimated from the product of the slice thickness (mm) and the sum of the areas ( $\text{mm}^2$ ) from the ROI per slice that contained the Gd-2[Gn]-DTPA dendrimers. All MRI experiments were conducted with a Bruker Biospec 70/20 system operating at 7 Tesla using a transmitter 86 mm diameter volume coil and receiver 2x2 phase array surface coil. For  $T_1$  weighted images flash sequence was used.  $T_R = 122.5$  ms, mean echo time (MET): 3.8 ms, 4 averages, FOV: 3 x 3 cm, Mtx: 256 x 256, Flip-angle:  $60^\circ$ , 11 slices with 1 mm thickness.  $T_1$  map parameters: Mtx: 128 x 128, 3 slices with 1 mm thickness, 4 repetition times: TR= 300, 800, 1300, 6000 ms, TE = 21.7 ms; FOV: 3 x 3 cm.



**S25.** F98 glioma rat ready to be put in the MRI system.

### Dual labeling with radioactive 188-rhenium and gadolinium.

The preparation of dual labeled [ $^{188}\text{Re}$ , Gd]-2[G3]-DTPA dendrimers was realized in a one pot reaction, consisting of two steps. Firstly, 1 mg 2[G3]-DTPA dendrimers was labeled with  $\text{Gd}^{3+}$ , as described above, followed by the radiolabeling with  $^{188}\text{Re}$ . Initially, 0.1 mL  $\text{SnCl}_2 \cdot 2\text{H}_2\text{O}$  solution (70 mg/mL  $\text{SnCl}_2 \cdot 2\text{H}_2\text{O}$  in 0.1M HCl) was mixed with the above solution of Gd-2[G3]-DTPA dendrimers (0.8 mL), followed by the addition of 200 MBq of  $^{188}\text{Re}$ -perrhenate ( $^{188}\text{ReO}_4^-$ ; in 0.1 mL saline solution).  $^{188}\text{Re}$  as carrier-free  $\text{Na}[^{188}\text{ReO}_4^-]$  in physiological solution was obtained by saline elution of  $^{188}\text{W}/^{188}\text{Re}$  generator (PRIMEX, IBS-CHU, and University of Angers, France). The reaction pH was arranged to  $\sim 5$  with 0.1 M NaOH and 0.1 M HCl, as necessary. The reaction was heated at  $90^\circ\text{C}$  and was followed by radio-ITLC at 15, 30, 45, and 90 min time intervals. The radio-ITLC strips were developed in acetone. Permeate traveled to the solvent front and the  $^{188}\text{Re}$  complexed in the dendrimers remained in the baseline ( $R_f=0$ ). Purification was done by centrifugation with Amicon 3K, while changing the buffer to PBS, followed by filtration through  $0.8\ \mu\text{m}$  sterile filters. The ITLC strips were cut in half and counted by a Gamma counter (Packard Auto-Gamma 5,000 series) to determine the radiochemical purity. The radiolabeling yield, as a measure of percent incorporation of the radionuclide during the synthesis procedure, was determined with an Activitymeter.

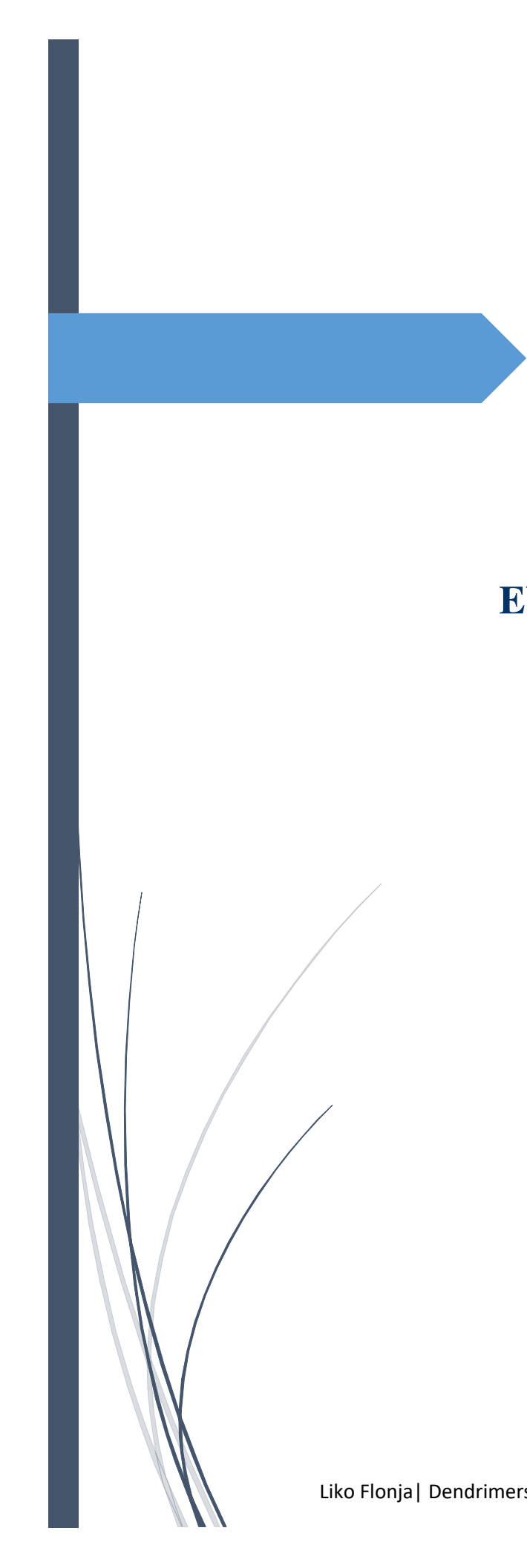
### Experimental conditions for the tissue distribution study following the CED of dual labeled dendrimers.

A tissue distribution study was carried out on 12 female Fischer rats 20 days following the F98 glioma cells implantation. The tumor development was monitored by  $T_2W$  MRI.  $T_2W$  MRI

parameters: RARE Factor = 4, FOV: 3 x 3 cm, Mtx: 256 x 256, 11 slices with 1 mm thickness, TR = 3200 ms, TE = 21.3 ms and 60 ms (2 echo time), 1 avg.

Animals were put in individual metabolic cages, in order to collect urine and feces and they were divided into two groups: one injected with 3.7 MBq of  $^{188}\text{ReO}_4^-$  solution (n=6), and the other with 3.7 MBq of  $[\text{Gd}+^{188}\text{Re}]-2[\text{G}3]-\text{DTPA}$  dendrimers (n=6). In both groups, the animals were sacrificed at post-injection interval times of 24 hours (n=3) and 96 hours (n=3). The organs were removed, washed, and weighed (blood, liver, kidney, spleen, pancreas, small intestines, large intestines, bladder, ovaries, heart, lungs, stomach, muscle (abdominal wall), skin, bones, left hemisphere of the brain, right hemisphere of the brain, and carcass). The content activity of urine, feces and each organ was determined using a gamma counter (Packard Auto-Gamma 5,000 series). The results were expressed as percentage of injected activity (IA) per organ (%IA).

**Statistical analysis:** Results are expressed as mean  $\pm$  standard deviation (SD). Statistical analysis was performed using the One Way Anova or Two Paired t test. Data was considered to be significant when  $p < 0.05$ .



## *Complementary Results*

### **EVALUATION OF 2[G<sub>n</sub>]-DOTA DENDRIMERS FOR MRI**



## **PREAMBLE**

During the course of this work, 2[Gn]-DOTA dendrimers (n=2, 3, 4) were synthesized and characterized, in addition to 2[Gn]-DTPA dendrimers. These dendrimers were designed with the objective of dual labeling with Gd for MRI and radiotherapeutic radionuclides, such as  $^{90}\text{Y}$  or  $^{177}\text{Lu}$ . However, this line of work is to be completed in a near future.

In the present work, 2[Gn]-DOTA dendrimers were labeled with Gd and their relaxivity properties were compared with those of Gd-2[Gn]-DTPA dendrimers in 7T MRI, as described below.

### **2.2.2. Results and Discussion**

Three generations of GATG dendrimers (Figure 1a) incorporating a divalent core and 18 to 162 terminal azide groups, 2[G<sub>n</sub>]-N<sub>3</sub> (n = 2, 3, 4) <sup>177, 212</sup> were fully functionalized with DTPA ligands in a one pot reaction consisting of azide reduction with triphenylphosphine (Ph<sub>3</sub>P) followed by thiourea coupling with an activated isothiocyanate DTPA derivative (*p*-SCN-Bn-DTPA). The resulting dendrimers possess 18 terminal DTPA ligands for 2[G<sub>2</sub>]-DTPA, 54 terminal DTPA ligands for 2[G<sub>3</sub>]-DTPA and 162 terminal DTPA ligands for 2[G<sub>4</sub>]-DTPA. Possession of a short and rigid isothiocyanatobenzyl linker is a positive feature of the incorporated DTPA ligands and a factor that contributes to the high relaxivity, among many others. As reported previously,<sup>44</sup> fast internal rotation of high molecular weight agents prohibits achievement of high relaxivity even though the rotation of the entire molecule is reasonably slow. This short and rigid linker has been reported to limit the rotation of the small Gd chelates, which is characterized as internal rotation.

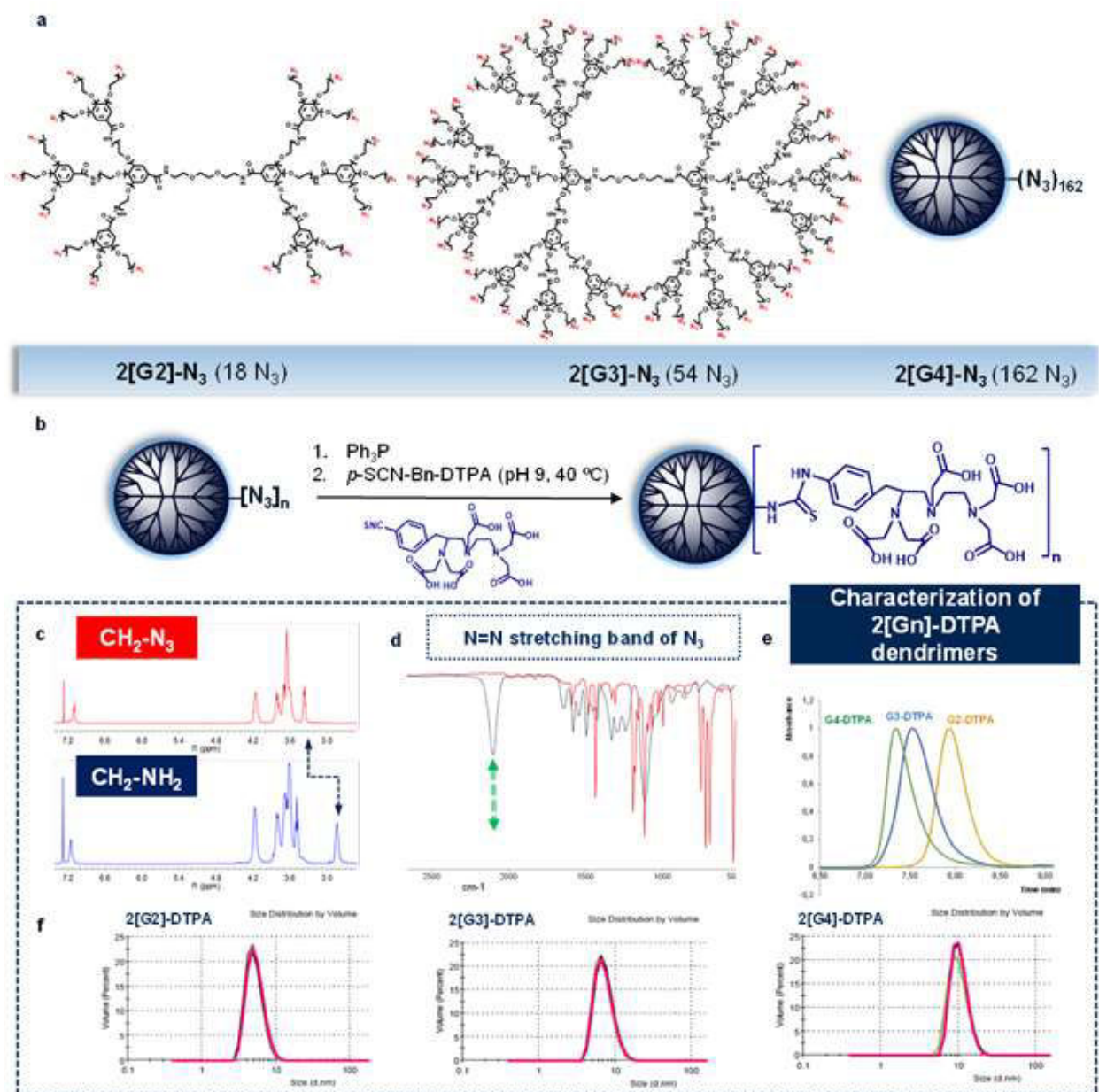


**Figure 2.18.** Functionalization of GATG dendrimers with DTPA ligands. (a) Chemical structure of 2[G<sub>n</sub>]-N<sub>3</sub> dendrimers. (b) One-pot DTPA functionalization reaction. (c, d) <sup>1</sup>H NMR and IR confirming complete reduction of azide groups. (e, f) GPC and DLS of 2[G<sub>n</sub>]-DTPA dendrimers with concentration of 1 mg/mL in 10 mM PB pH 7.4/ 150 mM LiCl.

The completion of the first step was easily monitored by IR spectroscopy thanks to the disappearance of the intense characteristic azide signal at *ca* 2100 cm<sup>-1</sup> (Figure 1c and 1d). The

procedure for the second step was modified from an established procedure in literature.<sup>215-216</sup> Ultrafiltration was the chosen method of purification to remove salts and small molecules, until gel permeation chromatography (GPC) showed a sole peak, confirming the purity of 2[Gn]-DTPA dendrimers. As seen in Figure 1e, dendrimers display monodisperse distributions and the expected increase in size with generation. In addition, they showed complete aqueous solubility and no sign of aggregation as revealed by dynamic light scattering (DLS, Figure 1f), with mean hydrodynamic diameters of 5.2 nm (2[G2]-DTPA), 8.9 nm (2[G3]-DTPA) and 11.7 nm (2[G4]-DTPA). Fully experimental details and characterization are described in the EI.

Afterwards, the solution was lyophilized to afford 2[Gn]-DTPA ( $n = 2, 3, 4$ ) as a white solid in excellent yields (97-98%). Relative NMR integration was used to calculate the degree of conjugation of DTPA ligands to the dendrimers, by determining the ratio of hydrogens that corresponded to one isolated signal, named as signal “a” versus the signal of the aromatic part of the 2[Gn]-DTPA dendrimers (Figure 2.19).

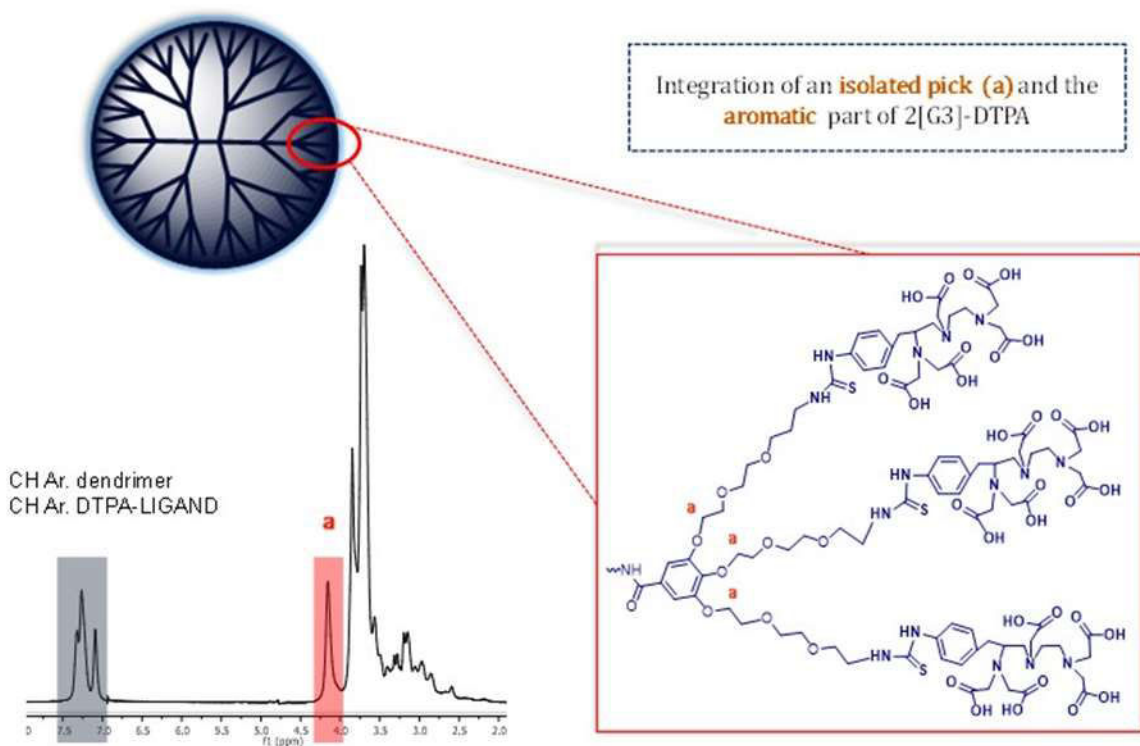


Figure 2.19 Degree of Conjugation of DTPA ligands to 2[Gn] dendrimers.

Technetium ( $^{99m}\text{Tc}$ ) was the radionuclide of choice for the investigation of the *in vivo* properties of the dendrimers, because of its wide availability, convenient half-life, and appropriate  $\gamma$  energy. The dominant role of technetium compounds in diagnostic procedures, strongly recommends the  $\beta$ -emitting rhenium isotope ( $^{188}\text{Re}$ ) for applications in nuclear-medical therapy, because it is possible to adopt general approaches from the established technetium chemistry for  $^{188}\text{Re}$  radiolabeling. Moreover,  $^{188}\text{Re}$  shows similar *in vitro* and *in vivo* behavior to that of  $^{99m}\text{Tc}$ , if labeled to the same nanovector.

Dendrimers were radiolabeled with  $^{99m}\text{Tc}$  with a yield of  $\sim 98\%$  and excellent radiochemical purity. 95-98% of the radioactivity was retained after 24 h in PBS, at room temperature (rt), demonstrating the high stability of the radiolabeled dendrimers (for the  $^{99m}\text{Tc}$  radiolabeling

procedure check EI).  $^{99m}\text{Tc}$  radiolabeling proved successful in assessing the biodistribution and clearance of the radiolabeled dendrimers once in the bloodstream. An *iv* dose of 3.7 MBq  $^{99m}\text{Tc}$ -2[G2]-DTPA (group 1),  $^{99m}\text{Tc}$ -2[G3]-DTPA (group 2), and  $^{99m}\text{Tc}$ -2[G4]-DTPA (group 3) was given to healthy female Wistar rats (n=3 per group). Blood samples were collected at various time intervals post-injection. Results are shown in Figure 2.20.

The  $^{99m}\text{Tc}$ -2[Gn]-DTPA dendrimers were removed rapidly from circulation irrespective of G. The distribution phase half-life  $t_{1/2}$  ( $\alpha$ ) was shorter for  $^{99m}\text{Tc}$ -2[G3]-DTPA dendrimers (12 min), followed by  $^{99m}\text{Tc}$ -2[G4]-DTPA dendrimers (13 min) and  $^{99m}\text{Tc}$ -2[G2]-DTPA dendrimers (18 min). The clear-phase half-life  $t_{1/2}$  ( $\beta$ ) was shorter for  $^{99m}\text{Tc}$ -2[G3]-DTPA (131 min), followed by  $^{99m}\text{Tc}$ -2[G4]-DTPA (134 min) and  $^{99m}\text{Tc}$ -2[G2]-DTPA dendrimers (198 min). In fact, despite their larger size,  $^{99m}\text{Tc}$ -2[G4]-DTPA dendrimers were distributed and cleared out similarly to  $^{99m}\text{Tc}$ -2[G3]-DTPA.  $^{99m}\text{Tc}$ -2[G3]-DTPA had a faster distribution and clearance to that of  $^{99m}\text{Tc}$ -2[G2]-DTPA. These findings are compatible with literature.<sup>210, 217-218</sup>

The major elimination route of the three generations of  $^{99m}\text{Tc}$ -2[Gn]-DTPA dendrimers was through urine. An increased accumulation in the liver with concomitant decreased uptake in the kidney was seen with increasing dendrimer generation. In line with this, an increased accumulation of the dendrimers in the feces was observed with the increase of the liver excretion. In the case of  $^{99m}\text{Tc}$ -2[G2]-DTPA (approx. 13 kDa) a higher kidney accumulation was present, if compared to  $^{99m}\text{Tc}$ -2[G3]-DTPA (approx. 40 kDa) and  $^{99m}\text{Tc}$ -2[G4]-DTPA (approx. 120 kDa). This could be attributed to the exponential increase in the molecular weight of the higher dendrimer generations, since it is known that the molecular structure and the molecular dimensions of a dendrimer are important factors in how dendrimers distribute in the body.

As a rule of thumb, the medically applied macromolecule should have a molecular weight larger than 20 kDa to act as a blood pool agent that stays in circulation for a prolonged period. Besides excretion via the liver, dendritic polyanions with molecular weights or hydrodynamic diameters below the renal threshold (approx. 40kDa) are generally excreted via the kidneys within a few hours.<sup>135, 219</sup> No activity was detected in the stomach, showing the *in vivo* stability of the <sup>99m</sup>Tc-2[Gn]-DTPA dendrimers. These dendrimers did not specifically accumulate in any organs, demonstrating no toxicity risks. Since this study was done in healthy rats, the fact that no activity was found in the brain makes clear that these dendrimers cannot surpass an intact BBB.

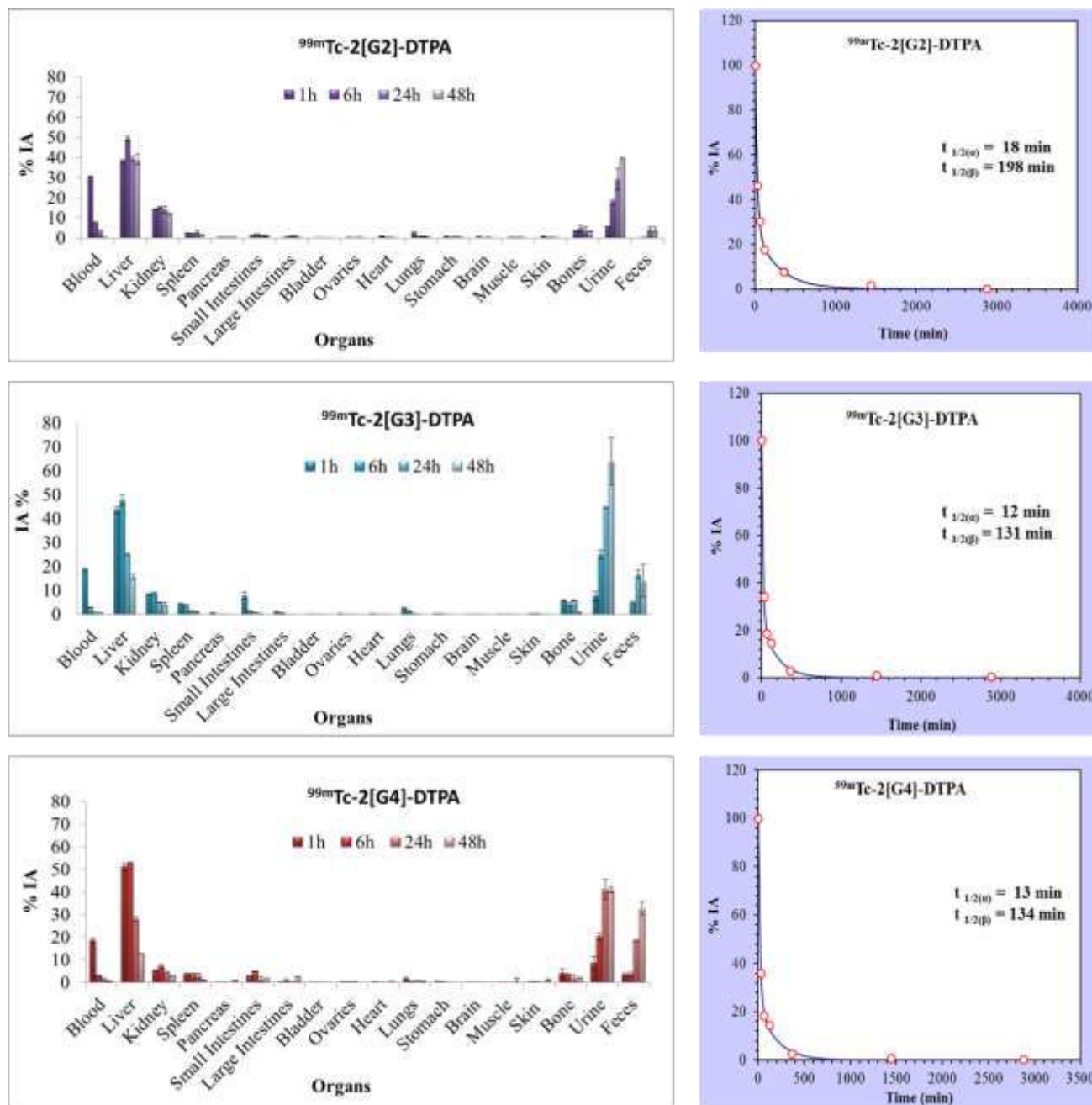


Figure 2.20 (a) Biodistribution analyses (n=3/group). (b) *In vivo* blood clearance in adult female Wistar rats, injected via the tail vein with 3.7 Mbq of <sup>99m</sup>Tc-2[Gn]-DTPA in 0,2 mL saline.

After gathering knowledge on the biodistribution and pharmacokinetics of these dendrimers as nanovectors, the next step was to evaluate their MRI properties and to exploit their brain retention by MRI, following their stereotactic injection in F98 glioma tumor bearing rats. F98 glioma tumor model closely resembles to human glioblastoma. With this aim, Gd complexes of 2[Gn]-DTPA dendrimers (Gd-2[Gn]-DTPA) were prepared with labeling yields ranging from 89 to 98%, as determined by ICP-MS (for Gd labeling procedure, check EI).

In MRI, the image intensity of a parametric image is known to be proportional to the longitudinal ( $T_1$ ) and transverse ( $T_2$ ) relaxation times and it can give a quick view of how these values differ across an image.  $T_1$  and  $T_2$  maps are quantitative images of  $T_1$  and  $T_2$  relaxation times, respectively. A Gd complex induces an increase of both the longitudinal and transverse relaxation rates, ( $R_1=1/T_1$  and  $R_2=1/T_2$ ) of the solvent nuclei. The plot of the observed relaxation rates versus the concentration of the paramagnetic species (Gd) gives a straight line and its slope defines the relaxivity,  $r_{1/2}$  (in units of  $\text{mM}^{-1}\text{s}^{-1}$ ).

Longitudinal ( $r_1$ ) and transverse ( $r_2$ ) relaxivities were determined accordingly, for all generations of Gd-2[Gn]-DTPA dendrimers by concentration dependent measurements of the relaxation times ( $T_{1,2}$ ) at 7T magnetic field strength, which gave good linear fits ( $R^2 > 0.99$ ). Plotting the ( $1/T_{1,2}$  sample- $1/T_{1,2}$  PBS) values of conjugated dendrimers with corresponding Gd concentrations provided the relaxivity of the each sample *in vitro* (Table 2.8). The plots of  $R_1$  versus [Gd] and  $R_2$  vs. [Gd] for the Gd-2[Gn]-DTPA dendrimers and the gold standard Gd-DTPA (both ranging from 0.03 to 1 mM) are depicted in Figure 2.21 c.

It is well known that small size and fast tumbling molecules like Gd-DTPA show a modest decrease in  $r_1$  in higher fields, while slow tumbling molecules, like dendrimers, have high relaxivity that peaks between 0.5-1 T and then show a sharp drop in  $r_1$  with increasing field strength.<sup>220-222</sup> The  $r_2$  has been reported to be static or increases with higher magnetic field strength, resulting in larger  $r_2/r_1$  ratios. Furthermore, molecular relaxivity is defined as the product of the number of the grafted Gd ions on the multimeric molecule per unit of ionic relaxivity. This provides molecules with larger molecular volume, but it is an efficient way to locally increase the metal concentration.

The ion  $r_1$  relaxivity of 2[G3]-DTPA-Gd is more than 2 times higher than the  $r_1$  of Gd-DTPA and higher than the  $r_1$  of 2[G2]-DTPA-Gd and 2[G4]-DTPA-Gd at 7T (Table 2.8).

The effect of the dendrimers, in increasing  $r_2$  at 7T is clear. Gd-2[G2]-DTPA-, Gd-2[G3]-DTPA and Gd-2[G4]-DTPA have an  $r_2$  respectively more than 8, 12 and 11 times higher than that of Gd-DTPA (Table 2.11).

**Table 2.11.** Relaxivities of macromolecular CAs compared with Gd-DTPA in 7T.

Compound	$r_2/\text{Gd}$ ( $\text{mM}^{-1}\text{s}^{-1}$ )*	$r_1/\text{Gd}$ ( $\text{mM}^{-1}\text{s}^{-1}$ )*	Molecular $r_2$ ( $\text{mM}^{-1}\text{s}^{-1}$ )	Molecular $r_1$ ( $\text{mM}^{-1}\text{s}^{-1}$ )	$r_2/r_1$ *
Gd-2[G2]-DTPA	24.5	6.2	318.5	80.6	4.0
Gd-2[G3]-DTPA	41.8	7	1797.4	301	6.0
Gd-2[G4]-DTPA	39.5	6.5	5135	845	6.1
Gd-DTPA	3.4	3.2	3.4	3.2	1.1

\* Ionic relaxivity per Gd

All the dendrimer generations after the labeling with Gd (Gd-2[G2]-DTPA (n=2), Gd-2[G3]-DTPA (n=3) and Gd-2[G4]-DTPA (n=2)) were stereotactically injected in F98 glioma rats. As shown in the Figure 2.21 c MRI scans were done at 0.5h post-CED. The presence of the Gd-2[Gn]-DTPA dendrimers is shown as hypo-intensity in the  $T_1$  maps and higher-intensity in the  $T_1W$  images.

Since for an efficient radiotherapy and follow-up MRI, nanovectors must combine efficient clearance profiles with sufficient retention of radiotherapeutic nuclides and paramagnetic nuclei at the tumor site, we decided to quantify the brain retention and clearance rate of the dendrimers following CED. With this aim we dual labeled the 2[G3]-DTPA dendrimers with Gd and  $^{188}\text{Re}$  and performed a tissue distribution study in rats bearing F98 glioma tumors, at day 20 following stereotactic tumor implantation ( $^{188}\text{Re}$ : 3.7 MBq + Gd: 1mM/ 10 $\mu\text{L}$  injection). The tissue distribution of these dendrimers was compared in parallel with that of the free radionuclide ( $^{188}\text{Re}$  perrhenate: 3.7 MBq/ 10 $\mu\text{L}$  injection) following identical experimental conditions. In this way, it was made possible to know the exact brain confinement properties of dendrimers as nanovectors. The preparation of dual labeled [ $^{188}\text{Re}$ , Gd]-2[G3]-DTPA dendrimers was realized in a one pot reaction with a radiolabeling yield of around 62%, and radiochemical purity exceeding 95% as determined by radio-ITLC. The radiolabeling process was finalized in 30 minutes. 97% of the radiolabeling was retained after 24 h in PBS at rt, demonstrating the high stability of ( $^{188}\text{Re}$ , Gd)-2[G3]-DTPA dendrimers (more information on the conditions of the dual labeling process available on the EI).

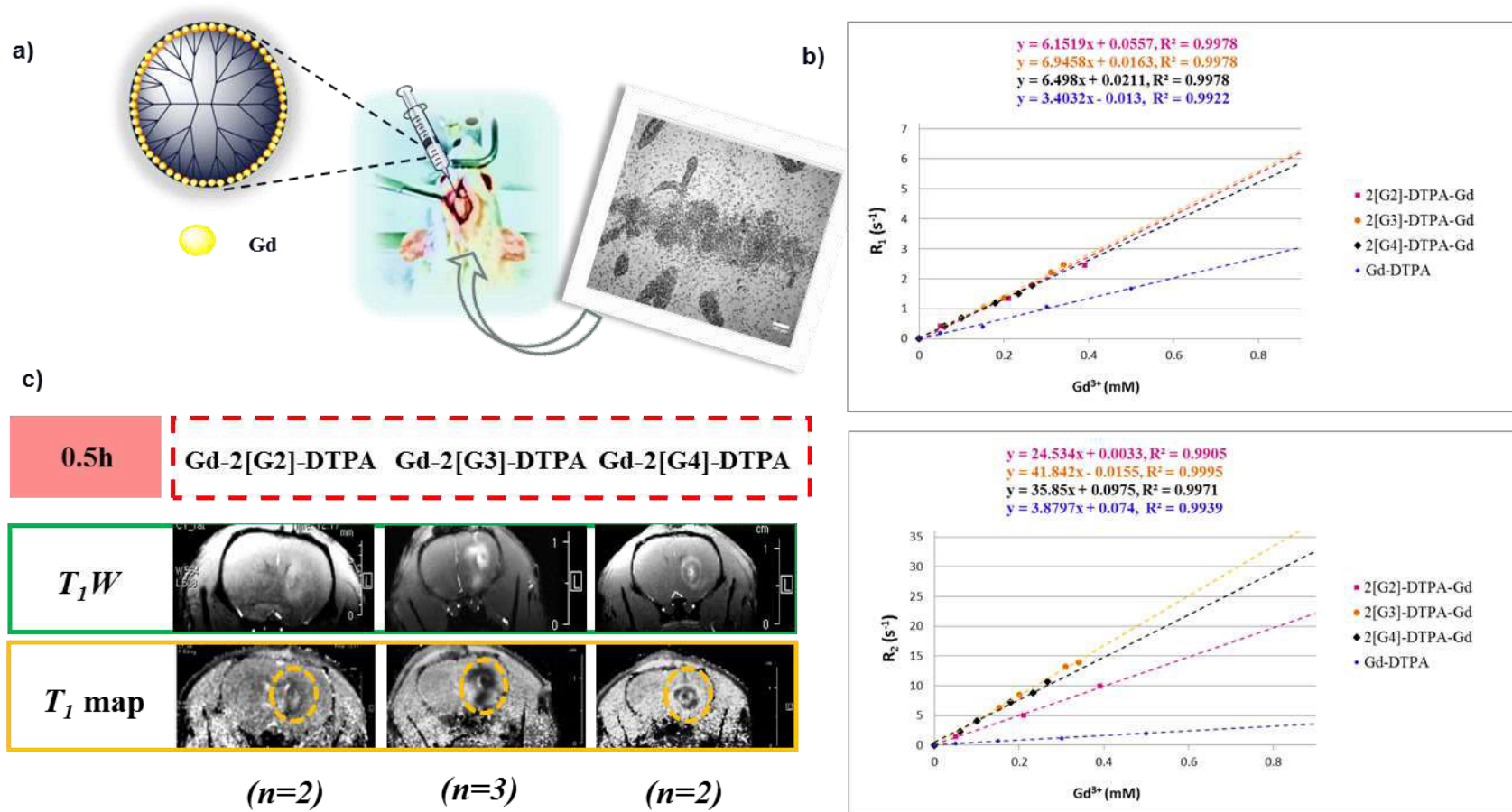


**Figure 2.21.** Evaluation of 2[Gn]-DTPA dendrimers by MRI following Gd labeling. (a) Schematic including CED of Gd-2[G3]-DTPA dendrimers in F98 glioma tumor bearing rats. An extensive invasion of normal brain with islands of F98 tumor cells at varying distances from the tumor mass is observed. (b)  $R_1$  and  $R_2$  plots for Gd-2[G2]-DTPA (pink), Gd-2[G3]-DTPA (orange), Gd-2[G4]-DTPA (black), and Gd-DTPA (blue); (c)  $T_1W$  and  $T_1$  maps of the F98 glioma rats 0.5h post-CED (7T MRI). Orange circles indicate the presence of 2[Gn]-DTPA-Gd.

The tissue distribution study was carried out on 12 female Fischer rats 20 days following the F98 glioma cells implantation. Rats were humanly sacrificed at days 21 and 24 after F98 tumor cell implantation (for more details on this procedure see EI). The levels of radionuclide brain retention and organ distribution were evaluated along with the  $^{188}\text{Re}$  elimination in feces and urine over 24 (Figure 2.22 a) and 96 h (Figure 2.22 b) following CED, in four groups of animals (n=3). While it has been largely described that  $^{188}\text{Re}$ -perrhenate is rapidly excreted via the urinary bladder following intravenous injection,<sup>223</sup> little was known about the elimination of such a solution following brain administration.

Gratifyingly, a significant difference between a CED infusion of  $^{188}\text{Re}$ -perrhenate and of ( $^{188}\text{Re}$ , Gd)-2[G3]-DTPA dendrimers was observed. While almost all of the injected activity (IA) of  $^{188}\text{Re}$  was eliminated via urine within 24h following CED of  $^{188}\text{Re}$ -perrhenate, only 14% IA of  $^{188}\text{Re}$  was found in urine for ( $^{188}\text{Re}$ , Gd)-2[G3]-DTPA dendrimers at the same time. Interestingly, 75% IA of ( $^{188}\text{Re}$ , Gd)-2[G3]-DTPA was retained at the injection site in the right brain hemisphere, not surpassing to the left brain hemisphere, as previously anticipated by  $T_1$  maps. After 96 h, with 88% IA of the  $^{188}\text{Re}$  radioactivity of ( $^{188}\text{Re}$ , Gd)-2[G3]-DTPA found in urine, still 8.6% IA resided at the injection site in the right brain hemisphere and no activity was detected in the left brain hemisphere.

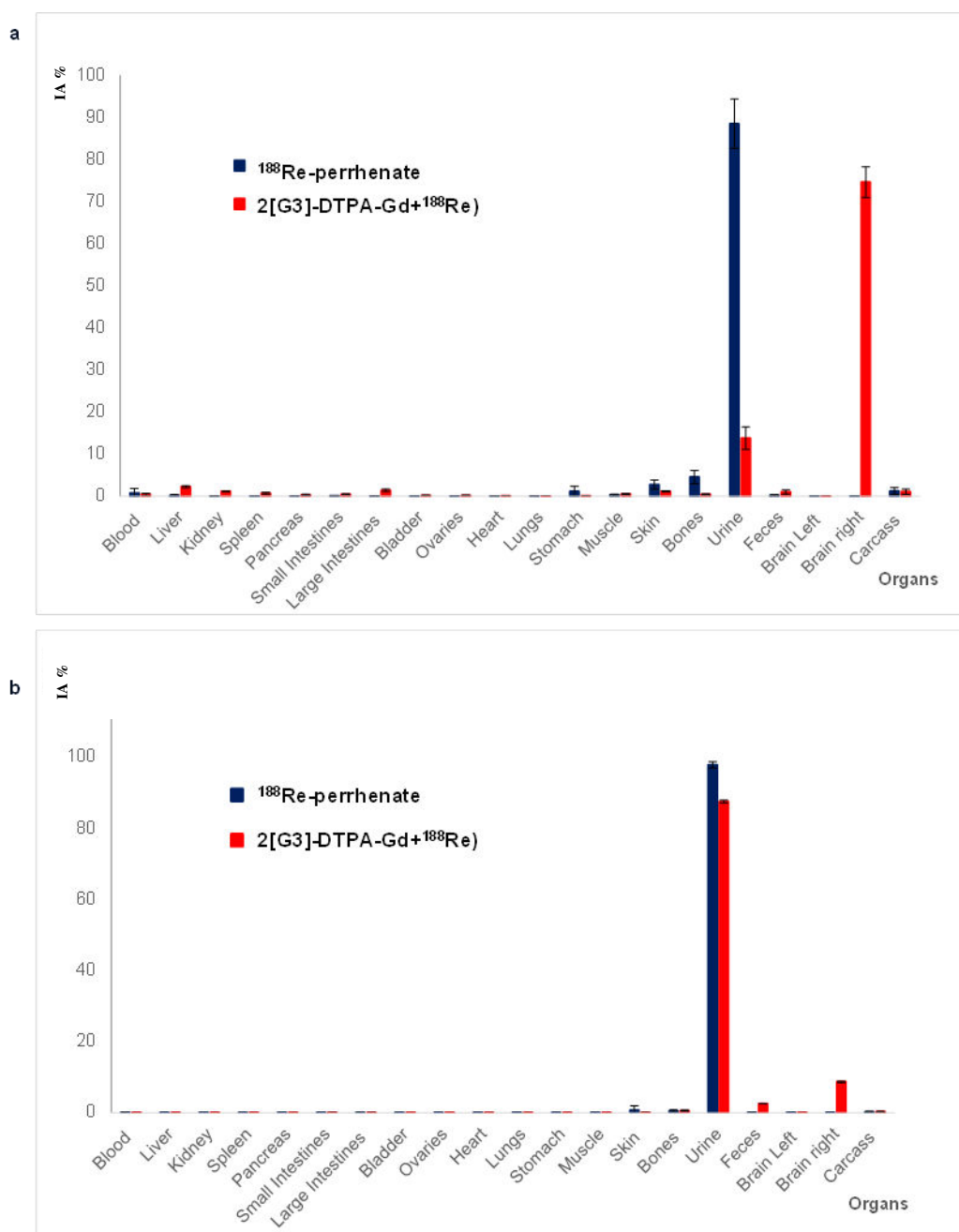


**Figure 2.22.** Brain retention and clearance of 2[Gn]-DTPA dendrimers following dual labeling with Gd and  $^{188}\text{Re}$ . Tissue distribution comparison between  $^{188}\text{Re-perrhenate}$  (3.7 MBq) and of [ $^{188}\text{Re}$ , Gd]-2[G3]-DTPA dendrimers (3.7 MBq) (a) 24 hours (b) and 96 hours following their CED in F98-glioma rats (n=3).

### Conclusions

In summary, we synthesized four generations of GATG dendrimers fully functionalized with DTPA ligands. Benefitting from the high-density functional groups on the surface of the dendrimer, a large number of DTPA ligands (ranging from 18 to 162 DTPA ligands/dendrimer from 2[G2]-DTPA to 2[G4]-DTPA) was available to be labeled with  $^{99m}\text{Tc}$ , Gd and  $^{188}\text{Re}$ . These dendrimers were radiolabeled with  $^{99m}\text{Tc}$  to determine and compare the *in vivo* properties of different generations, such as throughout body distribution, pharmacokinetics, clearance profiles and possible organ toxicity.

Molecular weight and architecture had an important role on the *in vivo* behavior of these dendrimers. With the increase in generation size, an increase in liver uptake with concomitant decrease in kidney uptake was observed. The third generation of dendrimers resulted as the best one for faster throughout body distribution and clearance. The MRI imaging properties of these Gd-labeled dendrimers, were evaluated at 7T and compared with those of the commercial Gd-DTPA. All the generations of dendrimers, with the third one being the best, had a higher  $r_1$  and  $r_2$  relaxivity in comparison with this gold standard.  $T_1$  maps confirmed the retention of the 2[G3]-DTPA-Gd dendrimers at the injection site, up to 24h post-CED.

The use of dual labeled dendrimers with  $^{188}\text{Re}$  and  $\text{Gd}^{3+}$  was evaluated following CED in an F98 glioma model and compared with  $^{188}\text{Re}$ -perrhenate. The use of dendrimers avoided the fast brain clearance of the radionuclide alone, and prolonged the confinement of the internal radiation at the tumor site. No radioactivity was found at the other brain hemisphere, showing that the dendrimers were confined at the injection site, before their unavoidable brain clearance.

For an efficient locoregional radiotherapy, the brain retention of these dendrimers needs to be improved, since at 96h post-CED approx. 8.6 % IA was counted at the injection site in the right brain hemisphere. Our ongoing research represents one of the first efforts in the field, to integrate multimodal dendrimers in nanovectorized radiotherapy and imaging of glioblastomas, following CED.

## 2.3. Complementary results

### 2.3.1. Materials and methods

#### Materials

Gadolinium (III) chloride hexahydrate, diethylenetriaminepentaacetic acid gadolinium (III) dihydrogen salt hydrate, 2,2-(ethylenethoxy)bis(ethylamine) (98%) and triphenyl phosphine (freshly crystallized from ethanol to remove triphenylphosphine oxide) were provided from Sigma-Aldrich. P-NCS-benzyl-DOTA-GA was ordered from CheMatech. Dendrimer's repeating unit (R.U.) 3,4,5-Tri-{2-[2-(2-azidoethoxy)ethoxy]ethyl}benzoic acid was prepared as described in reference <sup>178</sup>. All solvents were of HPLC grade and purchased from Sigma-Aldrich or Fisher Scientific and used without further purification. All reagents were of analytical grade. Dulbecco's Phosphate Buffered Saline- 0.0095 M (PO<sub>4</sub>) without Ca and Mg (DPBS) BioWhittaker<sup>®</sup> was purchased from Lonza as sterile and filtered. Deionized water was obtained from a Milli-Q plus system (Millipore).

#### Instrumentation

Automated column chromatography was performed on a MPLC Teledyne ISCO CombiFlash RF – 200 psi with a RediSepRf normal-phase 12 g silica column and with home-made RediSepRf reused columns, filled with basic aluminum oxide 70–230 mesh from Merck in the case of 2[G2]-N<sub>3</sub> dendrimers. Ultrafiltration was performed on Millipore<sup>®</sup> stirred cells using Ultracel<sup>®</sup> regenerated cellulose membranes discs Mw cutoff 3000 Da (YM3) for 2[G3]-N<sub>3</sub> and Mw cutoff 5000 (YM5) for 2[G4]-N<sub>3</sub> dendrimers. YM3 membrane was used for 2[G2]-DOTA dendrimers and YM5 membrane for 2[G3]-DOTA and 2[G4]-DOTA dendrimers. Molecular weight distributions of dendrimers were determined by size exclusion chromatography (SEC) on

an Agilent 1100 series separation module using a PSS SDV pre-column (5 $\mu$ m, 8 $\times$ 50 mm), a PSS SDV Linear S column (5 $\mu$ m, 8 $\times$ 300 mm), a PSS SDV Lux Linear M column (5 $\mu$ m, 8 $\times$ 300 mm) with an Agilent 1100 series refractive index (RI) detector. THF was used as eluent at 1 mL/min for azide dendrimers, and filtered through 0.45  $\mu$ m before injection. In the case of 2[Gn]-DOTA, 10 mM PB pH 7.4/ 150 mM LiCl was used as eluent at 1 mL/min with 1 mg/mL concentration and filtered through 0.45  $\mu$ m before injection.

NMR spectra were recorded on a Varian Mercury 300 MHz and Varian Inova 750 MHz spectrometers. Chemical shifts are reported in ppm ( $\delta$  units) referenced to residual solvent peaks. FT-IR spectra were recorded on a Bruker IFS-66v using neat samples (CsI window).

Dendrimer hydrodynamic diameters were measured by dynamic light scattering (DLS). Laser Doppler micro-electrophoresis on a Nano-S Zetasizer (Malvern Instrument Ltd) at 25°C. DLS of 2[Gn]-DOTA dendrimers was performed by dissolving the samples in 10 mM PB pH 7.4/150 mM LiCl (1 mg/mL). Gd-labeled 2[Gn]-DOTA (Gd-2[Gn]-DOTA) dendrimers were purified by centrifugation in a 320R Hettich centrifuge, using Amicon Ultra-4 centrifugal filters Ultracel<sup>®</sup> with a regenerated cellulose membrane Mw cutoff 3000 Da, provided from Merck Millipore<sup>®</sup>.

Gadolinium loading of the dendrimers was assessed by ICP-MS analysis at Pharmacology and Toxicology Laboratory, CHU Angers, France. MRI was performed with a Bruker Avance DRX 300 equipped with a magnet of 7T at the Primex platform IBS-CHU, University of Angers, France. When possible, experiments were done in triplicate. Mean values and standard deviations are reported unless otherwise stated.

### Synthesis and characterization of 2[Gn]-DOTA dendrimers

**2[G2]-DOTA:** Ph<sub>3</sub>P (43 mg, 0.16 mmol) was added to a solution of 2[G2]-N<sub>3</sub> (36 mg, 7 μmol) in MeOH/ CHCl<sub>3</sub>/ H<sub>2</sub>O 5:5:1 (1.45 mL; 0.1 M per N<sub>3</sub>). The mixture was stirred at rt under Ar until complete reduction of the terminal azides (16 h, as followed by FT-IR). Afterwards, it was reacted with an 18-fold molar excess of 2,2',2''-(10-(1-carboxy-4-((4-isothiocyanatobenzyl)amino)-4-oxobutyl)-1,4,7,10-tetraazacyclododecane-1,4,7-triyl)triacetic acid (p-NCS-Bz-DOTA-GA) (81 mg, 0.13 mmol) at 40 °C. The reaction mixture was heated at 40°C and the pH adjusted to 9.0 with 2.2 mL of 10 mM PB pH 9/150 mM LiCl solution. After 24h of stirring at 40 °C, acetone (1.1 mL) was added to homogenize the mixture. Another additional equal amount of p-NCS-Bz-DOTA-GA was added to the mixture after 24 h as a solid, and the pH was maintained as before for another 24 h. The resulting solution was purified by ultrafiltration [YM3, 10 mM PB pH 9/150 mM LiCl (5×30 mL) followed by milliQ water (2 × 30 mL)] and lyophilized to obtain 2[G2]-DOTA (108 mg, 95%) as a white powder. <sup>1</sup>H NMR (750 MHz, D<sub>2</sub>O) δ<sub>H</sub>: 7.23 (d, J = 56.6 Hz, 72H), 7.05 (d, J = 10.4 Hz, 16H), 4.32 (d, J = 70.6 Hz, 46H), 4.05 (d, J = 68.5 Hz, 57H), 3.94 – 2.11 (m, 817H), 1.89 (d, J = 98.0 Hz, 36H). <sup>13</sup>C NMR (101 MHz, D<sub>2</sub>O) δ<sub>C</sub>: 179.7, 177.7, 175.3, 171.4, 168.3, 168, 151.7, 139.6, 136.3, 129, 128.2, 125.1, 106.1, 72.1, 70.1, 69.9, 69.6, 69.1, 68.6, 68.3, 66.6, 62.4, 57.6, 56.5, 50.6, 45.9, 43.9, 42.5, 39.8, 34. IR ν max: 3266, 1584, 1514, 1408, 1329, 1101 cm<sup>-1</sup>.

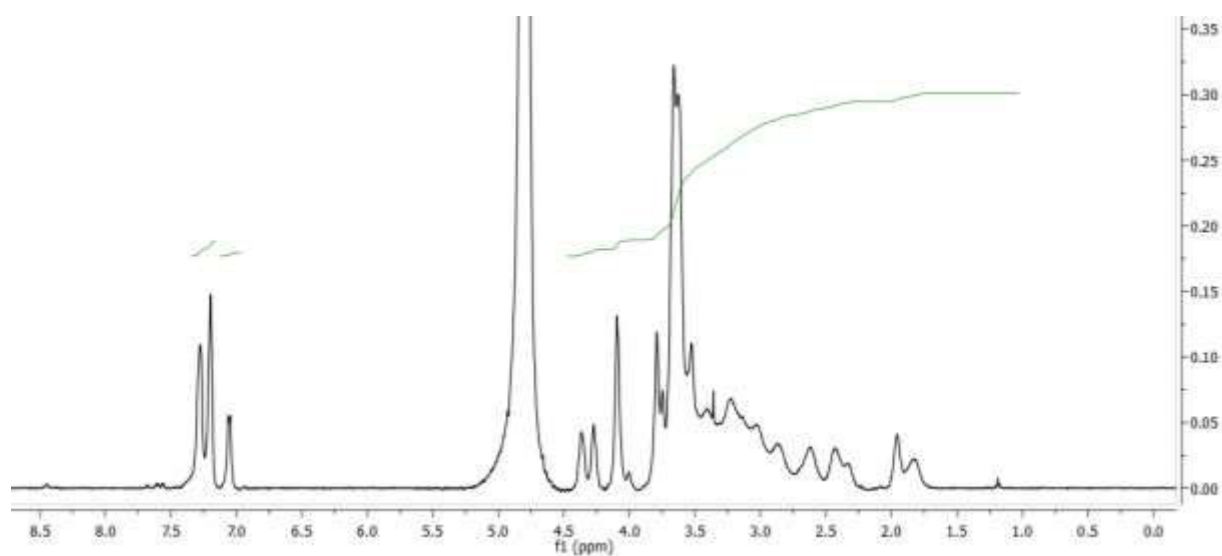
**2[G3]-DOTA:** Ph<sub>3</sub>P (45 mg, 0.17 mmol) was added to a solution of 2[G3]-N<sub>3</sub> (40 mg, 2.5 μmol) in MeOH/ CHCl<sub>3</sub>/ H<sub>2</sub>O 5:5:1 (1.5 mL; 0.1 M per N<sub>3</sub>). The mixture was stirred at rt under Ar until complete reduction of the terminal azides (36 h, as followed by FT-IR). Afterwards, it was reacted with a 54-fold molar excess of p-NCS-Bz-DOTA-GA (95.9 mg, 0.154 mmol). The

reaction mixture was heated at 40 °C and the pH adjusted to 9.0 with 4 mL of 10 mM PB pH 9/150 mM LiCl solution. After 24 h of stirring at 40 °C, acetone (1.5 mL) was added to homogenize the mixture. Another additional equal amount of p-NCS-Bz-DOTA-GA was added to the mixture after 24 h as a solid, and the pH was maintained as before for another 24 h. The resulting preparation was purified by ultrafiltration (YM5, 10 mM PB pH 9/150 mM LiCl (5×30 mL) followed by milliQ water (2 × 30 mL)] and lyophilized to obtain 2[G3]-DOTA (118 mg, 97%) as a white powder. <sup>1</sup>H NMR (750 MHz, D<sub>2</sub>O) δ<sub>H</sub>: 7.42 – 7.02 (m, 268H), 4.42 – 1.71 (m, 2735H). <sup>13</sup>C NMR (101 MHz, D<sub>2</sub>O) δ<sub>C</sub>: 179.7, 176.2, 175.1, 168.3, 151.7, 139.6, 137.6, 137.3, 136.3, 129, 128.2, 126.7, 125.1, 106, 72.1, 69.9, 69.6, 69.1, 68.6, 68.3, 66.5, 63.1, 56.4, 50.4, 46, 43.9, 42.5, 39.6, 39, 33.3. IR ν<sub>max</sub>: 3278, 1583, 1328, 1091 cm<sup>-1</sup>.

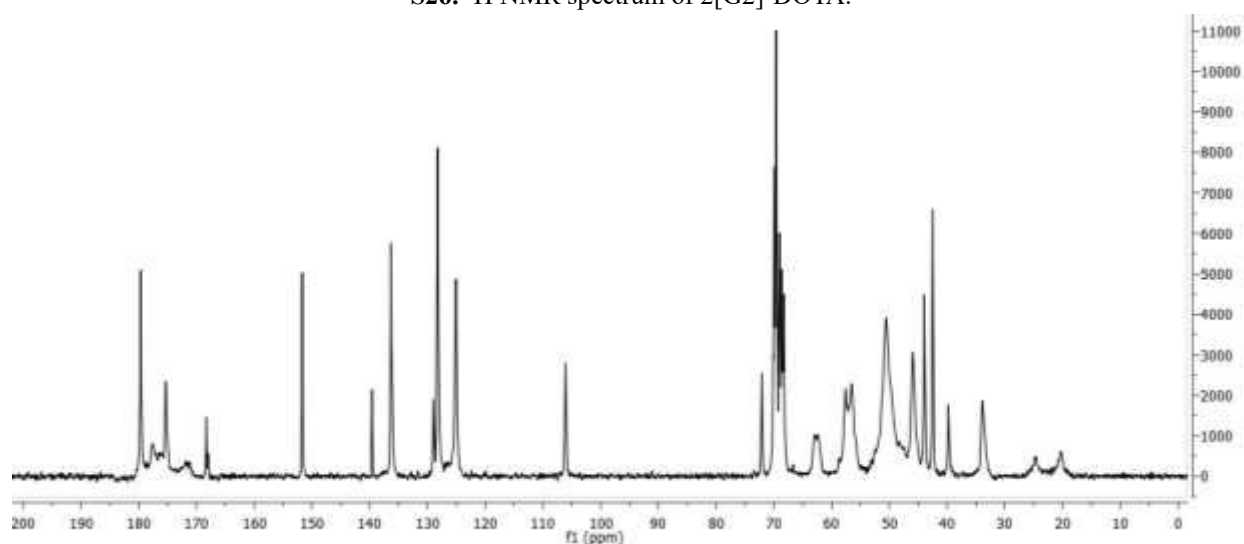
**2[G4]-DOTA:** Ph<sub>3</sub>P (44 mg, 0.17 mmol) was added to a solution of 2[G4]-N<sub>3</sub> (40 mg, 0.8 μmol) in MeOH/ CHCl<sub>3</sub>/ H<sub>2</sub>O 5:5:1 (1.3 mL; 0.1 M per N<sub>3</sub>). The mixture was stirred at rt under Ar until complete reduction of the terminal azides (48 h, as followed by FT-IR). Afterwards, it was reacted with a 162-fold molar excess of p-NCS-Bz-DOTA-GA (84 mg, 0.135 mmol) at 40°C. The reaction mixture was heated at 40°C and the pH adjusted to 9.0 with 3.5 mL of 10 mM PB pH 9/150 mM LiCl solution. After 24 h of stirring at 40 °C, acetone (1.3 mL) was added to homogenize the mixture. Another additional equal amount of p-NCS-Bz-DOTA-GA was added to the mixture after 24 h as a solid, and the pH was maintained as before for another 24 h. The resulting preparation was purified by ultrafiltration (YM5, 10 mM PB pH 9/150 mM LiCl (5×30 mL) followed by milliQ water (2 × 30 mL)] and lyophilized to obtain 2[G4]-DOTA (120 mg, 99%) as a white powder. <sup>1</sup>H NMR (750 MHz, D<sub>2</sub>O) δ<sub>H</sub>: 7.17 (t, J = 63.4 Hz, 1024H), 4.41 – 1.61 (m, 8699H). <sup>13</sup>C NMR (101 MHz, D<sub>2</sub>O) δ<sub>C</sub>: 170, 175.8, 168.1, 151.7, 139.6, 133.5, 128.9, 127.8,

124.5, 106.1, 72.3, 69.6, 69.1, 63.7, 58.8, 58.2, 51, 47, 46.1, 43.1, 42.7, 39.6, 34.3. IR v max: 2853, 1579, 1408, 1328, 1091  $\text{cm}^{-1}$ .

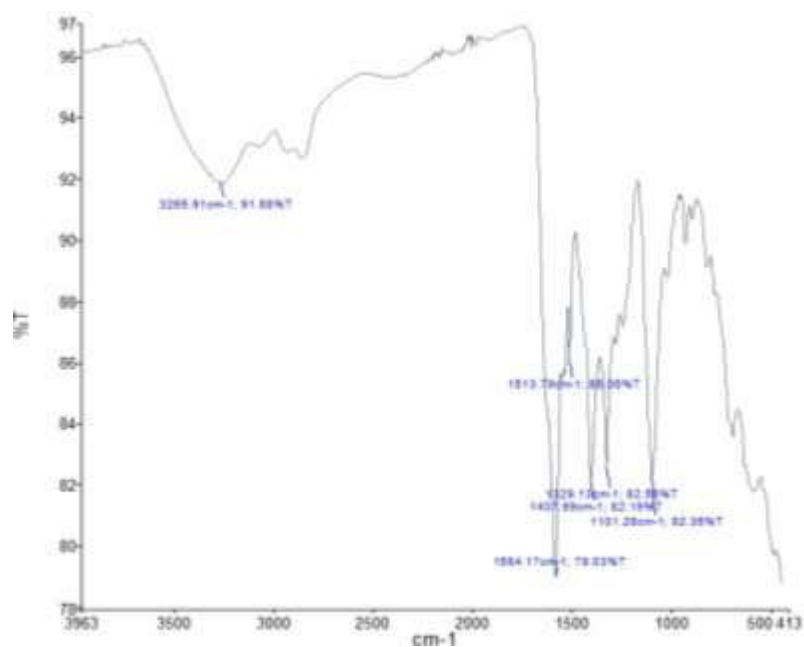
### Characterization of 2[Gn]-DOTA dendrimers



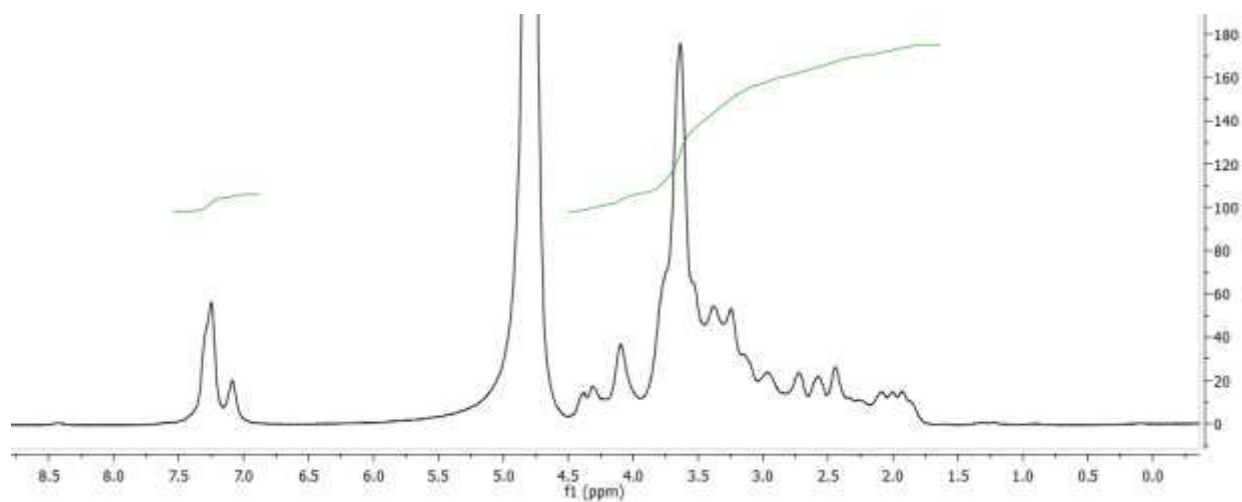
S26.  $^1\text{H}$  NMR spectrum of 2[G2]-DOTA.



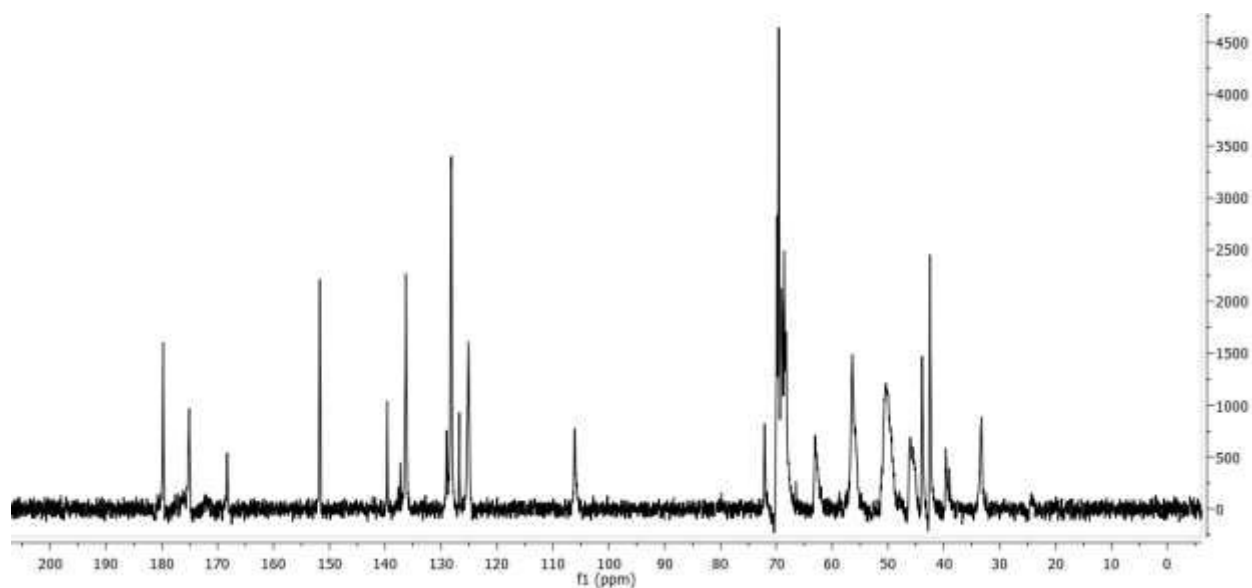
S27.  $^{13}\text{C}$  NMR spectrum of 2[G2]-DOTA.



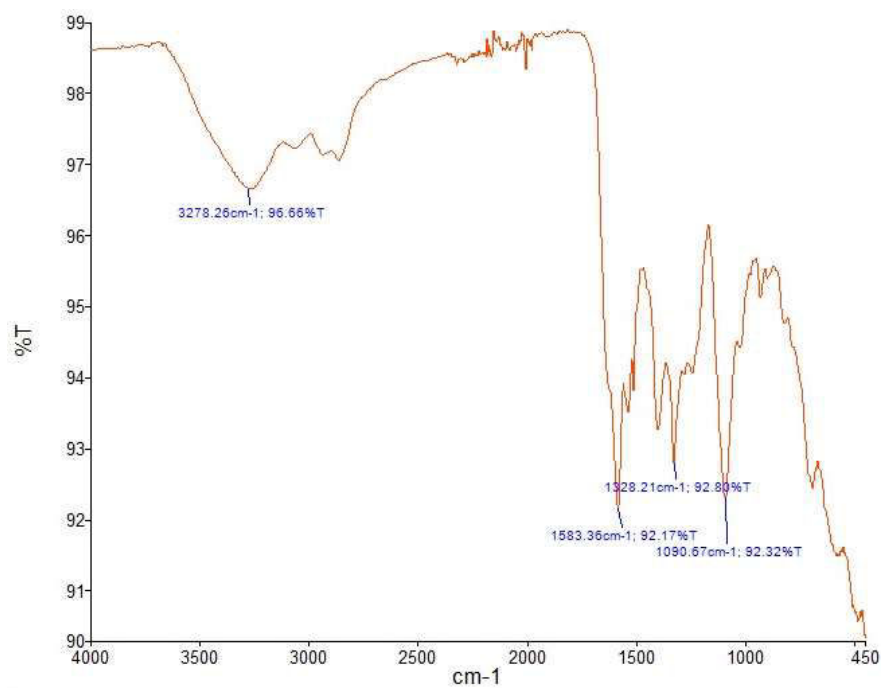
**S28.** IR spectrum of 2[G2]-DOTA.



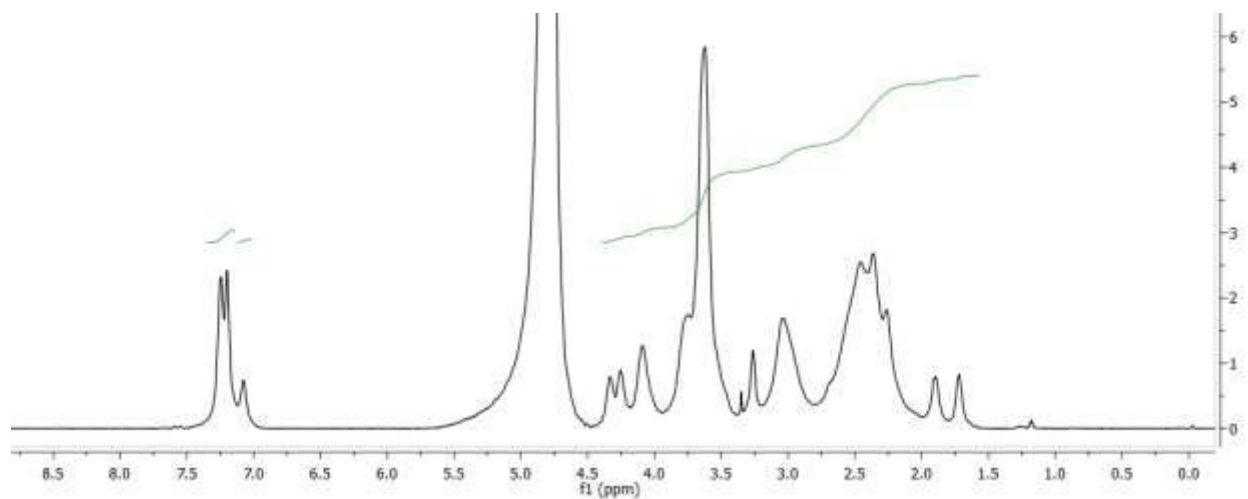
**S29.** <sup>1</sup>H NMR spectrum of 2[G3]-DOTA.



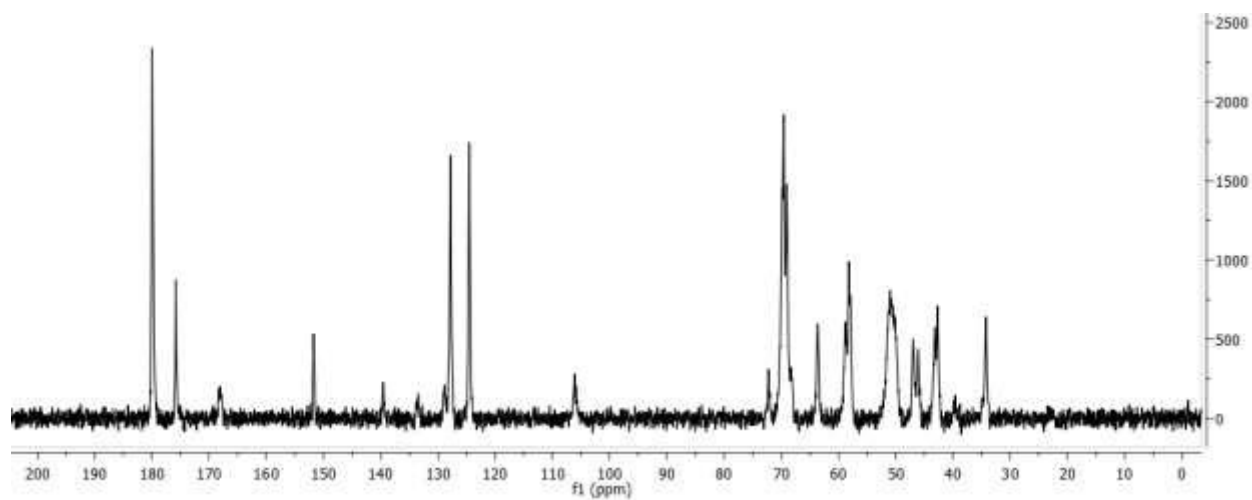
**S30.**  $^{13}\text{C}$  NMR spectrum of 2[G3]-DOTA.



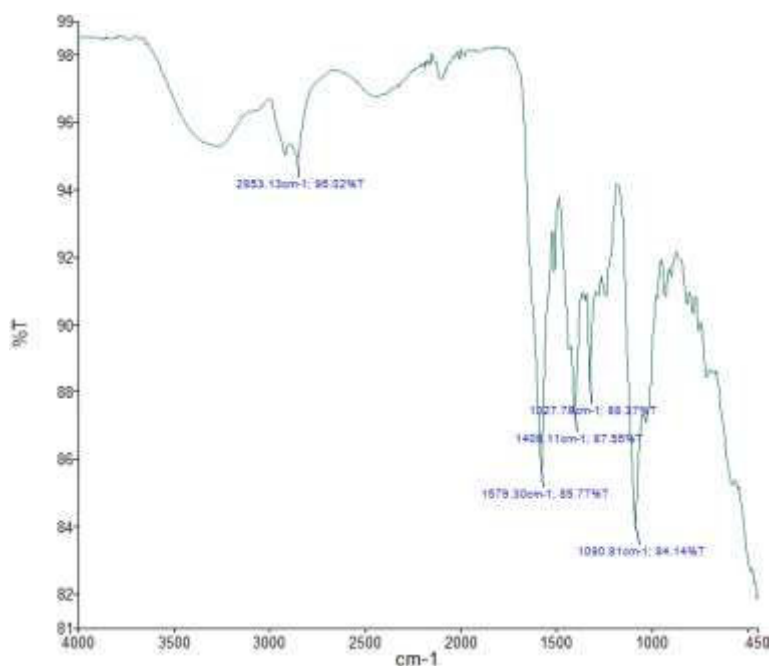
**S31.** IR spectrum of 2[G3]-DOTA.



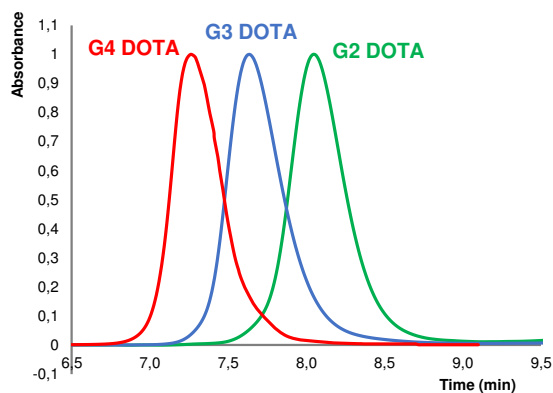
**S32.**  $^1\text{H}$  NMR spectrum of 2[G4]-DOTA.



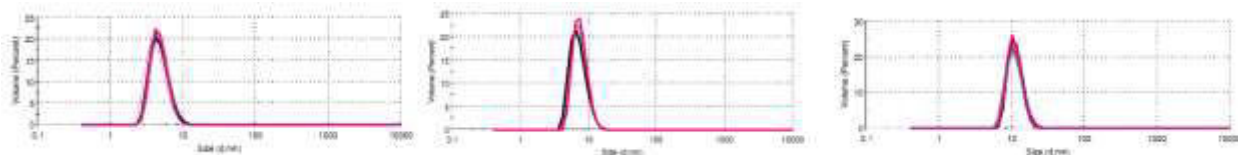
**S33.**  $^{13}\text{C}$  NMR spectrum of 2[G4]-DOTA.



S34. IR spectrum of 2[G4]-DOTA.



S35. Purity check of [Gn]-DOTA dendrimers by SEC.



S36. DLS measurements of 2[Gn]-DOTA dendrimers (2[G2]-DOTA-2[G4]-DOTA from left to right)

To determine <sup>1</sup>H-<sup>13</sup>C connectivity, 2D Heteronuclear Multiple-Quantum Correlation (<sup>13</sup>C-

$^1\text{H}$  HMQC) experiments were done respectively. 2D NMR Correlation Spectroscopy ( $^1\text{H}$ -  $^1\text{H}$  COSY) was run to evaluate which signals arose from neighboring protons, and Distortionless Enhancement of Polarization Transfer (DEPT)  $^{13}\text{C}$  NMR spectra was acquired to deduct the number of H attached to C. An example of the  $^{13}\text{C}$  NMR spectra characterization of 2[G2]-DOTA/DTPA dendrimers is given in the Figure 2.23-2.25.

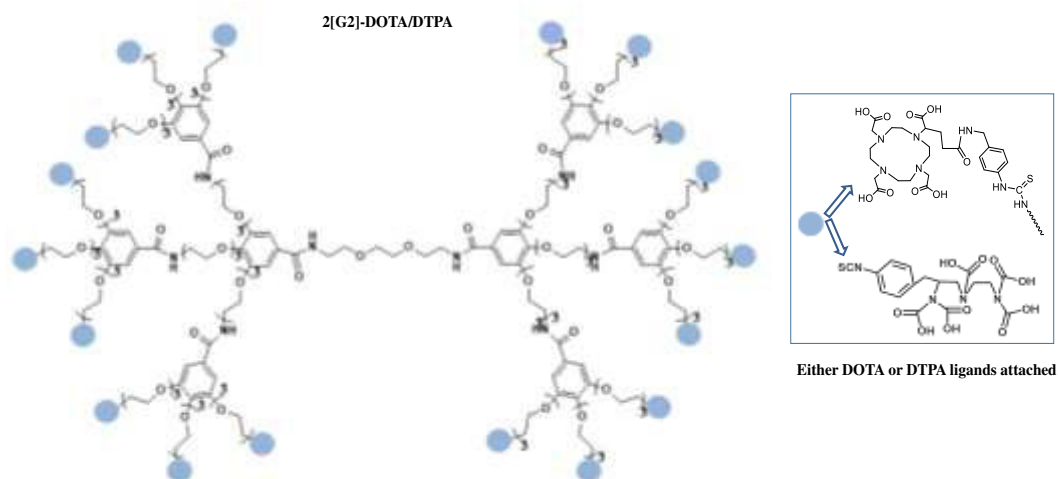


**Figure 2.23.** Chemical structure of 2[G2]-DOTA/DTPA

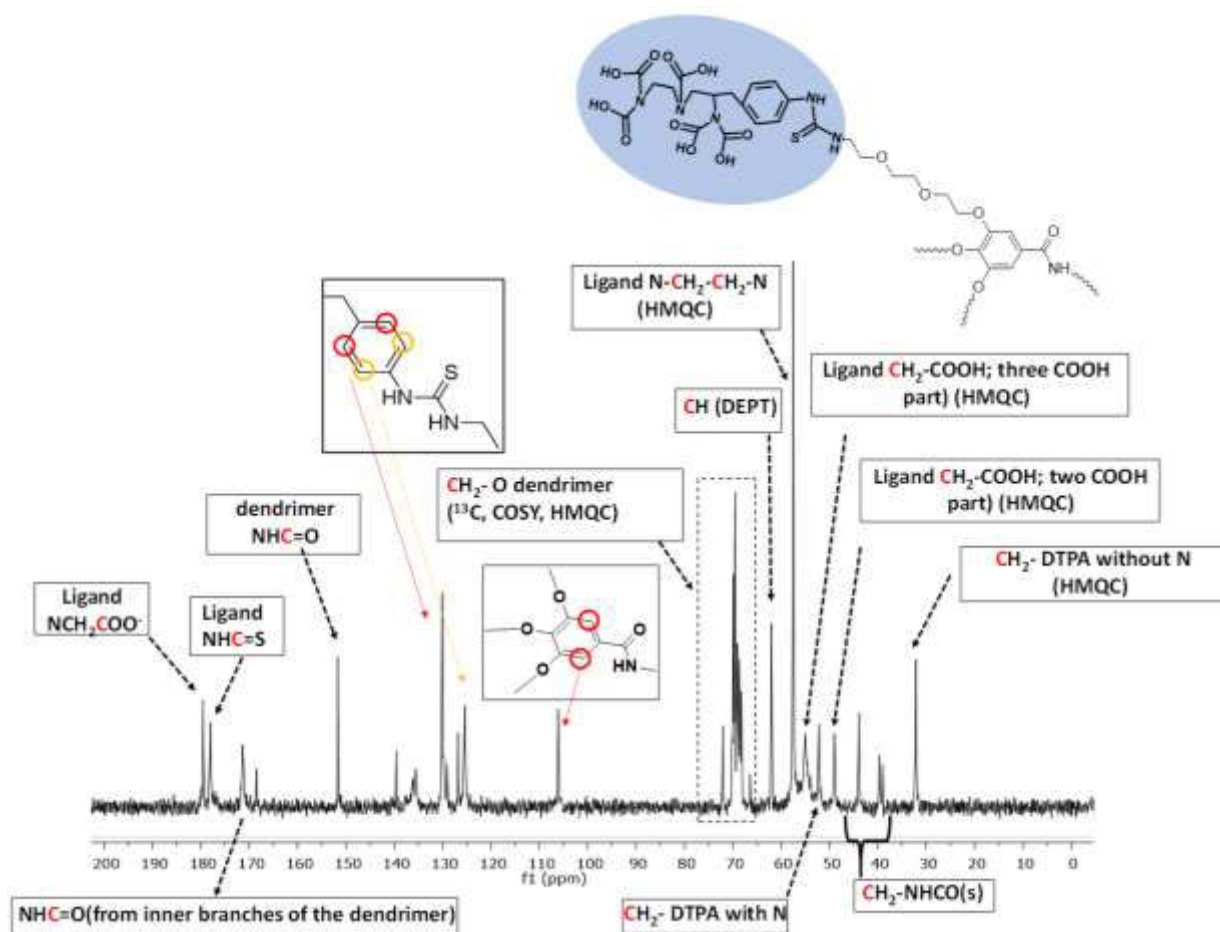


**Figure 2.24.** NMR interpretation of 2[G2]-DTPA structures

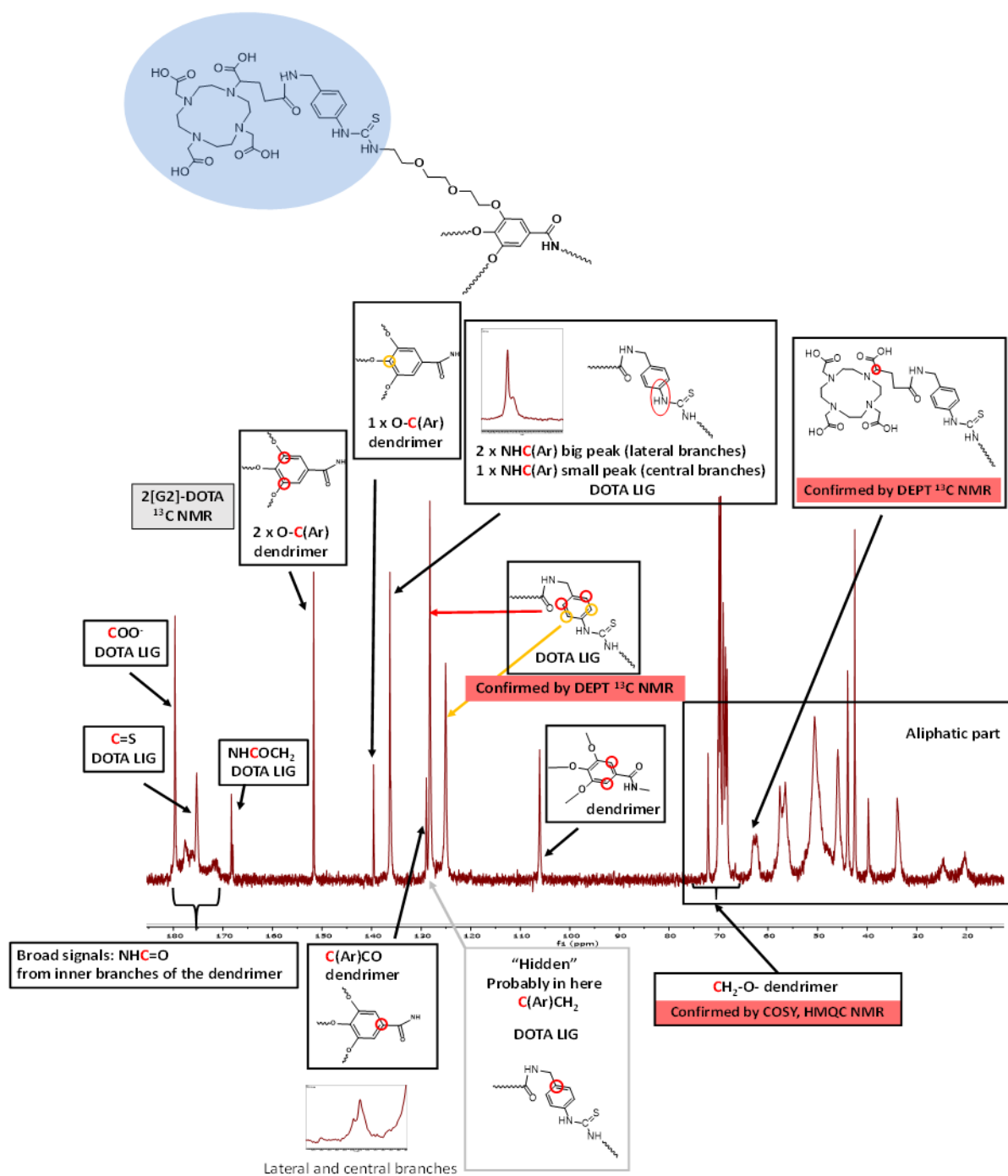


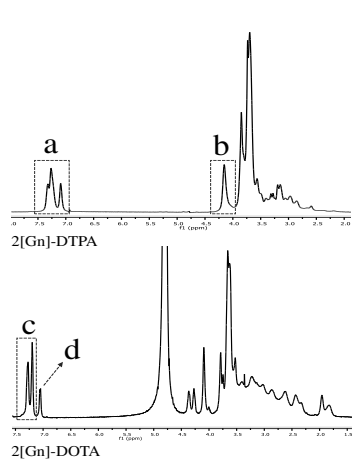
**Figure 2.25** NMR interpretation of 2[G2]-DOTA structures.

### Degree of Conjugation of DOTA derivatives to 2[Gn] dendrimers

Relative NMR integration was used to determine the ratio of hydrogens that correspond to

the signal, making it possible to calculate the degree of conjugation of DTPA and DOTA ligands to the dendrimers. Further information is given in the Table 2.12.

**Table 2.12** Relative NMR integration data to measure the % DC of chelates to 2[Gn]-DTPA/DOTA dendrimers



1H NMR integration				
Dendrimers	Exp. # of H	Exp. # of H	Total Theo. # of H	DC %
2[Gn]-DTPA	<b>a</b>	<b>b</b>	Theo. (a+b)	
2[G2]-DTPA	87.76	48	136	100
2[G3]-DTPA	268	150	424	98.6
2[G4]-DTPA	807.59	474.48	1282	100
2[Gn]-DOTA	<b>c</b>	<b>d</b>	Theo. (c+d)	
2[G2]-DOTA	72	16.34	88	100
2[G3]-DOTA	202.57	48	268	94
2[G4]-DOTA	715.78	95.84	808	99.6

Size, molecular weight and the number of chelates are all important parameters to consider when designing the macromolecular MRI CA (Table 2.13).

**Table 2.13** Characterization of 2[Gn]-DTPA and 2[Gn]-DOTA dendrimers

Abbreviation	Number of peripheral functional groups	MW <sup>a</sup> (g/mol)	Diameter ± SD (nm)
2[G2]-DTPA	18	12981	5.15 ± 0.04
2[G3]-DTPA	54	39723	8.94 ± 0.15
2[G4]-DTPA	162	121556	11.72 ± 0.19
2[G2]-DOTA	18	15721.62	5.4 ± 0.01
2[G3]-DOTA	54	48280.474	8.94 ± 0.03
2[G4]-DOTA	162	148414.338	12.96 ± 0.16

<sup>a</sup>: Based on calculated Molecular Weight.

### 2.3.2. Results and discussion

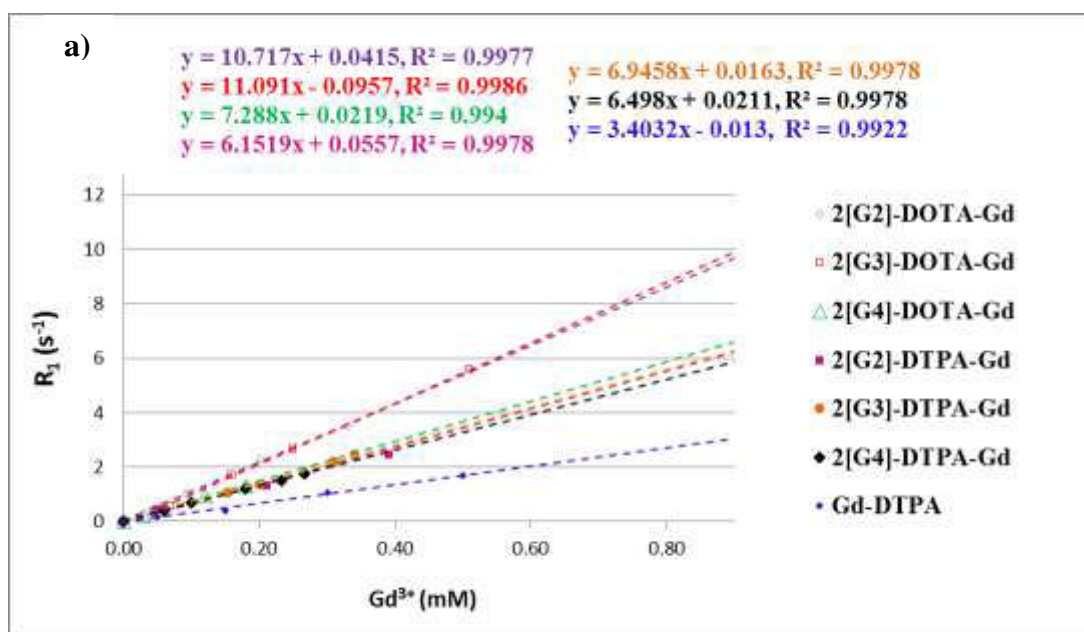
#### Comparison of relaxivity properties between Gd-2[Gn]-DTPA and Gd-2[Gn]-DOTA dendrimers

Longitudinal and transverse relaxivities were determined for all generations of the Gd-2[Gn]-DTPA and Gd-2[Gn]-DOTA dendrimers by concentration dependent measurements of the relaxation times, which gave good linear fits ( $R^2 > 0.99$ ). Plotting the  $(1/T_{\text{sample}} - 1/T_{\text{PBS}})$  values of conjugated dendrimers with corresponding Gd concentrations provided the relaxivity of the each sample. Stock solutions of the Gd-2[Gn]-DTPA and Gd-2[Gn]-DOTA dendrimers (1 mM in Gd), were diluted to concentrations of 0.1, 0.25, and 0.50 mM in 1X PBS (300  $\mu$ L) respectively. Solutions of Gd-DTPA (Sigma Aldrich) were prepared in 1X PBS (300  $\mu$ L) at the same concentration range and used as a reference standard. Relaxivity measurements were obtained at  $\sim 25^\circ\text{C}$  using a Bruker Biospec 70/20 system, operating at 7 Tesla. For the  $T_1$  map, a series of variable repetition times ( $T_R$ ) single slice fast spin echo images of all the solutions were acquired at the same time with an echo time ( $T_E$ ) of 7 ms, and 1 average. The total scan time was 18 min and 14 sec.  $T_1$  map parameters were as follows: Mtx: 256 x 256; 1 axial slice with 2 mm thickness 6 repetition times: TR = 200; 400; 800; 1500; 3000; 5500 ms; TE = 7 ms; FOV= 35 mm x 35 mm. The  $T_1$  values were calculated from the mean signal in the ROI for each repetition time, adjusted to the equation:  $S = S_0 \times (1 - e^{-\frac{TR}{T_1}})$ .

The  $T_2$  maps were calculated from multi spin echo images with a TR of 2 s. 25 echo images were acquired with a TE of 8.02 ms, which was the interval time between echo images acquisitions, too.  $T_2$ - map parameters were as follows: 1 axial slice of 2 mm thickness; TR = 3200 ms; TE = 8.02 ms (25 echo times with interval of 8.02 ms in between), 1 average. Field of view (FOV): 35 x 35

mm; Mtx: 256 x 256; The  $T_2$  values were calculated from mean signal in the ROI for each echo image, adjusted according to the equation:  $S = S_0 \times e^{-\frac{TE}{T_2}}$ . The software used for the calculations was Paravision 6.0 (Bruker Software).

The molar relaxivities,  $r_1$  and  $r_2$ , were obtained from the slope of the inverse of longitudinal relaxation time ( $1/T_1$ ), or of the inverse of transverse relaxation time ( $1/T_2$ ) vs. [Gd] plots, determined from ROI measurements. A plot of  $R_1$  versus [Gd] for the Gd-2[Gn]-DTPA, Gd-2[Gn]-DOTA conjugates and Gd-DTPA (ranging from 0.03 to 0.5 mM) is shown in Figure 2.26.a. Similarly, the plot of  $R_2$  vs. [Gd] for the Gd-2[Gn]-DTPA, Gd-2[Gn]-DOTA conjugates and Gd-DTPA, is depicted in Figure 2.26 b.



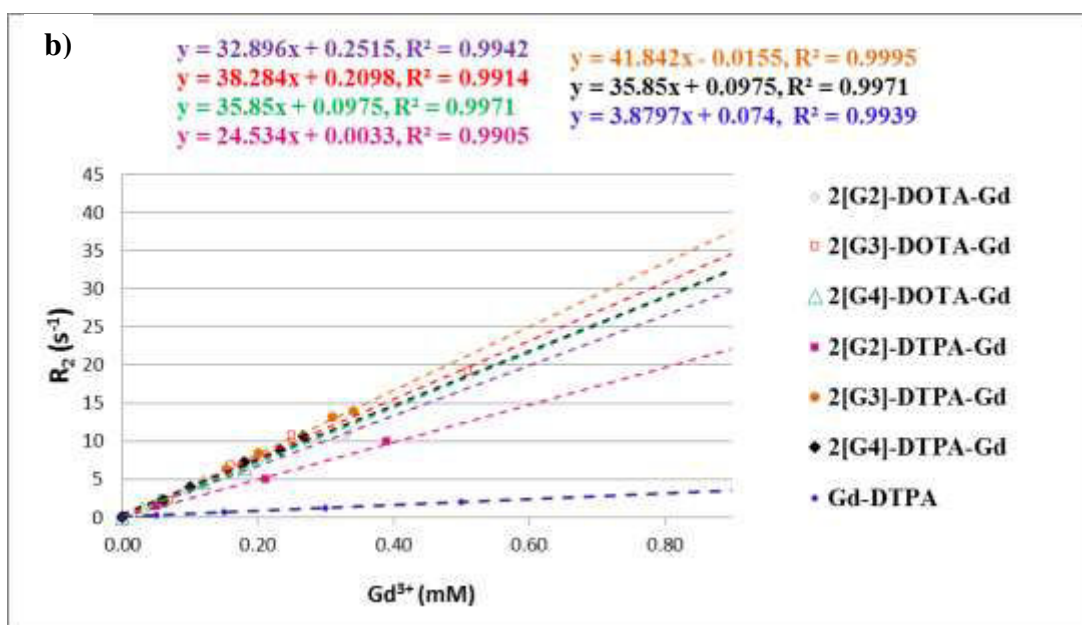


**Figure 2.26.** a)  $R_1$  plots for Gd-2[G2]-DOTA (violet), Gd-2[G3]-DOTA (red), Gd-2[G4]-DOTA (green), Gd-2[G2]-DTPA (pink), Gd-2[G3]-DTPA (orange), Gd-2[G4]-DTPA (black), and Gd-DTPA (blue); b)  $R_2$  plots for Gd-2[G2]-DOTA (violet), Gd-2[G3]-DOTA (red), Gd-2[G4]-DOTA (green), Gd-2[G2]-DTPA (pink), Gd-2[G3]-DTPA (orange), Gd-2[G4]-DTPA (black), and Gd-DTPA (blue).

The data shown in Table 2.14, indicates that the ionic  $r_1$  relaxivity of the Gd-2[G3]-DOTA ( $11.1 \text{ mM}^{-1} \cdot \text{s}^{-1}$ ) is slightly higher than that of Gd-2[G2]-DOTA ( $10.7 \text{ mM}^{-1} \cdot \text{s}^{-1}$ ), and more than three times higher than that of the Gd-DTPA ( $3.2 \text{ mM}^{-1} \cdot \text{s}^{-1}$ ). The  $r_1$  ionic relaxivity of the Gd-2[G4]-DOTA ( $7.3 \text{ mM}^{-1} \cdot \text{s}^{-1}$ ) is lower than that of the other two above mentioned dendrimer conjugates, but comparable with the  $r_1$  of Gd-2[G3]-DTPA ( $7 \text{ mM}^{-1} \cdot \text{s}^{-1}$ ), which is slightly higher than the  $r_1$  of Gd-2[G2]-DTPA ( $6.2 \text{ mM}^{-1} \cdot \text{s}^{-1}$ ), and Gd-2[G4]-DTPA ( $6.5 \text{ mM}^{-1} \cdot \text{s}^{-1}$ ). On the other hand, the molecular relaxivity shows an increased trend from the second to the fourth generations, given the exponential increase in the number of DTPA or DOTA ligands per generation. The  $r_2$  relaxivity of Gd-2[Gn]-DOTA is comparable for each generation, and  $\sim 11$  times higher than that of Gd-DTPA. The  $r_2$  relaxivity of Gd-2[G3]-DTPA is comparable with that of Gd-2[G4]-DTPA, but  $\sim 2$  times higher than that of Gd-2[G2]-DTPA.

**Table 2.14** Relaxivities of macromolecular CAs compared with Gd-DTPA in 7T.

Compound	$r_2/\text{Gd}$ ( $\text{mM}^{-1}\text{s}^{-1}$ )*	$r_1/\text{Gd}$ ( $\text{mM}^{-1}\text{s}^{-1}$ )*	Molecular $r_2$ ( $\text{mM}^{-1}\text{s}^{-1}$ )	Molecular $r_1$ ( $\text{mM}^{-1}\text{s}^{-1}$ )	Ion $r_2/r_1$
Gd-2[G2]-DOTA	32.9	10.7	457.31	148.73	3.1
Gd-2[G3]-DOTA	38.3	11.1	1600.94	463.98	3.5
Gd-2[G4]-DOTA	35.9	7.3	4379.8	890.6	4.9
Gd-2[G2]-DTPA	24.5	6.2	318.5	80.6	4.0
Gd-2[G3]-DTPA	41.8	7	1797.4	301	6.0
Gd-2[G4]-DTPA	39.5	6.5	5135	845	6.1
Gd-DTPA	3.4	3.2	3.4	3.2	1.1

\* ionic relaxivity per Gd

## 2.4. Conclusions

Three highest generations of GATG dendrimers were synthesized and fully conjugated to either DTPA or DOTA ligands. The relaxivity properties of both 2[Gn]-DOTA and 2[Gn]-DTPA dendrimers were compared with those of commercial Gd-DTPA at 7T, following their labeling with Gd. The Gd labeling was achieved with high efficiency and stability. All the dendrimer generations had a higher  $r_1$  and  $r_2$  relaxivity than the commercial Gd-DTPA. The ionic relaxivity of water per Gd ion of Gd-2[G3]-DOTA dendrimers was the highest, followed by Gd-2[G2]-DOTA, Gd-2[G4]-DOTA, Gd-2[G3]-DTPA, Gd-2[G4]-DTPA, Gd-2[G2]-DTPA and Gd-DTPA.

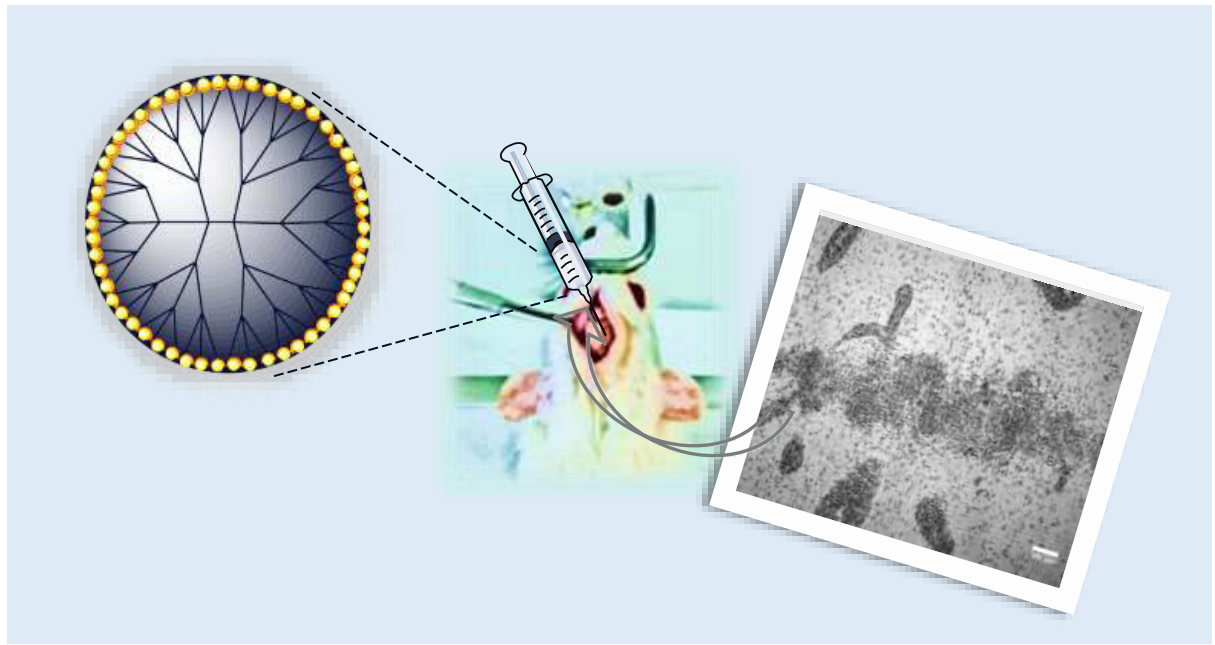
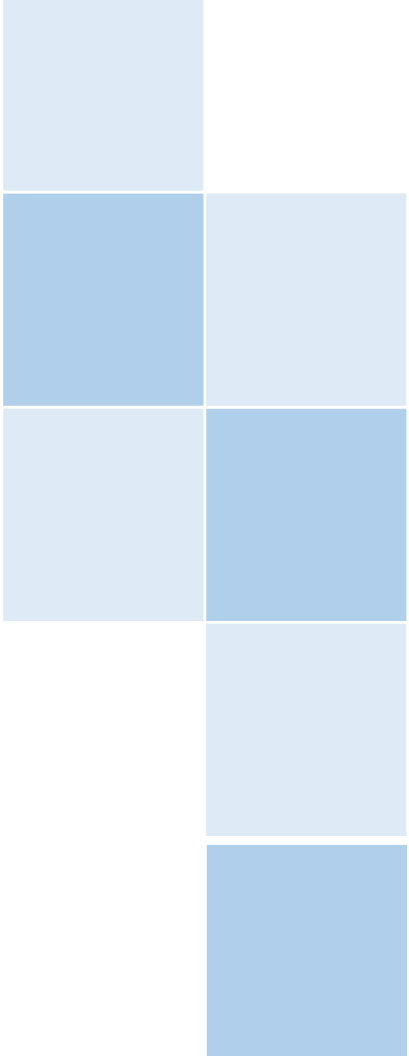
Possession of a short and rigid isothiocyanatobenzyl linker is a positive feature of the incorporated DTPA and DOTA conjugates and also a factor that contributes to the high relaxivity among many others. This short and rigid linker limits the rotation of the small Gd chelates, which is characterized as internal rotation. As reported previously,<sup>44</sup> fast internal rotation of high molecular weight agents prohibits achievement of high relaxivity even though the rotation of the

entire molecule is reasonably slow.

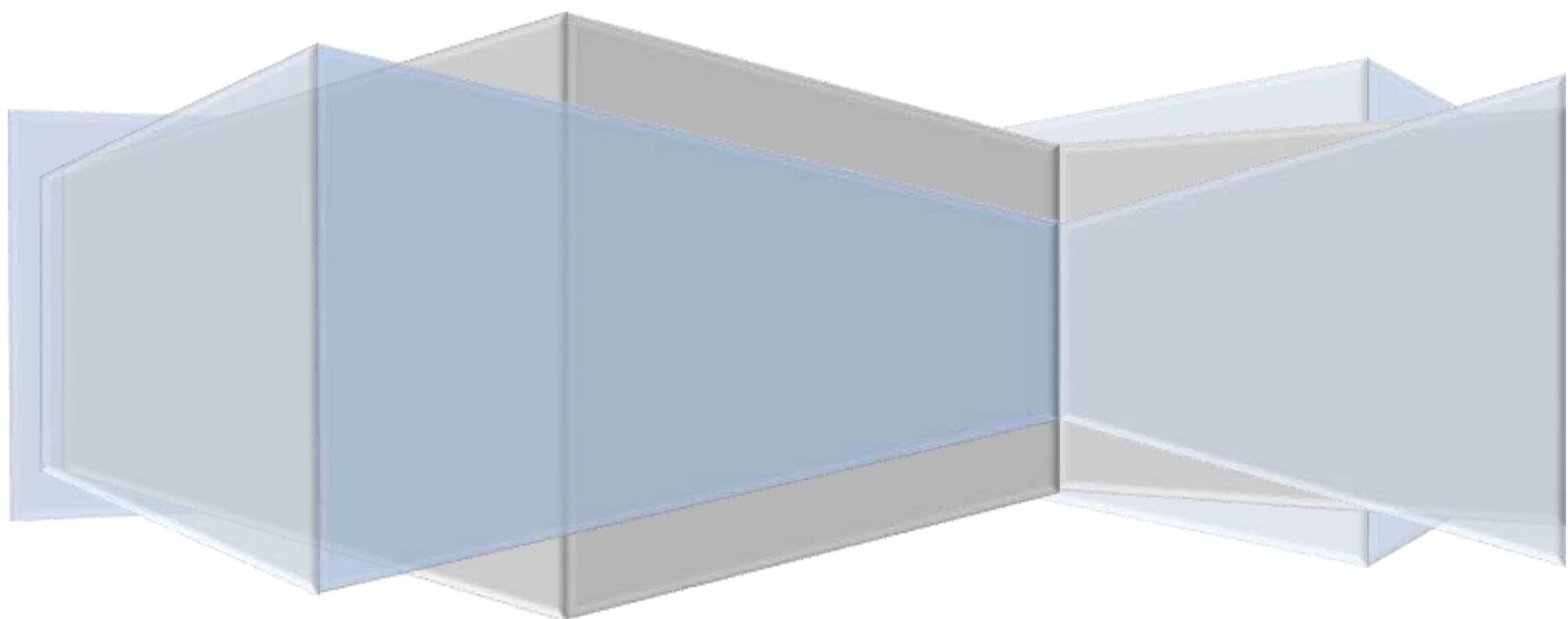
Furthermore, the macrocyclic DOTA ligand has a higher rigidity than the open chained DTPA, providing even a slower internal rotation for the 2[Gn]-DOTA dendrimers and leading to a higher  $r_1$ , in comparison with their 2[Gn]-DTPA twins. The  $r_1$  of Gd-2[G4]-DOTA dendrimers was comparable with that of Gd-2[G2]-DOTA dendrimers. For the Gd-2[G4]-DTPA dendrimers their  $r_1$  was less than Gd-2[G3]-DTPA but more than Gd-2[G2]-DTPA dendrimers. The reason for this phenomenon might be the back-folding of the dendritic arms for the fourth generation.

Macromolecules like dendrimers are described to have a decreasing  $r_1$  and increasing  $r_2$  with increasing magnetic field strength. This tendency might be observed in the case of GATG dendrimers as well, with Gd-2[G3]-DTPA and Gd-2[G3]-DOTA having the highest  $r_1$ , followed by Gd-2[G4]-DTPA, Gd-2[G4]-DOTA, Gd-2[G2]-DOTA, Gd-2[G2]-DTPA and lastly Gd-DTPA. Similarly to the results achieved for  $r_1$ , the third generation of dendrimers was better than the other two to increase the  $r_2$ .

It is known that the higher relaxivity and stability of Gd-DOTA makes it applicable as an alternative to Gd-DTPA for MRI.<sup>224</sup> Similarly Gd-2[Gn]-DOTA dendrimers showed a slightly higher relaxivity in comparison with Gd-2[Gn]-DTPA dendrimers. On the other hand, in a previous study,<sup>225</sup> no significant differences in enhancement of the brain image of rats were observed between Gd-DTPA and Gd-DOTA.



## **PART 3. General Conclusions**





### PART 3. General Conclusions

For the treatment of tumors current therapies involve the combination of external beam radiation and chemotherapies, which do not discriminate between healthy and tumor tissues. As a result, great efforts are being realized to synergistically integrate on nanosystems, technologies such as internal radiotherapy (delivery of radioisotopes to the site of action), diagnostic agents (for MRI or PET), and targeting. Localized internal radiotherapy is known to be the most promising treatment alternative for unresectable solid tumors. Recent innovative oncologic strategies have involved the nanovectorization approach, to efficiently target and retain radiation at the tumor site, avoiding side effects such as toxicity and tumor resistance. Selected nanovectors are labeled with radionuclides for the improvement of the treatment efficacy, while reducing the dose of radiolabeled materials *in vivo*.

Among several nanovectors that may be used for this purpose, dendrimers are seen as a powerful platform, due to their multivalency, tunable size and physicochemical properties as a function of the generation. Dendrimers are branched macromolecules prepared in a stepwise fashion, that oppositely to classical polymers are monodisperse and globular. The number of terminal groups on the periphery of dendrimers can be accurately controlled, which allows their selective decoration with targeting ligands, drugs, diagnostic and therapeutic agents. In addition, the possibility to prepare dendrimers with different sizes (generations) and to modulate their hydrodynamic radii, solubility, and distribution by PEGylation, renders dendrimers attractive scaffolds for the treatment and diagnosis of tumors.

Milestones in the development of dendrimers for nanovectorized radiotherapy include their functionalization with ligands for radiolabeling, targeting agents, and stealth functional groups to

potentially improve their biodistribution, circulation times, and stability *in vivo*. Radiolabeling of dendrimers with therapeutic radionuclides has previously resulted in tumor regression and longer survival, as described in our review. The biodistribution of dendritic conjugates could be improved by PEGylation, intratumoral application, saturation with cold metals, or by modulating their charge and molecular weight. In addition, the multifunctionality of dendrimers makes them excellent candidates for theranostics.

The development of radiotherapeutic dendrimers for use in image-guided radionuclide therapies; in combination with moAbs, with only minor changes in immunoreactivity; in radiovirotherapy as coatings of adenoviral vectors for effective liver detargeting and tumor retargeting, as well as nonviral gene delivery vectors for NIS-targeted radionuclide therapy of metastatic cancer, has attracted the attention of many researchers in the field. Although issues associated with *in vivo* properties and the toxicity of dendrimer conjugates are challenges to be addressed individually, as a whole there are considerable promise and benefits on current applications of dendrimers for radionanotherapy.

A proper evaluation of dendrimer-based radiopharmaceuticals must be done according to three criteria: the choice of radionuclide, the vector used, and the modalities of administration. Relatively recent results on dendrimer-based radiopharmaceuticals in preclinical models do not permit such a comparison yet. The physicochemical properties of the radionuclide are crucial, but differences between vectors (untargeted vs targeted dendrimer, different dendrimer generations) have been investigated after intravenous injections with the aim of qualifying the targeting rather than the efficacy. In fact, for medical applications with radiopharmaceuticals, locoregional

injection could be a preferred way, where dendrimers play the role of confining agent at the injection site, in order to reduce the associated radio toxicity on healthy tissues or organs.

Considering these observations two strategies were applied during the course of this work.

The initial synthetic strategy consisted in the design of dendrimers containing carbamate groups. The carbamate group was chosen to increase the plasma half-life of dendrimers due to their higher physical and proteolytic stability. Two types of first generation carbamate dendrimers were synthesized by azide-alkyne cycloaddition, avoiding the use of toxic catalyst and coupling agents. However, the synthetic yield of these products was low. For the synthesis and characterization of the second generation of these dendrimers, there were researched all the possible combinations of synthesis conditions available for now, such as synthesising two types of aromatic cores and a new aliphatic core for the carbamate dendrimers and combining each one of them with two kinds of repeating units that were synthesised with different physico-chemical characteristics. At the same time the AAC click conditions were changed and experimented in different microwave parameters (Power, Temperature, Time). After careful analysis of the results, it was decided that these systems were not stable to degradation in the microwave conditions applied for the AAC reactions.

Afterwards, it started the synthesis of another family of dendrimers. The synthesis of GATG dendrimers was done in thermal conditions, avoiding the use of toxic coupling agents and catalysts. By a synergistic combination of highly efficient reactions (amide formation and azide reduction), and efficient purifications (automated MPLC or ultrafiltration, depending on the generation), four generations (2[G1]-2[G4]) of GATG dendrimers, bearing azides in the periphery were synthesized with very good yields. The peripheral azides exponentially grew with each generation, starting

from 6 for the first generation (2[G1]) to 162 for the fourth generation (2[G4]). The increased number of terminal groups compared do GATG dendrons is expected to grant the resulting structures, increased affinities in multivalent recognition processes of biomedical interest. 2[G2] to 2[G4] of GATG dendrimers were fully functionalized with ligands of biomedical interest, such as DTPA and DOTA. A new method “One Pot” was developed for easy and efficient conjugation of the ligands to the peripheral groups of the dendrimers. Benefitting from the high-density functional groups on the surface of the dendrimer, a large number of either DTPA or DOTA ligands (ranging from 18 to 162 DTPA/DOTA ligands/dendrimer from 2[G2] - 2[G4] dendrimers) was available to be labeled with  $^{99m}\text{Tc}$ , Gd and  $^{188}\text{Re}$ .

For the characterization of GATG azide dendrimers  $^1\text{H}$  NMR,  $^{13}\text{C}$  NMR, and FTIR spectra were acquired. The purity of all azide dendrimers was confirmed by GPC through the examination of their elution profiles in THF. The hydrodynamic radius of hydrochloride amino dendrimers was determined experimentally in aqueous solution at 25°C by DLS.

For the characterization of 2[Gn]-DTPA/DOTA dendrimers,  $^1\text{H}$  NMR,  $^{13}\text{C}$  NMR, and FTIR spectra were acquired. DLS was used to determine the hydrodynamic radius of all Gn-GATG-Ligand dendrimers in buffer solution (pH 7.4) at 25°C. The purity of all 2[Gn]-DTPA/DOTA dendrimers was confirmed by GPC, through the examination of their elution profiles in a buffer solution (pH 7.4).  $^1\text{H}$  NMR and IR spectroscopy were most useful techniques for monitoring the couplings and activation steps during the preparation of dendrimers, ensuring that the reactions went to completion.

A simple and efficient synthetic method was reported herein for the construction of GATG dendrimers avoiding the use of toxic coupling agents and catalysts, with very good yields and a

fast-forward “One Pot” coupling procedure for the DTPA and DOTA ligands, with efficient purification through ultrafiltration, resulting in fully functionalized 2[Gn]-DTPA/DOTA dendrimers, with very good yields.

2[Gn]-DTPA dendrimers were radiolabeled with  $^{99m}\text{Tc}$  to determine and compare the *in vivo* properties of different generations, such as throughout body distribution, pharmacokinetics, clearance profiles and possible organ toxicity. Molecular weight and architecture had an important role on the *in vivo* behavior of these dendrimers. With the increase in generation size, an increase in liver uptake with concomitant decrease in kidney uptake was observed. The third generation of dendrimers resulted as the best one for faster throughout body distribution and clearance.

The MRI imaging properties of these Gd-dendrimers, were evaluated at 7T and compared with those of the commercial Gd-DTPA. All the generations of dendrimers, with the third one being the best, had a higher  $r_1$  and  $r_2$  relaxivity in comparison with Gd-DTPA. Possession of a short and rigid isothiocyanatobenzyl linker is a positive feature of the incorporated DTPA and DOTA conjugates and also a factor that contributed to the high relaxivity among many others. As expected, due to the higher rigidity of the conjugated macrocyclic ligand, Gd-2[Gn]-DOTA dendrimers had slightly better relaxivity properties in comparison with Gd-2[Gn]-DTPA ones. The ionic relaxivity of water per Gd ion of Gd-2[G3]-DOTA dendrimers was the highest, followed by Gd-2[G2]-DOTA, Gd-2[G4]-DOTA, Gd-2[G3]-DTPA, Gd-2[G4]-DTPA, Gd-2[G2]-DTPA and Gd-DTPA. The  $r_1$  of Gd-2[G4]-DOTA dendrimers was comparable with that of Gd-2[G2]-DOTA dendrimers. For the Gd-2[G4]-DTPA dendrimers their  $r_1$  was less than Gd-2[G3]-DTPA but more than Gd-2[G2]-DTPA dendrimers. The reason for this might be the back-folding of the dendritic arms for the fourth generation.

Macromolecules like dendrimers are known to have a decreasing  $r_1$  and increasing  $r_2$  with increasing magnetic field strength. In the case of GATG dendrimers, Gd-2[G3]-DTPA and Gd-2[G3]-DOTA had the highest  $r_2$ , followed by Gd-2[G4]-DTPA, Gd-2[G4]-DOTA, Gd-2[G2]-DOTA, Gd-2[G2]-DTPA and lastly Gd-DTPA. Similarly to the results achieved for  $r_1$ , the third generation of dendrimers was better than the other two to increase the  $r_2$ . The molecular relaxivity of these dendrimers increased with the increase in generation size in both DTPA and DOTA conjugated 2[Gn] dendrimers.

Since in the biodistribution study following iv injection, the third generation of  $^{99m}\text{Tc}$ -2[Gn]-DTPA dendrimers was the one that had the fastest throughout body distribution and clearance, and it was also the more suitable generation in improving the ionic relaxivity in 7T MRI, it was chosen for further evaluation. 2[G3]-DTPA dendrimers were injected stereotactically via CED in F98 glioma rats, following Gd labeling and their brain retention was investigated with MRI.  $T_1$  maps confirmed the retention of the Gd-2[G3]-DTPA dendrimers at the injection site, up to 24 h post-CED.

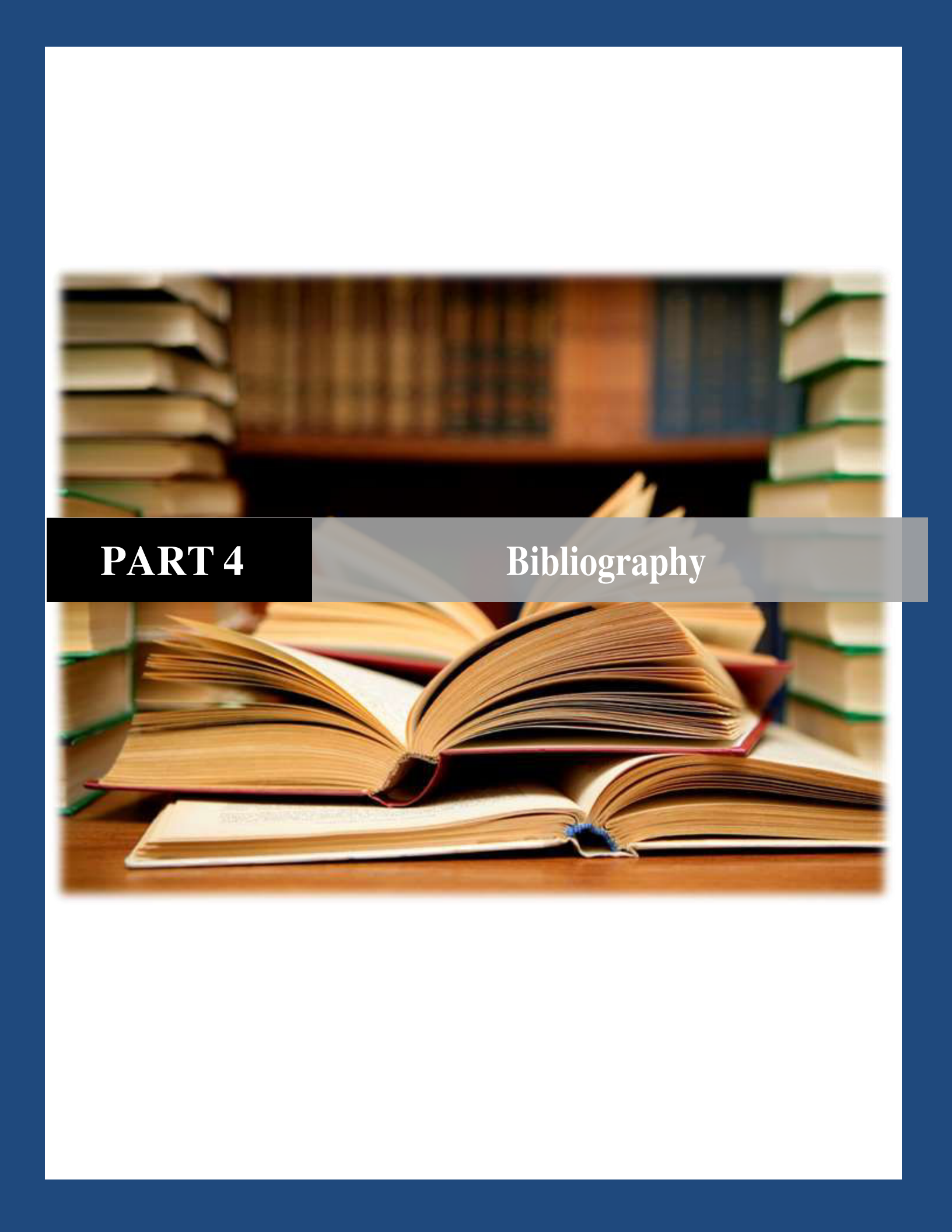
The brain retention of  $^{188}\text{Re}$  and  $\text{Gd}^{3+}$  dual labeled 2[G3]-DTPA dendrimers was quantified in a tissue distribution study, done following their CED in an F98 glioma rats and compared with  $^{188}\text{Re}$ -perrhenate injected using the same procedure. The use of dendrimers avoided the fast brain clearance of the radionuclide alone, and prolonged the confinement of the internal radiation at the tumor site. No radioactivity was found at the other brain hemisphere, showing that the dendrimers were confined at the injection site, before their unavoidable brain clearance. For an efficient locoregional radiotherapy, the brain retention of these dendrimers needs to be improved, since at 96 h post-CED approx. 8.6 % IA was counted at the injection site in the right brain hemisphere.

## *General Conclusions*

---

Our ongoing research represents one of the first efforts in the field, to integrate multimodal dendrimers in nanovectorized radiotherapy and imaging of glioblastomas, following CED.





**PART 4**

**Bibliography**



### PART 4. Bibliography

1. Ferlay, J.; Soerjomataram, I.; Dikshit, R.; Eser, S.; Mathers, C.; Rebelo, M.; Parkin, D. M.; Forman, D.; Bray, F., Cancer incidence and mortality worldwide: sources, methods and major patterns in GLOBOCAN 2012. *Int. J. Cancer* **2015**, *136* (5), E359-E386.
2. Louis, D. N.; Perry, A.; Reifenberger, G.; von Deimling, A.; Figarella-Branger, D.; Cavenee, W. K.; Ohgaki, H.; Wiestler, O. D.; Kleihues, P.; Ellison, D. W., The 2016 World Health Organization Classification of Tumors of the Central Nervous System: a summary. *Acta Neuropathol.* **2016**, *131* (6), 803-820.
3. Ohgaki, H.; Kleihues, P., The Definition of Primary and Secondary Glioblastoma. *Clin. Cancer Res.* **2013**, *19* (4), 764-772.
4. Kleihues, P.; Ohgaki, H., Primary and secondary glioblastomas: from concept to clinical diagnosis. *Neuro-Oncology* **1999**, *1* (1), 44-51.
5. Kleihues, P.; Cavenee, W. K., *Pathology and genetics of tumours of the nervous system*. International Agency for Research on Cancer: 2000.
6. Schiffer, D.; Valentini, C.; Melcarne, A.; Mellai, M.; Prodi, E.; Carrara, G.; Denysenko, T.; Junemann, C.; Casalone, C.; Corona, C., Spatial relationships of MR imaging and positron emission tomography with phenotype, genotype and tumor stem cell generation in glioblastoma multiforme. **2014**.
7. Michel Lacroix; Dima Abi-Said; Daryl R. Fourney; Ziya L. Gokaslan; Weiming Shi; Franco DeMonte; Frederick F. Lang; Ian E. McCutcheon; Samuel J. Hassenbusch; Eric Holland; Kenneth Hess; Christopher Michael; Daniel Miller; Raymond Sawaya, A multivariate analysis of 416 patients with glioblastoma multiforme: prognosis, extent of resection, and survival. *Journal of Neurosurgery* **2001**, *95* (2), 190-198.
8. Bauchet, L.; Mathieu-Daudé, H.; Fabbro-Peray, P.; Rigau, V.; Fabbro, M.; Chinot, O.; Palluseau, L.; Carnin, C.; Lainé, K.; Schlama, A.; Thiebaut, A.; Patru, M. C.; Bauchet, F.; Lionnet, M.; Wager, M.; Faillot, T.; Taillandier, L.; Figarella-Branger, D.; Capelle, L.; Loiseau, H.; Frappaz, D.; Campello, C.; Kerr, C.; Duffau, H.; Reme-Saumon, M.; Trétarre, B.; Daures, J.-P.; Henin, D.; Labrousse, F.; Menei, P.; Honnorat, J.; Neurochirurgie, w. t. p. o. S. F. d.; the Club de Neuro-Oncologie of the Société Française de Neurochirurgie, S. F. d. N.; Française, A. d. N.-O. d. E., Oncological patterns of care and outcome for 952 patients with newly diagnosed glioblastoma in 2004. *Neuro-Oncology* **2010**, *12* (7), 725-735.
9. Ostrom, Q. T.; Gittleman, H.; Farah, P.; Ondracek, A.; Chen, Y.; Wolinsky, Y.; Stroup, N. E.; Kruchko, C.; Barnholtz-Sloan, J. S., CBTRUS Statistical Report: Primary Brain and Central Nervous System Tumors Diagnosed in the United States in 2006-2010. *Neuro-Oncology* **2013**, *15* (suppl 2), ii1-ii56.
10. Pöpperl, G.; Kreth, F. W.; Mehrkens, J. H.; Herms, J.; Seelos, K.; Koch, W.; Gildehaus, F. J.; Kretzschmar, H. A.; Tonn, J. C.; Tatsch, K., FET PET for the evaluation of untreated gliomas: correlation of

FET uptake and uptake kinetics with tumour grading. *Eur. J. Nucl. Med. Mol. Imaging* **2007**, *34* (12), 1933-1942.

11. Jansen, N. L.; Schwartz, C.; Graute, V.; Eigenbrod, S.; Lutz, J.; Egensperger, R.; Pöpperl, G.; Kretschmar, H. A.; Cumming, P.; Bartenstein, P.; Tonn, J.-C.; Kreth, F.-W.; la Fougère, C.; Thon, N., Prediction of oligodendroglial histology and LOH 1p/19q using dynamic [18F]FET-PET imaging in intracranial WHO grade II and III gliomas. *Neuro-Oncology* **2012**, *14* (12), 1473-1480.
12. Kunz, M.; Thon, N.; Eigenbrod, S.; Hartmann, C.; Egensperger, R.; Herms, J.; Geisler, J.; la Fougere, C.; Lutz, J.; Linn, J.; Kreth, S.; von Deimling, A.; Tonn, J. C.; Kretschmar, H. A.; Pöpperl, G.; Kreth, F. W., Hot spots in dynamic18FET-PET delineate malignant tumor parts within suspected WHO grade II gliomas. *Neuro-Oncology* **2011**, *13* (3), 307-316.
13. Götz, I.; Grosu, A., [18F]FET-PET Imaging for Treatment and Response Monitoring of Radiation Therapy in Malignant Glioma Patients – A Review. *Front. Oncol.* **2013**, *3* (104).
14. Minn, H., PET and SPECT in low-grade glioma. *European Journal of Radiology* *56* (2), 171-178.
15. Bénard, F.; Romsa, J.; Hustinx, R., Imaging gliomas with positron emission tomography and single-photon emission computed tomography. *Semin. Nucl. Med.* *33* (2), 148-162.
16. Gotz, L.; Spehl, T. S.; Weber, W. A.; Grosu, A. L., PET and SPECT for radiation treatment planning. *The quarterly journal of nuclear medicine and molecular imaging : official publication of the Italian Association of Nuclear Medicine (AIMN) [and] the International Association of Radiopharmacology (IAR), [and] Section of the So* **2012**, *56* (2), 163-72.
17. Gulyas, B.; Halldin, C., New PET radiopharmaceuticals beyond FDG for brain tumor imaging. *The quarterly journal of nuclear medicine and molecular imaging : official publication of the Italian Association of Nuclear Medicine (AIMN) [and] the International Association of Radiopharmacology (IAR), [and] Section of the So* **2012**, *56* (2), 173-90.
18. Lee, J. D.; Kim, D. I.; Lee, J. T.; Chang, J. W.; Park, C. Y., Indium-111-Pentetreotide Imaging in Intra-axial Brain Tumors: Comparison with Thallium-201 SPECT and MRI. *J. Nucl. Med.* **1995**, *36* (4), 537-541.
19. Schillaci, O.; Filippi, L.; Manni, C.; Santoni, R., Single-Photon Emission Computed Tomography/Computed Tomography in Brain Tumors. *Semin. Nucl. Med.* *37* (1), 34-47.
20. Keunen, O.; Taxt, T.; Grüner, R.; Lund-Johansen, M.; Tonn, J.-C.; Pavlin, T.; Bjerkvig, R.; Niclou, S. P.; Thorsen, F., Multimodal imaging of gliomas in the context of evolving cellular and molecular therapies. *Adv. Drug Delivery Rev.* **2014**, *76*, 98-115.
21. Sharma, P.; Brown, S.; Walter, G.; Santra, S.; Moudgil, B., Nanoparticles for bioimaging. *Adv. Colloid Interface Sci.* **2006**, *123–126*, 471-485.

22. Holland, E. C., Glioblastoma multiforme: The terminator. *Proc. Natl. Acad. Sci. U. S. A.* **2000**, *97* (12), 6242-6244.
23. Doan, B.-T.; Meme, S.; Beloeil, J.-C., General Principles of MRI. In *The Chemistry of Contrast Agents in Medical Magnetic Resonance Imaging*, John Wiley & Sons, Ltd: 2013; pp 1-23.
24. Brown, M. A.; Semelka, R. C., *MRI: basic principles and applications*. John Wiley & Sons: 2011.
25. Bloembergen, N.; Purcell, E. M.; Pound, R. V., Relaxation Effects in Nuclear Magnetic Resonance Absorption. *Physical Review* **1948**, *73* (7), 679-712.
26. Li, X.; Wyatt, C. In *Brain segmentation performance using T1-weighted images versus T1 maps*, SPIE Medical Imaging, International Society for Optics and Photonics: 2010; pp 76233R-76233R-9.
27. Deoni, S. C. L.; Rutt, B. K.; Peters, T. M., Rapid combined T1 and T2 mapping using gradient recalled acquisition in the steady state. *Magnetic Resonance in Medicine* **2003**, *49* (3), 515-526.
28. Chen, P.-F.; Steen, R. G.; Yezzi, A.; Krim, H., Joint Brain Parametric T(1)-Map Segmentation and RF Inhomogeneity Calibration. *International Journal of Biomedical Imaging* **2009**, *2009*, 269525.
29. Chen, P.-F.; Steen, R. G.; Yezzi, A.; Krim, H., Brain MRI T1-Map and T1-weighted image segmentation in a variational framework. In *Proceedings of the 2009 IEEE International Conference on Acoustics, Speech and Signal Processing*, IEEE Computer Society: 2009; pp 417-420.
30. Coolen, B. F.; Geelen, T.; Paulis, L. E. M.; Nauerth, A.; Nicolay, K.; Strijkers, G. J., Three-dimensional T1 mapping of the mouse heart using variable flip angle steady-state MR imaging. *NMR Biomed.* **2011**, *24* (2), 154-162.
31. Coolen, B. F.; Geelen, T.; Paulis, L. E.; Nicolay, K.; Strijkers, G. J., Regional contrast agent quantification in a mouse model of myocardial infarction using 3D cardiac T1mapping. *Journal of Cardiovascular Magnetic Resonance* **2011**, *13* (1), 1-9.
32. Hamlin, S. A.; Henry, T. S.; Little, B. P.; Lerakis, S.; Stillman, A. E., Mapping the Future of Cardiac MR Imaging: Case-based Review of T1 and T2 Mapping Techniques. *RadioGraphics* **2014**, *34* (6), 1594-1611.
33. Glover, G. H., Handbook of MRI pulse sequences, M. A. Bernstein, K. F. King and X. J. Zhou. Elsevier Academic Press, 2004, ISBN: 0-12-092861-2. *NMR Biomed.* **2005**, *18* (3), 202-203.
34. Ananta, J. S.; Godin, B.; Sethi, R.; Moriggi, L.; Liu, X.; Serda, R. E.; Krishnamurthy, R.; Muthupillai, R.; Bolskar, R. D.; Helm, L.; Ferrari, M.; Wilson, L. J.; Decuzzi, P., Geometrical confinement of gadolinium-based contrast agents in nanoporous particles enhances T(1) contrast. *Nat. Nanotechnol.* **2010**, *5* (11), 815-821.

35. Werner, E. J.; Datta, A.; Jocher, C. J.; Raymond, K. N., High-Relaxivity MRI Contrast Agents: Where Coordination Chemistry Meets Medical Imaging. *Angewandte Chemie International Edition* **2008**, *47* (45), 8568-8580.
36. Alric, C.; Taleb, J.; Le Duc, G.; Mandon, C.; Billotey, C.; Le Meur-Herland, A.; Brochard, T.; Vocanson, F.; Janier, M.; Perriat, P.; Roux, S.; Tillement, O., Gadolinium chelate coated gold nanoparticles as contrast agents for both X-ray computed tomography and magnetic resonance imaging. *J. Am. Chem. Soc.* **2008**, *130* (18), 5908-15.
37. Hansen, E. W., FYS-KJM4740. **2015**.
38. Bulte, J. W. M., The chemistry of contrast agents in medical magnetic resonance imaging. edited by A. E. Merbach and E. Toth. Wiley, Chichester, 2001, £135. *NMR Biomed.* **2004**, *17* (4), 210-210.
39. Merbach, A. E.; Toth, E., *The Chemistry of Contrast Agents in Medical Magnetic Resonance Imaging*. Wiley: 2001.
40. Wiener EC, B. M., Brothers H, Magin RL, Gansow OA, Tomalia DA, Lauterbur PC, Dendrimer-based metal chelates: a new class of magnetic resonance imaging contrast agents. *Magn Reson Med.* **1994**, *31* (1), 1-8.
41. Wiener, E. C.; Auteri, F. P.; Chen, J. W.; Brechbiel, M. W.; Gansow, O. A.; Schneider, D. S.; Belford, R. L.; Clarkson, R. B.; Lauterbur, P. C., Molecular Dynamics of Ion-Chelate Complexes Attached to Dendrimers. *J. Am. Chem. Soc.* **1996**, *118* (33), 7774-7782.
42. Wang, S. J.; Brechbiel, M.; Wiener, E. C., Characteristics of a New MRI Contrast Agent Prepared From Polypropyleneimine Dendrimers, Generation 2. *Invest. Radiol.* **2003**, *38* (10), 662-668.
43. Aime, S.; Botta, M.; Crich, G. S.; Giovenzana, B. G.; Pagliarin, R.; Piccinini, M.; Sisti, M.; Terreno, E., Towards MRI contrast agents of improved efficacy. NMR relaxometric investigations of the binding interaction to HSA of a novel heptadentate macrocyclic triphosphonate Gd(III)-complex. *JBIC Journal of Biological Inorganic Chemistry* **1997**, *2* (4), 470-479.
44. Tóth, É.; Pubanz, D.; Vauthey, S.; Helm, L.; Merbach, A. E., The Role of Water Exchange in Attaining Maximum Relaxivities for Dendrimeric MRI Contrast Agents. *Chemistry – A European Journal* **1996**, *2* (12), 1607-1615.
45. Laus, S.; Ruloff, R.; Tóth, É.; Merbach, A. E., GdIII Complexes with Fast Water Exchange and High Thermodynamic Stability: Potential Building Blocks for High-Relaxivity MRI Contrast Agents. *Chemistry – A European Journal* **2003**, *9* (15), 3555-3566.
46. Bryant, L. H.; Brechbiel, M. W.; Wu, C.; Bulte, J. W. M.; Herynek, V.; Frank, J. A., Synthesis and relaxometry of high-generation (G = 5, 7, 9, and 10) PAMAM dendrimer-DOTA-gadolinium chelates. *Journal of Magnetic Resonance Imaging* **1999**, *9* (2), 348-352.

47. Nwe, K.; Bernardo, M.; Regino, C. A. S.; Williams, M.; Brechbiel, M. W., Comparison of MRI properties between derivatized DTPA and DOTA gadolinium-dendrimer conjugates. *Bioorg. Med. Chem.* **2010**, *18* (16), 5925-5931.
48. Stupp, R.; Tonn, J.-C.; Brada, M.; Pentheroudakis, G.; Group, O. b. o. t. E. G. W., High-grade malignant glioma: ESMO Clinical Practice Guidelines for diagnosis, treatment and follow-up. *Annals of Oncology* **2010**, *21* (suppl 5), v190-v193.
49. Tate, M. C., Surgery for Gliomas. In *Current Understanding and Treatment of Gliomas*, Raizer, J.; Parsa, A., Eds. Springer International Publishing: Cham, 2015; pp 31-47.
50. Villà, S.; Balañà, C.; Comas, S., Radiation and concomitant chemotherapy for patients with glioblastoma multiforme. *Chinese Journal of Cancer* **2014**, *33* (1), 25-31.
51. Friedman, H. S.; Kerby, T.; Calvert, H., Temozolomide and Treatment of Malignant Glioma. *Clin. Cancer Res.* **2000**, *6* (7), 2585-2597.
52. Sminia, P.; Mayer, R., External Beam Radiotherapy of Recurrent Glioma: Radiation Tolerance of the Human Brain. *Cancers* **2012**, *4* (2), 379-399.
53. Belka, C.; Budach, W.; Kortmann, R. D.; Bamberg, M., Radiation induced CNS toxicity – molecular and cellular mechanisms. *Br. J. Cancer* **2001**, *85* (9), 1233-1239.
54. Weller, M.; Cloughesy, T.; Perry, J. R.; Wick, W., Standards of care for treatment of recurrent glioblastoma—are we there yet? *Neuro-Oncology* **2013**, *15* (1), 4-27.
55. Bredel, M., Anticancer drug resistance in primary human brain tumors. *Brain Research Reviews* **2001**, *35* (2), 161-204.
56. Maysinger, D.; Morinville, A., Drug delivery to the nervous system. *Trends in Biotechnology* **15** (10), 410-418.
57. Yazici, G.; Cengiz, M.; Ozyigit, G.; Eren, G.; Yildiz, F.; Akyol, F.; Gurkaynak, M.; Zorlu, F., Hypofractionated stereotactic reirradiation for recurrent glioblastoma. *Journal of neuro-oncology* **2014**, *120* (1), 117-123.
58. Skeie, B. S.; Enger, P. Ø.; Brøgger, J.; Ganz, J. C.; Thorsen, F.; Heggdal, J. I.; Pedersen, P.-H., Gamma Knife Surgery versus Reoperation for Recurrent Glioblastoma Multiforme. *World Neurosurgery* **2012**, *78* (6), 658-669.
59. Hoebbers, F.; Rios, E.; Troost, E.; van den Ende, P.; Kross, K.; Lacko, M.; Lalisang, R.; Kremer, B.; de Jong, J., Definitive radiation therapy for treatment of laryngeal carcinoma. *Strahlentherapie und Onkologie* **2013**, *189* (10), 834-841.

60. Hall, W. A.; Djalilian, H. R.; Sperduto, P. W.; Cho, K. H.; Gerbi, B. J.; Gibbons, J. P.; Rohr, M.; Clark, H. B., Stereotactic radiosurgery for recurrent malignant gliomas. *Journal of Clinical Oncology* **1995**, *13* (7), 1642-8.
61. Bokstein, F.; Blumenthal, D. T.; Corn, B. W.; Gez, E.; Matcyevesky, D.; Shtraus, N.; Ram, Z.; Kanner, A. A., Stereotactic radiosurgery (SRS) in high-grade glioma: judicious selection of small target volumes improves results. *Journal of neuro-oncology* **2016**, *126* (3), 551-557.
62. Pantaleo Romanelli; Alfredo Conti; Antonio Pontoriero; Giuseppe Kenneth Ricciardi; Francesco Tomasello; Costantino De Renzis; Gualtiero Innocenzi; Vincenzo Esposito; Giampaolo Cantore, Role of stereotactic radiosurgery and fractionated stereotactic radiotherapy for the treatment of recurrent glioblastoma multiforme. *Neurosurgical Focus* **2009**, *27* (6), E8.
63. Brem, H.; Piantadosi, S.; Burger, P. C.; Walker, M.; Selker, R.; Vick, N. A.; Black, K.; Sisti, M.; Brem, S.; Mohr, G.; et al., Placebo-controlled trial of safety and efficacy of intraoperative controlled delivery by biodegradable polymers of chemotherapy for recurrent gliomas. The Polymer-brain Tumor Treatment Group. *Lancet (London, England)* **1995**, *345* (8956), 1008-12.
64. Vanpouille-Box, C.; Hindré, F., Nanovectorized radiotherapy: a new strategy to induce anti-tumor immunity. *Front. Oncol.* **2012**, *2*, 136.
65. Kassis, A. I., Therapeutic Radionuclides: Biophysical and Radiobiologic Principles. *Semin. Nucl. Med.* **2008**, *38* (5), 358-366.
66. Gudkov, S. V.; Shilyagina, N. Y.; Vodeneev, V. A.; Zvyagin, A. V., Targeted Radionuclide Therapy of Human Tumors. *Int. J. Mol. Sci.* **2016**, *17* (1), 33.
67. Cordier, D.; Krolicki, L.; Morgenstern, A.; Merlo, A., Targeted Radiolabeled Compounds in Glioma Therapy. *Semin. Nucl. Med.* *46* (3), 243-249.
68. Larson, S. M.; Carrasquillo, J. A.; Cheung, N.-K. V.; Press, O. W., Radioimmunotherapy of human tumours. *Nat. Rev. Cancer* **2015**, *15* (6), 347-360.
69. Press, O. W.; Rasey, J., Principles of radioimmunotherapy for hematologists and oncologists. *Seminars in oncology* **2000**, *27* (6 Suppl 12), 62-73.
70. Naruki, Y.; Carrasquillo, J. A.; Reynolds, J. C.; Maloney, P. J.; Frincke, J. M.; Neumann, R. D.; Larson, S. M., Differential cellular catabolism of <sup>111</sup>In, <sup>90</sup>Y and <sup>125</sup>I radiolabeled T101 anti-CD5 monoclonal antibody. *Int J Rad Appl Instrum B* **1990**, *17* (2), 201-207.
71. Geissler, F.; Anderson, S. K.; Press, O., Intracellular catabolism of radiolabeled anti-CD3 antibodies by leukemic T cells. *Cell. Immunol.* **1991**, *137* (1), 96-110.
72. Press, O. W.; Shan, D.; Howell-Clark, J.; Eary, J.; Appelbaum, F. R.; Matthews, D.; King, D. J.; Haines, A. M. R.; Hamann, P.; Hinman, L.; Shochat, D.; Bernstein, I. D., Comparative Metabolism and

- Retention of Iodine-125, Yttrium-90, and Indium-111 Radioimmunoconjugates by Cancer Cells. *Cancer Res.* **1996**, *56* (9), 2123-2129.
73. Kaminski, M. S.; Zelenetz, A. D.; Press, O. W.; Saleh, M.; Leonard, J.; Fehrenbacher, L.; Lister, T. A.; Stagg, R. J.; Tidmarsh, G. F.; Kroll, S.; Wahl, R. L.; Knox, S. J.; Vose, J. M., Pivotal Study of Iodine I 131 Tositumomab for Chemotherapy-Refractory Low-Grade or Transformed Low-Grade B-Cell Non-Hodgkin's Lymphomas. *Journal of Clinical Oncology* **2001**, *19* (19), 3918-3928.
74. Witzig, T. E.; Gordon, L. I.; Cabanillas, F.; Czuczman, M. S.; Emmanouilides, C.; Joyce, R.; Pohlman, B. L.; Bartlett, N. L.; Wiseman, G. A.; Padre, N.; Grillo-López, A. J.; Multani, P.; White, C. A., Randomized Controlled Trial of Yttrium-90–Labeled Ibritumomab Tiuxetan Radioimmunotherapy Versus Rituximab Immunotherapy for Patients With Relapsed or Refractory Low-Grade, Follicular, or Transformed B-Cell Non-Hodgkin's Lymphoma. *Journal of Clinical Oncology* **2002**, *20* (10), 2453-2463.
75. Press, O. W.; Eary, J. F.; Appelbaum, F. R.; Martin, P. J.; Nelp, W. B.; Glenn, S.; Fisher, D. R.; Porter, B.; Matthews, D. C.; Gooley, T.; et al., Phase II trial of 131I-B1 (anti-CD20) antibody therapy with autologous stem cell transplantation for relapsed B cell lymphomas. *Lancet (London, England)* **1995**, *346* (8971), 336-40.
76. Press, O. W.; Eary, J. F.; Appelbaum, F. R.; Martin, P. J.; Badger, C. C.; Nelp, W. B.; Glenn, S.; Butchko, G.; Fisher, D.; Porter, B.; Matthews, D. C.; Fisher, L. D.; Bernstein, I. D., Radiolabeled-Antibody Therapy of B-Cell Lymphoma with Autologous Bone Marrow Support. *N. Engl. J. Med.* **1993**, *329* (17), 1219-1224.
77. Argyrou, M.; Valassi, A.; Andreou, M.; Lyra, M., Rhenium-188 Production in Hospitals, by W-188/Re-188 Generator, for Easy Use in Radionuclide Therapy. *Int. J. Mol. Imaging* **2013**, *2013*, 7.
78. Vanpouille-Box, C. Les nanocapsules lipidiques chargées en Rhénium-188: nouvel outil pour la radiothérapie interne du carcinome hépatocellulaire et du gliome. Doctoral Thesis, University of Angers, 2011.
79. Zalutsky, M. R., Targeted  $\alpha$ -Particle Therapy of Microscopic Disease: Providing a Further Rationale for Clinical Investigation. *J. Nucl. Med.* **2006**, *47* (8), 1238-1240.
80. Jurcic, J. G.; Larson, S. M.; Sgouros, G.; McDevitt, M. R.; Finn, R. D.; Divgi, C. R.; Ballangrud, Å. M.; Hamacher, K. A.; Ma, D.; Humm, J. L., Targeted  $\alpha$  particle immunotherapy for myeloid leukemia. *Blood* **2002**, *100* (4), 1233-1239.
81. Hall, E. J.; Giaccia, A. J., *Radiobiology for the Radiologist*. Lippincott Williams & Wilkins: 2006.
82. Mulford, D. A.; Scheinberg, D. A.; Jurcic, J. G., The Promise of Targeted  $\alpha$ -Particle Therapy. *J. Nucl. Med.* **2005**, *46* (1 suppl), 199S-204S.
83. Zalutsky, M.; Pozzi, O., Radioimmunotherapy with [alpha]-particle emitting radionuclides. *The Quarterly Journal of Nuclear Medicine and Molecular Imaging* **2004**, *48* (4), 289.

84. Miederer, M.; McDevitt, M. R.; Sgouros, G.; Kramer, K.; Cheung, N.-K. V.; Scheinberg, D. A., Pharmacokinetics, Dosimetry, and Toxicity of the Targetable Atomic Generator, 225Ac-HuM195, in Nonhuman Primates. *J. Nucl. Med.* **2004**, *45* (1), 129-137.
85. Panchapakesan, B.; Wickstrom, E., Nanotechnology for Sensing, Imaging, and Treating Cancer. *Surg. Oncol. Clin. N. Am.* **2007**, *16* (2), 293-305.
86. Tröster, S. D.; Müller, U.; Kreuter, J., Modification of the body distribution of poly(methyl methacrylate) nanoparticles in rats by coating with surfactants. *International Journal of Pharmaceutics* **1990**, *61* (1-2), 85-100.
87. Brigger, I.; Morizet, J.; Aubert, G.; Chacun, H.; Terrier-Lacombe, M. J.; Couvreur, P.; Vassal, G., Poly(ethylene glycol)-coated hexadecylcyanoacrylate nanospheres display a combined effect for brain tumor targeting. *J. Pharmacol. Exp. Ther.* **2002**, *303* (3), 928-936.
88. Stella, B.; Arpicco, S.; Peracchia, M. T.; Desmaële, D.; Hoebeke, J.; Renoir, M.; D'Angelo, J.; Cattel, L.; Couvreur, P., Design of folic acid-conjugated nanoparticles for drug targeting. *J. Pharm. Sci.* **2000**, *89* (11), 1452-1464.
89. Kocbek, P.; Obermajer, N.; Cegnar, M.; Kos, J.; Kristl, J., Targeting cancer cells using PLGA nanoparticles surface modified with monoclonal antibody. *J. Control. Release* **2007**, *120* (1-2), 18-26.
90. Hdeib, A.; Sloan, A., Targeted radioimmunotherapy: the role of 131I-chTNT-1/B mAb (Cotara®) for treatment of high-grade gliomas. *Future Oncology* **2012**, *8* (6), 659-669.
91. Michael Y. Chen; Russell R. Lonser; Paul F. Morrison; Lance S. Governale; Edward H. Oldfield, Variables affecting convection-enhanced delivery to the striatum: a systematic examination of rate of infusion, cannula size, infusate concentration, and tissue—cannula sealing time. *Journal of Neurosurgery* **1999**, *90* (2), 315-320.
92. Sakka, L.; Coll, G.; Chazal, J., Anatomy and physiology of cerebrospinal fluid. *European Annals of Otorhinolaryngology, Head and Neck Diseases* **2011**, *128* (6), 309-316.
93. Meyers, J. D.; Cheng, Y.; Broome, A. M.; Agnes, R. S.; Schluchter, M. D.; Margevicius, S.; Wang, X.; Kenney, M. E.; Burda, C.; Basilion, J. P., Peptide-targeted gold nanoparticles for photodynamic therapy of brain cancer. *Particle and Particle Systems Characterization* **2015**, *32* (4), 448-457.
94. Dixit, S.; Miller, K.; Zhu, Y.; McKinnon, E.; Novak, T.; Kenney, M. E.; Broome, A.-M., Dual Receptor-Targeted Theranostic Nanoparticles for Localized Delivery and Activation of Photodynamic Therapy Drug in Glioblastomas. *Mol. Pharm.* **2015**, *12* (9), 3250-3260.
95. Shidhaye, S. S.; Vaidya, R.; Sutar, S.; Patwardhan, A.; Kadam, V. J., Solid lipid nanoparticles and nanostructured lipid carriers - Innovative generations of solid lipid carriers. *Curr. Drug Deliv.* **2008**, *5* (4), 324-331.

96. Allard, E.; Hindré, F.; Passirani, C.; Lemaire, L.; Lepareur, N.; Noiret, N.; Menei, P.; Benoit, J.-P., 188Re-loaded lipid nanocapsules as a promising radiopharmaceutical carrier for internal radiotherapy of malignant gliomas. *Eur. J. Nucl. Med. Mol. Imaging* **2008**, *35* (10), 1838-1846.
97. Béduneau, A.; Hindré, F.; Clavreul, A.; Leroux, J.-C.; Saulnier, P.; Benoit, J.-P., Brain targeting using novel lipid nanovectors. *J. Control. Release* **2008**, *126* (1), 44-49.
98. Ballot, S.; Noiret, N.; Hindré, F.; Denizot, B.; Garin, E.; Rajerison, H.; Benoit, J.-P., 99mTc/188Re-labelled lipid nanocapsules as promising radiotracers for imaging and therapy: formulation and biodistribution. *Eur. J. Nucl. Med. Mol. Imaging* **2006**, *33* (5), 602-607.
99. Christie, C.; Madsen, S. J.; Peng, Q.; Hirschberg, H., Macrophages as nanoparticle delivery vectors for photothermal therapy of brain tumors. *Therapeutic Delivery* **2015**, *6* (3), 371-384.
100. Antosh, M. P.; Wijesinghe, D. D.; Shrestha, S.; Lanou, R.; Huang, Y. H.; Hasselbacher, T.; Fox, D.; Neretti, N.; Sun, S.; Katenka, N.; Cooper, L. N.; Andreev, O. A.; Reshetnyak, Y. K., Enhancement of radiation effect on cancer cells by gold-pHLIP. *Proceedings of the National Academy of Sciences* **2015**, *112* (17), 5372-5376.
101. Phillips, W. T.; Goins, B.; Bao, A.; Vargas, D.; Gutierrez, J. E.; Trevino, A.; Miller, J. R.; Henry, J.; Zuniga, R.; Vecil, G.; Brenner, A. J., Rhenium-186 liposomes as convection-enhanced nanoparticle brachytherapy for treatment of glioblastoma. *Neuro-Oncology* **2012**, *14* (4), 416-425.
102. James, C. D., Nanoparticles for treating brain tumors: unlimited possibilities. *Neuro-Oncology* **2012**, *14* (4), 389.
103. Huang, F.-Y. J.; Lee, T.-W.; Chang, C.-H.; Chen, L.-C.; Hsu, W.-H.; Chang, C.-W.; Lo, J.-M., Evaluation of (188)Re-labeled PEGylated nanoliposome as a radionuclide therapeutic agent in an orthotopic glioma-bearing rat model. *Int. J. Nanomed.* **2015**, *10*, 463-473.
104. Vanpouille-Box, C.; Lacoeyille, F.; Belloche, C.; Lepareur, N.; Lemaire, L.; LeJeune, J.-J.; Benoît, J.-P.; Menei, P.; Couturier, O. F.; Garcion, E.; Hindré, F., Tumor eradication in rat glioma and bypass of immunosuppressive barriers using internal radiation with 188Re-lipid nanocapsules. *Biomaterials* **2011**, *32* (28), 6781-6790.
105. U. Boas, J. B. C. a. P. M. H. H., Dendrimers: Design, Synthesis and Chemical Properties. In *Dendrimers in Medicine and Biotechnology: New Molecular Tools*, Boas, U.; Christensen, J. B.; Heegaard, P. M. H., Eds. The Royal Society of Chemistry: 2006; pp 1-27.
106. Appelhans, D.; Oertel, U.; Mazzeo, R.; Komber, H.; Hoffmann, J.; Weidner, S.; Brutschy, B.; Voit, B.; Ottaviani, M. F. In *Dense-shell glycodendrimers: UV/Vis and electron paramagnetic resonance study of metal ion complexation*, Proceedings of the Royal Society of London A: Mathematical, Physical and Engineering Sciences, The Royal Society: 2010; pp 1489-1513.

107. Barth, R. F.; Adams, D. M.; Soloway, A. H.; Alam, F.; Darby, M. V., Boronated starburst dendrimer-monoclonal antibody immunoconjugates: Evaluation as a potential delivery system for neutron capture therapy. *Bioconjug. Chem.* **1994**, *5* (1), 58-66.
108. Chauhan, A. S.; Jain, N. K.; Diwan, P. V., Pre-clinical and behavioural toxicity profile of PAMAM dendrimers in mice. *Proceedings of the Royal Society A: Mathematical, Physical and Engineering Science* **2010**, *466* (2117), 1535-1550.
109. Hofacker, A. L.; Parquette, J. R., Amplification of local chirality within a folded dendrimer. An intramolecular 'sergeants and soldiers' experiment. *Proceedings of the Royal Society A: Mathematical, Physical and Engineering Science* **2010**, *466* (2117), 1469-1487.
110. Klajnert, B.; Pikala, S.; Bryszewska, M., Haemolytic activity of polyamidoamine dendrimers and the protective role of human serum albumin. *Proceedings of the Royal Society A: Mathematical, Physical and Engineering Science* **2010**, *466* (2117), 1527-1534.
111. Howell, B. A.; Fan, D., Poly(amidoamine) dendrimer-supported organoplatinum antitumour agents. *Proceedings of the Royal Society A: Mathematical, Physical and Engineering Science* **2010**, *466* (2117), 1515-1526.
112. Kobayashi, H.; Kawamoto, S.; Jo, S.-K.; Bryant, H. L.; Brechbiel, M. W.; Star, R. A., Macromolecular MRI Contrast Agents with Small Dendrimers: Pharmacokinetic Differences between Sizes and Cores. *Bioconjug. Chem.* **2003**, *14* (2), 388-394.
113. Simanek, E. E.; Abdou, H.; Lalwani, S.; Lim, J.; Mintzer, M.; Venditto, V. J.; Vittur, B., The 8 year thicket of triazine dendrimers: strategies, targets and applications. *Proceedings of the Royal Society A: Mathematical, Physical and Engineering Science* **2010**, *466* (2117), 1445-1468.
114. Solassol, J.; Crozet, C.; Perrier, V.; Leclaire, J.; Béranger, F.; Caminade, A.-M.; Meunier, B.; Dormont, D.; Majoral, J.-P.; Lehmann, S., Cationic phosphorus-containing dendrimers reduce prion replication both in cell culture and in mice infected with scrapie. *J. Gen. Virol.* **2004**, *85* (6), 1791-1799.
115. Thayumanavan, S.; Bharathi, P.; Sivanandan, K.; Rao Vutukuri, D., Towards dendrimers as biomimetic macromolecules. *C. R. Chim.* **2003**, *6* (8-10), 767-778.
116. Tomalia, D. A.; Baker, H.; Dewald, J.; Hall, M.; Kallos, G.; Martin, S.; Roeck, J.; Ryder, J.; Smith, P., A New Class of Polymers: Starburst-Dendritic Macromolecules. *Polym. J.* **1985**, *17* (1), 117-132.
117. Newkome, G. R.; Yao, Z.; Baker, G. R.; Gupta, V. K., Micelles. Part 1. Cascade molecules: a new approach to micelles. A [27]-arborol. *J. Org. Chem.* **1985**, *50* (11), 2003-2004.
118. Hawker, C. J.; Frechet, J. M. J., Preparation of polymers with controlled molecular architecture. A new convergent approach to dendritic macromolecules. *J. Am. Chem. Soc.* **1990**, *112* (21), 7638-7647.

119. Ngoc Quyen, T.; Cuu Khoa, N.; Thi Phuong, N., Dendrimer-based nanocarriers demonstrating a high efficiency for loading and releasing anticancer drugs against cancer cells in vitro and in vivo. *Advances in Natural Sciences: Nanoscience and Nanotechnology* **2013**, *4* (4), 045013.
120. Wooley, K. L.; Hawker, C. J.; Lee, R.; Frechet, J. M. J., One-Step Synthesis of Hyperbranched Polyesters. Molecular Weight Control and Chain End Functionalization. *Polym J* **1994**, *26* (2), 187-197.
121. Fischer, M.; Vögtle, F., Dendrimers: From Design to Application—A Progress Report. *Angewandte Chemie International Edition* **1999**, *38* (7), 884-905.
122. De Gennes, P.-G.; Hervet, H., Statistics of «starburst» polymers. *Journal de Physique Lettres* **1983**, *44* (9), 351-360.
123. Mansfield, M. L.; Klushin, L. I., Monte Carlo studies of dendrimer macromolecules. *Macromolecules* **1993**, *26* (16), 4262-4268.
124. Bhalgat, M. K.; Roberts, J. C., Molecular modeling of polyamidoamine (PAMAM) Starburst™ dendrimers. *Eur. Polym. J.* **2000**, *36* (3), 647-651.
125. Hodge, P., Polymer science branches out. *Nature* **1993**, *362* (6415), 18-19.
126. Klajnert, B.; Bryszewska, M., Dendrimers: properties and applications. *Acta Biochim. Pol.* **2001**, *48* (1), 199-208.
127. Chai, M.; Niu, Y.; Youngs, W. J.; Rinaldi, P. L., Structure and Conformation of DAB Dendrimers in Solution via Multidimensional NMR Techniques. *J. Am. Chem. Soc.* **2001**, *123* (20), 4670-4678.
128. Boas, U.; Heegaard, P. M. H., Dendrimers in drug research. *Chem. Soc. Rev.* **2004**, *33* (1), 43-63.
129. Farin, D.; Avnir, D., Surface Fractality of Dendrimers. *Angewandte Chemie International Edition in English* **1991**, *30* (10), 1379-1380.
130. Noriega-Luna, B.; Godínez, L. A.; Rodríguez, F. J.; Rodríguez, A.; Zaldívar-Lelo de Larrea, G.; Sosa-Ferreira, C. F.; Mercado-Curiel, R. F.; Manríquez, J.; Bustos, E., Applications of Dendrimers in Drug Delivery Agents, Diagnosis, Therapy, and Detection. *Journal of Nanomaterials* **2014**, *2014*, 19.
131. Emrick\*, T.; Fréchet†, J. M. J., Self-assembly of dendritic structures. *Curr. Opin. Colloid Interface Sci.* **1999**, *4* (1), 15-23.
132. Zheng, Y.-R.; Ghosh, K.; Yang, H.-B.; Stang, P. J., Coordination-Driven Self-Assembly of Three-Dimensional Supramolecular Dendrimers. *Inorg. Chem.* **2010**, *49* (11), 4747-4749.
133. Mintzer, M. A.; Grinstaff, M. W., Biomedical applications of dendrimers: a tutorial. *Chem. Soc. Rev.* **2011**, *40* (1), 173-190.

134. Tekade, R. K.; Kumar, P. V.; Jain, N. K., Dendrimers in Oncology: An Expanding Horizon. *Chem. Rev.* **2009**, *109* (1), 49-87.
135. Medina, S. H.; El-Sayed, M. E. H., Dendrimers as Carriers for Delivery of Chemotherapeutic Agents. *Chem. Rev.* **2009**, *109* (7), 3141-3157.
136. Dufès, C.; Uchegbu, I. F.; Schätzlein, A. G., Dendrimers in gene delivery. *Adv. Drug Delivery Rev.* **2005**, *57* (15), 2177-2202.
137. Rolland, O.; Turrin, C.-O.; Caminade, A.-M.; Majoral, J.-P., Dendrimers and nanomedicine: multivalency in action. *New J. Chem.* **2009**, *33* (9), 1809-1824.
138. Astruc, D.; Boisselier, E.; Ornelas, C., Dendrimers designed for functions: from physical, photophysical, and supramolecular properties to applications in sensing, catalysis, molecular electronics, photonics, and nanomedicine. *Chem. Rev.* **2010**, *110* (4), 1857-1959.
139. Reek, J. N. H.; Arévalo, S.; van Heerbeek, R.; Kamer, P. C. J.; van Leeuwen, P. W. N. M., Dendrimers in Catalysis. In *Adv. Catal.*, Bruce, C. G.; Helmut, K., Eds. Academic Press: 2006; Vol. Volume 49, pp 71-151.
140. Abbasi, E.; Aval, S. F.; Akbarzadeh, A.; Milani, M.; Nasrabadi, H. T.; Joo, S. W.; Hanifehpour, Y.; Nejati-Koshki, K.; Pashaei-Asl, R., Dendrimers: synthesis, applications, and properties. *Nanoscale Research Letters* **2014**, *9* (1), 247-247.
141. Tomalia, D. A.; Wilson, L. R.; Hedstrand, D. M.; Tomlinson, I. A.; Fazio, M. J.; Kruper, W. J.; Kaplan, D. A.; Cheng, R. C.; Edwards, D. S.; Jung, C. W., Dense star polymer conjugates. Google Patents: 1996.
142. Tomalia, D. A., Dendritic effects: dependency of dendritic nano-periodic property patterns on critical nanoscale design parameters (CNDPs). *New J. Chem.* **2012**, *36* (2), 264-281.
143. Caminade, A.-M.; Ouali, A.; Laurent, R.; Turrin, C.-O.; Majoral, J.-P., The dendritic effect illustrated with phosphorus dendrimers. *Chem. Soc. Rev.* **2015**, *44* (12), 3890-3899.
144. Blodgett, T. M.; Meltzer, C. C.; Townsend, D. W., PET/CT: Form and Function. *Radiology* **2007**, *242* (2), 360-385.
145. Talanov, V. S.; Regino, C. A. S.; Kobayashi, H.; Bernardo, M.; Choyke, P. L.; Brechbiel, M. W., Dendrimer-Based Nanoprobe for Dual Modality Magnetic Resonance and Fluorescence Imaging. *Nano Lett.* **2006**, *6* (7), 1459-1463.
146. Freemantle, M., DOWNSIZING CHEMISTRY. *Chemical & Engineering News Archive* **1999**, *77* (8), 27-36.

147. Jansen, J. F. G. A.; de Brabander-van den Berg, E. M. M.; Meijer, E. W., Encapsulation of Guest Molecules into a Dendritic Box. *Science* **1994**, *266* (5188), 1226-1229.
148. Ottaviani, M. F.; Montalti, F.; Turro, N. J.; Tomalia, D. A., Characterization of Starburst Dendrimers by the EPR Technique. Copper(II) Ions Binding Full-Generation Dendrimers. *The Journal of Physical Chemistry B* **1997**, *101* (2), 158-166.
149. Esfand, R.; Tomalia, D. A., Poly(amidoamine) (PAMAM) dendrimers: from biomimicry to drug delivery and biomedical applications. *Drug Discov. Today* **2001**, *6* (8), 427-436.
150. Cheng, Y.; Zhao, L.; Li, Y.; Xu, T., Design of biocompatible dendrimers for cancer diagnosis and therapy: current status and future perspectives. *Chem. Soc. Rev.* **2011**, *40* (5), 2673-2703.
151. Lee, D. S.; Im, H.-J.; Lee, Y.-S., Radionanomedicine: Widened perspectives of molecular theragnosis. *Nanomed. Nanotech. Biol. Med.* **2015**, *11* (4), 795-810.
152. Lee, D.-E.; Koo, H.; Sun, I.-C.; Ryu, J. H.; Kim, K.; Kwon, I. C., Multifunctional nanoparticles for multimodal imaging and theragnosis. *Chem. Soc. Rev.* **2012**, *41* (7), 2656-2672.
153. Choi, H.; Lee, Y.-S.; Hwang Do, W.; Lee Dong, S., Translational radionanomedicine: a clinical perspective. In *European Journal of Nanomedicine*, 2016; Vol. 8, p 71.
154. Hare, J. I.; Lammers, T.; Ashford, M. B.; Puri, S.; Storm, G.; Barry, S. T., Challenges and strategies in anti-cancer nanomedicine development: An industry perspective. *Adv. Drug Delivery Rev.* **2016**.
155. Abi-Ghanem, A. S., Radionuclide Therapy of Leukemias. In *Nuclear Medicine Therapy: Principles and Clinical Applications*, Aktolun, C.; Goldsmith, J. S., Eds. Springer New York: New York, NY, 2013; pp 27-47.
156. Baetke, S. C.; Lammers, T.; Kiessling, F., Applications of nanoparticles for diagnosis and therapy of cancer. *The British Journal of Radiology* **2015**, *88* (1054), 20150207.
157. Khan, M. K.; Nigavekar, S. S.; Minc, L. D.; Kariapper, M. S. T.; Nair, B. M.; Lesniak, W. G.; Balogh, L. P., In Vivo Biodistribution of Dendrimers and Dendrimer Nanocomposites — Implications for Cancer Imaging and Therapy. *Technol. Cancer Res. Treat.* **2005**, *4* (6), 603-613.
158. Qiao, Z.; Shi, X., Dendrimer-based molecular imaging contrast agents. *Prog. Polym. Sci.* **2015**, *44* (0), 1-27.
159. Liu, K.; Xu, Z.; Yin, M., Perylenediimide-cored dendrimers and their bioimaging and gene delivery applications. *Prog. Polym. Sci.* **2015**, *46* (0), 25-54.
160. Tomalia, D. A., Dendrimers as multi-purpose nanodevices for oncology drug delivery and diagnostic imaging. *Nanomed. Nanotech. Biol. Med.* **2006**, *2* (4), 309.

161. Svenson, S.; Tomalia, D. A., Dendrimers in biomedical applications—reflections on the field. *Adv. Drug Delivery Rev.* **2005**, *57* (15), 2106-2129.
162. Koo, O. M.; Rubinstein, I.; Onyukel, H., Role of nanotechnology in targeted drug delivery and imaging: a concise review. *Nanomed. Nanotech. Biol. Med.* **2005**, *1* (3), 193-212.
163. Wolinsky, J. B.; Grinstaff, M. W., Therapeutic and diagnostic applications of dendrimers for cancer treatment. *Adv. Drug Delivery Rev.* **2008**, *60* (9), 1037-1055.
164. Menjoge, A. R.; Kannan, R. M.; Tomalia, D. A., Dendrimer-based drug and imaging conjugates: design considerations for nanomedical applications. *Drug Discov. Today* **2010**, *15* (5–6), 171-185.
165. Kesharwani, P.; Iyer, A. K., Recent advances in dendrimer-based nanovectors for tumor-targeted drug and gene delivery. *Drug Discov. Today* **2015**, *20* (5), 536-547.
166. Kolb, H. C.; Finn, M. G.; Sharpless, K. B., Click Chemistry: Diverse Chemical Function from a Few Good Reactions. *Angewandte Chemie International Edition* **2001**, *40* (11), 2004-2021.
167. Rostovtsev, V. V.; Green, L. G.; Fokin, V. V.; Sharpless, K. B., A Stepwise Huisgen Cycloaddition Process: Copper(I)-Catalyzed Regioselective “Ligation” of Azides and Terminal Alkynes. *Angewandte Chemie International Edition* **2002**, *41* (14), 2596-2599.
168. Lee, C. Y.; Held, R.; Sharma, A.; Baral, R.; Nanah, C.; Dumas, D.; Jenkins, S.; Upadhaya, S.; Du, W., Copper-Granule-Catalyzed Microwave-Assisted Click Synthesis of Polyphenol Dendrimers. *J. Org. Chem.* **2013**, *78* (22), 11221-11228.
169. Huisgen, R., Kinetics and reaction mechanisms: selected examples from the experience of forty years. In *Pure Appl. Chem.*, 1989; Vol. 61, p 613.
170. Wu, P.; Feldman, A. K.; Nugent, A. K.; Hawker, C. J.; Scheel, A.; Voit, B.; Pyun, J.; Fréchet, J. M. J.; Sharpless, K. B.; Fokin, V. V., Efficiency and Fidelity in a Click-Chemistry Route to Triazole Dendrimers by the Copper(I)-Catalyzed Ligation of Azides and Alkynes. *Angewandte Chemie International Edition* **2004**, *43* (30), 3928-3932.
171. Joralemon, M. J.; O'Reilly, R. K.; Matson, J. B.; Nugent, A. K.; Hawker, C. J.; Wooley, K. L., Dendrimers Clicked Together Divergently. *Macromolecules* **2005**, *38* (13), 5436-5443.
172. **!!! INVALID CITATION !!!**
173. Killops, K. L.; Campos, L. M.; Hawker, C. J., Robust, Efficient, and Orthogonal Synthesis of Dendrimers via Thiol-ene “Click” Chemistry. *J. Am. Chem. Soc.* **2008**, *130* (15), 5062-5064.
174. Appukkuttan, P.; Van der Eycken, E., Recent Developments in Microwave-Assisted, Transition-Metal-Catalysed C–C and C–N Bond-Forming Reactions. *Eur. J. Org. Chem.* **2008**, *2008* (7), 1133-1155.

175. Oliver Kappe, C., Microwave dielectric heating in synthetic organic chemistry. *Chem. Soc. Rev.* **2008**, 37 (6), 1127-1139.
176. Walter, M. V.; Malkoch, M., Simplifying the synthesis of dendrimers: accelerated approaches. *Chem. Soc. Rev.* **2012**, 41 (13), 4593-4609.
177. Fernandez-Megia, E.; Correa, J.; Riguera, R., "Clickable" PEG-dendritic block copolymers. *Biomacromolecules* **2006**, 7 (11), 3104-11.
178. Amaral, S. P.; Fernandez-Villamarin, M.; Correa, J.; Riguera, R.; Fernandez-Megia, E., Efficient Multigram Synthesis of the Repeating Unit of Gallic Acid-Triethylene Glycol Dendrimers. *Organic Letters* **2011**, 13 (17), 4522-4525.
179. Bondy, M. L.; Scheurer, M. E.; Malmer, B.; Barnholtz-Sloan, J. S.; Davis, F. G.; Il'yasova, D.; Kruchko, C.; McCarthy, B. J.; Rajaraman, P.; Schwartzbaum, J. A.; Sadetzki, S.; Schlehofer, B.; Tihan, T.; Wiemels, J. L.; Wrensch, M.; Buffler, P. A., Brain Tumor Epidemiology: Consensus from the Brain Tumor Epidemiology Consortium (BTEC). *Cancer* **2008**, 113 (7 Suppl), 1953-1968.
180. Stupp, R.; Mason, W. P.; van den Bent, M. J.; Weller, M.; Fisher, B.; Taphoorn, M. J. B.; Belanger, K.; Brandes, A. A.; Marosi, C.; Bogdahn, U.; Curschmann, J.; Janzer, R. C.; Ludwin, S. K.; Gorlia, T.; Allgeier, A.; Lacombe, D.; Cairncross, J. G.; Eisenhauer, E.; Mirimanoff, R. O., Radiotherapy plus Concomitant and Adjuvant Temozolomide for Glioblastoma. *N. Engl. J. Med.* **2005**, 352 (10), 987-996.
181. Nieder, C.; Adam, M.; Molls, M.; Grosu, A. L., Therapeutic options for recurrent high-grade glioma in adult patients: Recent advances. *Crit. Rev. Oncol. Hemat.* **2006**, 60 (3), 181-193.
182. Muldoon, L. L.; Soussain, C.; Jahnke, K.; Johanson, C.; Siegal, T.; Smith, Q. R.; Hall, W. A.; Hynynen, K.; Senter, P. D.; Peereboom, D. M.; Neuwelt, E. A., Chemotherapy Delivery Issues in Central Nervous System Malignancy: A Reality Check. *Journal of Clinical Oncology* **2007**, 25 (16), 2295-2305.
183. Claes, A.; Idema, A. J.; Wesseling, P., Diffuse glioma growth: a guerilla war. *Acta Neuropathol.* **2007**, 114 (5), 443-458.
184. Grossman, S. A.; Batara, J. F., Current management of glioblastoma multiforme. *Seminars in Oncology* **2004**, 31 (5), 635-644.
185. Sawyer, A. J.; Piepmeier, J. M.; Saltzman, W. M., New Methods for Direct Delivery of Chemotherapy for Treating Brain Tumors. *The Yale Journal of Biology and Medicine* **2006**, 79 (3-4), 141-152.
186. Bobo, R. H.; Laske, D. W.; Akbasak, A.; Morrison, P. F.; Dedrick, R. L.; Oldfield, E. H., Convection-enhanced delivery of macromolecules in the brain. *Proc. Natl. Acad. Sci. U. S. A.* **1994**, 91 (6), 2076-80.

187. Boiardi, A.; Eoli, M.; Salmaggi, A.; Lamperti, E.; Botturi, A.; Solari, A.; Di Meco, F.; Broggi, G.; Silvani, A., Local drug delivery in recurrent malignant gliomas. *Neurological Sciences* **2005**, *26* (1), s37-s39.
188. Butowski, N. A.; Sneed, P. K.; Chang, S. M., Diagnosis and Treatment of Recurrent High-Grade Astrocytoma. *Journal of Clinical Oncology* **2006**, *24* (8), 1273-1280.
189. Combs, S. E.; Thilmann, C.; Edler, L.; Debus, J.; Schulz-Ertner, D., Efficacy of Fractionated Stereotactic Reirradiation in Recurrent Gliomas: Long-Term Results in 172 Patients Treated in a Single Institution. *Journal of Clinical Oncology* **2005**, *23* (34), 8863-8869.
190. Tsao, M. N.; Mehta, M. P.; Whelan, T. J.; Morris, D. E.; Hayman, J. A.; Flickinger, J. C.; Mills, M.; Rogers, C. L.; Souhami, L., The American Society for Therapeutic Radiology and Oncology (ASTRO) evidence-based review of the role of radiosurgery for malignant glioma. *International Journal of Radiation Oncology\*Biophysics\*Physics* **2005**, *63* (1), 47-55.
191. Wang, P. P.; Frazier, J.; Brem, H., Local drug delivery to the brain. *Adv. Drug Delivery Rev.* **2002**, *54* (7), 987-1013.
192. Kaiser, M. G.; Parsa, A. T.; Fine, R. L.; Hall, J. S.; Chakrabarti, I.; Bruce, J. N., Tissue Distribution and Antitumor Activity of Topotecan Delivered by Intracerebral Clysis in a Rat Glioma Model. *Neurosurgery* **2000**, *47* (6), 1391-1399.
193. Bruce, J. N.; Falavigna, A.; Johnson, J. P.; Hall, J. S.; Birch, B. D.; Yoon, J. T.; Wu, E. X.; Fine, R. L.; Parsa, A. T., Intracerebral Clysis in a Rat Glioma Model. *Neurosurgery* **2000**, *46* (3), 683-691.
194. Lopez, K. A.; Waziri, A. E.; Canoll, P. D.; Bruce, J. N., Convection-enhanced delivery in the treatment of malignant glioma. *Neurological Research* **2006**, *28* (5), 542-548.
195. Yang, W.; Barth, R. F.; Huo, T.; Nakkula, R. J.; Weldon, M.; Gupta, N.; Agius, L.; Grecula, J. C., Radiation therapy combined with intracerebral administration of carboplatin for the treatment of brain tumors. *Radiation Oncology* **2014**, *9* (1), 1-9.
196. Shi, M.; Fortin, D.; Paquette, B.; Sanche, L., Convection-enhancement delivery of liposomal formulation of oxaliplatin shows less toxicity than oxaliplatin yet maintains a similar median survival time in F98 glioma-bearing rat model. *Invest. New Drugs* **2016**, *34* (3), 269-276.
197. Zhou, J.; Atsina, K.-B.; Himes, B. T.; Strohbahn, G. W.; Saltzman, W. M., Novel Delivery Strategies for Glioblastoma. *Cancer journal (Sudbury, Mass.)* **2012**, *18* (1), 10.1097/PPO.0b013e318244d8ae.
198. Miyata, S.; Kawabata, S.; Hiramatsu, R.; Doi, A.; Ikeda, N.; Yamashita, T.; Kuroiwa, T.; Kasaoka, S.; Maruyama, K.; Miyatake, S.-I., Computed Tomography Imaging of Transferrin Targeting Liposomes Encapsulating Both Boron and Iodine Contrast Agents by Convection-Enhanced Delivery to F98 Rat Glioma for Boron Neutron Capture Therapy. *Neurosurgery* **2011**, *68* (5), 1380-1387.

199. Ren, H.; Boulikas, T.; Lundstrom, K.; Soling, A.; Warnke, P. C.; Rainov, N. G., Immunogene therapy of recurrent glioblastoma multiforme with a liposomally encapsulated replication-incompetent Semliki forest virus vector carrying the human interleukin-12 gene--a phase I/II clinical protocol. *Journal of neuro-oncology* **2003**, *64* (1-2), 147-54.
200. Voges, J.; Reszka, R.; Gossmann, A.; Dittmar, C.; Richter, R.; Garlip, G.; Kracht, L.; Coenen, H. H.; Sturm, V.; Wienhard, K.; Heiss, W.-D.; Jacobs, A. H., Imaging-guided convection-enhanced delivery and gene therapy of glioblastoma. *Annals of Neurology* **2003**, *54* (4), 479-487.
201. Sawyer, A. J.; Saucier-Sawyer, J. K.; Booth, C. J.; Liu, J.; Patel, T.; Piepmeier, J. M.; Saltzman, W. M., Convection-enhanced delivery of camptothecin-loaded polymer nanoparticles for treatment of intracranial tumors. *Drug Delivery and Translational Research* **2011**, *1* (1), 34-42.
202. Emfietzoglou, D.; Kostarelos, K.; Sgouros, G., An Analytic Dosimetry Study for the Use of Radionuclide-Liposome Conjugates in Internal Radiotherapy. *J. Nucl. Med.* **2001**, *42* (3), 499-504.
203. Mufamadi, M. S.; Pillay, V.; Choonara, Y. E.; Du Toit, L. C.; Modi, G.; Naidoo, D.; Ndesendo, V. M. K., A Review on Composite Liposomal Technologies for Specialized Drug Delivery. *Journal of Drug Delivery* **2011**, *2011*, 939851.
204. Wilbur, D. S.; Hamlin, D. K.; Pathare, P. M.; Weerawarna, S. A., Biotin Reagents for Antibody Pretargeting. Synthesis, Radioiodination, and in Vitro Evaluation of Water Soluble, Biotinidase Resistant Biotin Derivatives. *Bioconjug. Chem.* **1997**, *8* (4), 572-584.
205. del Rosario, R. B.; Wahl, R. L., Biotinylated Iodo-Polylysine for Pretargeted Radiation Delivery. *J. Nucl. Med.* **1993**, *34* (7), 1147-1151.
206. Svenson, S., The dendrimer paradox - high medical expectations but poor clinical translation. *Chem. Soc. Rev.* **2015**, *44*, 4131-4144.
207. Liko, F.; Hindré, F.; Fernandez-Megia, E., Dendrimers as Innovative Radiopharmaceuticals in Cancer Radionanotherapy. *Biomacromolecules* **2016**.
208. Kannan, R. M.; Nance, E.; Kannan, S.; Tomalia, D. A., Emerging concepts in dendrimer-based nanomedicine: from design principles to clinical applications. *J. Intern. Med.* **2014**, *276* (6), 579-617.
209. Casacó, A.; López, G.; García, I.; Rodríguez, J.; Fernández, R.; Figueredo, J.; Torres, L.; Perera, A.; Batista, J.; Leyva, R., Phase I single-dose study of intracavitary-administered Nimotuzumab labeled with <sup>188</sup>Re in adult recurrent high-grade glioma. *Cancer biology & therapy* **2008**, *7* (3), 333.
210. Boas, U.; Christensen, J. B.; Heegaard, P. M., *Dendrimers in medicine and biotechnology: new molecular tools*. Royal Society of Chemistry: 2006.
211. Fernandez-Megia, E.; Correa, J.; Rodríguez-Meizoso, I.; Riguera, R., A Click Approach to Unprotected Glycodendrimers. *Macromolecules* **2006**, *39* (6), 2113-2120.

212. Amaral, S. P.; Correa, J.; Riguera, R.; Fernandez-Megia, E., Unpublished work.
213. Reddy, L. H.; Sharma, R. K.; Chuttani, K.; Mishra, A. K.; Murthy, R. R., Etoposide-incorporated tripalmitin nanoparticles with different surface charge: Formulation, characterization, radiolabeling, and biodistribution studies. *The AAPS Journal* **2004**, *6* (3), 55-64.
214. Zhang, Y.; Huo, M.; Zhou, J.; Xie, S., PKSolver: An add-in program for pharmacokinetic and pharmacodynamic data analysis in Microsoft Excel. *Computer Methods and Programs in Biomedicine* **2010**, *99* (3), 306-314.
215. Wei Cui, Y. Z., Xiaoping Xu, and Yu-Mei Shen, Synthesis and 188Re Radiolabelling of Dendrimer Polyamide Amine (PAMAM) Folic Acid Conjugate. *Med. Chem.* **2012**, *8* (4), 727-731.
216. Kobayashi, H.; Sato, N.; Hiraga, A.; Saga, T.; Nakamoto, Y.; Ueda, H.; Konishi, J.; Togashi, K.; Brechbiel, M. W., 3D-micro-MR angiography of mice using macromolecular MR contrast agents with polyamidoamine dendrimer core with reference to their pharmacokinetic properties. *Magnetic Resonance in Medicine* **2001**, *45* (3), 454-460.
217. Nel, A. E.; Madler, L.; Velegol, D.; Xia, T.; Hoek, E. M.; Somasundaran, P.; Klaessig, F.; Castranova, V.; Thompson, M., Understanding biophysicochemical interactions at the nano-bio interface. *Nature materials* **2009**, *8* (7), 543-57.
218. Malik, N.; Wiwattanapatapee, R.; Klopsch, R.; Lorenz, K.; Frey, H.; Weener, J. W.; Meijer, E. W.; Paulus, W.; Duncan, R., Dendrimers:: Relationship between structure and biocompatibility in vitro, and preliminary studies on the biodistribution of 125I-labelled polyamidoamine dendrimers in vivo. *J. Control. Release* **2000**, *65* (1-2), 133-148.
219. Nigavekar, S. S.; Sung, L. Y.; Llanes, M.; El-Jawahri, A.; Lawrence, T. S.; Becker, C. W.; Balogh, L.; Khan, M. K., 3H dendrimer nanoparticle organ/tumor distribution. *Pharm. Res.* **2004**, *21* (3), 476-83.
220. Rohrer, M.; Bauer, H.; Mintonovitch, J.; Requardt, M.; Weinmann, H.-J., Comparison of Magnetic Properties of MRI Contrast Media Solutions at Different Magnetic Field Strengths. *Invest. Radiol.* **2005**, *40* (11), 715-724.
221. Caravan, P., Strategies for increasing the sensitivity of gadolinium based MRI contrast agents. *Chem. Soc. Rev.* **2006**, *35* (6), 512-523.
222. Swanson, S. D.; Kukowska-Latallo, J. F.; Patri, A. K.; Chen, C.; Ge, S.; Cao, Z.; Kotlyar, A.; East, A. T.; Baker, J. R., Targeted gadolinium-loaded dendrimer nanoparticles for tumor-specific magnetic resonance contrast enhancement. *Int. J. Nanomed.* **2008**, *3* (2), 201-210.

## Bibliography

---

223. Hsieh, B. T.; Hsieh, J. F.; Tsai, S. C.; Lin, W. Y.; Huang, H. T.; Ting, G.; Wang, S. J., Rhenium-188-Labeled DTPA: a new radiopharmaceutical for intravascular radiation therapy. *Nucl. Med. Biol.* **1999**, *26* (8), 967-72.
224. Magerstadt, M.; Gansow, O. A.; Brechbiel, M. W.; Colcher, D.; Baltzer, L.; Knop, R. H.; Girton, M. E.; Naegele, M., Gd(DOTA): an alternative to Gd(DTPA) as a T1,2 relaxation agent for NMR imaging or spectroscopy. *Magn Reson Med* **1986**, *3* (5), 808-12.
225. Runge, V. M.; Jacobson, S.; Wood, M. L.; Kaufman, D.; Adelman, L. S., MR imaging of rat brain glioma: Gd-DTPA versus Gd-DOTA. *Radiology* **1988**, *166* (3), 835-838.



## Flonja LIKO



**PhD student: European Doctorate in Nanomedicine and Pharmaceutical Innovation**

 **Angers- France**

 flonjaliko@yahoo.com



<https://fr.linkedin.com/in/flonjaliko>

**LANGUAGES: English | Italian | Turkish | Spanish | Albanian**

### CORE QUALIFICATIONS

- Research experience in synthetic organic chemistry and pharmaceutical technology/ radiopharmacy.
- Practical experience with the following analytical techniques: Nuclear magnetic resonance spectroscopy (NMR), Absorption spectrophotometry (UV-visible), Absorption spectrophotometry (IR), Thin Layer Chromatography (TLC), DLS technique, Gamma counting, Gamma camera, etc.
- Knowledge of radioactivity handling ( $^{188}\text{Re}$ -Perrhenate and  $^{99\text{m}}\text{Tc}$ -Perrhenate)
- Experience with preclinical research., convection enhanced delivery procedures, biodistribution and pharmacokinetic studies.
- Good command of the software Mestre Nova<sup>TM</sup> (Mestrelab Research<sup>TM</sup>).
- Good command of the software Office<sup>TM</sup> (Word<sup>TM</sup>, Excel<sup>TM</sup> e PowerPoint<sup>TM</sup>).

### EDUCATION

**Oct 2013- Oct 2016**

**European Doctorate in Nanomedicine and Pharmaceutical Innovation**

University of Angers, INSERM U1066 Micro et Nanomédecines Biomimétiques (France)

University of Santiago de Compostela, Center for Research in Biological Chemistry and Molecular Materials (CiQUS) (Spain)

Dissertation title: Dendrimers as a powerful tool for theranostic applications (Double doctorate). This PhD was financed and organized by the NanoFar program. NanoFar is proposed by leading European academic teams working together on the integrative approaches to nanomedicine.

**Sept. 2008- Oct. 2011**

**Master of Science in Pharmaceutical Technology**

University of Hacettepe, Faculty of Pharmacy, Division Head of Pharmaceutical Technology,

Department of Radiopharmacy (Turkey)

Dissertation title: *In vitro* studies on 5-florouracil loaded DTPA-PE containing nanosized PEGylated different charged liposome formulations for diagnosis and treatment of tumor. Formulations of anionic, cationic and neutral PEGylated liposome

nanoparticles with different phospholipid types, decorated with DTPA-PE ligands for radiolabeling with  $^{99m}\text{Tc}$  and loaded with 5-fluorouracil, aimed to be used as a theranostic platform for diagnosis and treatment of breast cancer.

**Oct. 2004- Jul. 2008**

**Licentiate in Pharmacy**

**University of Ankara, Faculty of Pharmacy (Turkey)**

### GRANTS AND AWARDS

- **EACEA EMJD** PhD fellowship.
- **Excellence** scholarship within the Bilateral Education Agreement between Albania and Turkey for her undergraduate degree.

### PUBLICATIONS

- **Liko, F.;** Hindré, F.; Fernandez-Megia, E., Dendrimers as Innovative Radiopharmaceuticals in Cancer Radionanotherapy. *Biomacromolecules* 2016, *17* (10), 3103-3114.
- **Liko, F.;**Tetaud, C.; Galopin,N.;Amaral,S.; Fernandez-Megia,E.; Hindré, F. Novel dendritic construct as a prospective theranostic agent for radiotherapy and MRI of glioblastoma (manuscript in preparation).
- **Liko, F.;** Erdoğan, S.; Özer, Y. A.; Vural, I. In vitro Studies on 5-Fluorouracil-Loaded DTPA-PE Containing Nanosized PEGylated Liposomes for Diagnosis and Treatment of Tumor. *Journal of Liposome Research* 2013, *23*, 61–69.

### ACADEMIC CONFERENCES

- 2016** **ORAL COMMUNICATION: Evaluation of theranostic dendrimers for radiotherapy and MRI of gliomas;** [Flonja Liko](#); Eduardo Fernandez-Megia; Francois Hindre; ICONAN 2016 (Sep. 2016), Paris, France
- 2015** **POSTER: Multifunctional dendrimers for multimodality Imaging;** [Flonja Liko](#); Natacha Galopin, Clement Tetaud, Eduardo Fernandez-Megia; Francois Hindre; SFNano 2015 (Dec. 2015), Grenoble, France.
- ORAL COMMUNICATION: Dendrimers as a powerful tool in radionanomedicine;** [Flonja Liko](#); Eduardo Fernandez-Megia; Francois Hindre; New Advances in animal models and preclinical imaging for translational research in Cancerology; 9th edition; (Oct. 2015), Pen Bron, La Turballe, France.
- POSTER: Functionalized dendrimers as dual modality systems;** [Flonja Liko](#); Eduardo Fernandez-Megia; Francois Hindre; NanoFar Autumn School (Oct. 2015), University of Nantes, France.
- 2014** **POSTER: Synthesis and generation growth of a new family of carbamate dendrimers;** [Flonja Liko](#); Eduardo Fernandez-Megia; Francois Hindre; NanoFar Autumn School (Oct. 2014), Université Catholique de Louvain, Belgium.
- 2013** **ORAL COMMUNICATION: Overview of dendrimers, advantages for applications in cancer theranostics;** [Flonja Liko](#); Eduardo Fernandez-Megia;

Francois Hindre; NanoFar Autumn School (Oct. 2013), University of Santiago de Compostela), Spain.

- 2012** **ORAL COMMUNICATION: In vitro Studies on 5-Fluorouracil-Loaded DTPA-PE Containing Nanosized PEGylated Liposomes for theranostics of breast cancer;** Flonja Liko, Suna Erdogan, Yekta Ozer; 8<sup>th</sup> World Meeting on Pharmaceutics, Biopharmaceutics and Pharmaceutical Technology”, (Mar. 2012), Istanbul, Turkey.

### TRAINING COURSES

- 2016** “MRI practical background course” (1-2 Mar.)  
Primex-MRI facility, IBS-CHU, University of Angers, Angers (France)
- 2015** “NanoFar Autumn School” (26 -30 Oct.)  
University of Nantes, Nantes (France)
- 2014** “Biobusiness Week: How to turn Bioscience into Biobusiness?” (10 -13 Jun.)  
Atlanpole Biotherapies, Nantes (France).  
“EDEN 4, Fourth Spanish Dendrimer Meeting” (23-24 Jan.)  
Center for Research in Biological Chemistry and Molecular Materials, Santiago de Compostela (Spain)  
“NanoFar Autumn School” (20 -24 Oct.)  
Université Catholique de Louvain, Brussels (Belgium)
- 2013** “Utilisation of the spectrometer AGILENT (Varian) Mercury-300” (7-8 Nov.)  
Center for Research in Biological Chemistry and Molecular Materials, Santiago de Compostela (Spain)  
“NanoFar Autumn School” (21 -25 Oct.)  
Center for Research in Biological Chemistry and Molecular Materials, Santiago de Compostela (Spain)

# Thèse de Doctorat

## Flonja LIKO

### Potentiel des dendrimères comme outil d'applications théranostiques

#### Dendrimers as a powerful tool in theranostic applications

##### Résumé

Une nouvelle stratégie oncologique, basée sur l'intégration de la radiothérapie nanovectorisée et l'administration loco-régionale, a été évaluée pour le traitement et l'imagerie du glioblastome, le type le plus commun des tumeurs cérébrales primaires. Les dendrimères Gallic Acid-Triéthylène Glycol (GATG) sont des nanovecteurs de choix pour délivrer simultanément l'agent thérapeutique (le radioisotope  $^{188}\text{Re}$  par son rayonnement bêta a été retenu) et l'agent diagnostique (le gadolinium est un agent paramagnétique utilisé en Imagerie par Résonance Magnétique (IRM)). Leur évaluation a été réalisée par administration loco-régionale par stéréotaxie sur un modèle de rat F98. Les données pharmaco-cinétiques ont été également obtenues après injection intraveineuse permettant d'apprécier les propriétés des différents dendrimères synthétisés. Leur apport en terme de confinement au site d'injection représente un avantage majeur de ce nouveau type de radiopharmaceutiques.

##### Mots clés

GATG, dendrimères, radiothérapie interne, MRI, glioblastoma,  $^{188}\text{Re}$ ,  $\text{Gd}^{3+}$ ,  $^{99\text{m}}\text{Tc}$ .

##### Abstract

A new oncologic strategy, based on the integration of nanovectorized radiotherapy and locoregional delivery, was evaluated for the treatment and imaging of glioblastomas, the most common and lethal type of primary brain tumors. Gallic acid-triethylene glycol (GATG) dendrimers were the nanovectors of choice to deliver the radiotherapeutic  $^{188}\text{Re}$  and paramagnetic nuclei  $\text{Gd}^{3+}$ , with a minimally invasive stereotactic injection, directly depositing the radiotherapeutic dose to the tumor site in a F98 rat glioma model. Intravenous injection was used to further investigate the pharmacokinetics, throughout body distribution and clearance profiles of these dendrimers. Molecular weight and architecture had an important role on the *in vivo* behavior of the dendrimers. Their use as nanovectors prevented the fast brain clearance of the radionuclide alone, and prolonged the confinement of the internal radiation at the tumor site.

##### Key words

GATG, dendrimer, internal radiotherapy, MRI, glioblastoma,  $^{188}\text{Re}$ ,  $\text{Gd}^{3+}$ ,  $^{99\text{m}}\text{Tc}$ .